Feasibility Study Report for the Next Generation CFHT. I. Science

Submitted by P. Côté on behalf of the ngCFHT Feasibility Study Science Team

December 2, 2012

Contributing Authors

Nobou Arimoto	National Astronomical Observatory of Japan	Japan
Michael Balogh	University of Waterloo	Canada
Patrick Boissé	Institut dAstrophysique de Paris	France
James Bolton	University of Melbourne	Australia
Piercarlo Bonifacio	GEPI, Université Paris Diderot	France
Francois Bouchy	Institut d'Astrophysique de Paris/Obs. de Haute Provence	France
Andrew Cole	University of Tasmania	Australia
Patrick Côté	National Research Council	Canada
Len Cowie	Institute for Astronomy, University of Hawaii	United States of America
David Crampton	National Research Council	Canada
Scott Croom	University of Sydney	Australia
Katia Cunha	Observatório Nacional-MCT	Brazil
	National Optical Astronomy Observatory	United States of America
Richard de Grijs	Kavli Institute for Astronomy and Astrophysics	China
Magali Deleuil	Laboratoire d'Astrophysique de Marseille	France
Ernst de Mooij	University of Toronto	Canada
Simon Driver	International Centre for Radio Astronomy Research	Australia
Patrick Dufour	Université de Montréal	Canada
Sara Ellison	University of Victoria	Canada
Sebastien Foucaud	National Taiwan Normal University	Taiwan
Ken Freeman	Australian National University	Australia
Karl Glazebrook	University of Swinburne	Australia
Patrick Hall	York University	Canada
Zhanwen Han	Yunnan Observatory	China
Michael Hudson	University of Waterloo	Canada
John Hutchings	National Research Council	Canada
Rodrigo Ibata	Université de Strasbourg	France
Pascale Jablonka	Observatoire de Paris	France
Jean-Paul Kneib	Laboratoire d'Astrophysique de Marseille	France
	Ecole Polytechnique Federale de Lausanne	Switzerland
Chiaki Kobayashi	Australian National University	Australia
	University of Hertfordshire	United Kingdom
Rolf-Peter Kudritzki	Institute for Astronomy, University of Hawaii	United States of America
Rosine Lallement	GEPI, Observatoire de Paris	France
Damien Le Borgne	Institut dAstrophysique de Paris	France
Yang-Shyang Li	Kavli Institute for Astronomy and Astrophysics	China
Lihwai Lin	Academia Sinica Institute of Astronomy and Astrophysics	Taiwan
Yen-Ting Lin	Inst. for the Physics & Math. of the Universe, Univ. of Tokyo	Japan
Martin Makler	Centro Brasilerio de Pesquisas Fisicas	Brasil
Nicolas Martin	Université de Strasbourg	France
Alan McConnachie	National Research Council	Canada
Norio Narita	National Astronomical Observatory of Japan	Japan
Changbom Park	Korea Institute for Advanced Study	Republic of Korea
Eric Peng	Peking University	China
Patrick Petitjean	Institut dAstrophysique de Paris	France
Céline Peroux	Laboratoire d'Astrophysique de Marseille	France
Ryan Ransom	Okanagan College/DRAO	Canada
Swara Ravindranath	Inter-University Centre for Astronomy and Astrophysics	India
Bacham Eswar Reddy	Indian Institute of Astrophysics	India

Contributing Authors (cont'd)

Marcin Sawicki	St. Mary's University	Canada
Carlo Schimd	Laboratoire d'Astrophysique de Marseille	France
Luc Simard	National Research Council	Canada
Raghunathan Srianand	Inter-University Centre for Astronomy and Astrophysics	India
Else Starkenburg	University of Victoria	Canada
Thaisa Storchi-Bergmann	Universidade Federal do Rio Grande do Sul	Brasil
Charling Tao	Centre de Physique des Particules de Marseille	France
	Tsinghua University	China
Sivarani Thirupathi	Indian Institute of Astrophysics	India
Keiichi Umetsu	Academia Sinica Institute of Astronomy & Astrophysics	Taiwan
Kim Venn	University of Victoria	Canada
Chris Willott	National Research Council	Canada
Ting-Gui Wang	University of Science and Technology of China	China
Jong-Hak Woo	Seoul National University	Republic of Korea
Xue-Bing Wu	Peking University	China

Contents

Summary

The Next Generation CFHT (ngCFHT) is a proposal to replace the 3.6m CFHT with a 10m, dedicated spectroscopic survey telescope. The new facility would be installed on the existing telescope pier and equipped with a wide-field (1.5 deg^2), massively-multiplexed ($N_{\rm fib} = 800$–3200) fibre spectrograph. This document evaluates the science drivers for the proposed facility, including technical requirements and possible survey strategies. We compare the expected performance of ngCFHT with a number of existing, planned or proposed spectroscopic facilities, and show how it would be unrivaled in its ability to perform panoramic, multi-object spectroscopy of the faint universe, thanks to its combination of large collecting area, wide field of view, high multiplexing, range of spectral resolutions ($\mathcal{R} =$ 2000, 6500, 20000), and dedicated scheduling for surveys. Two major scientific thrusts highlight ngCFHT's potential for discovery:

1. *Galactic Archaeology.* ngCFHT would provide the ultimate spectroscopic complement to the Gaia mission, with a multi-year, bright/grey-time survey that would map a quarter of the volume of the Milky Way and yield medium-resolution spectra for a sample of 20 million stars, 5 million of which would also have high-resolution data. No planned or proposed survey could rival this programme in its ability to characterize the halo metallicity distribution function, perform chemical tagging of Galactic stars, or explore the three-dimensional, phase-space structure of our Galaxy.

2. *Galaxy Evolution and Cosmology*. A suite of dark-time surveys covering many thousands of square degrees would yield spectra for more than 10 million galaxies, allowing a study of galaxy evolution at seven distinct epochs between $0.5 < z < 1.5$ (each with the same statistical power as the SDSS) while providing BAO distances (accurate to better than 1%) to be used in a precise measurement of dark energy and its possible evolution with redshift. No planned or proposed spectroscopic survey would provide comparable constraints on the growth factor, the law of gravitation on large scales, or the shape of the power spectrum.

Many other transformational science programmes would also be enabled, on a wide range of topics: i.e., the three-dimensional structure of the ISM, time-domain spectroscopy, rare and exotic stellar types, chemo-dynamical mapping of nearby galaxies, the structure of dark matter halos, star formation efficiency as a function of halo mass, the galaxy-IGM connection from Ly-α absorbers, and reverberation mapping of AGN. We highlight the integral role ngCFHT could play in a long-term, strategic vision for astronomy on Mauna Kea.

An accompanying technical feasibility report shows how the proposed redevelopment could utilize the existing pier and building with only minor modifications, and how the conversion would not increase the visual footprint of CFHT on Mauna Kea; it also presents possible telescope optical designs, and spectrograph design options that demonstrate the overall feasibility of the concept.

1 Strategic Vision

1.1 Scope and Context of this Study

The diverse and exciting scientific opportunities enabled by a wide-field, large-aperture, spectroscopic survey telescope have long been recognized by the international astronomical community. Indeed, the initial calls for such a facility appeared more than a decade ago (e.g., Brown & Dey 2001; Dey et al. 2003), and the suite of powerful imaging and astrometric telescopes that are scheduled to begin survey operations in the near future have only sharpened the need for wide-field spectroscopic follow up. Yet, despite its obvious and enduring scientific appeal, such a facility remains a "missing capability" in the portfolio of international astronomical projects.

Here we examine the science drivers and technical requirements for such a facility: i.e., the Next Generation CFHT (ngCFHT), which aims to replace the 3.6m CFHT[1] with a 10m survey telescope, to be installed on the existing pier and equipped with a dedicated, wide-field, highly multiplexed fibre spectrograph. The ngCFHT concept began as a grassroots movement within the CFHT user communities in late 2010, and, in early 2011, a feasibility study was initiated to explore both the facility's scientific requirements and its overall technical feasibility. This facility, which could see first light as soon as the early 2020s, has been developed to fill what is arguably the single most important missing capability in astrophysics — a dedicated, 10m-class telescope for the comprehensive spectroscopic follow up (at both low and high spectral resolution) of upcoming imaging and astrometric surveys.

This document presents results from the scientific component of the ngCFHT feasibility study; an accompanying document focuses on the technical and design aspects. Because the proposed facility would have a broad, multi-national appeal, and because the proposed redevelopment is beyond the scope of the existing CFHT partnership, a number of science working groups were assembled in early 2011, with membership not limited to existing partner communities. The science working groups were chosen to cover the broadest possible range of science topics: the interstellar medium, stellar astrophysics and exoplanets, the Milky Way, the Local Group, nearby galaxies and clusters, galaxy evolution, QSOs and AGN, the intergalactic medium, and cosmology. The $\sim$60 astronomers who make up the science working groups represent a number of communities that have a presence on Mauna Kea, either now or in the near future (e.g., Australia, Brazil, Canada, China, France, Hawaii, India, Japan, the Republic of Korea, Taiwan, the UK, and the USA).

In this chapter, we briefly review the rationale that underlies a redevelopment of the existing telescope (§1.2), and look ahead to ngCFHT's anticipated scientific legacy (§1.3). The many imaging and astrometric surveys that motivate such a facility are briefly reviewed in §1.4. In §1.5 we compare the expected performance of ngCFHT with a number of existing, planned or proposed spectroscopic facilities, showing that its capabilities would be unrivaled for stellar, Galactic, extragalactic and cosmological science. A brief overview of ngCFHT's design, technical specifications, and provisional operating scenarios is presented in §1.6, while §1.7 explains the integral role ngCFHT could play in a long-term, strategic vision for astronomy atop Mauna Kea. A large (but incomplete) selection of scientific investigations that could be undertaken with ngCFHT are discussed in §2. Subsections examine the facility's competition and synergy in various subfields, identify probable "legacy" science, and present preliminary strategies for spectroscopic surveys.

1.2 Redevelopment of the Existing Facility

Mauna Kea is widely regarded as one of the finest astronomical sites on earth, enjoying excellent atmospheric stability (i.e., a median seeing of the free atmosphere of $0\farcs4$ with a 10th percentile quality of $0\farcs25$), low precipitable water vapour (median $\approx$ 0.9 mm) and a high percentage of useable nights ($\approx$ 300 annually for spectroscopy). It has superb infrastructure for astronomy, with a dozen telescopes operating from this location (see §1.7), and its geographical location offers convenient access for many astronomical communities located along the Pacific Rim. At an equatorial latitude of $19\fdg8$ N, it allows complete visibility of the northern skies (an important consideration for those communities whose observing resources are located primarily in the south), and significant access to the southern skies as well (see §1.4 and Figure 2). CFHT, which in 1979 became the first 4m-class telescope to go into operation on Mauna Kea, occupies what is arguably the best site on the mountain: i.e., at the northern edge of the $\sim$4200m summit ridge.

However, space for expansion on Mauna Kea is limited, particularly along the summit ridge, which is already fully developed. The redevelopment of existing sites, including that of CFHT, has therefore been anticipated for some

[1]The Canada-France-Hawaii Telescope (CFHT) is jointly operated by Canada (through the National Research Council of Canada), France (through the Centre National de la Recherche Scientique) and the University of Hawaii. The observatory has active collaborative agreements with Brazil (2002 – present), China (2011 – present), the Republic of Korea (2000 – 2003, 2012 – present), and Taiwan (2002 – present).

time. A framework for such redevelopment was established in the *Mauna Kea Science Reserve Master Plan* (2000) (hereafter Master Plan), which noted that up to 3–4 of the facilities situated on the summit ridge (i.e., NASA/IRTF, CFHT, UH 2.2m, UKIRT, and the UH 0.6m) could be redeveloped over a 20-year period. This comprehensive study — prepared in consultation with a diversity of communities to ensure that scientific requirements were balanced with cultural and environmental considerations — presciently anticipated

> *"... a trend toward specialization for these conventional-size optical/infrared telescopes facilities.... Specialization will allow the telescope facility to achieve the ultimate in performance within the chosen area of research, while at the same time simplifying the operation and thereby reducing costs. Specialization will provide a strong incentive for joint operating arrangements and shared use among the observatory organizations."*

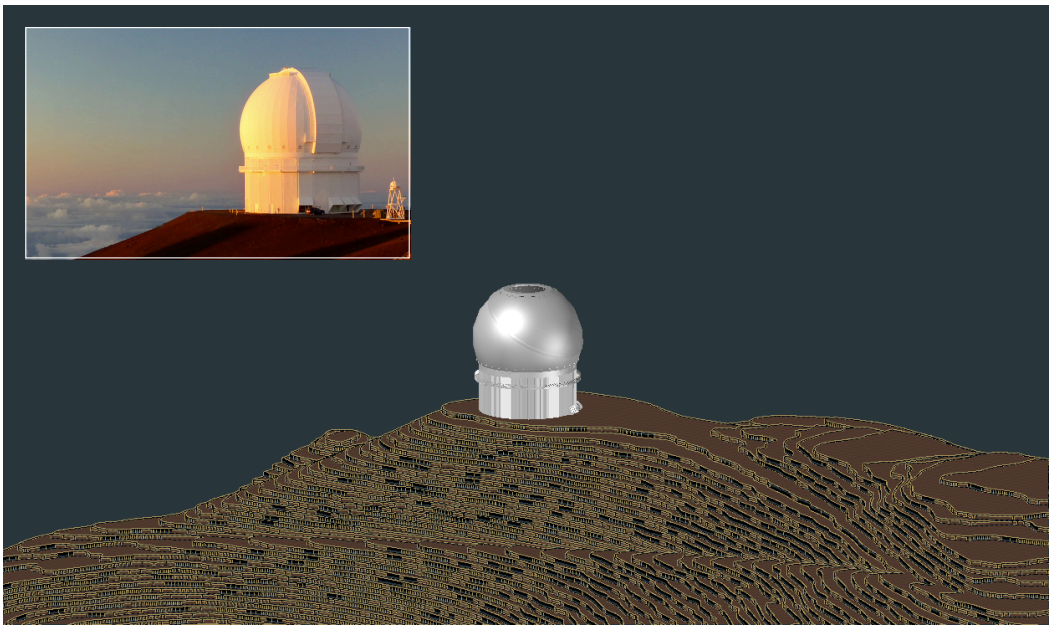

Figure 1: Projection of a three-dimensional rendering of ngCFHT by *Empire Dynamic Structures*, showing the facility as it would appear on the summit ridge. The facility, with the Calotte pointed at the zenith, is shown in 1:1 scale with the true mountain-top topography. The inset shows an image of the existing CFHT taken from a similar perspective.

The Master Plan presented a number of guidelines intended to direct future development in a manner that smoothly integrates new facilities into the summit environment. Mindful of these guidelines, the ngCFHT concept explored here has been developed subject to the following, additional, design constraints:

1. It does not disturb the ground beyond what has already been done.
2. It stays within the current CFHT space envelope.
3. It minimizes work at the summit by reusing the existing telescope and enclosure piers.

The development philosophy for the ngCFHT concept has thus been to "stay within the three-dimensional footprint of the existing facility". This is in full accord with all guidelines laid out in the Master Plan, and would ensure that the appearance of the summit ridge is effectively unchanged by redevelopment (see Figure 1).

1.3 Science Drivers and Facility Legacy

Astronomy is on the cusp of a new era. A new generation of powerful, optical/IR imaging telescopes will soon be carrying out panoramic sky surveys — sometimes on timescales of days or weeks as they undertake the first systematic exploration of the transient universe. In 2013, ESA's Gaia satellite will commence its 5-year mission to compile an astrometric catalogue of $\sim$ one billion Galactic stars, while in 2014, the eROSITA satellite will begin the first all-sky

X-ray survey since ROSAT (but with a ∼30-fold improvement in survey efficiency). In the radio region, powerful new SKA Pathfinder telescopes will soon begin surveys to map much of the sky at unprecedented depth and resolution. Collectively, these facilities will produce rich datasets that will be used by astronomers to address many of the coming decade's most pressing scientific questions — from the assembly history of the Milky Way to the nature of dark energy.

As we show below, ngCFHT would be unrivaled in its ability to perform panoramic, multi-object spectroscopy of the faint universe, and thus take the leading role in the scientific exploitation of these surveys. Although a vast scientific heritage is virtually guaranteed, we highlight two broad areas in which ngCFHT's impact would be especially profound:

1. **Galactic Archaeology.** ngCFHT would carry out the ultimate spectroscopic follow up of the Gaia mission, with a multi-year, bright/grey-time survey yielding medium-resolution spectra for a sample of 20 million stars, 5 million of which would also have high-resolution data. Covering ∼1/4 of the sky to a depth of $g \simeq 20$–21 mag, no planned or proposed survey could rival this programme in its ability to characterize the halo metallicity distribution function, perform chemical tagging of Galactic stars, or explore the three-dimensional phase space structure of the Milky Way.

2. **Galaxy Evolution and Cosmology.** A suite of dark-time surveys covering many thousands of square degrees would yield spectra for more than 10 million galaxies, allowing a study of galaxy evolution at seven distinct epochs between $0.5 < z < 1.5$, *each with the same statistical power as the SDSS*, while providing BAO distances accurate to <1% to be used in a precise measurement of dark energy and its possible evolution with redshift. No planned or proposed spectroscopic survey would provide comparable constraints on the growth factor, the law of gravitation on large scales, or the shape of the power spectrum.

ngCFHT's impact would, however, be felt far beyond these fields. Its combination of large collecting area, wide field of view, high multiplexing, range of spectral resolution, and dedicated operations mode, would allow it to undertake *transformational* research across a wide range of subfields. A representative selection of other science results that would be enabled by such a facility include:

– An extraordinary, three-dimensional map of the Galactic ISM, with the density structure and kinematics measured along hundreds of thousands of sight lines using high-resolution, absorption-line spectroscopy of molecular, atomic and ionized gas.

– The homogeneous measurement of fundamental parameters (e.g., spectroscopic masses, distances, metallicities, rotation rates) for a large sample of high-mass stars belonging to the Milky Way and nearby galaxies, which would revolutionize our understanding of stellar evolution and feedback in star-forming galaxies.

– The first panoramic, time-domain spectroscopic surveys ever conducted, including unprecedented studies of stellar multiplicity, pulsating and eclipsing stars, novae and supernovae.

– The identification of rare but important stellar types, such as solar twins, white dwarfs associated with the Milky Way thick disk or halo, and extremely metal-poor stars.

– A complete and unbiased chemo-dynamical survey of Local Group galaxies, from lowest-mass, dark-matter-dominated dwarfs to M31, the nearest example of an $L^\star$ galaxy.

– The measurement of gravitational masses and density profiles for a complete sample of dark matter halos, down to the scales of dwarf galaxies, in a rich cluster environment based on radial velocities for hundreds of thousands of candidate baryonic substructures in the nearby Virgo cluster.

– A comprehensive study of the relationship between stellar and gravitational mass, baryon dynamics, and star formation efficiency in dark matter halos spanning a range of $\sim 10^6$ in stellar mass. Covering an area four times larger than the GAMA survey, and reaching 2 magnitudes deeper, this survey would yield spectra for half a million galaxies within $z \lesssim 0.15$

– A spectroscopic survey of ∼100 bright quasar fields allowing an order-of-magnitude improvement in our ability to probe the Galaxy-IGM connection based on ≥40000 Ly-α absorbers, and spectroscopy for 1000–2000 damped Ly-α systems that would dramatically improve our knowledge of early nucleosynthesis and the evolution of metals out to $z \sim 4$.

– A thorough study of AGN feedback through high-S/N, high-resolution, time-domain spectroscopy, as well as an independent determination of the redshift evolution of dark energy through BAOs in the Lyα forest, and an AGN Hubble diagram calibrated through reverberation mapping.

Details on these and other science programmes may be found in §2 of this report. Although the above list is incomplete, it illustrates the expected breadth of ngCFHT's scientific legacy.

1.4 Wide-Field Imaging and Astrometric Surveys

The remarkable success of several public surveys carried out in recent years — most notably the Sloan Digital Sky Survey (SDSS), but also the CFHT Legacy Survey (CFHTLS), the UKIRT Infrared Deep Sky Survey (UKIDSS), and others — has demonstrated the impressive power offered by large, homogeneous, and well-characterized datasets. It should perhaps come as no surprise that the science that ultimately emerged from each of these surveys was far more diverse than anticipated at their outset. For instance, SDSS had a profound impact on topics as far ranging as small bodies in the solar system to the reionization of the universe — a broad appeal that underlies its repeated ranking as the highest-impact telescope of the last decade (e.g. Madrid & Macchetto 2006, 2009; Chen et al. 2009).

Despite this very high level of impact, the next generation of surveys should far exceed SDSS in terms of overall capacity for multidisciplinary research. For instance, Table 1 summarizes the large (i.e., $\Omega_{\rm tot} >$ a few thousand deg^2) optical/IR photometric surveys that are either recently completed, are currently underway, or are being planned for space- and ground-based (1–8m class) telescopes. Collectively, these facilities will cover the entire sky to unprecedented depths, at a range of wavelengths (as illustrated in Figure 2).

However, as we have already noted, there are no plans at present for a dedicated, 10m-class telescope capable of providing the wide-field spectroscopy needed to fully capitalize on these surveys. The importance of this spectroscopic component can scarcely be overestimated: e.g., it is universally recognized that the science impact of SDSS would have been greatly diminished without its spectroscopic element, for the simple reason that broadband photometry alone provides only zeroth-order information on the physical properties of astrophysical sources.[2]

Table 1: Existing, Planned and Proposed Imaging and Astrometric Survey Facilities

Telescope/Instrument	$D_{\rm M1}$ (m)	Status	Wavelength/Filters	Available	Ω (deg^2)	$A\Omega$ (m^{2}deg^2)	$\Omega_{\rm tot}$ (10^3 deg^2)	$f^{\ddagger}_{\rm MK}$
Ground-Based								
SDSS	2.5	Existing	u,g,r,i,z	2000	1.54	7.6	14.6	1
CFHT/MegaPrime	3.6	Existing	u,g,r,i,z	2003	0.90	9.2	6.1	1
UKIRT/WFCam	3.8	Existing	Z,Y,J,H,K	2005	0.19	2.1	4.0	1
PanSTARRS-1	1.8	Existing	g,r,i,z,y,w	2009	7.3	18.6	30.9	1
VISTA/VIRCam	4.1	Existing	Z,Y,J,H,K$_s$	2010	0.6	7.5	20.0	0.48-0.64*
VST/OmegaCam	2.6	Existing	u,v,g,r,i,z	2011	1.0	5.3	4.5	0.60-0.64*
Subaru/HSC	8.2	Existing	g,r,i,z,y	2012	1.7	90	2.0	1
Blanco/DEC	4.0	Existing	g,r,i,z,y	2012	3.0	38	5.0	0.33
WIYN/ODI	3.5	Planned	u,g,r,i,z	2013	1.0	9.6	....	1
Skymapper	1.35	Planned	u,v,g,r,i,z	2013	5.7	8.2	20.6	0.46
PanSTARRS-2	2×1.8	Planned	g,r,i,z,y,w	2013	7.3	37.2	30.9	1
LSST	6.7¶	Planned	u,g,r,i,z,y	2020	6.7	370	24.2	0.39
Space-Based								
Gaia	2×(1.4×0.5)	Planned	0.85–0.87 μm	2013	all sky survey (V $<$ 17)		41.2	0.75
Euclid	1.2	Planned	RIZ,Y,J,H	2020	0.55	0.62	15	$\simeq$ 0.77
WFIRST	1.5	Proposed	Z,Y,J,H,K	2025:	0.5	0.9	3.4†	$\sim$0.5$^{\otimes}$

‡ – *Fraction of survey area visible from Mauna Kea at an airmass of* $X \leq 1.5$.

$\star$ – *Quoted range refers to multiple public surveys.*

¶ – *Effective clear aperture including obscuration.*

† – *According to the Final Report of the WFIRST Science Definition Team, an area of* $\sim$*10 000 deg*^{2} *could be covered during a possible extended lifetime phase.*

$\otimes$ – *Assumes that the primary survey area is equally divided between two fields near the northern and southern ecliptic poles.*

[2]For broadband imaging on 2–4m telescopes (with a spectral resolution of $\mathcal{R} \equiv \lambda/\Delta\lambda \sim 5$), the measurement of distances, kinematics and abundances for the faintest sources requires a spectral resolution that is hundreds, or thousands, of times higher. Thus, spectroscopic follow up requires a roughly order-of-magnitude increase in telescope collecting area.

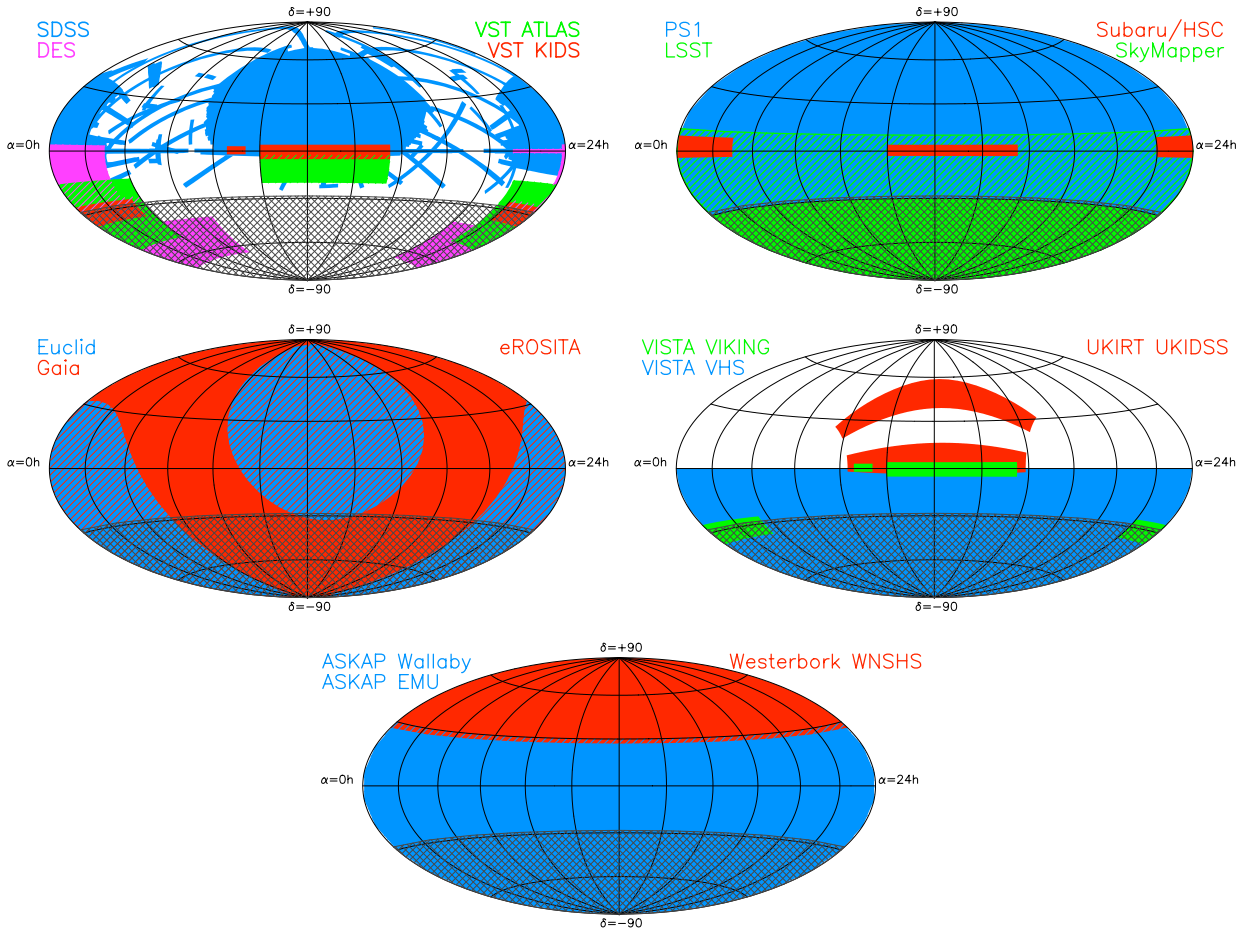

Figure 2: Sky coverage for a selection of existing or upcoming wide-field surveys at optical, IR, X-ray and radio wavelengths. The surveys shown are SDSS, DES, VST-KIDS, VST-ATLAS, VISTA-Viking, Pan-STARRS 1, LSST, Skymapper, Subaru/PFS, VISTA-VHS, VISTA-VIKING, Eucid, eROSITA, Gaia, ASKAP-WALLABY, ASKAP-EMU and Westerbork-WNSHS. The $\sim 3\pi$ region visible from Mauna Kea lies above the hatched region in the south. See also Table 1.

1.4.1 Ground- and Space-Based Imaging Facilities

A number of existing, planned and proposed imaging or astrometric facilities are listed in Table 1. In the northern hemisphere, the entire 3π steradians of sky visible from Mauna Kea are currently being surveyed with the 1.8m PanSTARRS (PS1) telescope. This survey will provide complete optical $(grizyw)$ coverage to approximate limiting magnitudes of $g_{\rm lim} \sim 23.6, r_{\rm lim} \sim 23.3$, and $i_{\rm lim} \sim 23.2$ mag. The PS2 telescope (a near-clone of PS1) is scheduled to begin operations in 2013; it will survey the same area of sky as PS1, effectively doubling its collecting area. In the south, SkyMapper is now being commissioned and will soon undertake its Southern Sky Survey. This all-hemisphere survey (in $uvgriz$) will reach to a limit of $g_{\rm lim} \sim 22.9$ mag, or roughly 0.5–1 mag deeper than the SDSS. In the longer term, the Large Synoptic Survey Telescope (LSST) — the top-ranked, ground-based facility in the recent decadal survey for US astronomy (Blandford et al. 2010) — will undertake a 10-year programme to monitor the entire sky below $\delta \simeq -10^\circ$ in the $ugrizy$ bandpasses. A single 20s exposure with LSST will reach $g_{\rm lim} \simeq 25.0$, with a final (co-added) survey depth of $g_{\rm lim} \simeq 27.5$.

In addition to these all-hemisphere optical surveys, a number of other wide-field imaging projects are either completed, underway or planned. An area of nearly 15 000 deg^2 has already been mapped in the optical by the SDSS (DR9), albeit to shallower limits than planned for PS1+PS2, and the Hyper-Suprime-Cam (HSC) instrument on the 8.2m Subaru telescope will begin regular operations soon. Beginning in 2013, this impressive instrument — the largest mosaic camera ever commissioned on an 8m-class telescope — will undertake a 5-year strategic survey to map $\simeq 1500$

deg^2 along the celestial equator to unprecedented depth. From the south, the Dark Energy Survey will use the Dark Energy Camera (DEC) on the 4m Blanco telescope to map an area of 5000 deg^2, while OmegaCam on the 2.6m VST will survey an area of comparable size. In the infrared, several surveys are underway with 4.1m VISTA telescope, the largest being the VISTA Hemisphere Survey (VHS) which will map the entire southern sky and provide an important complement to the optical studies.

For space-based imaging, two major wide-field missions are in active development: Euclid (ESA) and WFIRST (NASA). Euclid, which is scheduled for launch around 2020, is a 1.2m IR/optical telescope that will image a minimum area of 15 000 deg^2 at $|b| > 30^\circ$ during its anticipated 5-year lifetime. Limiting AB magnitudes are expected to be 24 in YJH, and 24.5 in a single, broad optical filter (RIZ). For WFIRST, two possible Design Reference Missions are being considered according to the *Final Report of the WFIRST Science Definition Team* (Green et al. 2012). Both are restricted to the 0.7–2.4 μm wavelength range, although the first calls for a primary mirror of 1.3m and the second for a primary of 1.1m. In either case, WFIRST would survey an area of $\sim$ 3500 deg^2 to a K-band depth of $\sim$26 AB mag. With a launch no sooner than 2025, the WFIRST reference missions are highly complementary to Euclid.

From the perspective of ngCFHT, these surveys will be extraordinary resources for spectroscopic study. Note, however, that in an unimaginable, worst case scenario in which none of the planned facilities will become operational, SDSS (DR9) already provides 14 555 deg^2 of multi-colour imaging that is already deeper than the nominal limits of many spectroscopic surveys. In addition, thousands of square degrees of imaging are already available from CFHT/MegaCam, Subaru/Suprime-Cam, as well as the various southern surveys. Thus, the existing imaging alone forms a strong foundation for a dedicated spectroscopic campaign, and the new surveys planned for the next decade will simply sharpen the need for complementary spectroscopy. Moreover, as Table 1 and Figure 2 show, Mauna Kea would be an excellent location from which to mount a such a spectroscopic campaign, providing full access to the northern skies and extensive coverage in the south as well.[3]

1.4.2 The Gaia Mission

In addition to the photometric surveys discussed above, a landmark *astrometric* space telescope (i.e., Gaia) will launch in the near future. This mission will produce a three-dimensional (3-D) stellar map of unprecedented precision. Between 2013 and 2018, it will conduct an all-sky survey to measure the positions of roughly *1 billion* stars — approximately 1% of the entire stellar content of the Milky Way. In fact, all astronomical objects brighter than $V \simeq 20$ mag will be catalogued, and objects brighter than $V \simeq 15$ mag will have their position measured to better than 20 *micro*-arcseconds — the approximate width of a human hair viewed at a distance of 1000 km. Objects with $V \simeq 20$ mag will have their positions measured with accuracies $\sim$10 times larger than this (with a dependence on stellar type).

Beyond its astrometric component, Gaia will also obtain multi-band photometry for all sources, and it is additionally equipped with a Radial Velocity Spectrometer (RVS) that will measure velocities for objects brighter than $V \sim 17$ mag (roughly 150 million stars) to an accuracy of 1–10 km s^{-1}. Basic astrophysical information — including interstellar reddening and atmospheric parameters — will be acquired for the brightest $\sim$ 5 million stars, and elemental abundances for the brightest $\sim$ 2 million stars.

Gaia's level of astrometric precision is entirely unprecedented, and the dataset that will ultimately emerge from this survey will certainly redefine astrometric systems and transform our understanding of the Milky Way. Still, high-quality spectral data will be available for only a tiny fraction of the overall sample, and will be limited to the brightest stars. Not only does this introduce a bias for the nearest stars, but it undersamples those components of the Milky Way that are poorly represented in the solar neighbourhood: i.e., the Galactic halo and thick disk. For these reasons, comprehensive spectroscopic follow-up for the Gaia mission is widely recognized by the international astronomical community as both urgent and essential.

The scientific exploitation of data from the Gaia mission will likely be a central element of international astronomy for the next few decades, and will certainly extend beyond the areas of stellar astrophysics, stellar populations, and Galactic structure that comprise Gaia's core science programme. Indeed, the *Report by the ESA-ESO Working Group on Galactic Populations, Chemistry and Dynamics* (Turon et al. 2008) made some prescient recommendations on the need to improve wide-field spectroscopic capabilities worldwide, with an eye towards maximizing Gaia's legacy. These recommendations include the development of dedicated, highly multiplexed, 4m- and 8m-class spectroscopic telescopes, noting that:

"Our terms of reference were to propose a set of recommendations to ESA and ESO for optimizing the

[3]Approximately half of the southern hemisphere is visible from the Mauna Kea at an airmass less than $X = 1.5$.

exploitation of their current and planned missions. However, the Galaxy is an all-sky object; in fact, from the ground, the outer parts of the Galaxy are best observed from the Northern hemisphere, as the extinction is on-average lower there. In parallel with Recommendations 2(a) to 2(d), there is a real need for dedicated highly multiplexed spectrographs in the northern hemisphere."

1.4.3 Surveys at Other Wavelengths

While the discussion to this point has focused largely on imaging and astrometric surveys in the optical and IR regions, it is important to note that the coming decade will also see a number of highly anticipated, wide-field surveys at other wavelengths — most notably at radio and X-ray wavelengths.

In the radio, a pair of eagerly anticipated 3π surveys will be conducted using the Australian Square Kilometre Array Pathfinder (ASKAP) facility between 2014 and 2017. The first of these, WALLABY (Widefield ASKAP L-band Legacy All-sky Blind surveY), is an extragalactic neutral hydrogen survey that will cover the entire sky below $\delta = +30^\circ$. This same region will also be mapped by EMU (Evolutionary Map of the Universe) — a deep (10 μJy/beam rms), radio continuum (1.4 GHz) survey. It is believed that WALLABY and EMU will detect $\sim$ 500 000 and 70 million sources, respectively. Clearly, combining these radio data with optical/IR imaging *and optical spectroscopy* would dramatically boost their overall scientific return, particularly for the EMU survey. Two-thirds of the area covered by these ASKAP surveys (i.e., about half the entire sky) would be observable by ngCFHT, whose 10m aperture would be particularly well-suited to the identification and study of the faintest sources.

At X-ray wavelengths, the eROSITA mission (extended ROentgen Survey with an Imaging Telescope Array) is expected to launch in 2014. It will perform the first all-sky imaging survey in the medium-energy X-ray range. With excellent energy resolution (138 eV at 6 keV) and spatial resolution ($\approx 25''$–$30''$), eROSITA will detect $\sim 10^5$ galaxy clusters up to redshifts of $z \sim 1.3$. The characterization of even a fraction of these clusters (to say nothing of other eROSITA sources) will also require a large-aperture, wide-field spectroscopic facility (see §2.9).

Finally, a number of telescopes that will operate at other wavelengths, including the ultraviolet (Astrosat/UVIT) and submm (CCAT) regions, are also developing plans for large-area surveys in the coming years, and these too would benefit from a 10m-class facility that could efficiently collect optical/IR spectra for sources distributed over wide fields.

1.5 Wide-Field Spectroscopy: An International Priority for the Coming Decade

Prompted by the need for wide-field spectroscopy, several new instruments and/or programmes have been developed that make use of existing existing telescope resources (see Table 2 for a summary of existing, planned or proposed facilities). Notable projects that are either underway or will begin operations in the immediate future are the ESO-Gaia survey and the AAT/HERMES project, both of which focus on high-resolution ($\mathcal{R} > 20\,000$) spectroscopy and are thus squarely focused on Gaia science. In addition, a lower resolution stellar survey is now underway at the recently commissioned Large Sky Area Multi-Object Fiber Spectroscopic Telescope (LAMOST, also known as the Guo Shou Jing Telescope).

Some 300 co-investigators are involved in the ESO-Gaia survey (Gilmore et al. 2012), which is a dedicated effort to use the VLT's high-resolution, multiplexed spectrographs to observe $\sim 10^5$ stars with FLAMES/GIRAFFE ($V \lesssim 20$) and $\sim 10^4$ stars with FLAMES/UVES ($V \lesssim 15$). This project saw first light in December 2011 and has been allocated 300 nights over a 5-year period. Meanwhile, Australia is finishing work on the HERMES instrument, which will use the $\sim$400-fibre, 2dF positioner on the 3.9m Anglo-Australian Telescope. Currently undergoing commissioning, it will operate at a resolution of $\mathcal{R} = 28\,000$ and undertake the "Galactic Archaeology with HERMES" (GALAH) survey. GALAH aims to observe $\sim 10^6$ stars brighter than $V \sim 14$ mag, measuring for each a radial velocity as well as chemical abundances for ≥ 15 elements. Finally, LAMOST (Cui et al. 2012) — a recently commissioned 4m telescope with a dedicated, 4000-fibre spectrograph and a 5°-diameter field of view — is carrying out an low-resolution "bright star" ($r < 18$) survey that will provide be a powerful complement to the Gaia mission.

Of course, the science drivers for wide-field spectroscopy extend well beyond the Gaia mission. While the "Astro 2010 Decadal Review" (Blandford et al. 2010) made no specific recommendations on highly multiplexed spectroscopy, it did note that:

"The properties of dark energy would be inferred from the measurement of both its effects on the expansion rate and its effects on the growth of structure (the pattern of galaxies and galaxy clusters in the universe). In doing so it should be possible to measure deviations from a cosmological constant larger than about

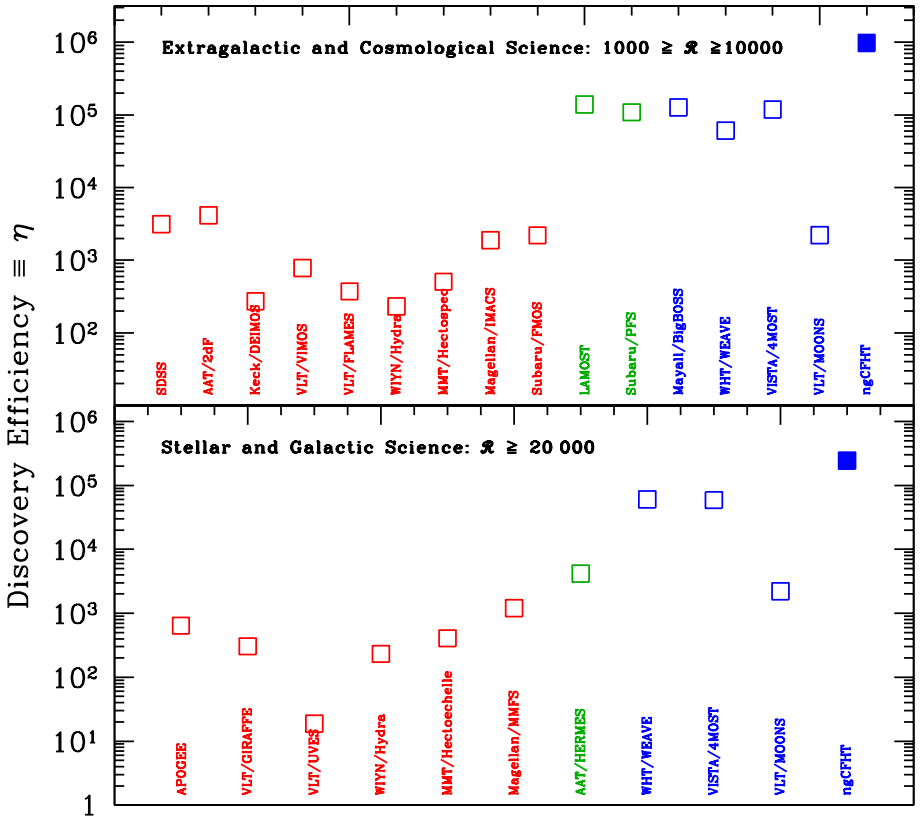

Figure 3: Comparison of the "discovery efficiency" parameter, η, for existing (red), planned (green) and proposed (blue) multi-object spectroscopic facilities (see also Table 2). The upper panel shows facilities that operate at low to intermediate spectral resolutions ($1\,000 \lesssim \mathcal{R} \lesssim 10\,000$), and which are consequently optimized for extragalactic astrophysics and cosmology. The lower panel shows those facilities that operate at a spectral resolution of $\mathcal{R} = 20\,000$ or higher, and which are thus optimized for stellar and Galactic research. No existing, planned or proposed facility would rival ngCFHT in its capacity to perform wide-field spectroscopic mapping of the faint universe.

a percent. Massively multiplexed spectrographs in intermediate-class and large- aperture ground-based telescopes would also play an important role."

Such considerations prompted the development of the Prime Focus Spectrograph (PFS; Vives et al. 2012; Sugai et al. 2012) for the 8.2m Subaru telescope. PFS recently passed its Conceptual Design Review and is now under construction with first light expected around 2017. Upon completion, it will be the world's most powerful multi-object spectrograph, and plans are underway for a Subaru Strategic Program to use this instrument for $\sim$ 300 nights distributed over a 5-year period. Note that the PFS instrument emerged following the cancellation of the Wide Field Multi-Object Spectrograph (WFMOS) and, in some ways, represents a spectroscopic complement to Subaru's Hyper-SuprimeCam instrument. Demand for this unique pair of instruments is expected to be extremely high.

Finally, several other notable spectrographs are in the proposal or evaluation stage. These include: (1) BigBOSS, which would be deployed on the 4m Mayall telescope (Schlegel et al. 2009); (2) WEAVE, which would be installed on the 4.2m William Herschel Telescope (Balcells et al. 2010); (3) MOONS, a "GIRAFFE-like", near-IR spectrograph that would be installed on one the 8.2m VLT telescopes (Cirasuolo et al. (2012); and (4) 4MOST, an optical spectrograph for the 4.1m VISTA telescope (de Jong et al. 2012). At present, none of these instruments has been approved, although ESO is expected to select one of MOONS or 4MOST for future development in the spring of 2013.

How would ngCFHT compare to existing, planned and proposed facilities? Although it is difficult to capture the performance of an instrument/facility in a single metric, we define a parameter, η, that loosely represents the "discovery efficiency" of a given facility:

$$\eta \equiv D_{\rm M1}^2 \Omega N_{\rm mos} f/IQ^2.$$

Table 2: Existing, Planned and Proposed Multi-Object Spectroscopic Facilities

Telescope/Instrument	$D_{\rm M1}$ (m)	Status	Available	λ (μm)	Ω (deg^2)	$A\Omega$ (m^2 deg^2)	$N_{\rm mos}$	$\mathcal{R}$	f	IQ	$\log \eta$
Ground-Based											
AAT/AAOmega	3.9	Existing	1996	0.37–1.00	3.14	37.5	392	1000–17000	0.5	1.5	3.5
SDSS	2.5	Existing	2000	0.38–0.92	1.54	7.6	640	1800	1.0	1.4	3.6
Keck/DEIMOS	10.0	Existing	2002	0.41–1.10	0.023	1.8	150	2500–5500	0.4	0.7	2.1
VLT/VIMOS	8.2	Existing	2002	0.37–1.00	0.062	3.3	600	180–2500	0.2	0.8	2.9
VLT/FLAMES	8.2	Existing	2003	0.37–0.95	0.136	7.2	8–130	5600–25000	0.2	0.8	1.3–2.6
MMT/Hectospec	6.5	Existing	2004	0.36–0.92	0.79	26.1	240–300	1000-40000	0.2	1.0	2.6–2.7
WIYN/Hydra	3.5	Existing	2005	0.37–1.00	0.79	7.5	90	800–40000	0.2	0.8	2.4
Magellan/IMACS	6.5	Existing	2008	0.36–1.00	0.16	5.3	400	1100–16000	0.2	0.6	3.3
SDSS/APOGEE	2.5	Existing	2011	1.51–1.70	1.54	7.6	300	27000–31000	0.5	1.4	2.8
Subaru/FMOS	8.2	Existing	2012	0.8–1.8	0.20	10.4	400	600-2200	0.2	0.7	3.3
LAMOST†	4.0	Existing	2012	0.37-0.90	19.6	247	4000	1000–10000	1.0	3.0	5.1
AAT/HERMES	3.9	Planned	2013	4 windows	3.14	37.5	392	28000	0.5	1.5	3.6
Subaru/PFS	8.2	Planned	2017	0.38–1.30	1.1	70	2400	1900-4500	0.3	0.7	5.0
WHT/WEAVE	4.2	Proposed	2018	0.37–1.00	3.14	41	$\sim$1000	5000–20000	0.7	0.8	4.8
Mayall/BigBOSS	4.0	Proposed	2018	0.36–1.05	7.1	89	5000	3000–4800	0.5	1.5	5.1
VLT/MOONS	8.2	Proposed	2018	0.8–1.8	0.14	7.3	1000	4000-20000	0.3	0.8	3.3
VLT/4MOST	4.1	Proposed	2019	4 windows	3.0	40	1500	3000-20000	1.0	0.8	5.1
ngCFHT	10.0	Proposed	2021	0.37–1.30	1.5	118	3200	2000	1.0	0.7	6.0
				0.37–1.00			3200,800	6500,20000	1.0	0.7	5.4
Space-Based											
Gaia	2$\times$(1.4$\times$0.5)	Planned	2013	0.85–0.87	all sky survey (V $<$ 17)		....	11500	....	....	....
Euclid	1.2	Planned	2020	1.10–2.00	0.55	0.62	....	250	....	....	....
WFIRST	1.5	Proposed	2025:	1.10–2.00	0.5	0.89	....	75–320	....	....	....

† – *Also known as the Guo Shou Jing Telescope (GSJT).*

Here $D_{\rm M1}$ is the diameter of the primary mirror, Ω is the instantaneous field of view, $N_{\rm mos}$ is the number of simultaneous spectra, f is the fractional time available for scheduling, and IQ is the typical image quality (FWHM) delivered by the site and facility. Figure 3 compares this parameter for a number of facilities. Note that the facilities have been divided into "low/intermediate" ($1000 \lesssim \mathcal{R} \lesssim 10\,000$) and "high" ($\mathcal{R} \gtrsim 20\,000$) resolution categories. Broadly speaking, this division corresponds to most of the "extragalactic/cosmology" and "stellar/Galactic" science cases considered in §1.6.2. As Figure 3 shows, ngCFHT would, for both high and low resolution science, outperform all other facilities by a wide margin. Compared to planned or proposed facilities (shown in green and blue, respectively), this higher efficiency is the result of several factors, including large aperture, range of spectral resolution, excellent site quality, and dedicated scheduling for surveys. This last factor is particularly relevant in the case of PFS, whose performance is comparable to that of ngCFHT for low/intermediate resolution science, but would likely be limited to only $\sim$60 nights per year on a general use telescope (see Ellis et al. 2012).

1.6 Overview of the ngCFHT Concept

1.6.1 Basic Design and Performance Specifications

An accompanying document[4] examines the technical issues relating to the ngCFHT feasibility study, with performance specifications established by the science requirements discussed in this report (see §1.6.2). The reader is referred to this companion report for full details on the technical elements of the study, including telescope and pier load capacities, telescope and enclosure configurations, telescope and feed optics, spectrograph conceptual designs, aerothermal performance, and preliminary schedules and cost estimates. As a reference for the discussion of science drivers that follows in §2, Table 3 summarizes the basic performance specifications and characteristics for ngCFHT.

1.6.2 Technical Requirements for Science

Figure 1.6.2 summarizes the top-level science requirements derived from the scientific studies discussed in §2. These requirements have been split by science topic, and further divided into the key questions relating to each area. While

[4]Feasibility Study Report for the Next Generation CFHT. II. Technical

Table 3: Next Generation CFHT Specifications and Characteristics.

Parameter	Specification
Primary Mirror (M1) Diameter	10m (segmented, equivalent)
M1 Segments	1.45m (hexagonal, corner-to-corner)
Overall f-ratio	f/2.1
Instantaneous Field of View	1.5 deg^2 (hexagonal)
Telescope Image Quality$^{\diamond}$	EE80 diameter $< 0\farcs45$ (FWHM $\sim 0\farcs3$)
Site Image Quality	FWHM = $0\farcs40 \pm 0\farcs05$ (free atmosphere median)
Vignetting	0% on axis, 13% max at edge of field
Total System Throughput†	$>$ 25% over 90% of the wavelength range
Plate Scale	102 arcsec/mm
Observing Modes	low resolution (LR)
	medium resolution, high multiplexing (MR-HM)
	medium resolution, full coverage (MR-FC)
	high resolution (HR)
Wavelength Range	370 – 1300 nm (LR)
	370 – 1000 nm (MR-HM)$^{\otimes}$
	370 – 1000 nm (MR-FC)
	370 – 1000 nm (HR)
Multiplexing	N = 3200, with full coverage from 370 – 1300 nm (LR)
	N = 800, with full coverage from 370 – 1000 nm (MR-FC)$^{\otimes}$
	N = 3200, with two (selectable) windows ($\lambda/7$) in the visible (MR-HM)
	N = 800, with two (selectable) windows ($\lambda/7$) in the visible (HR)
Resolving Power	2 000 (low)
	6 500 (medium)
	20 000 (high)
Fibre Configuration Timescale	$\leq$ 40s
Time Dedicated to Survey Observations	$\geq$ 80%
Available Zenith Angles	0° – 60°
Location	$19\fdg8250$ N, $155\fdg4683$ W
Median Precipitable Water	0.9 mm
Useable Nights	80% spectroscopic, 55% photometric

$\diamond$ – *Telescope optical quality without atmospheric or dome/mirror seeing, as seen at fibre entrance. Specification but includes nominal image quality, residual atmospheric dispersion, manufacturing, alignment and control errors. This value should be convolved with the observed seeing profile to give the total object PSF.*

† – *Includes telescope optics, wide field corrector optics, ADC optics, geometrical vignetting, fibre train, spectrograph optics, and detectors. No entrance losses (which are strongly seeing dependent) or atmospheric extinction (which are zenith dependent) are taken into account.*

$\otimes$ – *Spectra at reduced resolution ($\mathcal{R} \simeq 2\,000$) also available in the near-IR (1000 – 1300 nm) region.*

this list is far from complete, it nevertheless provides a representative sample of the requirements needed to make significant progress in each science area. Numbers highlighted by red fonts inside blue boxes represent the *driving* science requirements for ngCFHT; taken together, these requirements set the key specifications on the overall performance of the facility.

Although the science programmes considered in Figure 1.6.2 have different requirements for spectral resolution, field size, limiting magnitude, etc, a few general points are readily apparent:

- A large survey area is essential for nearly every programme. In some cases, this reflects the rarity of the targets themselves (e.g., solar twins, extremely metal-poor stars, ultra compact dwarf galaxies). For the most part, though, it reflects a need to obtain statistically robust samples. Clearly, this important consideration impacts both the field of view of the telescope and its "survey efficiency" — how quickly can the facility acquire and observe an individual field, reach the requisite S/N ratio, and move on to the next set of observations.

- In nearly every case (and nearly irrespective of the requested spectral resolution), the targets are faint, reflecting the need for a large (i.e., 10m-class) aperture and high system throughput. Although some planned and proposed facilities are competitive with ngCFHT for wide-field spectroscopy of *bright* targets (e.g., LAMOST, HERMES, 4MOST), only PFS has a comparable performance for faint-object spectroscopy (but not at high spectral resolution, and subject to limits on the number of nights available for scheduling).

- The majority of the driving science requirements are set jointly by science cases in the general areas of Galactic Archaeology, and Galaxy Evolution and Cosmology. Generally speaking, the former topics require high spectral resolution and sensitivity at blue wavelengths, while the latter requires lower spectral resolutions and red/IR wavelengths. No other planned or proposed facility meets the joint requirements on high spectral resolution and large collecting area that is essential for most Galactic Archaeology science cases.

From an examination of the requirements matrix in Figure 1.6.2, the essential scientific capabilities of ngCFHT can be summarized as follows:

For maximum scientific impact, the facility must be able to obtain efficiently very large numbers (>10^6) of low- ($R \simeq 2\,000$), moderate- ($R \simeq 6\,500$) and high-resolution ($R \simeq 20\,000$) spectra for faint ($20 \lesssim g \lesssim 24$) science targets over large areas of the sky ($10^3 - 10^4$ deg^2) and spanning blue/optical to near-IR wavelengths ($0.37 - 1.3\mu$m). At the highest resolutions, it should have a velocity accuracy of $\lesssim$ 1 km s^{-1}, and at low resolution, complete wavelength coverage should be possible in a single observation.

1.6.3 Survey Implementation, Programme Scheduling and Operations Model

There are presently 14 optical/IR telescope worldwide with primary mirrors in the range $8.1\text{m} \leq D_{\rm M1} \leq 10.4\text{m}$. Together, these facilities offer a large selection of instruments that are capable of imaging, spectroscopy, polarimetry, interferometry, and coronography. However, with the notable exception of the planned PFS instrument for Subaru, wide-field, highly-multiplexed spectroscopy is a critical capability that is not provided by any of these facilities. In part, this reflects the cost and complexity of such an instrument (the implementation of which can even involve modifications to the basic telescope architecture). However, another factor is also at play: all existing 8–10m telescopes are *general use* facilities, with time divided among a variety of instruments according to community demand.

By the end of this decade, an important exception will be LSST, a 6.7m (effective aperture) survey telescope that is seen as the heir apparent to SDSS (although it of course lacks SDSS' spectroscopic component). Like LSST, ngCFHT would have a science-driven mandate to focus heavily, if not exclusively, on dedicated surveys. This operational strategy, which is unique among existing 8–10m telescopes, would give ngCFHT a distinct advantage compared with these facilities, as it enables an array of scientific analyses that would otherwise be difficult or impossible to schedule.

Examples of such surveys are given in Section 2. They are discussed throughout the remainder of this document, and we will just highlight a few here. A *Galactic Archaeology Survey* would utilize a large fraction of the available bright/grey time over a decade ($\approx$ 1450 nights) to collect moderate- and high-resolution spectroscopy for millions of stars distributed over a quarter of the volume of the Milky Way (i.e., two fibre configurations in each of $\sim$ 7000 fields). A *Galaxy Evolution Survey* would use $\approx$ 1100 nights of dark time to examine the evolution of galaxies using a "wedding cake" survey strategy (i.e., wide, medium and deep surveys). A *BAO/Cosmology Survey*, possibly implemented in coordination with the previous survey, would explore the expansion acceleration of the universe with BAO, and measure redshift space distortions and the shape of the power spectrum using a $\sim$10 000 deg^2 redshift survey

Parameter	ISM	Stellar Astrophysics		Milky Way / Galactic Archaeology			Local Group		Nearby galaxies	
	3D mapping	*Time domain*	*Rare objects*	*Chemodynamics of the stellar halo*	*Disk evolution*	*Bulge science*	*Global chemodynamics of M31/M33*	*Structure of dwarf galaxies*	*Structure of DM halos*	*Rich clusters*
Spectral resolutions	≥ **20000**	≥ 20000	~ 20000	**6000**, **20000**	6000, **20000**	≥ **20000**	**6000**	6000	2000	2000
Magnitude limit (AB) §	g=16	g=16	g=19.5	g=**21.5, 19.5**	g=21.5, 19.5	g=18	g=**23**	g=**23**	i=22	r=22
Wavelength range (μm)	0.38 - 0.88	0.37 - 0.95	0.37 - 0.89	**0.37** - 0.90	**0.37** - 0.90	**0.37** - 0.90	0.4 - 0.95	0.4 - 0.95	0.37 - 1.3	0.37 - 1.3
(complete wavelength coverage required?)										
Target density (# / sq. degree)	~500	1300	rare *	~500 ♮	> 10^4	>1000	~ 1000s	~ 1000s	1400	~10^4
Survey area (sq. degrees)	5000 - 10000	~ 100	10000	**10000**	10000	~ 200	350	1 <--> 10	1000	30
# science objects	> 10^6	> 10^5	n x 10^6 *	**n x 10^6**	n x 10^6	> 10^5	n x 10^5	n x 10^3	5 x 10^5	20 cluster fields
Velocity accuracy (km/s)	n/a	*0.15 (goal)*	< 2	**< 2**	**< 2**	**< 2**	< 5	< 5	15 - 30	15 - 30
Survey synergies	Gaia, multi-wavelength surveys	Kepler, Gaia, AAT/HERMES, SDSS, PS1 ...		Gaia, SDSS, PS1, AAT/HERMES, LSST...large number of current and upcoming photometric+spectroscopic surveys			Dedicated pre-imaging surveys (e.g. CFHT MegaCam, Subaru HSC...)		eRosita, PS1, ASKAP, GAMA, GALEX, LSST, Euclid...	
Other notes	Early-type stars preferred	Time resolved spectroscopy of Kepler fields (115 sq. degrees)		RV accuracy to match that of Gaia transverse velocities at the faint end. Extension to NIR and higher resolution desirable for bulge science			Foreground contamination likely high in outer regions of galaxies (identify using gravity sensitive features)		Study of nearest galaxies (e.g., Virgo cluster) could additionally use R ~ 6000	

Parameter	Galaxy Evolution			IGM		QSOs / AGN		Cosmology	
	Environment	*Clustering/halo models*	*Epoch of formation*	*Lyman alpha forest*	*DLAs*	*Clustering*	*Reverberation mapping*	*BAO/RSD*	*Cosmological clusters*
Spectral resolutions	**2000**	**2000**	**2000**	2000 - 20000	2000 - 20000	2000	≤ 2000	**2000**	**2000**
Magnitude limit (AB) §	i=**23.5**	i=**24.25**	i=**26**	B ~ 20	i ~ 19.5	i=23.5	g=22.95	g=**23.7**	i=23.5
Wavelength range (μm)	0.37 - **1.3**	0.37 - **1.3**	0.37 - **1.3**	0.37 - 1.3	0.37 - 1.3	0.37 - 1.3	0.37 - 1.3	0.37 - 1.3	0.37 - 1.3
(complete wavelength coverage required?)	yes	yes	yes	desirable	desirable	desirable	desirable	yes	yes
Target density (# / sq. degree)	**~3 x 10^4**	**~8 x 10^4**	**> 10^5**	1 - 10s	few	~200	~ 350	tracer dependant	>10^4
Survey area (sq. degrees)	**4300**	100	1.5	1000 - 10000	1000 - 10000	**4300**	1.5	10000	~750
# science objects	**~ 7 x 10^6**	~ 2 x 10^6	~ 30000	~ 1000	~1000s	~ 5 x 10^5	~ 500	n x 10^6	~ 500 clusters
Velocity accuracy (km/s)	resolution limited	resolution limited	resolution limited	n/a	n/a	resolution limited	resolution limited	resolution limited	resolution limited
Survey synergies	SDSS, LSST, PS1, DES, Euclid, DEEP2, zCOSMOS,...			SDSS, VLT UVES, Keck HIRES, ...		SDSS, CFHTLS, Plank, Herschel, SKA pathfinders, Chandra, eRosita, Gaia, ...		eRosita, PS1, Euclid, LSST, ASKAP, Planck...	
Other notes	Study galaxies over seven different epochs between 0.5 < z < 1.5 each with the same statistical power as SDSS			High resolution for chemical abundance analysis; see also Cosmology/BAO		Deep field same as for Galaxy Evolution study? High resolution also useful (absorbers, AGN feedback)		BAO calculations can be made for multiple source populations (LRGs, ELGs, Lyα forest, QSOs...)	

§ magnitude limits that drive facility requirements (bold, red font) correspond to SNR = 5 - 10 (point source detection limit)

* rare objects (e.g., white dwarfs) will be a small fraction of the number of stars targetted in a single field (e.g., expect ~8 white dwarfs per NFCFHT field of view)

♮ measured at the North Galactic Cap for g ≤ 21

Figure 4: Top-level requirements matrix for ngCFHT based on a subset of the science programmes from §2. See §1.6.2 for details.

carried out over $\approx$ 600 nights. Clearly, ngCFHT's operations model would enable programmes of a scope that would be unthinkable on a general use telescope.

At the same time, ngCFHT should exploit its unique operations model to accomodate not just large, "legacy-style" surveys, but also a limited number of smaller, PI-style programmes. The above surveys are prime examples of the former type of programme, which we provisionally assume would be allocated $\sim 80\%$ of the telescope time. The remaining $\sim$ 20% of time would then be available for smaller, strategic programmes. Of course, frequent calls for proposals (of both types) should be solicited from the member communities, for review by an international time allocation committee.

The scientific relevance, productivity and effectiveness of ngCFHT surveys should be continually reviewed, particularly for programmes operating on multi-year timescales. For instance, a Science Advisory Board with rotating membership from the ngCFHT community, could conduct annual reviews of long-term programmes, to ensure the programmes are making demonstrable progress and effectively disseminating data (and data products) within the user communities. Furthermore, the fraction of time available for allocation to strategic programmes should be frequently examined in order to respond effectively to community needs and the latest scientific developments. While long-term surveys that capitalize upon the capabilities of ngCFHT (or any wide field spectroscopic facility) are an essential component of operations, the discovery space of ngCFHT would be entirely unique. It is therefore essential that a science-driven operations model is developed that recognizes and takes advantage of these opportunities.

1.6.4 Data Products, Calibrations and Reduction Pipelines

As one of the most highly multiplexed spectrographs ever constructed, ngCFHT would obtain of order 3200 spectra per hour. This equates to $\gtrsim 20\,000$ spectra per 7.5-hr night, or around 7 million spectra per year. While this is a large number of spectra, the overall data-rate for ngCFHT would be relatively small by the standards of current and future surveys. As a baseline, the tri-resolution spectrograph design described in the accompanying technical feasibility report uses a total of sixteen 9k$\times$9k CCDs ($\sim$ 160 MB per frame) and eight 4k$\times$4k FPAs ($\sim$ 32 MB per frame) to accommodate all the spectra over the required wavelength ranges. This corresponds to around 3 GB per exposure.[5] As a rough estimate of the data rate, if we assume 15-min (sub)exposures, there will be of order 30 science exposures per night. Allowing for calibration frames, this equates to an anticipated raw data rate for ngCFHT of order 100 – 200 GB per night. To put this in the context of future surveys, the anticipated raw data-rate from LSST is $\sim$15 TB per night.[6]

Given the demands imposed by the large number of science targets, and by the anticipated scope of the Legacy Surveys, an automated and efficient pipeline is needed to facilitate data reduction and calibration, and to produce science-ready spectra. This pipeline must include (but will not necessarily be limited to) the following elements:

- Correction of 2-D spectra for bias and flat-fielding (including fringe removal if necessary);
- Optimal extraction of 2-D spectra;
- Measurement and subtraction of scattered light;
- Wavelength calibration, and subtraction of sky;
- Coaddition of science spectra (including optimized cosmic ray rejection);
- Flux calibration;
- Computation of error matrices.

Both the raw data and the fully reduced, extracted and calibrated spectra would be made available in a data archive for general distribution. The precise location and structure of the archive will need to be determined during subsequent design phases. Note that CFHT and its partners have considerable experience in the archiving and distribution of survey datasets, and the overall functionality requirements for the ngCFHT pipeline are similar to those for pipelines that have already been implemented successfully (e.g., SDSS/SEGUE). In addition to the full data processing pipeline, a "quick-look" data reduction package should be implemented to allow for data validation immediately after acquisition.

Calibration frames will need to be obtained regularly, while calibration stars (i.e., spectrophotometric, radial velocity and/or spectral standards) must be targeted for observation in an automated but robust manner. In particular:

[5] For comparison, MegaCam, the current wide-field imager on CFHT, produces $\sim$ 0.7 GB per exposure.

[6] §2.6.3 of "LSST: from Science Drivers to Reference Design and Anticipated Data Products", v2.0.9, www.lsst.org/files/docs/overviewV2.0.pdf

- Flat fields, bias frames and arcs for wavelength calibration should be obtained at the start and end of every night. More regular observations of arcs may be needed when particularly accurate wavelength calibration is required (e.g., bracketing a science observation).

- Sky subtraction in survey mode will be achieved by allocating a significant number of fibres (typically 5–10%) to sky locations during the main science observations. These fibres — which may be evenly distributed across the focal plane or have different distributions depending on the programme — would monitor the sky simultaneously with the science observation. Many innovative techniques have now been developed for sky subtraction with multi-object fibre spectrographs using this general strategy, notably with FLAMES-GIRAFFE and FLAMES-UVES (e.g., Battaglia et al. 2008; see also Bolton & Schlegel 2010). These allow the creation of a "master-sky" spectrum that can be scaled and subtracted from each object spectrum, with the line and continuum components treated separately. Alternate methods, such as "beam-switching" and "cross beam-switching", may also be implemented, depending on the science requirements of the specific programme.

- In addition to sky subtraction, some fibres will be allocated to calibration stars. The most common of these will be spectrophotometric standards for flux calibration and correction of telluric absorption where necessary. During future design stages, science requirements on the spectrophotometric performance will be developed. This will set technical requirements such as the fibre-to-fibre transmission of ngCFHT (which can be calculated and monitored from the large library of flat fields that will be created) to ensure that flux measurements observed using one fibre can be related accurately to other fibres. The space density and luminosity function of all possible calibration stars will also be explored and alternative strategies investigated (i.e., normalization of spectra using broadband photometry).

The automated analysis of astronomical spectra (at both low and high resolution) for large stellar and extragalactic surveys has developed significantly over the last few years. This rapid progress was driven, in large part, by a number of recent and upcoming spectroscopic surveys including, e.g., SDSS/SEGUE, AAT/HERMES, the ESO/GAIA survey, and Subaru/SuMIRe. At a minimum, the automated analysis of ngCFHT data will include star/galaxy classification and redshift determination. The level of additional analysis — e.g., the automated measurement of $T_{\rm eff}$, $\log g$, [Fe/H], [α/Fe] and individual elemental abundances for stellar spectra — must be defined during the next phase of study. Clearly, such pipelines will need to be constructed for the main scientific analysis of many of the envisioned programmes. This type of analysis may be better performed by the survey and science teams rather than by the observatory, although it is likely that, at a minimum, some form of "zero order" science parameters will be provided automatically to better facilitate the scientific exploitation of the data.

1.7 A Strategic Vision for Mauna Kea

Mauna Kea Observatories (MKO) is an collection of independent astronomical research facilities atop the $\sim$4200m summit of Mauna Kea. MKO features a 2 km^2 "astronomy precinct", established in 1967, within the Mauna Kea Science Reserve. The first telescope on the mountain (the now decommissioned UH 0.6m) was installed in 1969, followed quickly by the UH 2.2m in 1970. CFHT, commissioned in 1979, was the first 4m-class facility on Mauna Kea. Today, MKO is home to a dozen optical, IR and submm telescopes that represent a collective scientific investment of more than $2 billion dollars. Mauna Kea has also been chosen as the site for the $\sim$$1 billion Thirty Meter Telescope (TMT) project, a 30m segmented-mirror telescope that is expected to begin operations in the early 2020s. Although MKO is managed by the University of Hawaii, the telescopes that comprise MKO are distinctly multi-national in flavour, representing the international astronomical community's primary centre for optical, IR and submm research in the northern hemisphere.

The centrepoint of optical, IR and submm astronomy in the southern hemisphere is the European Southern Observatory (ESO), an intergovernmental research organization that presently consists of 15 participating countries and maintains two sites in Chile — La Silla (the original ESO site) and Paranal (which is located $\sim$ 500 km north of La Silla). ESO also plans to build the 40m-class, European Extremely Large Telescope (E-ELT) on Cerro Armazones, which is located 22 km to the east of Paranal. Like TMT, E-ELT is expected to begin operations early in the coming decade. Although ESO's organizational structure would not be appropriate for Mauna Kea, it has undeniably established itself as a leader in the strategic deployment of astronomy resources, including the recent commissioning of two dedicated survey telescopes on Paranal: the 4m Visible and Infrared Survey Telescope for Astronomy (VISTA) and the 2.6m VLT Survey Telescope (VST). These facilities were developed not only to address important scientific questions in their own right, but to maximize the scientific return from ESO's VLT telescopes, and ultimately, the E-ELT.

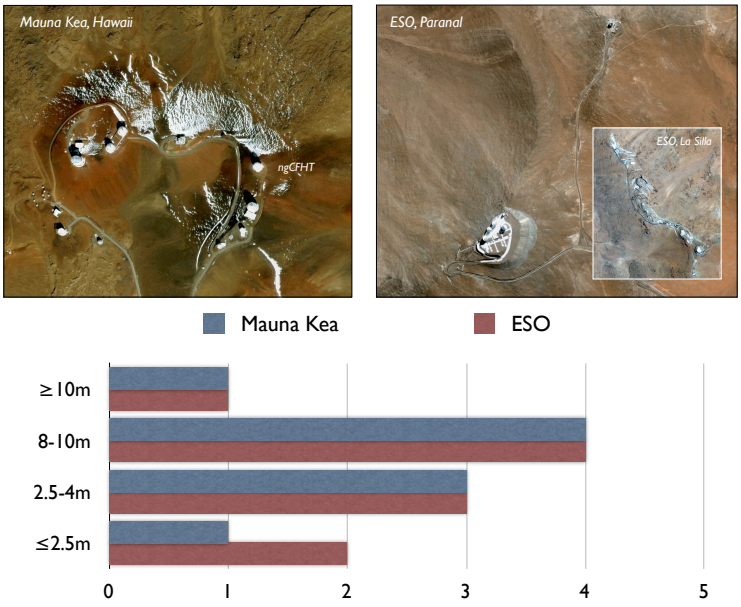

Figure 5: Comparison of optical and IR telescope resources on Mauna Kea to those of the European Southern Observatory (Paranal and La Silla combined). The comparison includes both the E-ELT (39m) and TMT (30m), which could be operational within a decade. The transformation of the 3.6m CFHT into a dedicated, wide-field, spectroscopic survey telescope would be a unique capability among 8-10m-class telescopes worldwide, and offer powerful synergies with existing or planned telescopes on the ground and in space.

In terms of current and projected resources, the suite of telescopes at MKO and ESO are quite similar in terms of their overall number and capabilities (see Figure 5). The primary distinction between the two observatories is in their operational philosophy. To date, the telescopes on Mauna Kea have tended to act autonomously in both the implementation of research programmes and the setting of priorities for future instruments and facilities (although there are limited, but highly successful, time exchange programmes between some MKO telescopes; e.g., Gemini-Subaru, Subaru-Keck, CFHT-Gemini, etc).[7] This operational model has served well for many years, but by $\sim$2020, the cost and scope of forefront astronomical facilities will have reached the point that a greater level of cooperation and coordination may become critical for minimizing expenditures, and maximizing scientific return on investments.

The international communities that are either presently represented on Mauna Kea, or will be when TMT begins operations in the next decade, include Argentina, Australia, Brazil, Canada, Chile, China, France, India, Japan, the Netherlands, the Republic of Korea, Taiwan, the United Kingdom, and the United States. This list, which encompasses all participants in the ngCFHT feasibility study, includes communities that have active collaborative agreements with one or more MKO telescopes, including CFHT. The international scope of the research being carried out on Mauna Kea is thus comparable to that at ESO.

As we will show in this document, ngCFHT would be a revolutionary research facility that represents an urgently needed, but as yet missing, capability in international astronomy. It would serve a broad and diverse base of users while maximizing the scientific return from existing facilities on Mauna Kea (and across the world), including some of the most ambitious projects planned for the coming decade (i.e., Pan-STARRS, LSST, Euclid, Gaia, eROSITA, etc). It would also serve as the ultimate spectroscopic survey instrument with which to feed the forthcoming ELTs, including TMT (the future "crown jewel" of MKO astronomy). In short, ngCFHT would be a timely, strategic, and scientifically exciting step towards a more coordinated and cooperative vision for international astronomy on Mauna Kea, which is to the benefit of all MKO stakeholders.

[7]On 19 October 2012, the timesharing agreement between Subaru and Gemini was expanded such that the amount of time exchanged each semester would be set by *scientific demand*. As noted in Nature, this "points to a closer collaboration among large telescopes" (E. Hand, November 2, 2012 issue).

2 Science Cases

2.1 The Interstellar Medium

2.1.1 Abstract

The Next Generation CFHT — with its wide field of view, highly-multiplexed spectrograph, and 10m aperture — would be a unique and powerful tool for studying the interstellar medium (ISM) of the Milky Way. Whereas only primitive maps of the ISM exist at present, ngCFHT could be used in different observing modes to address definitively some of the foremost problems in ISM research. For instance, a dedicated bright-time survey — when combined with data from a large Galactic Archaeology Survey — would yield the first detailed, three-dimensional maps of ISM density and kinematics. A second, related, project could target individual objects/clouds that are presently interacting with the ISM to probe the detailed physics of ISM interactions. In either case, the power of ngCFHT would lie in the combination of high spectral resolution, wide field of view and extreme multiplexing. In the case of large-scale ISM mapping, ngCFHT's high observing efficiency would reduce survey durations to manageable levels, putting it far beyond the reach of any existing or planned facility/instrument. For detailed study of individual structures, ngCFHT's wide field and dense fibre coverage would be well matched to many Galactic features, such as stellar streams, astrospheres, and individual interstellar clouds — targets that would otherwise be accessible (in a limited capacity) in the radio region alone.

2.1.2 Introduction

Multi-wavelength observations of the Galactic ISM have never been so detailed nor so abundant as now. Yet, paradoxically, our understanding of its origin and evolution remain surprisingly limited — primarily because we lack the accurate distances that are needed to map out its three-dimensional (3-D) structure. High-quality emission maps of the ISM have been produced (or are currently underway) thanks to a wide range of ground- or space-based facilities that operate at almost all wavelengths, including the γ–ray (FERMI), X–ray (ROSAT, Chandra, XMM, Suzaku), UV (GALEX), IR (ISO, Spitzer), sub-mm (Herschel, Planck) and radio (DRAO, LOFAR) regions. Such data usually come in the form of two-dimensional images in specific spectral bands, or in data cubes (i.e., two spatial dimensions plus a spectral, or polarimetric, dimension). Unfortunately, there is almost no information available on the distances of the features that are responsible for the observed ISM emission. As a result, we lack the realistic 3-D density and velocity distributions for the Galactic ISM that are needed to identify the sources of those emissions and to construct quantitative, physically-motivated models.

This situation is regrettable since a number of prominent astrophysical facilities and/or surveys require an increasingly detailed understanding of the Galactic ISM. For instance, interpreting observations of the cosmic microwave background (CMB) and its polarization is strongly dependent on optimal modeling of Galactic dust emission and its spectral characteristics; these in turn depend on the spatial distribution and temperature of the dust, and on the intensity of the interstellar radiation field that heats it. To produce realistic models of this radiation field, it is therefore necessary to compute the propagation of photons through the 3-D dust and gas distributions. Similarly, the analysis and modeling of diffuse γ–ray emission (which is generated by the interaction of cosmic rays with ISM nuclei and by up-scattering of the interstellar radiation field by cosmic electrons) doubly requires a 3-D knowledge of the ISM distribution — on the one hand because it is needed to compute the cosmic ray trajectories accurately, and on the other hand, because the radiation field itself is governed by this distribution. Finally, obscuration by dust poses a significant obstacle to our understanding of stellar populations within the Milky Way. Extinction and reddening are not always estimable to the level of precision that is needed to characterize the properties of distant stars. Most notably, the upcoming Gaia mission would benefit immeasurably from detailed Galactic extinction maps (see below and §2.2 and §2.3).

Independent of the above objectives, the number and variety of potential applications for 3-D ISM maps are vast: i.e., the identification of foreground or background contaminants in absorption/emission studies of specific objects, stellar-ISM interactions (including the heliosphere), and environmental studies of Galactic objects in general. Clearly, high-quality, 3-D maps covering a significant fraction of the sky would be a powerful resource with widespread applications in many subfields of modern astrophysics (see, e.g., Lallement et al. 2003; Marshallet al. 2006; Welsh et al. 2010).

2.1.3 ngCFHT in Context: Competition and Synergies

As we explain below, the key synergy for ngCFHT in the study of the Galactic ISM is with Gaia — an ESA "cornerstone" mission that is scheduled to launch in 2013 (see §2.1.4.1). 3-D mapping of the ISM based on spectroscopy Gaia target stars is most efficacious when the number of sightlines is maximized. This in turn depends on the number of fibres, the field and survey size, and the telescope/instrument efficiency (i.e., system throughput). Since high spectral resolution ($\mathcal{R} = 20,000$ to $30,000$) is a pre-requisite for ISM studies, the competition in the immediate future would come primarily from AAT/HERMES, although ngCFHT would be much more efficient thanks to its greater wavelength coverage (a factor of $\sim$1.5$\times$), multiplexing ($8\times$) and throughput ($6.5\times$). The Gaia/RVS, PFS and BigBOSS have spectral resolutions that are too low by factors of $\sim$ 2–5$\times$ while the proposed MOONS instrument for VLT focuses on the 0.8–1.8μm spectral region, thereby missing most of the traditional ISM diagnostics (see §2.1.4.1). Among proposed facilities, 4MOST comes closest to rivaling ngCFHT in ISM mapping speed; reaching the requisite S/N for individual stars will be $\sim 5\times$ slower for 4MOST based on the difference in telescope collecting area, although is roughly compensated by its larger field of view (i.e., 5 deg^2 when deployed on VISTA). Of course, there is also a powerful synergy with 4MOST since it and ngCFHT would be located in different hemispheres — an important consideration when mapping the large-scale structure of the ISM.

2.1.4 Legacy Science

2.1.4.1 A Three-Dimensional Study of the Galactic Interstellar Medium (ISM)

Gaia and the Need for Multi-Object Spectroscopy. Any programme to map out the 3-D structure of the ISM requires, directly or directly, an immense database of distance-limited absorption data. The highest spatial resolution and also the possibility of coupling with the emission spectra (through the velocity identifications) can be achieved only through the inversion of large amounts of spectroscopic absorption data towards individual stars of known distance. Unfortunately, neither high-resolution absorption databases, nor precise stellar distances within Galaxy, are available at the present time. The situation will soon change with launch of ESA's astrometric mission, Gaia, that will measure the positions of all stars down to $\approx$ 20th magnitude, and create an extraordinarily precise three-dimensional map of more than a billion stars throughout the Milky Way. This remarkable dataset — once combined with new information on absorption lines, diffuse interstellar bands (DIBs), reddening and extinction from optical spectroscopy — has the potential to revolutionize studies of the ISM and its three-dimensional structure.

Table 4: Important ISM Diagnostic Features.

Site of Orgin	Species	Wavelength (nm)	Window	Notes
dense molecular gas	CN	387.4	ISM Survey (blue)	
dense molecular gas	CH	430	ISM Survey (blue)	
dense molecular gas	CH^+	423.3	ISM Survey (blue)	
dense molecular gas	Ca I	427.7	ISM Survey (blue)	
dense molecular gas	K I	769.9	ISM Survey (red)	
dense molecular gas	C_2	772.5, 876.0	ISM Survey (red)	
atomic lines	Na I	588.9–689.5	GA Survey (red)	
atomic lines	K I	769.9	ISM Survey (red)	
atomic lines	Ca II	393.4–396.8	ISM Survey (blue)	
ionized gas	Ti II	336.1	....	
ionized gas	Ca II	393.4–396.8	ISM Survey (blue)	
DIB	....	578	....	Strong feature. Tightly correlated with HI and with E(B-V), except in high radiation field.
DIB	....	628	GA Survey (red)	Strong feature. Moderately correlated with HI and E(B-V).
DIB	....	661	GA Survey (red)	
DIB	....	862	ISM Survey (red)	Tightly correlated with E(B-V).

However, building 3-D maps of the ISM in the post-Gaia era will require spectroscopy for a vast number of

targets, ideally distributed over a range of distances, in as many directions as possible, and at spectral resolutions and S/N levels that are high enough to enable the detection and measurement of key ISM absorption features. Clearly, this is not feasible using single-object spectrographs as the observations would be far too time consuming. It would also be impossible using small-field multi-object spectrographs, since observations need to be carried out over a significant fraction of the sky. In short, a high-resolution mapping of the three-dimensional structure gas and dust in the Milky Way will require a telescope/spectrograph combination that has both a wide-field and a high level of multiplexing.

Absorption Data for Mapping. It is worth bearing in mind that an interstellar tracer does not need to be strictly proportional to the column density of interstellar hydrogen, or to the total column of dust, to be useful in locating interstellar clouds, since distance assignments are based on the *gradients* of the absorbing columns. It is for this reason that absorption lines arising from any interstellar species, and diffuse bands of all kinds, can potentially be used in the analysis (in addition to the reddening).

We list in Table 4 the major gaseous lines and the interstellar gas phases they are tracing (see also Figure 2.1.4.1). Since the ISM is composed of several phases, tracers should ideally allow these different phases to be explored, particularly the main ones: i.e., the dense molecular, diffuse atomic, and diffuse ionized phases. The combination of three or more tracers for each phase is best. However, as mentioned above, once the main structures are located in space — thanks to the measured radial velocity structure — then independent emission line data (mainly H I, CO and Hα) can be included to refine the phase distribution. Since absorbing lines contain information on the gas dynamics, both radial velocities and columns (including volumic densities from inversion) can be used in models. Angular variations over the sky of the line centres can also be used to constrain the *transverse* motions.

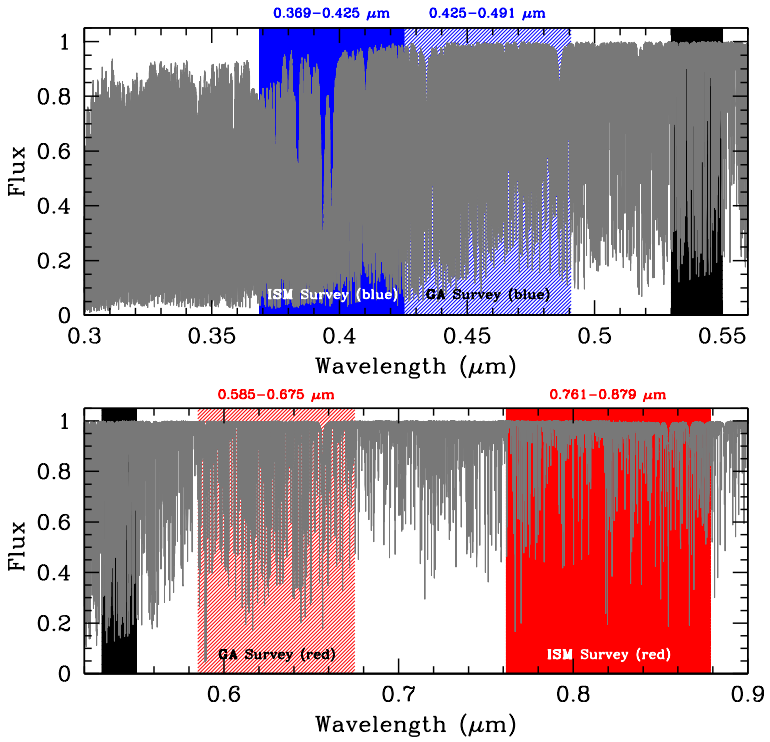

Figure 6: One possible strategy for large-scale, three-dimensional mapping of the Galactic ISM. The shaded red and blue areas show four distinct wavelength regions that could be targeted in the course of a Galactic Archaeology Survey (the lightly shaded red and blue regions) and a supplemental ISM survey (the heavily shaded regions). Taken together, these spectral bands contain more than a dozen of the key ISM diagnostics listed in Table 4. Note that the black area indicates an inaccessible region of width $\sim \pm 10$ nm centred on the central wavelength of the spectrograph dichroic at ≈ 540 nm. For reference, the grey curves show the residual solar irradiance spectrum of Kurucz (2005).

Depending on the range of column densities, some tracers may not be fully appropriate. Strong interstellar lines suffer from saturation close to the disk or towards very opaque clouds, and should thus be replaced by other, weaker, lines for large distances or columns. DIBs — whose carriers are still unknown, but are strongly suspected to be macro-

molecules in the gas phase — also trace the amount of interstellar matter along a given line of sight. While they have never been considered seriously for mapping purposes, recent work shows that they are ubiquitous, being present even in the spectra of distant cool stars (e.g., Chen et al. 2012). Some DIBs have been shown to be very tightly correlated with the colour excess, some with the atomic gas, and some with the molecular gas. Combining measurements for different DIBs is the ideal approach, though any one can be used for mapping purposes. For the most part, DIBs are broader than gaseous lines, but they contain important kinematic information as they are Doppler-shifted according to the radial velocity of their carriers. They can also be quite numerous: optical spectra have been shown to contain as many as 400 DIBs. Depending on their relationship to the extinction or the gas columns, their detection can require high S/N and/or highly extincted stars. It is therefore impossible to list all possibilities, but rather note that one may adapt the DIB choice to a particular combination of S/N, distance and extinction.

Finally, we emphasize that medium- or high-resolution stellar spectra may be used to determine both the reddening and fundamental stellar parameters. Of course, if distances are known from measurements (Gaia) or photometry, then the reddening data may also be inverted to derive three-dimensional dust maps.

Inversion Methods. The small number of 3-D maps published to date are based on inversion techniques that have been applied to absorption or extinction data. A Bayesian method adapted to individual measurements of gas columns (or extinctions) has been developed by Vergely et al. (2001) and applied to published neutral sodium columns. Lallement et al. (2003) used the same method to compute maps based on data acquired specifically for this purpose. Additional maps were produced by Welsh et al. (2010) for neutral sodium and singly ionized calcium. Figure 7 shows a cut through a 3-D interstellar density cube in the solar neighborhood, computed from an updated Na I database and Hipparcos parallaxes (Puspitarini et al. 2012). The limited number of targets imposes regularization conditions under the form of a spatial correlation, i.e. interstellar clouds have a minimum size, here of 20 pc. This map is based on just 1900 stars, and barely reaches to $\sim$ 250 pc. The same method has also been applied recently to reddening measurements, making use of all precise determinations to date (i.e., Vergely et al. 2010). The map shown in Figure 8 shows an updated analysis based on 17,000 colour excess measurements. While this map reaches 1500 pc in some directions, the extent along any given line of sight is typical is 1/2 or 1/3 this, and the spatial resolution is clearly limited.

Table 5: Technical Requirements and Survey Implementation: A Three-Dimensional Study of the Galactic ISM.

Survey Area (Ω)	Galactic Disk ($b < \mid \pm 10^\circ \mid$) : $\Omega \approx 5\,000$ deg^2.
Field Location	$l \simeq 0 - 360^\circ$ and $b < \mid \pm 10^\circ \mid$ subject to $X < 1.5$
Number of Configurations ($n_{\rm config}$)	$n_{\rm config} = 1$
Primary Imaging Resources for Target Selection	Gaia, Pan-STARRS (3π)
Observing Conditions	Lunar illumination: 75%–100%
Number of Visits and Exposure Time per Visit	$N_{\rm visit} = 2$ per configuration, $T_{\rm exp} = 1.25$ hr per visit
Wavelength Coverage	0.369–0.425μm and 0.761–0.879μm at $\mathcal{R} = 20,000$ (ISM survey)
	0.425–0.491μm and 0.585–0.675μm at $\mathcal{R} = 20,000$ (Galactic Archaeology Survey)
Limiting (point source) Magnitude per Visit	$g_{\rm AB} \simeq 16$
Total Time Needed for Program ($T_{\rm tot}$)	$T_{\rm tot}$ = 3300 $\times$ (1$\times$0.25 hr) + 20% overhead $\approx$ 990 hrs over 10 yrs
	[in addition to 3300 $\times$ (1$\times$1 hr) + 20% overhead $\approx$ 3960 hrs available from the Galactic Archaeology Survey]

Considering that Figures 7 and 8 represent the "state of the art" for three-dimensional mapping of the Galactic ISM, it is obvious that ngCFHT has the potential to completely revolutionize this field. Table 5 summarizes one possible survey that could be undertaken, perhaps as an ngCFHT "Key Project", to map out the three-dimensional distribution of gas and dust in the Milky Way. As noted in §1 and §2.3, it is expected that ngCFHT would devote a large fraction of its bright time observing to Galactic Archaeology (GA) surveys. A leading candidate for a GA survey aims to survey $\sim$1/4 of the sky and observe Galactic field stars brighter than $g \approx 20.4$ at $\mathcal{R} = 20,000$. Stellar targets would be selected primarily to belong to the halo, but would also include thin- and thick-disk stars.

Such a survey would produce a wealth of data useful for ISM studies, despite the fact that GA observations would likely be carried out in spectral windows that are chosen to maximize information content for halo stars, and not necessarily for the ISM (see Table 4). By supplementing these GS data with observations in blue and red spectral windows chosen specifically to contain the largest possible number of ISM species (see Figure 6), it would be possible to carry out an unprecedented mapping of the Galactic ISM along a million or more sightlines. This ISM survey would also be extremely efficient since high-quality spectra (i.e., S/N $\sim$ 100 and 250 per Å near 400 and 800 nm) could be obtained in just 15 min exposures for $g = 16$ stars of spectral types O, B and A. For reference, a survey of 4950 deg^2 covering a swath of 20 deg centreed on the Galactic plane would require $\sim$ 1000 hrs of ngCFHT time, or about two

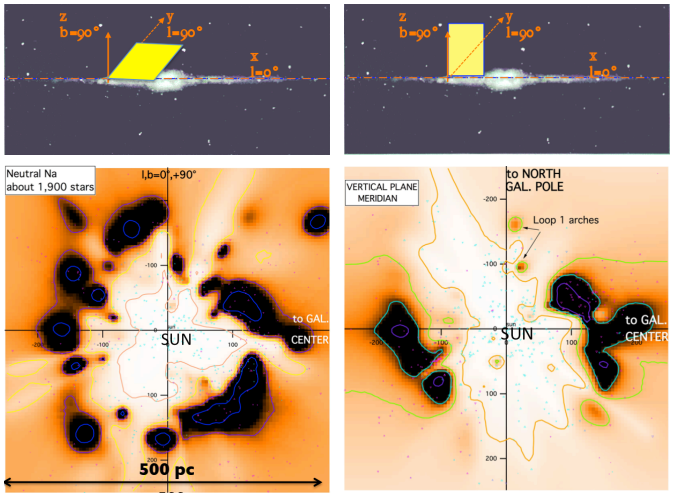

Figure 7: Planar cuts in the three-dimensional distribution of neutral sodium in the Galactic (left) and meridian (right) planes in the vicinity of the Sun (Puspitarini et al. 2012). The (imposed) resolution is 20 pc. Regions more distant than 200 pc and having a uniform colour correspond to a lack of information in the initial homogenous distribution. The main feature visible in these maps is the Local Cavity, which is devoid of dense gas. Note that, in the vertical plane, the Local Cavity is inclined by about 20° with respect to the polar direction. These maps are based on a very small amount of NaI columns measured from high-resolution spectra.

weeks per year over the course of a decade-long survey. Such observations could be undertaken in conditions of very high sky brightness.

2.1.4.2 Absorption Studies in Support of Radio Observations

Small-Scale Structures seen in Polarization: The Interface between Stars and the ISM. Detailed information on small-scale ($\sim 1''$) structures in the ISM is now available from radio polarization data (e.g., Landecker et al. 1999; Ransom et al. 2010; Wolleben et al. 2010; Wolleben 2007). Some of these structures correspond to shells generated by stellar winds or supernovae. Other structures trace the interfaces between evolved stars or planetary nebulae (PNe) and the ambient ISM, including "tails" behind fast-moving PNe. Such interfaces, albeit much larger, are also seen at other wavelengths, most notably in the infrared (e.g., Spitzer "arcs" in Orion) or in the UV (i.e., the spectacular case of Mira's tail; Wareing et al. 2007). In many (and perhaps most) cases, the origins of the detected polarization signatures are far from clear. The lack of information on the distance and the extent of these objects makes their true nature obscure and undermines efforts to construct quantitative models.

Observations with ngCFHT would be ideal for advancing this area of study. Dedicated observations of target stars located in the field and associated absorption measurements would yield more accurate distances to the radio polarization sources, and thus provide accurate physical dimensions. Moreover, the ability of the new observations to detect variations in the velocity structure at very small angular scales ($\sim 1''$ in a single exposure, less if observing several times and moving the fibres) would allow for direct comparison to hydrodynamic simulations of the star-ISM interaction, and provide critical information for the construction of rotation measure models. These models, in particular, would give important information on the magnetic-field structure in the interaction and tail regions, and could lead to the construction of better magneto-hydrodynamic models of the star-ISM interaction. Moreover, emission lines might also be detected and their variability studied as a function of the location in the bow-shock and tail structures, when present. Multi-fibre spectra would be particularly adaptable for such observations.

Supernova Remnants (SNRs) Increasingly detailed radio, optical and X-ray observations of SNRs have raised a number of important questions. Why are there such large differences in the ratios between X-ray and radio emissions for supernovae of the same type and with comparable radio emissions? Why are there radiative recombination continua (interpreted as freely expanding and recombining gas) in X-ray spectra of mixed-morphology SNRs that are known to be interacting with molecular gas (e.g., Miceli 2010)? The nature of the SNR, and the detailed distribution of the ISM surrounding it, are key parameters in understanding these interactions which play a major role in galactic

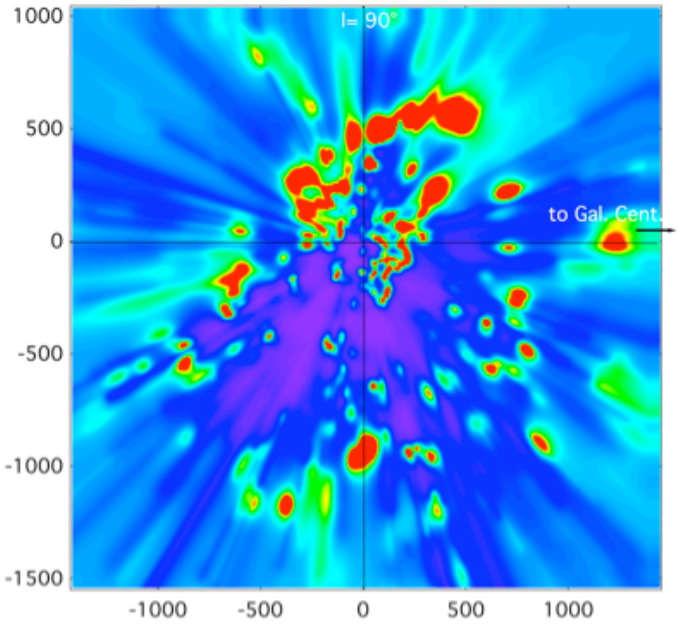

Figure 8: Planar cut in the three-dimensional opacity distribution inverted from 17,000 reddening measurements (see Lallement et al. 2003 for details on the methodology). The Sun is located at coordinates (0,0) where the units are parsecs. Violet indicates regions of very low density, while red shows high-density regions. External areas with a homogenous colour correspond to the absence of constraints (i.e., the paucity of target stars whose line-of-sight crosses this region of space). The Local Cavity at the centre is seen in these maps to be surrounded by a large number of *other* cavities, including a large region in the third quadrant that is almost entirely devoid of dust. This cavity is thought to be the counterpart of the radio supershell GSH 238+07 (Heiles 1998).

ISM recycling. Observations of the field stars around SNRs would allow the measurement of absorption or emission features that hold clues to the ISM structure, enable correlation studies, and ultimately lead to models that describe the ejecta expansion and shock properties.

The requirements for such programmes are similar in terms of wavelength coverage and S/N to those required for three-dimensional mapping of the ISM (§2.1.4.1). Such studies are probably best carried out in PI/GO time, as the necessary exposure times per field (though they depend of course on target distance) are on the order of a few hours for objects within a few kpc.

2.1.4.3 Small-Scale Structure of Diffuse Molecular Clouds and the CH^+ Problem

Whether or not diffuse interstellar clouds are "clumpy" remains a hotly debated issue. In particular, any structure in the spatial distribution of the major molecule, H_2, is very difficult to identify since the column density of this species can be measured only in the far UV, which requires spectral observations of bright, background stars with O or B spectral types. The degree of H_2 clumpiness is critically important for modeling the abundances within these clouds as it affects the penetration of UV photons and thus photo-destruction processes. Because H_2 is known to be closely correlated with CH (Federman 1982), observations of the blue lines of this radical can be used as a surrogate for H_2. By selecting appropriate clouds at intermediate latitudes where the confusion is minimal and the surface density of background stars is still high, one could map the distribution of CH and infer that of H_2. The use of background stars make it possible to probe the spatial structure over a surprisingly broad range of scales, with a dynamic range of about 3000. While the largest separations (1.5° or $\approx$ 3 pc for a cloud at 100 pc) can be used to delineate the overall geometry of the cloud and its boundaries, the smallest ones (a few arcseconds, or about 0.001 pc) would probe the structure at very small scales. ngCFHT spectra taken at a resolution of $\mathcal{R} = 20,000$ would be sufficient to reach these objectives because, apart from the main transition at 4300 Å, several additional weaker features are available around 3890 Å, allowing the measurement of line opacities and, hence, CH column densities even if line profiles are unresolved. The ISM project described above (see §2.1.4.1 and Table 5) would be ideal for such studies since it focuses on these blue

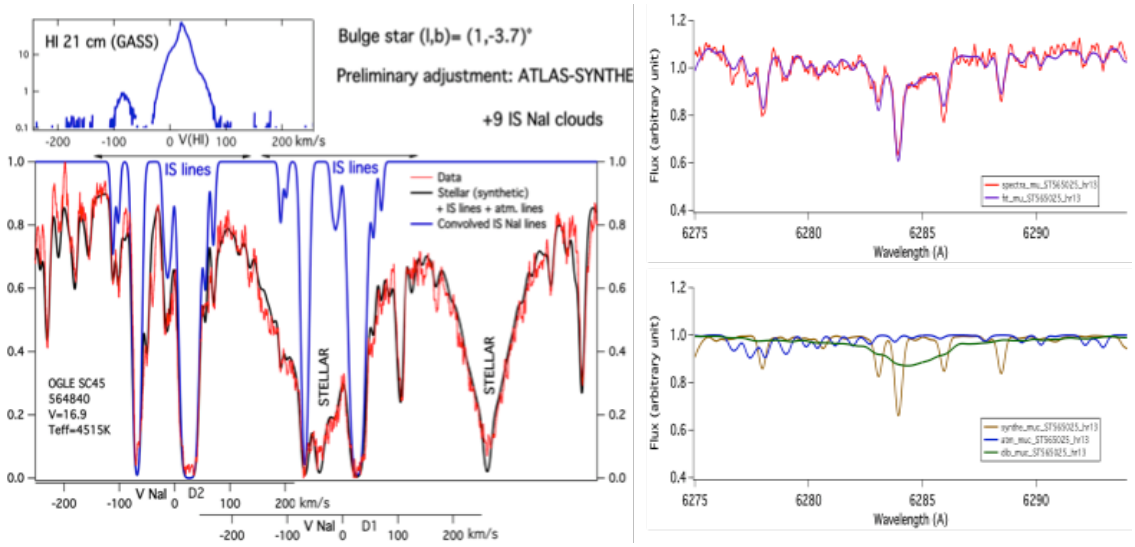

Figure 9: Examples of spectral extractions for the interstellar sodium absorption doublet (left) and a diffuse interstellar band (the 6284 Å band; right) from $\mathcal{R} = 20,000$ spectra of cool giant stars in the Galactic bulge (Chen et al. 2012). Spectra were obtained with the FLAMES/GIRAFFE instrument on the 8.2m VLT. In both cases, the data are fitted with a combination of stellar, atmospheric and interstellar spectral models. We show an example of nine interstellar clouds (i.e., 18 lines) detected towards OGLE-564840, and of a 600 mÅ equivalent width DIB towards OGLE-565025. The S/N here is of the order of 40 per resolution element. In high-resolution mode, data of this quality can be obtained with ngCFHT for a $g \approx 19.2$ star in an exposure of 1 hr.

wavelengths. Moreover, a vast number of background stars would be available: i.e., a $\sim$ 5,000 deg^2 region along the plane of the Galactic disk ($b < |\pm 10^\circ|$) and visible ($X < 1.5$) from Mauna Kea at some point during the year would contain more than 80,000 stars of type O or B (and 1.3 million A-type stars) brighter than $g = 16$ according to the Besançon models (Robin et al. 2003).

Such observations would provide simultaneous, and invaluable, information on the "CH^+ problem". The high abundance of CH^+ in the ISM is presently not understood: the $C^+ + H_2 \rightarrow CH^+ + H$ reaction presents an energy barrier of 4600 K and is insufficient to produce the observed amounts of CH^+ in the conditions prevailing in diffuse molecular gas. Similarly, the large abundance of H_2 in $J > 2$ rotational states requires energetic processes that have yet to be identified and which can play an important role in the physics and chemistry of diffuse molecular gas. CH^+ is thus an important species in that it can be used to investigate the nature of non-thermal processes that may play a key role in the physics of interstellar clouds. Several scenarios involving either shocks (Pineau des Forêts et al. 1986), vortices (Godard et al. 2009) or cloud/intercloud interfaces have been suggested as the additional energy source required to overcome the CH^+ formation energy barrier. All these scenarios imply the presence of localized regions heated to higher temperatures but with very different geometries (i.e., shocks and interfaces are essentially 2-D structures) while in the scenario involving turbulence, vortices are distributed over the whole cloud volume. Thus, a detailed study of the spatial distribution of CH^+ with a facility like ngCFHT would allow astronomers to identify conclusively the process at work. Furthermore, in this same spectral range, lines from CN are also present, and these can be used to provide additional constraints on cloud models. The technical and programmatic requirements for such a study would be similar to those described above for the study of radio structures.

2.1.4.4 The Nature of Diffuse Interstellar Bands (DIBs)

A large number of the absorption lines between 420 and 900 nm are DIBs. They are abundant, with more than 400 having been identified to date (see, e.g., Hobbs et al. 2009; Friedman et al. 2011). At present, no definitive identification exists for any of the carriers, despite decades of study (although large gaseous carbon molecules are strongly favored). Most observations have tended to focus on measuring correlations between specific bands and gas or dust columns. While some families that share some properties have been found, there is a strong variability in the degrees of correlation. Recent studies have shown that the strength of some DIBs is governed by the stellar/interstellar radia-

tion field, reflecting their degree of ionization. The cloud history and physical state (i.e., shocks, ionization, cooling, condensation, shielding against UV photons, etc) must play a role not only in the cloud chemistry and molecular content, but also in the formation of DIBs.

Building on these studies, ngCFHT would offer a new way to approach the longstanding problem of their identification, as well as characterizing the properties of the clouds to which they belong. Determining the detailed spatial distribution of the DIB carriers within a given cloud at high spatial resolution, through spectroscopic measurements of multiple targets, would give information on how those carriers evolve within the cloud. Although challenging, such observations might also reveal DIBs that originate from the same types of molecules since they should display the same spatial structure. No such studies have yet been attempted because they require not just DIB measurements, but also absorption data (needed to constrain the physical and chemical structure of the ISM). ngCFHT would be the ideal facility for such a study. Targets should in this case include cool, evolved stars in order to maximize spatial resolution. Such a programme could be carried out in PI mode, or using a subset of stars targeted in bright time surveys.

2.2 Stellar Astrophysics

2.2.1 Abstract

In many ways, stellar astrophysics forms the backbone of modern astronomy. Stellar evolutionary theory, guided by measurements for fundamental parameters from high-resolution spectroscopy, underpins our models of galaxy evolution and cosmology. Furthermore, it is now recognized that the formation of planetary systems is closely connected to that of the stellar hosts, as evidenced by the apparent high efficiency of planet formation among metal-rich stars. In the coming decade, a number of the key questions in stellar astrophysics will need to be addressed using very large, systematic spectroscopic surveys conducted at high spectral resolution: i.e., roughly an order of magnitude higher than that of the SDSS ($\mathcal{R} \simeq 1\,800$). We describe how an ambitious, wide-area stellar survey with ngCFHT could uncover rare and important stellar types, such as solar twins and faint, metal-poor white dwarfs associated with the Milky Way thick disk or halo. The detection and characterization of such objects using $\mathcal{R} = 20\,000$ optical spectroscopy would deepen our understanding of, e.g., planetary formation processes and their dependence on environment, the chronology of disk and halo formation, and the end stages of stellar evolution for low-mass stars. A Galactic Archaeology Survey of this sort (§2.3) could be complemented by smaller, more targeted programmes that explore the evolution and chemistry of massive stars in the local volume, or pioneer the field of time-domain stellar spectroscopy, which has the potential to improve dramatically our understanding of stellar multiplicity (including the interconnections between companions of all sorts, from low-mass stars, to brown dwarfs and exoplanets) and pulsating, eclipsing or eruptive stars.

2.2.2 Introduction

Stellar spectroscopy has long been a cornerstone of astrophysics. While its best known applications lie in the determination of fundamental stellar parameters — such as mass, temperature, luminosity, radius, magnetic field strength, and chemical abundance — it has increasingly been used as a tool for studying broader questions such as: how do galaxies evolve, how does planet formation unfold, and how and when did the first (and most metal-poor) stars in the Milky Way form? Examples of recent, high-impact results include the characterization of extremely metal-poor Galactic stars (e.g., Bonifacio et al. 2012, Frebel & Norris 2011, Placco et al. 2011), chemodynamical analyses of stars in the Local Group galaxies, halo streams, and ultra-faint dwarf galaxies (e.g., Tolstoy et al. 2009, Norris et al. 2010, Okamoto et al. 2012, Walker et al. 2009, Kirby et al. 2008b), and the study of stars that host planetary systems (e.g., Buchhave et al. 2012, Melendez et al. 2012, Sousa et al. 2011, Schuler et al. 2011, Ramirez et al. 2010).

For studies of the Galactic halo, the most detailed spectroscopic analyses to date have been carried out for individual stars or, at best, small groups of stars. The most important results have come from spectra collected with UVES and FLAMES (VLT), HIRES and DEIMOS (Keck), HDS (Subaru), and/or MIKE, IMACS and MMFS (Magellan). While most of the facilities mentioned above are capable of delivering high-resolution optical spectra, they can only do so for small, carefully selected samples of stars distributed over limited fields. Yet some of the key questions in stellar astrophysics can be addressed only by using large (and perhaps even blind) surveys containing large numbers of stars spread over wide fields (see also §2.1 and 2.3). Representative questions include:

1. *Is the Sun unusual because it hosts a planetary system?* Detailed spectroscopic analyses for a handful of "solar twins" have shown that their chemistry differs from that of the Sun: i.e., they contain higher fractions of refractory elements. In the case of the Sun, such elements may have been consumed by its surrounding planetary system (e.g., Rameriz et al. 2010). However, the interpretation of this result is difficult because the effects are subtle and there are alternative explanations for the observed abundance patterns (e.g., chromospheric activity, stellar seismology, or even first ionization potential effects). Because fewer than a few dozen solar twins are presently known, a larger sample is essential if we are to understand the origin of this difference.

2. *How old is the Galactic halo?* White dwarfs can be used to age-date their host stellar population using cooling curves. Unfortunately, they are so faint that most known white dwarfs are restricted to the solar neighbourhood. A handful (2–4) of white dwarfs has been found with high proper motions, suggesting they are members of the Galactic halo, yet only $\sim$ 30 pc away. The ages of 11–12 Gyr measured for these stars (Kilic et al. 2012, Bergeron et al. 2005) are in good agreement with white dwarf cooling curve ages in the globular clusters NGC 6397 and M4 (Hanson et al. 2007, 2004). Nevertheless, a much larger sample of more distant halo white dwarfs (with medium-resolution spectroscopy) could be combined with detailed white dwarf model atmospheres

calibrated using nearby objects (having high-resolution spectroscopy) to provide an independent measurement of the age distribution for the Galactic halo.

3. *Where are the minority populations in the Galactic Bulge?* Stars in the Galactic bulge tend to be metal-rich, as would be expected when star formation occurs rapidly (e.g., Lecureur et al. 2007, Fulbright et al. 2007, McWilliam et al. 2008). However, microlensing studies toward the bulge (Bensby et al. 2010, 2011) and some recent spectroscopic surveys (Gonzalez et al. 2011) find some stars with lower metallicities. Very metal-poor stars have yet to be found though, including any extreme metal-poor stars (if they exist, e.g., Gao et al. 2010 vs. Cescutti & Matteucci 2011). Clearly, very large sample sizes are needed to identify and characterize the most metal-poor stellar populations in the bulge (see also §2.3.4.2).

4. *How does environment impact the chemical evolution of disk galaxies?* Precise stellar parameters for massive stars can be determined using low-resolution spectroscopy and narrowband photometric indices (e.g., Kudritzk et al. 2012; Firnstein & Przybilla 2012). Because these stars are bright, they can be studied individually in galaxies out to ~ 4 Mpc: i.e., at the distance of the Sculptor and M81 groups. In principle, metallicity and reddening maps can be determined for the disks of star-forming galaxies in order to test the effects of environment on disk evolution. While individual galaxies can be examined with present-day instruments, a comprehensive study will require homogeneous observations for many stars belonging to a large, statistically robust sample of galaxies.

5. *Time domain stellar spectroscopy.* By the end of this decade, a large number of imaging surveys will have explored and characterized the transient sky down to very faint magnitudes. Spectral monitoring of many of these transients will be required to understand their nature. Multi-epoch spectral monitoring over wide areas will in turn require a large-aperture, highly-multiplexed spectrograph. Obvious applications include spectroscopic follow-up of transit-selected planetary host candidates, binary stars, pulsating and/or eclipsing variables, but also supernovae, gamma ray bursts, and AGNs.

Loosely speaking, for stellar astrophysics, the transformational role of ngCFHT would be two-fold: first, in the collection of spectra for stellar samples of unprecedented size, depth and resolution and, second, in the spectral monitoring of time variable sources (see, e.g., §2.2.4.4).

2.2.3 ngCFHT in Context: Competition and Synergies

Astronomy is entering an era that will be dominated by large surveys, most of which will be restricted to broad-band imaging. Surveys like Pan-STARRS, DES, Skymapper, LSST, and Euclid will together image most of the sky in optical and near-IR filters. These datasets will be outstanding resources for blind target selections and all-sky spectroscopic surveys. In addition, unique objects uncovered in these surveys (e.g., possibly objects related to the first stars, or rare metal-line white dwarfs that may have accreted planets; see Melis et al. 2012 and references therein) will require spectroscopic follow-up for detailed analyses.

While high-resolution, single-object spectrographs on 8m- to 10m-class telescopes can be used to study *individual* sources, ngCFHT would be a uniquely powerful resource for conducting wide-field spectroscopic surveys that build comprehensively on future imaging and astrometric surveys. Two *high-resolution* projects that are now underway will present some short-term competition to ngCFHT, although, ultimately, neither will rival ngCFHT in terms of its combined spectral resolution, areal coverage, depth and sample size. These are the APOGEE and ESO-Gaia surveys:

- APOGEE is an H-band survey at $\mathcal{R}$ = 30,000 with a priority of characterizing the stellar populations in the Galactic bulge (Eisenstein et al. 2011; Majewski 2012). Conducted as a SDSS-III programme with the small 2.5m telescope at Apachee Point, it is expected to yield spectra for $\approx$ 100 000 stars. Unfortunately, near-IR spectroscopy provides only a limited range of chemical elements (e.g., no neutron capture heavy elements, Origlia et al. 2012; Ryde et al. 2010; Smith et al. 2002). Still, APOGEE should reach through the Galactic Bulge and even observe bright red giants located on the other side of the Galactic disk. A similar VLT/FLAMES large programme is also underway, gathering optical spectra for several thousand stars towards the Galactic bulge, albeit in small, sparsely distributed fields. As it is being carried out in the optical region, this survey will not reach across the bulge.

- The ESO-Gaia survey is intended to provide high-resolution, VLT spectra for faint stars observed by Gaia, and thus give improved stellar parameter determinations, chemical abundances, and radial velocities (see Gilmore

et al. 2012). Gaia will provide distances from parallax measurements and space velocities from proper motions for $\sim$1 billion stars down to $m_v \approx 20$. Gaia will itself provide radial velocities and stellar parameters for $\sim$ 150 million stars, but its sensitivity is limited to the range m_v = 12–16 mag. While improved radial velocities and chemical abundances for Gaia stars will be provided by this survey, it will ultimately observe only a small fraction of possible Gaia targets and will cover a tiny fraction of the sky. As amply demonstrated by SDSS, a proper characterization of the Galactic halo requires coverage over a significant fraction of the sky. Of course, sky coverage will be further limited to just the southern hemisphere, which is unfortunate since, as noted by Turon et al. (1999), the outer parts of the Galaxy are best observed from the northern hemisphere, where the extinction is on average lower.

Other surveys that are presently in the commissioning or planning stages should also have an impact in this field (e.g., HERMES, LAMOST, 4MOST, MOONS, BigBoss, PFS, etc).[8] However, with the exception of MOONS and PFS, these surveys would be conducted on much smaller telescopes than ngCFHT. If the MOONS instrument is approved by ESO in 2013, it would be deployed (probably in 2017 or 2018) on one of the VLT unit telescopes and, consequently, would almost certainly be available for stellar surveys for a fraction of the available time.[9] The PFS instrument is presently limited to low spectral resolution (i.e., slightly higher than SDSS-I) and, like MOONS, would be deployed (around $\sim$ 2018) on a general user telescope. Hence, it would not be available for dedicated surveys.

The high-resolution spectroscopic surveys on 4m-class telescopes include HERMES, WEAVE, and possibly, 4MOST. These 4m surveys can be expected to observe the brightest stars and therefore have their most signficant impact on the characterization of the Galactic disk and local halo. For example, 4MOST anticipates gathering over 20 million spectra at $\mathcal{R}$ $\sim$5 000 and 2 million at $\mathcal{R}$ $\sim$20 000 during its 5-year lifetime (de Jong et al. 2012). The 4MOST team aims to determine radial velocities $\sim$4 mag fainter than Gaia (i.e., to m_v $\sim$20), which would permit substructure measurements with red giant branch stars to $\sim$60 kpc. The larger aperture of ngCFHT could reach intrinsically fainter stars locally, and reach stars into the outer halo; in medium resolution mode, ngCFHT could reach $\sim$3 magnitudes fainter again, or to distances of $\sim$1 Mpc. Also, different stellar types could be used to map substructure, since not only red giants could be observed over large distances. This means that spectra of the most luminous stars in all Local Group galaxies could be obtained, as well other nearby sparse group disk galaxies (see below). In particular, luminous A- and B-type supergiants (with $M_v \sim -6$ could be reached out to 4 Mpc with ngCFHT in medium resolution mode ($m_g \sim 23.1$), making it possible to estimate distances and metallicities in star-forming galaxies in other environments. We note that Magellan's M2FS may also have this capability depending on its throughput after commissioning (i.e., for spectroscopic surveys over smaller fields of view, suitable for the luminous stars belonging to nearby galaxies).

2.2.4 Legacy Science

As a point of departure, we consider a number of "legacy" science programmes in the field of stellar astrophysics that would be enabled by a wide-field, high-resolution spectroscopic survey of Milky Way stars, as described in §2.3 (see Table 7). Such a survey would cover nearly a quarter of the Galactic volume and would sample all major Galactic components (including the halo, the thin and thick disk, and the bulge), ultimately yielding high-resolution spectra for more than 5 million stars over its decade-long lifetime. We also consider a number of smaller, more targeted programmes that could complement this Galactic Archaeology Survey and address some key questions in stellar astrophysics.

2.2.4.1 Solar Twins: The Sun and Solar System in Context

Solar-type stars are obvious targets in the search for exoplanetary systems. In recent years, possible connections between the "architecture" of planetary systems and the fundamental parameters of their host stars, including their chemical makeup, have emerged as key constraints on proposed mechanisms of planet formation.

It has been recognized for some time that the stars found to host planets in radial velocity surveys tend to have rather high metallicities (e.g., Gonzalez 1997). With the ever-increasing number of Doppler-selected exoplanetary systems, it has been shown many times that the shift in metallicity — usually characterized by [Fe/H] — between planet-hosting FGK dwarf stars, and those known *not* to host closely orbiting giant planets, is of high statistical significance. Most studies agree (e.g., Fischer & Valenti 2005) that, in the majority of cases, the metal-rich nature of the planet-hosting

[8]There will also be significant survey potential for M2FS once it is commissioned on Magellan.

[9]The MOONS field of view (500 arcmin^2) is also just $\sim$ 1/10th that of ngCFHT, further reducing its efficiency for very wide-field surveys.

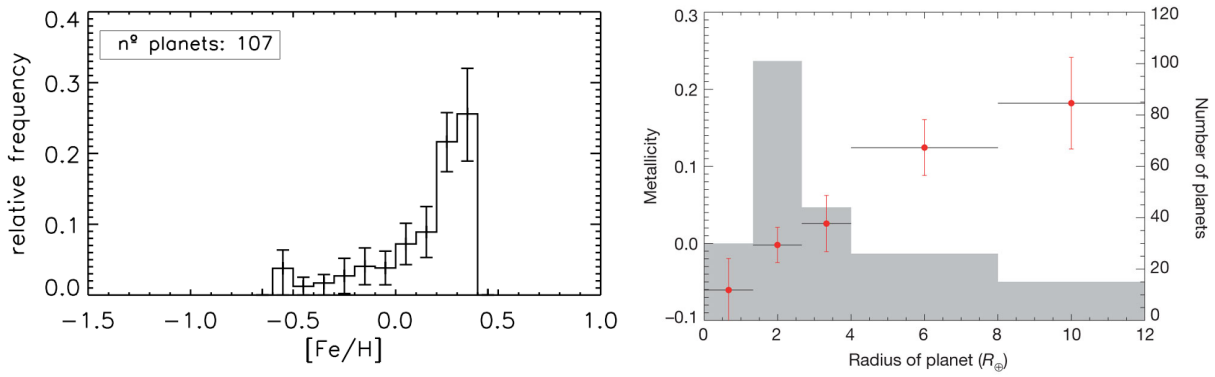

Figure 10: (Left Panel). Metallicity distributions for the combined CORALIE and HARPS samples plotted against the frequency of planet detections (Sousa et al. 2011). (Right Panel). Plot of stellar metallicity, on the left axis, versus planet radius from Buchhave et al. (2012). The right axis shows a histogram of detected planets as a function of their radius.

stars is intrinsic to the star itself. This suggests that planets — at least giant planets of the type that are found most easily in RV surveys — are preferentially formed in metal-rich environments. Indeed, data on 582 low-activity FGK stars in the HARPS volume-limited sample confirm that planet-hosting stars tend to be enhanced in metals (see the left panel of Figure 10).

Interestingly, some recent studies have noted that stars which host Jovian-mass planets tend to be more metal-rich than those stars which have only Neptunian-mass planets or smaller (e.g., Ghezzi et al. 2010; Buchhave et al. 2012). This result suggests that metallicity plays a role not just in the formation of giant planets, but also in the distribution of planetary masses within exosolar systems. The number of stars with Neptunian-sized planets or smaller that have been analyzed in detail has recently increased significantly thanks to the Kepler mission; Buchhave et al. (2012) report this trend down to the level of terrestrial-sized planets in 226 targets (Figure 10).

Additional, intriguing, chemical abundance trends have been noted in stars that may be related to the presence of planets. Using a technique in which spectral lines in "solar twins" (i.e., stars having stellar parameters similar to those of the sun) are compared in a careful differential abundance analysis, Melendez et al. (2009) found that the chemical composition of the sun is anomalous with respect to most (85%) solar twins. Compared with its twins, the sun exhibits a deficiency of refractory elements (i.e., those with high condensation temperatures, T_c) relative to volatile elements (those with low T_c). This finding may be a sign that planet formation occurred more efficiently around the sun compared with the majority of solar twins. Furthermore, within the context of this scenario, it seems likely that the observed abundance patterns are specifically related to the formation of terrestrial planets: i.e., while refractory material is missing in the sun, those dust-forming elements are overabundant in meteorites and terrestrial planets. If correct, this would be an exciting result, as it points the way to using chemical abundance distributions as diagnostics of inner, terrestrial-type planetary architectures. If the chemical signature found in the sun is indeed due to the formation of terrestrial planets, then the study of metal-rich solar analogs and F-type dwarfs can provide further clues to planetary formation mechanisms (Ramirez et al. 2010). In short, exploring the possibility that planet mass may be correlated with the chemical composition of the stellar host, using a large and homogeneous stellar sample, is of utmost importance.

These studies have demonstrated that there are subtle, but fascinating, patterns in the chemical abundance distributions of stars hosting exoplanets. Such patterns have a potential significance beyond a simple empirical shift towards higher metallicities. Probing the trends in chemical abundance distributions requires an ability to derive stellar parameters and chemical abundances for many different elements in a very large sample of solar-type stars. With a sample of $\sim$100 000 or more FGK main-sequence stars, the intrinsic dispersions of particular chemical families could be measured. This would make it possible to establish whether or not the peculiar signatures seen in the small numbers of planet-hosting and non-planet-hosting stars to-date are found in a general census of solar-type main-sequence stars. In particular, the availability of the Kepler field is a resource to be exploited by future large surveys from the Northern hemisphere as proposed with ngCFHT (see also §2.2.4.4). At a resolution of $\mathcal{R}$ = 20 000, a well-calibrated, uniform spectral dataset could be used to extract accurate chemical abundance distributions of a wide variety of elements,

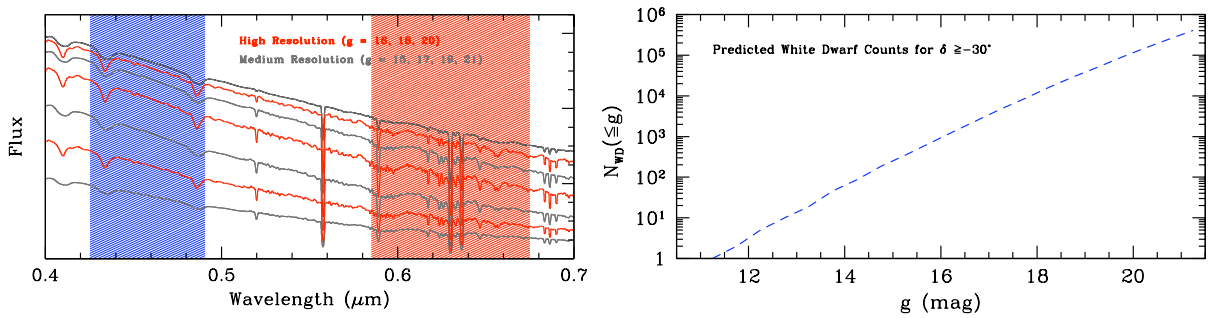

Figure 11: (Left Panel). Simulated high- and medium-resolution ngCFHT spectra (red and grey curves, respectively) for Milky Way white dwarfs spanning the magnitude range g = 15 to 21. Exposure times are 1 hr in all cases. The blue and red shaded regions show the proposed wavelength intervals for the $\mathcal{R} = 20\,000$ Galactic Archaeology Survey. (Right Panel). Cumulative luminosity function of Galactic white dwarfs based on the Besançon models of Robin et al. (2003). According to these models, there are more than 170 000 white dwarfs brighter than faint cutoff of the Galactic Archaelology survey ($g \approx 20.4$) and at $\delta \gtrsim -30^{\circ}$.

covering all nucleosynthetic origins and chemical behaviour.

2.2.4.2 White Dwarfs as Probes of Galactic Formation and Evolution

Prior to the SDSS, only $\sim$ 2500 white dwarfs were known. The SDSS DR4 catalogue of white dwarfs (Eisenstein et al. 2006) more than doubled this number, all with spectroscopic confirmations. This catalogue has since been used for statistical studies of white dwarf stellar physics and parameters (e.g., Kepler et al. 2007; Tremblay et al. 2011) as well as for studies of the ages of the Galactic thin and thick disks (e.g., Harris et al. 2006). The catalogue includes rare sub-classes of magnetic and pulsating white dwarfs, and white dwarfs in binary systems (which have also been identified by the UKIDSS survey, Steele et al. 2011). These latter systems can be further studied using time-resolved spectroscopy in order to identify compact, post common-envelope binaries; these objects — which are the precursors of cataclysmic variables, X-ray binaries and possibly SN Ia — allow the various formation mechanisms proposed for these systems to be carefully examined. The SDSS DR7 catalogue of white dwarfs, when released in the near future, should increase to more than 20 000 our census of spectroscopically confirmed white dwarfs.

At present, SDSS catalogues contain few white dwarfs belonging to the Galactic halo (i.e., the SDSS "20 pc" sample is estimated to be only 80% complete, Holberg et al. 2008). However, analyses of four, inner-halo white dwarfs moving through the solar neighbourhood (Kilic et al. 2012; Kalirai 2012) yield ages in good agreement with those of old stellar clusters having measured white dwarf ages (e.g., NGC 6397 and M4; Hanson et al. 2007, 2004). This is an area where ngCFHT can be expected to have a profound impact on white dwarf studies — by finding and identifying new white dwarfs in the Galactic halo, which are critical for improved age estimates, as well as the discovery of additional rare objects, e.g., white dwarfs polluted by accretion of terrestrial objects, magnetic stars, etc.

ngCFHT would play an invaluable role by providing good S/N spectra (15–50 was shown to be ideal in the analysis of SDSS spectra by Tremblay et al. 2011) for a volume-limited sample: e.g., within a distance of $\sim$ 100 pc. The left panel of Figure 11 shows simulated ngCFHT spectra (based on the models of Bohlin 2000) for white dwarfs in the range $15 \lesssim g \lesssim 21$, at both high- and medium-resolution. Exposure times in all cases are 1 hour, which is appropriate for the proposed Galactic Archaeology Survey. The right panel of Figure 11 illustrates the possibility for transformational gains with ngCFHT relative to SDSS for white dwarf studies. The dashed curve shows the predicted, cumulative number of white dwarfs down to $g \sim 21$ for declinations $\delta \gtrsim -30^{\circ}$. Down to this limiting magnitude, we expect roughly $\sim$ 8 white dwarfs per ngCFHT field, averaged over this $\sim 3 \times 10^4$ deg^2 region.

The measurement of precise stellar parameters for white dwarfs is only possible by combining photometry, from surveys like SDSS, Gaia, Pan-STARRS or LSST, with follow-up spectroscopy. For most systems, ngCFHT would be the *de facto* provider of spectroscopy, given its much deeper limiting magnitude than SDSS, Gaia, or 2-4m-class telescopes in general. For a subset of the newly discovered white dwarfs, proper motions and distances from Gaia would further improve the precision of the measured stellar parameters. In most cases, intermediate-resolution spectroscopy, for instance from the $\mathcal{R} = 6\,500$ component of the Galactic Archaeology Survey, would be sufficient. Indeed, spectra at $R = 2\,000$ would be adequate for most white dwarfs (i.e., DA and DB) where $\log g \approx 8$ and the H and He lines

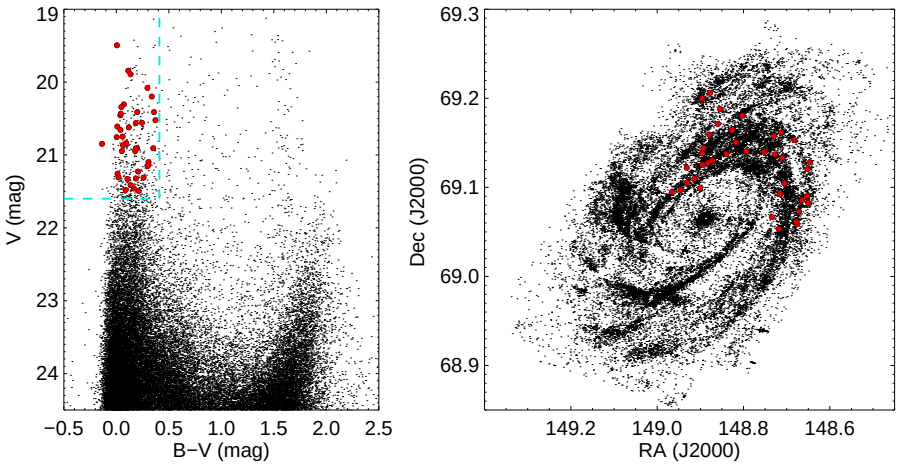

Figure 12: (Left Panel). HST/ACS colour-magnitude diagram used to select blue supergiant star candidates in M81. (Right Panel). Location of the blue supergiant star targets in M81. Figure from Kudritzki et al. (2012).

used for stellar parameter determinations are very broad. Higher resolution would be particularly interesting for other subtypes. For example, those with metal lines, which may have been polluted by the accretion of planets, could be used to determine the chemical composition of the former rocky planets. Needless to say, it would also be possible to analyse those systems with magnetic fields to a level of precision that is impossible with SDSS.

2.2.4.3 Fundamental Parameters for High-Mass (B/A) Stars: The Chemical Evolution of Disk Galaxies

Both high-and low-resolution spectroscopic surveys can play an important role in the derivation of fundamental parameters for massive stars. Detailed stellar parameters and chemical abundances for massive, hot stars can be determined with exquisite precision from high-resolution spectroscopy (e.g., Firnstein & Przybilla 2012), while medium-resolution spectroscopy can be used to measure basic parameters and metallicities. For example, Kudritzki et al. (2012) have shown that Keck/LRIS spectroscopy ($\mathcal{R} \sim 2\,000$) can be used to measure reliable temperatures and luminosities for hot, massive stars by fitting the Balmer jump and Balmer line profiles. Because these stars are intrinsically bright (i.e., $M_v > -6$), medium-resolution spectra can be used to examine stars in distant galaxies (e.g., star-forming galaxies in the Sculptor and M81 groups). Spectral templates can then be used to estimate metallicities in individual stars, and thus examine directly the metallicity gradients of disk galaxies.

In the simplest picture of disk formation, in which a disk forms through "inside out" gravitational collapse, one expects the metallicity to decrease as a function of Galactocentric radius (see Cheng et al. 2012). On the other hand, the existence of radial flows (e.g., Spitoni & Matteucci 2011) or the presence of a turbulent disk at early times (Brooks et al. 2009; Dekel et al. 2009) could alter this picture significantly. Strong radial migration mechanisms might also wash out an existing gradient in the stars (Roskar et al. 2008; Schoenrich & Binney 2009), while radial breaks may indicate either dynamical interactions within disks, or merger events in outer disks (e.g., Pohlen & Trujillo 2006; Younger et al. 2007; Bigiel et al. 2010). The measurement of disk metallicity gradients from individual stars means not only that coverage is more homogeneous than would be possible with H II regions, but it ensures that metallicity and reddening are sampled together, rather than relying on just oxygen abundances. Needless to say, metallicity measurements in a large and diverse sample of galaxies beyond the Milky Way will provide crucial environmental information that can be used to disentangle competing disk formation scenarios.

To illustrate the transformational role that ngCFHT could play in this field, we consider the case of M81, the nearby Sab galaxy at a distance of ≈ 3.5 Mpc. In this galaxy, stars as faint as $V \approx 21.5$ have been observed with Keck/LRIS at S/N $\sim$ 50, and the metallicity gradients were found to be consistent with the oxygen abundance gradients from HII regions, with comparable uncertainties (see Figure 12). It is interesting that the gradient in M81 seems to have evolved over the last $\sim$5 Gyr, as the oxygen gradient derived from PNe is steeper (see Figure 13). With the ngCFHT, a dedicated survey of nearby disk galaxies would be possible, including galaxies spanning a range in group and field environments. Previously, this kind of work was restricted to UV and high-resolution spectroscopic analyses; new

techniques, combined with a wealth of high-quality spectra from ngCFHT, would allow an ambitious, comprehensive survey to be mounted from the ground.

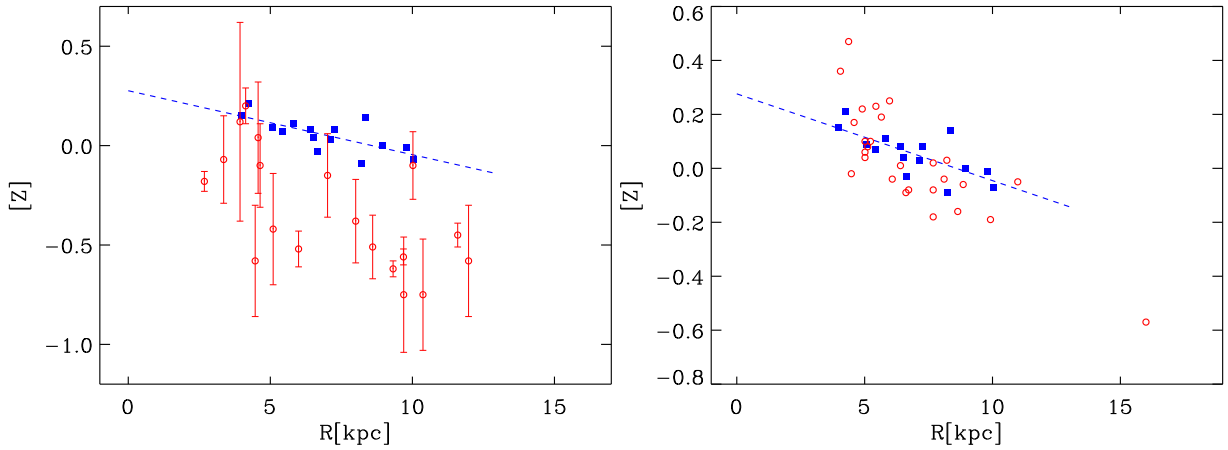

Figure 13: (Left Panel). Comparison of metallicities in M81 deduced from blue supergiant stars with planetary nebulae oxygen abundances (blue and red, respectively). (Right Panel). Comparison of metallicities deduced from blue supergiant stars with oxygen abundances derived from HII regions (blue and red, respectively). The random uncertainties in these measurements are $\sim$ 0.1 to 0.2 dex. Figure from Kudritzki et al. (2012).

With ngCFHT, the high-resolution spectroscopy could be used to study massive stars further, particularly in providing a large statistical sample of chemistries and rotation rates. These data would be useful in addressing issues related to rotational mixing (e.g., Maeder & Meynet 2010; Ekstrom et al. 2012). Since the inclination angle for any individual star is rarely known, a large statistical sample is one of the best ways to look for correlations between stellar line strengths/chemical abundances and stellar rotation rate (e.g., Hunter et al. 2009; Brott et al. 2011). Rotation is a fundamental parameter in the analysis of massive stars since it is thought to affect core masses, and therefore, ages, of these stars. In addition, rotation drives the mixing of nuclear processed material from a stellar interior to its surface, and it is thus one of the key observational constraints in stellar astrophysics (see, e.g., Venn et al. 2002). For very massive stars, rotation rates are thought to affect Eddington luminosities, and therefore mass loss rates as well, and ultimately to lead to the development of Wolf-Rayet stars and luminous blue variables. There is also some speculation that rotation is affected by stellar metallicity (Penny & Gies 2009), and that these parameters combine to influence stellar evolution predictions, including evolutionary masses. A large statistical sample of measured chemical abundances and rotation rates for massive, bright stars in M31, M33, and other Local Group, northern hemisphere star-forming galaxies (see also §2.4.4.1) would be the obvious way in which to test this prediction. These stars typically have $V \lesssim 18$ and are thus easily within reach of ngCFHT in its high resolution mode.

Of course, rotation is also important for the (main sequence) evolution of lower mass stars, as it affects directly convective mixing efficiencies and, ultimately, the interpretation of surface chemistry measurements (including the lithium isotopic abundances that are compared to Standard Big Bang predictions; Asplund et al. 2006; Suda et al. 2011). With a large sample of accurate, homogeneous rotation rates measured for many thousands of bright stars with ngCFHT in high-resolution mode, it would be possible to study these effects statistically.

2.2.4.4 Time Domain Spectroscopy

An increasing fraction of astronomical resources are being devoted to characterizing the transient, moving and variable universe. ngCFHT, thanks to its large aperture, wide field and high multiplexing, would be well positioned to pioneer the field of wide-field, time domain optical/IR spectroscopy. In this section, we consider two areas in stellar astrophysics where ngCFHT could make unique and important contributions: i.e., in the study of (1) stellar multiplicity and exoplanetary systems, and (2) variable stars and stellar pulsation.

Table 6: Technical Requirements and Survey Implementation: Multiplicity and Exoplanet Survey

Survey Area (Ω)	$\Omega = 115$ deg^2.
Field Location	Kepler field: $\alpha_{2000} \approx 290^\circ$, $\delta_{2000} \approx +44^\circ$.
Number of ngCFHT Fields ($N_{\rm field}$)	$N_{\rm field} = \Omega/{\rm FOV}_{\rm ngCFHT} = 84$.
Number of Configurations per Field ($n_{\rm config}$)	$\langle n_{\rm config} \rangle = 2$.
Total Number of Exposures ($N_{\rm exp}$)	$N_{\rm exp} = N_{\rm field} \times \langle n_{\rm config} \rangle \approx 84$ per epoch for radial velocity monitoring.
Primary Imaging Resources for Target Selection	Kepler + supplementary data.
Observing Conditions	Lunar illumination $\gtrsim 80\%$. Some cloud cover would be acceptable.
Instrumental Configuration(s)	(1) $\mathcal{R} = 20\,000$, $T_{\rm exp} = 0.15$ hr per epoch for radial velocity monitoring. (2) $\mathcal{R} = 2\,000$, $T_{\rm exp} = 0.3$ hr
Wavelength Coverage and Spectral Resolution	(1) 0.42–0.49μm and 0.59–0.67μm at $\mathcal{R} = 20\,000$ (2) 0.37–1.3μm at $\mathcal{R} = 2\,000$
Velocity Precision (ϵ_v)	$\epsilon_v \approx 150$ m s^{-1} at high resolution.
Limiting (point source) Magnitude	$g_{\rm AB} \simeq 16$.
Stellar Sample Size	$N_* \simeq 1.3 \times 10^5$.
Total Time Needed for Program ($T_{\rm tot}$)	$T_{\rm tot}$ = [84×0.15 hr] + 20% overhead ≈ 15 hrs per epoch. = 750 hrs for 50 epochs over 10 years, for high resolution monitoring. $T_{\rm tot}$ = [84×0.1 hr] + 20% overhead ≈ 30 hrs for a low resolution survey.

A. Stellar Multiplicity and Exoplanet Environments

More than 800 exoplanets have now been detected through a variety of methods: i.e., (1) radial velocity searches; (2) photometric transits; (3) astrometric searches; (4) direct imaging; (5) timing variations; and (6) microlensing surveys. While the radial velocity method still accounts for the majority of the known planets, transit surveys are now responsible for about one-third of the detections, with several thousand planet candidates awaiting validation. Different methods probe different planetary parameters, and each approach has its own advantages and biases. However, by combining results from the various methods, it is possible to build up a surprisingly complete picture of planetary systems. For instance, radial velocities provide important constraints on planetary masses, while planetary radii can be measured using photometric transits. Thus, it has been possible in recent years to lay important groundwork in the burgeoning field of comparative planetology.

Even the relatively well-characterized population of giant planets shows a surprising diversity in properties, with orbital configurations of all kinds observed: i.e., very short orbital periods, large eccentricities, large inclinations, etc. Thanks to a wealth of new data from space-based observatories (most notably CoRoT and Kepler), we are now able to detect planets with masses and radii not much larger than those of the Earth (and even identify some intriguing multiple-planet systems containing rocky planets). In general, a planet's fundamental parameters (e.g., radius, mass, density and orbit) provide the basic data needed for a characterization of extrasolar planets. These allow an assessment of the overall nature of a given planet (i.e., whether it is a gas giant, a Neptune-like system, or a terrestrial planet) and provide important insights into its interior structure. A measured orbit also allows us to investigate the dynamical evolution of the planet, and to set constraints on the current theories of planetary formation.

For the coming decade, the major thrusts of exoplanet research will likely be:

1. Surveys sensitive to planets in the lower part of the mass-radius diagram, covering an extend range in orbital period. A major goal continues to be the discovery of an Earth-like planet in the habitable zone of a G-type star. For Doppler searches, this requires a radial velocity precision of about 10 cm s^{-1} over a period of several years. For a photometric detection, it requires a measurement of the transit signal of a few 0.001%.

2. The detection of giant planets beyond the snow line (3–5 AU), including the discovery of Jovian analogs.

3. A thorough assessment of how the bulk properties of planets depend on the properties of their stellar hosts. This will require the detection of planets (and other companions) around a large sample of diverse stars, from F- to M-type dwarfs, as well as moderately evolved stars.

4. A determination of the uniqueness of our solar system, and a comparison of its properties to those of planetary systems in different environments and at different evolutionary stages.

No single facility will be capable of addressing all of the issues. For instance, a number of ongoing or planned surveys are focusing on improved detection limits via extended time coverage and/or increased radial velocity precision. At present, there are about fifteen instruments worldwide that can deliver a radial velocity accuracy of ~ 10 m s^{-1} or better. Some have been monitoring bright stellar samples for more than a decade, and some can achieve a precision of ~ 1 m s^{-1}: i.e., HARPS (ESO 3.6m), HIRES (Keck 10m), SOPHIE (OHP 1.9m) and HARPS-N (TNG 3.6m). Thus,

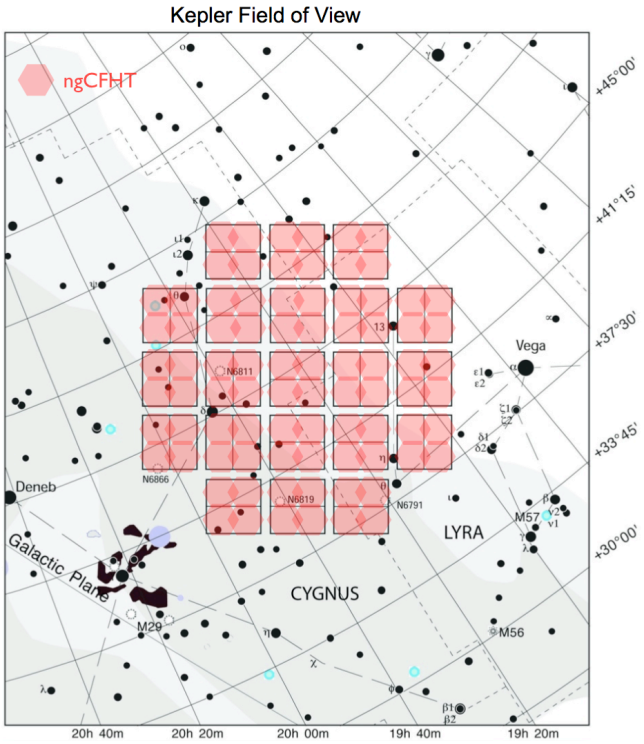

Figure 14: One possible survey geometry for spectroscopic monitoring of stars in the Kepler survey field (the 21 square regions covered by 42 CCDs) . The total $\sim$115 deg^2 survey area could be covered, with high spatial completeness, in 84 ngCFHT pointings.

the domain of massive planets should be relatively well explored in a decade's time. For low-mass planets (or those having long orbital periods), there are plans for ultra-high-precision instruments that should make significant progress on this front: e.g., ESPRESSO, a high-resolution spectrograph that is scheduled for delivery to one of the 8.2m VLTs in 2015, aims to achieve a precision of a few 10 cm s^{-1} (Pepe et al. 2010).

For ngCFHT, the maximum radial velocity precision attainable in high-resolution mode is likely to be of the order $\simeq$ 150 m s^{-1}. While this could certainly not compete with dedicated Doppler-search instruments, ngCFHT's large aperture, wide field and extreme multiplexing should allow it to make a unique contribution to the question how exoplanet properties depend on *environment*, a recurring theme in the above list. As an illustration, we consider the role ngCFHT might play in characterizing the stellar and planetary environments for $\sim 10^5$ stars in the Kepler fields. The Kepler mission, launched in 2009, is searching for transiting, Earth-like planets through continuous monitoring of $\approx$ 145 000 main sequence stars distributed over a $\sim$ 115 deg^2 field. To date, more than 2 000 planetary candidates have been identified and are awaiting verification. In 2012, the mission lifetime was extended until at least 2016.

Figure 14 shows how ngCFHT could survey the entire Kepler region in $\sim$ 84 pointings. A survey of this sort would have a two-fold purpose. First, low-resolution ($\mathcal{R} = 2\,000$) spectroscopy over the entire 0.37 to 1.3 μm range for a complete sample of Kepler targets would be ideal for homogeneous spectral typing and metallicity estimates for all (mostly late-type) stars using a common set of spectral features (e.g., Hα, TiO, CaH, etc). There is emerging evidence that the correlation between planetary frequency and host metallicity (see the left panel of Figure 10) exhibited by massive planets may not hold for the lowest-mass planets, so homogeneous metallicity estimates for the host stars of planetary systems of all sorts, based on high-S/N, homogeneous low-resolution, optical/IR spectroscopy, would be an important dataset to complement the extensive transit observations. Secondly, Kepler has proved to be very sensitive to "hot Jupiters", whose formation is thought to involve scattering and/or migration processes. The physical interpretation of these systems would benefit from a thorough characterization of companions of all sorts — from the regime of low-mass stars down to brown dwarfs. Although ngCFHT's velocity precision in $\mathcal{R} = 20\,000$ mode would not be sufficient to detect exoplanets themselves, it would be more than adequate to perform a complete census of low-mass stellar companions and brown dwarfs. Because the targets are bright, exposures of only 10–15 minutes

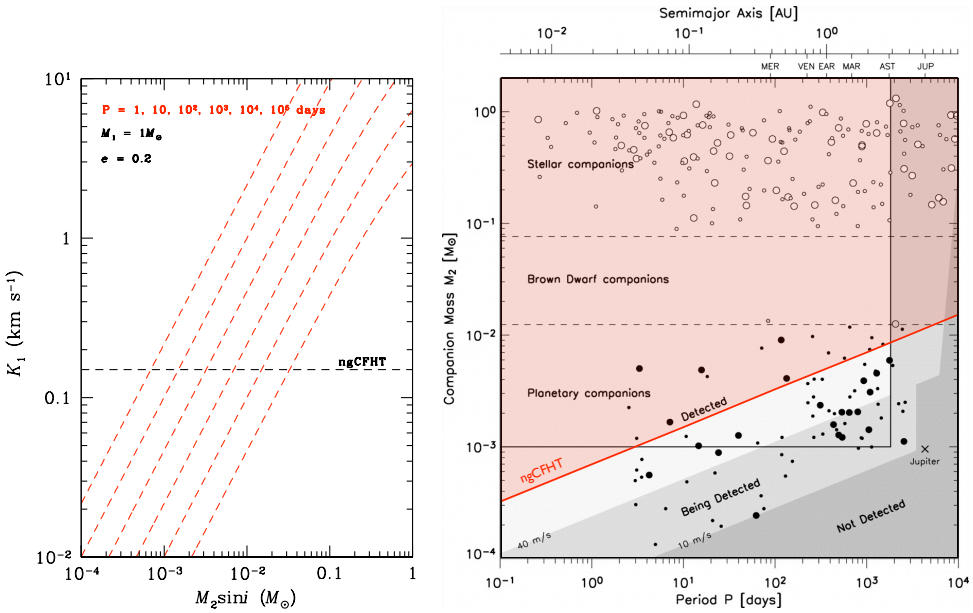

Figure 15: Illustration of the possible role of ngCFHT in characterizing the low-mass companions of solar-type stars. The panel on the left shows velocity induced by a companion plotted against (minimum) companion mass. The dashed red curves show the reflex velocities expected for companions with orbital periods between 1 and 10^5 days, as indicated in the figure. All calculations assume a 1 $M_\odot$ primary and an orbital eccentricity of $e = 0.2$. The dashed horizontal line shows the typical precision of ngCFHT radial velocity measurements for stars brighter than $g \sim 16.5$. The panel on the right, which is adapted from Grether & Lineweaver (2006), shows the sensitivity of ngCFHT in terms of companion mass and orbital period.

would be required to measure radial velocities to a level of a few hundred m s^{-1} for $\sim$10^5 stars in a few tens of hours. Thus, one could consider an ambitious, longterm monitoring programme to measure stellar multiplicity for this sample, requiring about 750 hrs over a ten year period (50 epochs).

Finally, this example considers the specific case of the Kepler mission, but there are several other space missions devoted to the study of exoplanets that are still in the development stage (e.g., TESS, FINESSE, CHEOPS, EChO, EXCEDE). As with the Kepler mission, TESS aims to detect large numbers of exoplanets using the transit method. However, like PLATO, the recently proposed (but not selected) ESA mission, it would concentrate on the detection of planets associated with brighter ($V \lesssim 13.5$) stars distributed over the entire sky. It is expected to monitor more than 2 million stars, and identify thousands of transiting exoplanets. Thus, there would continue to be a pressing need for wide-field, multi-object spectroscopic capabilities in order to characterize the target stars, particularly those showing possible evidence for transiting planets. At the same time, a major component of exoplanetary research will continue to be exoplanet detection via direct imaging studies. In such surveys, panoramic spectroscopy for millions of Galactic stars would be invaluable for optimizing the target selection by providing accurate stellar parameters, such as effective temperature, surface gravity, and also [Fe/H] or some elementary abundances of key elements; continued radial velocity monitoring would also allow a part of the companion populations in the target stars to be identified and characterized, as described above. A particularly exciting approach would be to select imaging targets using a combination of multi-band imaging and wide-field spectroscopy — to identify stars of various ages using Ca II H and K strength, Li abundances, rotational velocities, and/or UVW space motions. Combined with direct imaging data and radial velocity monitoring, this would allow a more complete characterization of the time evolution of planetary systems.

B. Variable and Pulsating Stars

For the study of variable stars — including eclipsing and pulsating variables — the yields from the next generation of imaging telescopes (Pan-STARRS, Skymapper, ATLAS, LSST, etc) promise to be immense. As an indication of what the future may hold, the left panel of Figure 16 shows results from a search for RR Lyrae variables based on

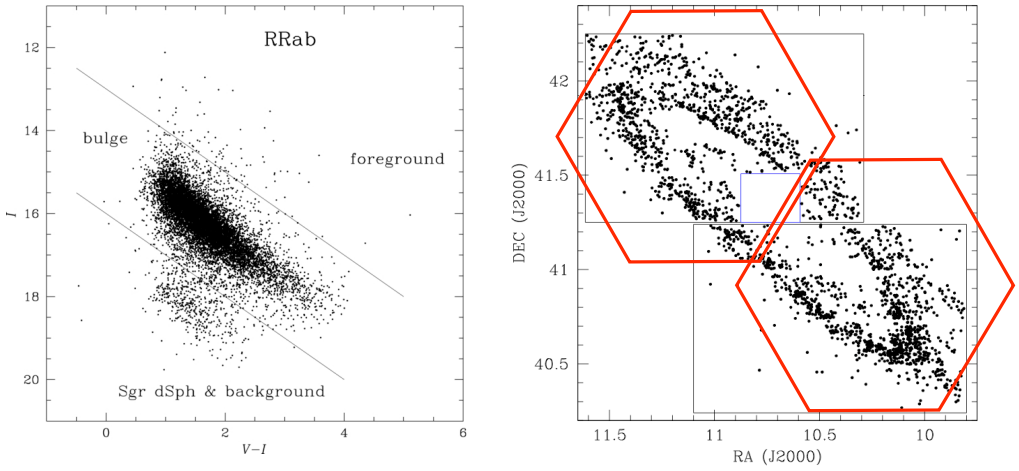

Figure 16: (Left Panel). Composite colour-magnitude diagram for 11 124 RR Lyr variables of type RRab from the OGLE-III survey, which carried out an 8-year monitoring campaign of a ~ 100 deg^2 region in the direction of the Galactic bulge. A roughly five-fold increase in the number of bulge RR Lyr variables is expected when the VVV survey is completed in ~ 2015 (Minniti et al. 2010). Figure from Pietrukowicz et al. (2012). (Right Panel). The distribution of Cepheids in M31 from the POMME survey (Pixel Observations of M31 with MEgacam). The red hexagons show possible ngCFHT fields for spectroscopic monitoring campaigns. Note that the Cepheid distribution is similar to that of the brightest stars in M31, although there are small differences due to reddening variations, gas content and changes in underlying star formation history. Figure adapted from Fliri & Vals-Gabaud (2012).

the OGLE-III microlensing survey of the Galactic bulge. This survey, covering a total area of ~ 100 deg^2, discovered more than 16 000 RR Lyr variables of all types, producing phased light and colour curves for each object (Pietrukowicz et al. 2012). The ongoing VISTA Variables in the Via Lactea survey (VVV; Minniti et al. 2010) is expected to increase the bulge RR Lyrae sample to 40 000–70,000 by 2015. The gains expected for other types of variables will be equally dramatic; for example, the right panel of Figure 16 show early results from the POMME survey (Fliri & Vals-Gabaud 2012) which used CFHT to monitor the disk of M31 over a period of about 2.5 months. This figure shows the distribution of more than 2 500 Cepheids with periods in the range 2 to 80 days, highlighting the familiar ring-like distribution of massive, bright stars in M31. In short, the coming decade should see a revolution in the study of variable stars.

Cepheids, RR Lyraes and other types of pulsating stars are not only cornerstones of the cosmic distance ladder, but also important testbeds for stellar evolutionary models. While there is much to be learned from photometry alone, the addition of multi-epoch spectroscopy would make possible a number of investigations that have heretofore been impossible. For instance, RR Lyr variables in the bulge region have magnitudes in the range $15 \lesssim I \lesssim 18$ and velocity semi-amplitudes of $A \simeq 20$ km s^{-1} or more, while Cepheids in M31 with periods longer than 3–4 days have $19 \lesssim r \lesssim 23$ and $A \gtrsim 15$ km s^{-1}. These magnitudes and pulsation velocities make it prudent to consider spectroscopic monitoring campaigns with ngCFHT: i.e., repeated radial velocity measurements, at a resolution of $\mathcal{R} \simeq 6\,500$ (i.e., $\epsilon_v \sim 3$ km s^{-1}), for hundreds or thousands of variables in selected fields. Such data could then be combined with contemporaneous, multi-colour, photometric data to carry out Baade-Wesselink studies for stellar samples of unprecedented size. Because the Baade-Wesselink method represents a direct route to the measurement of fundamental parameters including stellar radius and distance, such programmes would have obvious implications for our understanding of the mechanisms that drive stellar pulsation and the evolution of stars through the instability strip. In the case of M31, a number of other attractive targets for spectroscopic monitoring would also be available including bright, eclipsing binaries (which would provide direct mass measurements for stars at the upper end of the main sequence) and novae,[10] where pioneering efforts in spectral classification based on a handful of objects in Local Group galaxies has revealed an unexpected diversity in spectral properties (Shafter et al. 2012).

For the role ngCFHT might play in the study of explosive transients, including high-z supernovae, see §2.9.

[10]Novae in M31 occur at a rate of 30–65 yr^{-1} and, depending on maximum brightness, have decay timescales of 1–2 weeks to many months.

2.3 The Milky Way

2.3.1 Abstract

The success of the Lambda Cold Dark Matter (ΛCDM) cosmological paradigm on large scales is impressive. However, this model can now make relatively detailed predictions on smaller (i.e., galactic) scales, and it is here that observations and theory show important discrepancies. Advancing our understanding of the galaxy formation process in general requires detailed observations of individual systems, and, naturally, our Galaxy provides the most important laboratory for exploring chemodynamical evolution on these scales. Indeed, the Milky Way is now recognised as being a complex ensemble of stellar populations, each having characteristic age and metallicity distributions, and unique dynamical properties. Here, we summarize some of the ways in which ngCFHT could have a transformational impact in this burgeoning field. In particular, we emphasize the need to make the best use of its aperture and sensitivity by focusing on the faintest Galactic sources. We describe an ambitious, longterm Galactic Archaeological Survey that will provide a unique and powerful dataset with a broad range of scientific applications, from Gaia follow-up to the deconstruction of our Galaxy into its primordial building blocks. Over a period of $\sim$ 10 years, nearly 20 million medium-resolution stellar spectra would be obtained, down to a limiting magnitude of $g \sim 23$ and distributed over roughly a quarter of the sky. Approximately 5 million of these stars would have high-resolution spectra as well, extending to the furthest reaches of the Galaxy and covering more than 25% of its volume. Such a dataset would be both unprecedented and unrivaled.

2.3.2 Introduction

The measurement of the fluctuations in the CMB allow us to determine key cosmological parameters, including the total density, matter density and baryonic density of the universe. The picture that emerges is of a Universe dominated by a cosmological constant, with a mass budget largely dominated by non-baryonic matter (Komatsu et al. 2011). Within this context, cosmological simulations indicate that primordial fluctuations grew and gave rise to overdensities where galaxies and large-scale structures may have formed. However, the details of galaxy formation and evolution within this framework are not well understood due to the complexities of baryonic physics. It is on these small scales that the prevailing cosmological paradigm faces its toughest challenges.

Eggen et al. (1962) were the first to show that stellar abundances and kinematics could be used to understand the formation and evolution of our Galaxy, and thus guide ideas of galaxy formation in general. Indeed, their analysis of 221 very nearby stars remains, arguably, the single most influential observational paper on galaxy formation. In it, they proposed that metal-poor stars in the halo of the galaxy were formed during the rapid collapse of the protocloud that eventually became the Milky Way. An alternative proposal was offered by Seale & Zinn (1978), whose analysis of the stellar populations of a number of Galactic globular cluster led them to infer that they were formed in independent "protogalactic fragments" that later assembled the outer parts of the Galaxy. The current paradigm — whereby gas collapses in dark matter structures that form disks and eventually merge together or are accreted by larger systems — contains key elements of both of these original scenarios.

These seminal papers demonstrated that information relating to the chemical and dynamical characteristics of the early protogalaxy, its constituent building blocks, and the subsequent evolutionary processes that have produced the Milky Way (and its subcomponents) can be explored through chemodynamical studies of modern-day stellar populations. Freeman & Bland-Hawthorne (2002), for example, proposed identifying stars that were born from the same gas cloud by the measurement of abundances for many chemical species, and "tagging" those with similar abundance patterns. Helmi (2001) and others showed that stars that were accreted into the Milky Way from the same merger event can still be identified through their energies and angular momenta, even if they no longer form an obvious stellar stream across the sky (in contrast to coherent, present-day features such as the Sagittarius and Orphan streams, and other prominent substructures).

The chemical signatures, energies and angular momenta of the individual stars in the Galaxy encode its formation and evolutionary history, and can provide us with the most precise understanding of the processes through which the Milky Way was assembled. In contrast to the early study of Eggen et al. (2962), ngCFHT has the ability to provide these parameters for *millions* of stars throughout every component and subcomponent of the Galaxy, and contribute to the creation of the most detailed dataset ever assembled for a single galaxy.

Gaia, an ESO Cornerstone Mission. The Hipparcos astrometric space mission (Perryman et al. 1997; Perryman 1997) provided a major breakthrough in our understanding of the structure of the Galaxy. It measured accurate positions, proper motions and parallaxes for 118 218 stars, providing a revolutionary vision of the solar neighborhood.

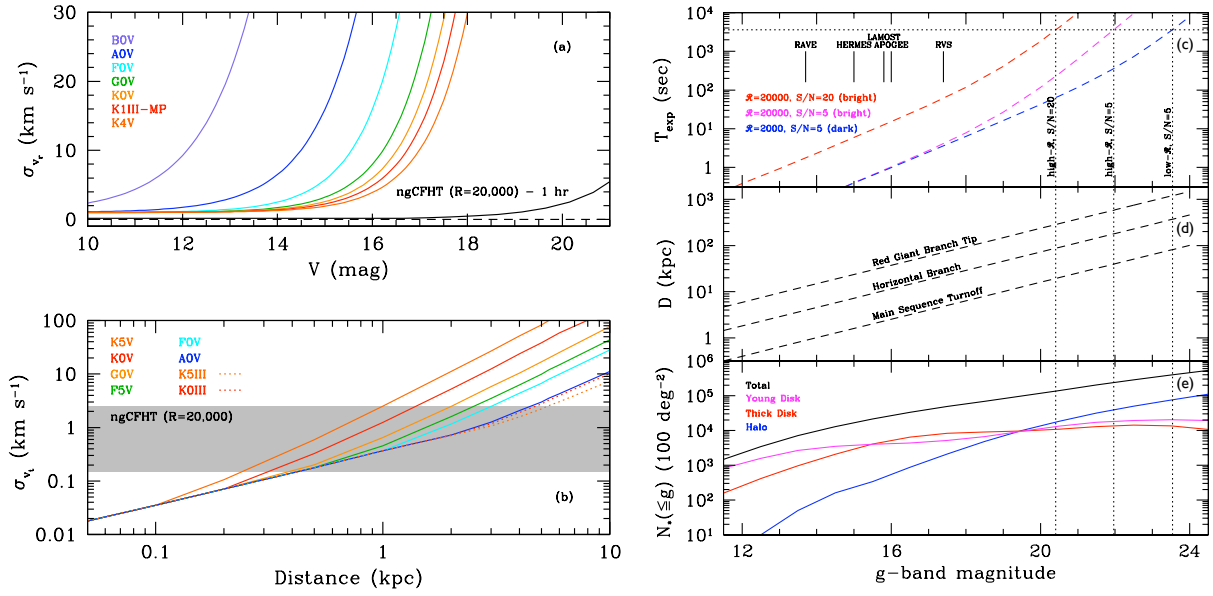

Figure 17: (Panel a). Expected radial velocity accuracy for the RVS instrument aboard GAIA. The coloured curves show the typical errors expected for stars of different spectral types. The lower black curve shows the radial velocity accuracy expected for a G2V star observed for a total of 1 hour with ngCFHT in high-resolution mode. (Panel b). Typical error in transverse velocity as a function of distance for stars observed with GAIA. The different curves correspond to stars of different spectral type. The shaded grey region shows the errors calculated for G2V stars with $g \lesssim 20.5$. (Panel c) Exposure time required for ngCFHT to reach target signal-to-noise ratios, plotted as a function of g-band magnitude. The three curves show results for different survey components and instrument configurations (as indicated in the legend). The horizontal dotted line indicates the nominal survey exposure time of 1 hr; from left to right, the vertical dashed curves show the corresponding limiting magnitudes for the different surveys. (Panel d) Depth reached for old, metal-poor halo populations as a function of g-band magnitude. Results are shown for three different tracer populations: red giant branch tips stars, horizontal branch stars, and main-sequence turnoff stars. (Panel e) Cumulative number counts for Milky Way stars in a 100 deg^2 region at the north Galactic cap (black curve). Star counts for three separate Galactic components (young disk, think disk and halo) are shown in colour.

The satellite was not equipped with a spectroscopic instrument, however, so it could not measure radial velocities; these were intended to be acquired from ground based facilities. Unfortunately, as of today, only $\sim$ 1/3 of the Hipparcos stars have a measured radial velocity.

The successor to Hipparcos is the ESA "Cornerstone" misson Gaia, which will be launched in 2013. Gaia will measure positions and magnitudes for every object in the sky brighter than 20th magnitude, or approximately *1 billion* objects. Postions of nearly 26 million stars will have accuracies of order 10 *micro*-arcseconds. In contrast to Hipparcos, Gaia will also be equipped with a medium-resolution ($\mathcal{R} \sim 11\,500$) spectrometer (the Radial Velocity Spectrograph, RVS), that will access the region around the Ca II Triplet (CaT). RVS will measure radial velocities for stars down to $V \sim$ 16–17 to an accuracy of 1–10 km s^{-1}. Chemical abundance information will also be provided for a few elements (i.e., Mg, Si, Ca, Ti and Fe for stars of spectral type F-G-K), but only for stars brighter than 12th magnitude. For fainter stars, only the mean "metallicity" and basic atmospheric parameters will be available. For the hundreds of millions of stars fainter than 17th magnitude, no spectral information at all will be available from RVS.

The Gaia dataset will represent a unique and comprehensive resource for astronomy, given the unprecedented accuracy with which it will measure the 3-D positions of Galactic stars. There will also be a near-perfect synergy with ngCFHT, since Gaia lacks, for all but the brightest subset of its targets, an equivalent accuracy in the measurement of velocities and compositions — an area in which ngCFHT would excel.

2.3.3 ngCFHT in Context: Competition and Synergies

Even prior to the Gaia mission, there has been significant ongoing effort to obtain spectroscopy for large numbers of stars in the Galaxy. Notable among these has been SDSS (York et al. 2000) and its extension, SEGUE (Yanny et al. 2009), that have provided low-resolution ($\mathcal{R} \sim 2\,000$) spectra of over 600 000 stars. Photometric data from SDSS were fundamental in discovering stellar streams in the Galactic halo (Belokurov et al. 2006), and the SDSS spectroscopic data have been used to measure radial velocities and basic astrophysical parameters (e.g., $T_{\rm eff}$, log g, [Fe/H], [α]/Fe], etc) and hence enable a wealth of follow-up studies. At brighter magnitudes ($I \leq 12$), the Radial Velocity Experiment (RAVE; Steinmetz et al. 2006) has accumulated around 500 000 stellar spectra for stars covering 20 000 deg^2 in the southern hemisphere. RAVE, which is using the 6dF spectroscopic facility on the 1.2m UK Schmidt in Australia, operates at intermediate resolution ($\mathcal{R} \sim 7\,000$). It is set to conclude in 2012.

The 4m LAMOST telescope (Zhao et al. 2012) is now undergoing science commissioning; it is a highly multiplexed (N = 5000), wide field (3 deg^2) survey telescope that will soon undertake the LAMOST Experiment for Galactic Understanding and Exploration (LEGUE) survey. This programme aims to acquire spectra, at a resolution of $\mathcal{R} = 1\,800$, for about 5 million stars brighter than $r = 17$ and $\sim$ 2.5 million stars brighter than $r = 19$.[11] Among 8m-class telescopes, PFS will be the most highly multiplexed spectrograph when it sees first light around 2017 (Ellis et al. 2012). It will have complete coverage from the optical at ~ 0.36 μm into the near-IR at ~ 1.3 μm, and will operate at a resolution of around $\mathcal{R} \simeq 2\,000$. Up to 2400 spectra will be collected simultaneously over a 1.3 deg^2 field. The design of PFS is based heavily on a concept put forward for Gemini (WFMOS) prior to its cancellation. As such, it bears many similarities to the low-resolution component of the ngCFHT design discussed in §1 and elsewhere.

Since all of the surveys discussed to this point rely on low or intermediate spectral resolution, individual abundances can only be derived from the strongest lines. However, the need for a suitable spectroscopic follow-up for the Gaia mission has brought tremendous focus by the international astronomical community on wide-field, *high-resolution* spectroscopy. There are now several ongoing or planned programmes on 4m- to 8m-class telescopes intended to address this shortcoming. A notable programme on a small telescope is the SDSSIII/APOGEE survey (Eisenstein et al. 2011; see also §2.2), that operates at a resolution of $\mathcal{R} \sim 20\,000$ at near-IR wavelengths in order to observe $\sim$100 000 stars to $H = 12.5$. As a near-IR survey, APOGEE focus on the inner Galaxy where extinction is strong.

The Gaia-ESO survey began in 2012 and represents a concerted effort by ESO to use existing spectroscopic resources (FLAMES/GIRAFFE and FLAMES/UVES) to maximize Gaia's impact (Gilmore et al. 2012) . It is a five-year project with $\sim$ 300 CoIs that aims to obtain 10 000 UVES spectra ($\mathcal{R} \sim 40\,000$) and 100 000 GIRAFFE spectra ($\mathcal{R} \sim 20\,000$) in relatively narrow spectral regions. This programme likely marks the start of a concerted effort by ESO to enhance its spectroscopic capabilities. For instance, two significant new spectroscopic capabilities are presently under consideration at ESO, with a decision expected in the spring of 2013. The first proposed instrument is the Multi-Object Optical and Near-infrared Spectrograph (MOONS; Cirasuolo et al. 2012), which is being considered for the VLT. It consists of a "GIRAFFE-like", multi-object spectrograph ($N \sim 500$ science objects) that would operate over a modest ~ 0.14 deg^2 field at red/near-IR wavelengths (0.8–1.8 μm). As with all current VLT instruments, it would share the telescope with the rest of the VLT instrumentation suite. The second proposed instrument is the 4m Multi-Object Spectroscopic Telescope (4MOST), a fibre-fed spectrograph that would be installed on the VISTA telescope (de Jong et al. 2012). It would operate at both high and low resolutions in a quasi-dedicated survey mode (sharing the available observing time with VISTA's IR mosaic camera). We note that 4MOST, as a nearly dedicated spectroscopic facility, is in some ways the smaller aperture equivalent of ngCFHT. Needless to say, both proposed ESO instruments would be best suited to observations of the southern skies.

In the immediate future, AAT/HERMES will likely begin science observations in 2013 (Barden et al. 2010). The primary survey to be undertaken by this instrument will be GALAH, which will make use the $N = 400$ multiplex gain at $\mathcal{R} = 28\,000$ to observe a total of $\sim$ one million stars to a limiting magnitude of $V \sim 14$. The abundances of ≥ 15 individual elements will be measured for each GALAH target. In the north, WHT/WEAVE (Balcells et al. 2010) will target nearly 1 000 objects simultaneously and achieve $\mathcal{R} = 5\,000$ with complete optical wavelength coverage, or $\mathcal{R} = 20\,000$ in a smaller interval. WEAVE will target $\sim$ one million stars to $V = 20$ with the former configuration and 50 000 halo giants with the latter configuration, to a depth of $V = 18$.

Compared with all existing and proposed multi-object spectrographs — of which there are many — ngCFHT occupies a unique and exciting discovery space. Existing and proposed spectrographs on 8–10m-class telescopes lack: (1) the flexibility in spectral resolution (i.e., low, medium and high resolution) to successfully measure the abundances

[11] Some higher-resolution ($\mathcal{R} = 5\,000$) spectroscopy is also planned for LEGUE (Deng et al. 2012).

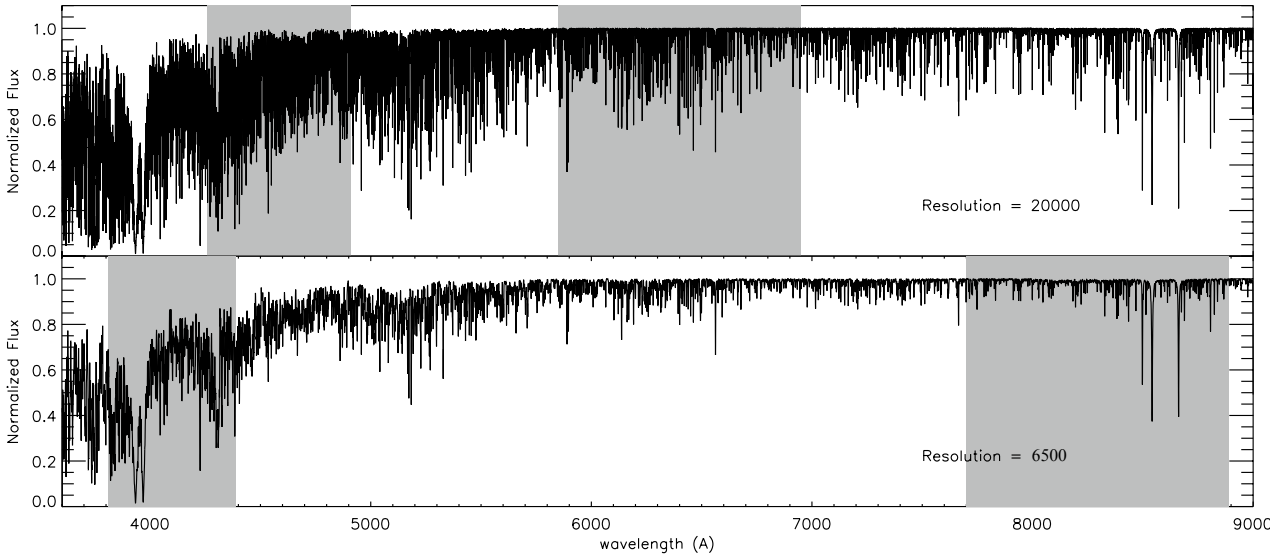

Figure 18: Synthesized spectrum for an [Fe/H] = –1 red giant at a resolution of both 20 000 and 6 500, illustrating representative spectra from the ngCFHT Galactic Archaeology Survey. The shaded regions in the upper and lower panels show the blue and red windows that would be observed at high and medium resolution (upper and lower panels, respectively).

of all but the strongest elements; (2) the wide field needed to survey the large areas required to sample faithfully the Galactic halo population; and /or (3) the ability to operate as a dedicated facility, and hence accumulate the vast datasets that motivate the development of highly-multiplexed spectrographs in the first place. There are several "equivalent" 4m instruments or facilities that are in various stages of implementation, and the large aperture of ngCFHT would, of course, be a natural complement to them that would allow access to targets beyond the reach of these smaller facilities. To take full advantage of the gain in aperture and survey efficiency that ngCFHT would provide, focus must therefore be placed on pushing to faint magnitude limits. The following reference survey illustrates one possible implementation of how a transformational Galactic Archaeology programme could be undertaken with ngCFHT.

2.3.4 Legacy Science

2.3.4.1 The ngCFHT Galactic Archaeology Survey: Decoding the Galactic DNA

We propose the following legacy survey as a means of exploiting the capabilities of ngCFHT for the purposes of Galactic Archaeology, GAIA follow-up, and the study of resolved stellar populations in our Galaxy. It is a longterm survey (i.e., to be scheduled during of fraction of the available bright/grey time for a period of $\approx$ 10 years) to map an area of $\sim$ 10 000 deg^2 at both intermediate ($\mathcal{R} = 6\,500$) and high ($\mathcal{R} = 20\,000$) spectral resolution. Key aspects of this survey include:

- Two pairs of spectral windows: one pair from 381–439 nm and 770–889 nm at $R = 6\,500$, and a second pair from 426–491 nm and 585–675 nm at $R = 20\,000$. These windows are shown graphically in Figure 18. Key chemical species that will typically be identified in these spectra are listed in Table 8.

- A survey strategy whereby 3200 spectra are obtained per field (i.e., $\sim$ 3000 stellar targets as well as spectra for sky subtraction, calibrations, etc) at $\mathcal{R} = 6\,500$ using relatively short exposures (of order 15 min) during grey/dark time. This medium-resolution survey would target stars to a limiting magnitude of $g_{\rm lim} \sim 21.5$ at S/N = 5. The brightest 25% of these targets would also observed for 1 hr at $\mathcal{R} = 20\,000$ during bright time, down to a limiting magnitude of $g_{lim} \sim 19.5$ at S/N = 20.

- The input catalogue would consist entirely of stellar sources (or nearly so; see, e.g., §2.7) with preselection from colour-magnitude diagrams to weight against thin-disk stars. Over the course of a *1-year period* observing in grey and bright time, and assuming 7 hrs observing per night with 1.5 hours per field (i.e., intermediate- and

high-resolution observations, plus overheads), and observing for 80% of the available time, ngCFHT would accumulate $\sim$ 1.8 million stellar sources at $\mathcal{R} = 6\,500$, with high-resolution observations for over 400 000 of these targets.

- Amortized over a 10 year survey lifetime, nearly 20 million stellar spectra would be obtained to a limiting magnitude of $g \sim 21.5$ covering roughly 10 000 deg^2 (i.e., a quarter of the volume of the Milky Way). About half of all stars observed at these magnitudes are halo stars; see Figure 17. (Note that this is *without* taking into account preselection against disk stars.) For the high-resolution component, around 30% of all stars at the S/N=20 limit will be halo giants. These would be identified out to a distance of a couple of hundred kpc from the centre of the Galaxy. Such a dataset would be both unprecedented and unrivaled.

Table 7: Technical Requirements and Survey Implementation: Galactic Archaeology Survey

Survey Area (Ω)	$\Omega \approx 10000$ deg^2.
Number of ngCFHT Fields ($N_{\rm field}$)	$N_{\rm field} = \Omega/{\rm FOV}_{\rm ngCFHT} \approx 6700$
Number of Configurations per Field ($n_{\rm config}$)	$\langle n_{\rm config} \rangle = 2$.
Total Number of Exposures ($N_{\rm exp}$)	$N_{\rm exp} = N_{\rm field} \times \langle n_{\rm config} \rangle \approx 6700 \times 2$
Primary Imaging Resources for Target Selection	Likely Pan-STARRS (3π); Subaru HSC, CFHT LS also possible for some regions)
Observing Conditions	Lunar illumination grey/bright; Cloud cover $< 20\%$.
Instrumental Configuration(s)	(1) $\mathcal{R} = 6\,000$ $N_{\rm point} = 6700$, $T_{\rm exp} = 0.25$ hr
	(2) $\mathcal{R} = 20\,000$ $N_{\rm point} = 6700$, $T_{\rm exp} = 1$ hr
Wavelength Coverage and Velocity Precision (ϵ_v)	(1) 381–439nm and 770–889nm and $\epsilon_v \lesssim 2$ km s^{-1} for $g \simeq 20$
	(2) 426–491nm and 585–675nm and $\epsilon_v \lesssim 2$ km s^{-1} for $g \simeq 20$
Limiting (point source) Magnitude	(1) $g_{\rm AB} \simeq 21.5$
	(2) $g_{\rm AB} \simeq 19.5$
Total Time Needed for Program ($T_{\rm tot}$)	$T_{\rm tot}$ = [(6700$\times$1.25 hr) + 20% overhead $\approx$ 1450 nights.
	Equivalent to $\sim 40\%$ of observing time per year

We now consider some of the key science questions that could be addressed with such a survey, highlighting when appropriate how additional ngCFHT observations would be profitable.

Key Science. A. Chemical Tagging of the Stellar Halo

The halo contains some of the oldest stars in the Galaxy — including those that formed a few Myr after the Big Bang. Both the kinematics and chemical compositions of these old stars provide us with strong constraints on the formation and evolution of our Galaxy, as demonstrated by the early work of Eggen et al. (1962) and also Searle & Zinn (1978). Many of the "proto-galactic fragments" whose existence in the outer halo was implied in the latter work have since been identified photometrically in the SDSS, most notably in the "field of streams" (Belokurov et al. 2006, and references therein). However, such streams are generally only observable if the time that has passed since they merged with the Galaxy is short compared to the dynamical timescales at their location. Streams in the outer halo tend to be longer lived and thus easier to recognize as coherent structures.

ngCFHT would provide detailed abundances, based on high-resolution spectroscopy, for a sample of several million stars at magnitudes $g \approx 18$–19. A large fraction of these will be halo stars in the outer Galaxy. The precision of the radial velocity measurements from ngCFHT would match those of the transverse velocities from Gaia at the faint end, and so provide the perfect complement to this important space mission. Typically, $\sim$ 2/3 of the stars will be dwarf/turnoff stars at distances of 2 to 10 kpc; giants would probe the halo at distances of 10 to $\sim$ 100 kpc or more. As such, this dataset would allow the first through exploration of the outer regions of the Milky Way.

Detailed abundances, with abundance ratios for elements formed through different nucleosynthetic channels, represents the single most important dataset for unraveling the formation and history of stellar Galactic halo components (Figure 19). Indeed, Freeman & Bland-Hawthorne (2002) suggested that "the major goal of near-field cosmology is to tag individual stars with elements of the protocloud". Of course, this applies not just to the stellar halo but also to other Milky Way components, including the disks and bulge (see below). However, the study of the chemical properties of the halo has relied, with a few exceptions, on local samples of halo stars that pass near enough to the Sun to be observable at high spectral resolution. Unfortunately, the number of such stars is dwarfed by the number of disk stars, given the latter components much higher volume density. Unlike any existing or proposed facility, ngCFHT would enable *in situ* studies of the halo and so trace directly, for the first time, spatial variations (such as gradients and substructures) in the chemical and dynamical properties of this (and every other) Galactic component (see Figure 20). Empirically,

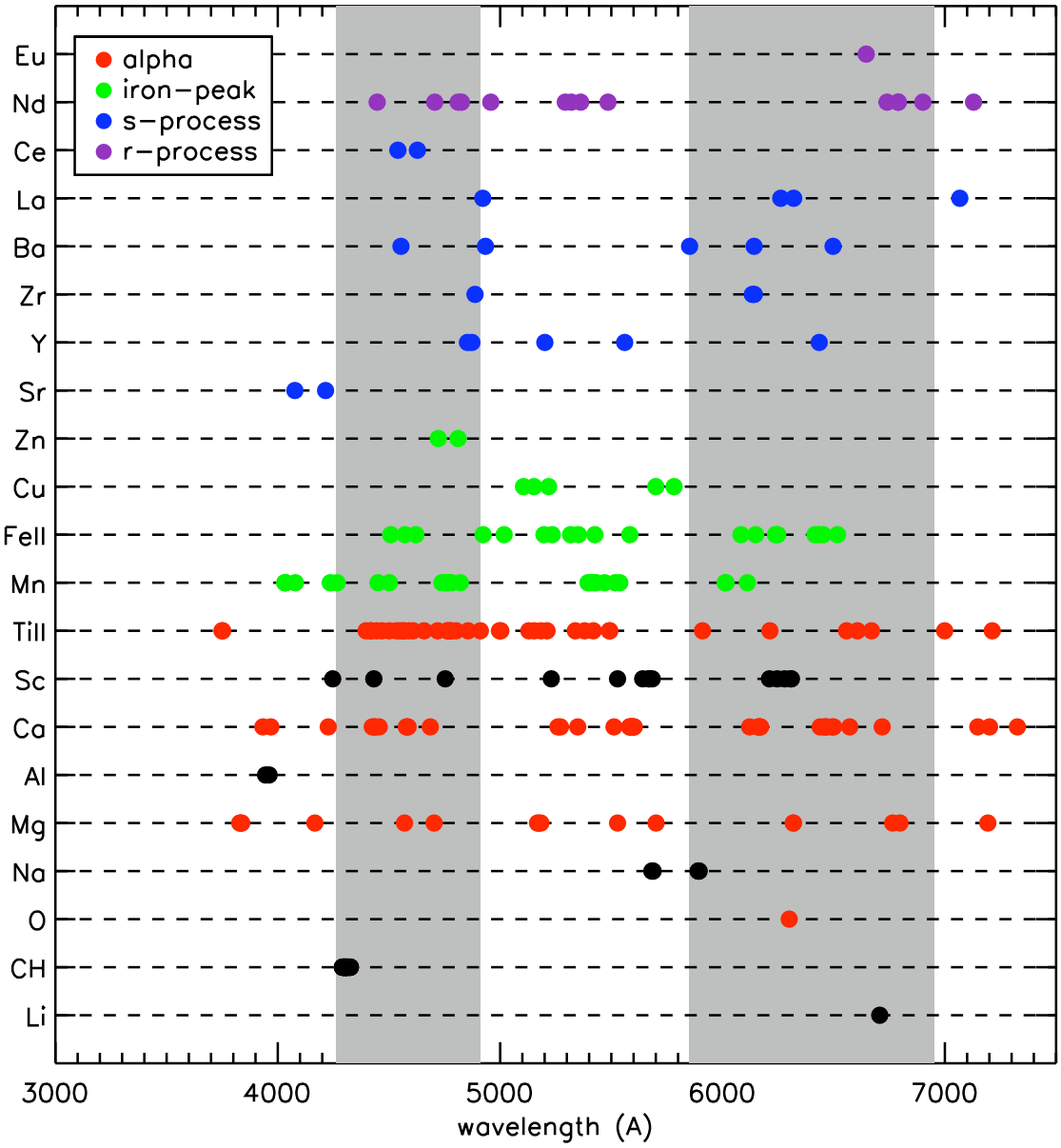

Figure 19: Schematic representation of the spectral diagnostics available for various elements in the ngCFHT Galactic Archaeology Survey. Note that these diagnostics are based on the synthetic metal-poor red giant spectrum shown in Figure 18; the available diagnostics will of course depend on the exact stellar target. Individual elements have been colour coded according to primary formation route: i.e., alpha, iron-peak, s– and r–process elements. The grey regions show the blue and red windows proposed for the primary, 10 000 deg^2 survey in high-resolution mode. For a subset ($\sim$ 10%) of this survey area, additional configurations high-resolution would be included to give complete spectral coverage over the optical regime for the purpose of ultra-precision chemical tagging.

Table 8: The Galactic Halo Survey: Principal Spectral Diagnostics

λ (Å)	Feature	Notes
Intermediate Resolution ($R \simeq 6\,500$), Blue Window (381 – 439 nm)		
3835, 3880, 3970,		
4101, 4340	H I	Balmer series
3933, 3968	Ca II	H, K
3883	CN	(band)
4320	CH	(band)
4077, 4215	Sr II	Resonance lines
4227	Ca I	Strong
Intermediate Resolution ($R \simeq 6\,500$), Red Window (770 – 889 nm)		
8542, 8600, 8662	Ca II	Calcium triplet
8806	Mg I	Gravity sensitive
High Resolution ($R \simeq 20\,000$) – Blue Window (∼426 – 491 nm)		
4554	Ba I	Critical; tests s/r, also 2nd peak s-process ratio.
4722, 4810	Zn I	Critical; tests metallicity dependent SNIa/AGB yields; line at 4722 weaker
4883, 4900	Y I	s process
		Also Nd (neutron capture), Sc& Mn (odd elements) and Ca, Ti & Mg (alphas)
High Resolution Survey ($R \simeq 20\,000$) – Red Window (585 – 675 nm)		
6300	O I	Critical
6645	Eu	Critical r-process
6707	Li	Unique
		Also Ba, La, Zr, Nd (s-process), Al, Mn, Na, Sc (odd elements), and Ca, Mg

it appears that to separate stars into groups associated with different chemical evolution by their abundance pattern requires a precision in the abundances of the order of 0.1 dex. For example, we are now becoming aware of the existence in the halo of stars with different [α/Fe] ratios but the same [Fe/H] (e.g., Bonifacio et al. 2011).

In addition to high-order abundance information, the unprecedented size of the stellar spectroscopic dataset for ngCFHT would facilitate detailed analysis of the metal-weak tail of the halo metallicity distribution function (MDF). This key observable has a direct bearing on models for the formation of the first stars, and on the dark baryonic content of galaxies. The first stars to be formed after the Big Bang were formed with the "primordial" chemical composition: i.e., hydrogen and helium, plus traces of lithium. A protogalactic cloud consisting of such a gas may have had difficulty in providing cooling mechanisms efficient enough to allow the formation of low-mass stars. Several theories on star formation postulate the existence of a "critical metallicity" below which only extremely massive stars can form (Bromm & Loeb 2003; Schneider et al. 2011 and references therein). Other theories invoke fragmentation to produce low-mass stars at any metallicity (Nakamura & Umemura 2011; Clark et al. 2011; Greif et al. 2011). The implication for the baryonic content of galaxies is obvious: if the first generation of massive stars that reionized the universe formed along with low-mass stars, a large fraction of these would now be present as old, cool white dwarfs (see §2.2). On the other hand, a small fraction of these (essentially those of mass less than 0.8 $M_\odot$) would still shining today and could be observed. If there is a critical metallicity, then the metal-weak tail of the MDF ought to show a sharp drop at this value. In Figure 21 the MDF derived from the Hamburg-ESO Survey (Schörck et al. 2009) is shown compared to several models for star formation at low metallicity. These models rely on dust cooling and fragmentation (Salvadori et al. 2007). Although a sharp drop does indeed appear around metallicity –3.5, many stars have already been discovered below this metallicity, the most metal-poor to date being SDSS J102915+172927 (Caffau et al. 2011) with a metallicity of –5.0 ($Z \leq 6.9 \times 10^{-7}$). Below [Fe/H = –3.5, the metallicity must be determined from high-resolution spectra since the metallic lines become too weak to measure at the resolution of $\mathcal{R} \sim 2\,000$ that has typically been used for this kind of work.

It is worth noting that the Hamburg-ESO MDF is based on only 1638 stars. The ngCFHT Galactic Archaeology Survey would represent close to the final word on this key issue by providing metallicities for a sample of several million stars at resolution $\mathcal{R} = 20\,000$. If ultra-metal-poor halo stars do indeed exist, then this extraordinary dataset would allow a complete characterization of the halo MDF down to [Fe/H] $\sim$ –7.

2.3.4.2 Key Science. B. The Evolution of the Galactic Disk

As noted above, the study by Eggen et al. (1962) established that stars of low metallicity have orbits that are eccentric compared with their metal-rich counterparts. This finding has been attributed to the rapid collapse of a proto-galactic

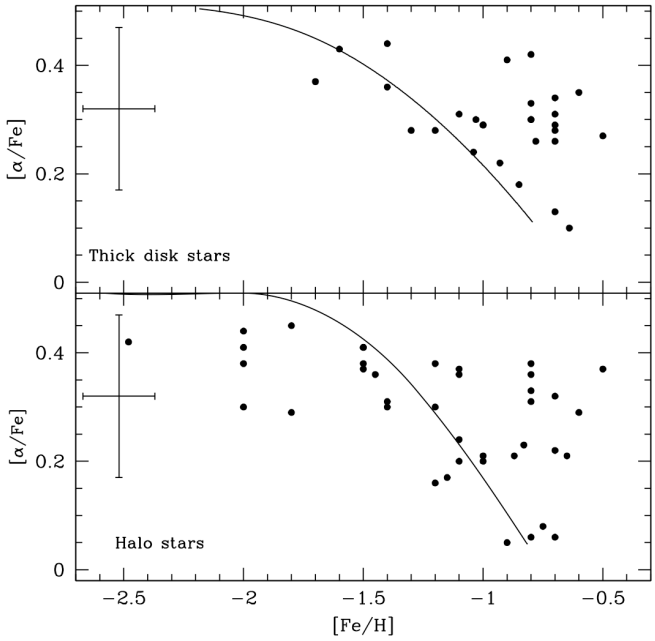

Figure 20: Diagram of [α/Fe] vs. [Fe/H] from Smiljanic et al. (2009). Results for thick disk stars are shown in the upper panel, while the halo stars are shown in the lower panel. The curves are model predictions from Valle et al. (2002). Accurate chemical abundances make it possible to discriminate between different populations. In the case of the halo and thick disk, it would be possible to identify and study individual streams.

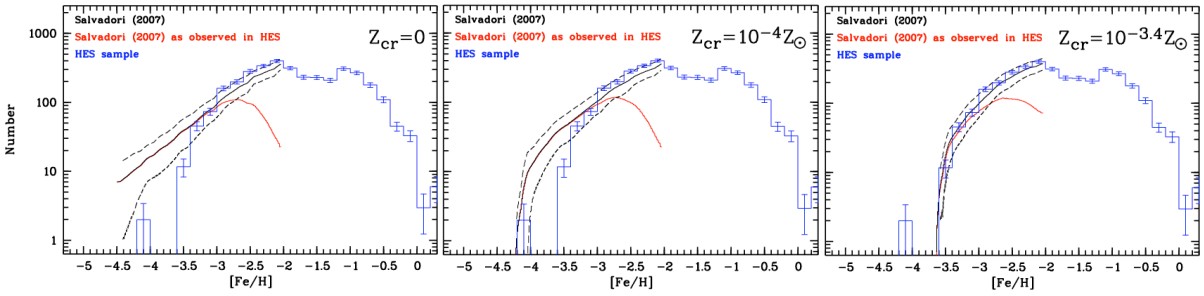

Figure 21: The halo star metalllicity distribution function from the Hamburg-ESO Survey (blue histogram) compared with the theoretical models of Salvadori et al. (2007) having different values of the critical metallicity. Figure from Schörck et al. (2009).

cloud that ultimately formed the (metal-poor) halo, with the rotationally-supported, metal-rich disk component forming afterwards. As a result of gas concentration, disks continued to evolve and form stars over the last 9–10 Gyrs, with the result that stellar metallicities in the disk span the range from about [Fe/H] ~ -1.0 to $\sim +0.4$ dex. Until very recently, it was believed that the chemical evolution of the halo merged seamlessly with that of the disk. In fact, the chemistry in the halo stars is dominated by SN II products, unlike the disk, where SN Ia contribute significantly. The transition occurs at about [Fe/H] $\sim$ –1.0. However, the simplistic view of the Galaxy formation through a halo, disk and bulge was somewhat complicated by the discovery of a fourth component known as the thick disk (Gilmore and Reid 1983). Today, we understand that the disks are an integral part of galaxy formation, with recent surveys having shown that thick disks are present in most disk galaxies (see, e.g., Yoachim & Dalcanton 2008 and references therein). Understanding the origin of the Galactic thick disk, and its connection to the other Galactic components, is intimately connected to the bigger question of how galaxies form and evolve (e.g., Freeman 1987; Majewski 1993; Freeman & Bland-Hawthorn 2002).

Until recently, there were important questions regarding the nature of the thick disk and its connection to the young disk. Is the thick disk a distinctive component from the thin disk? If so, how did its formation proceed? There continues to be progress towards answering such questions; for instance, the Hipparcos astrometric data on about 100 000 nearby stars provided a great opportunity to study disk stellar populations in more detail. Within the disk, many subgroups were identified, including some stellar streams. In the case of thick disk component, a more precise kinematic definition was established. High-resolution spectroscopic surveys (Fuhrmann 1998, Reddy et al. 2003, 2006, Bensby et al. 2003, 2004, 2005) for a couple of hundred stars yielded the following kinematic definitions (all in km s^{-1}):

$$\begin{aligned} \text{thin disk}: &\quad V_{\rm lag} = -12 \quad \sigma_{\rm u},\ \sigma_{\rm v},\ \sigma_{\rm w} = 39, 20, 20 \\ \text{thick disk}: &\quad V_{\rm lag} = -51 \quad \sigma_{\rm u},\ \sigma_{\rm v},\ \sigma_{\rm w} = 63, 39, 39 \\ \text{halo}: &\quad V_{\rm lag} = -220 \quad \sigma_{\rm u},\ \sigma_{\rm v},\ \sigma_{\rm w} = 131, 106, 85 \end{aligned} \tag{1}$$

[See Dehnen & Binney 1998; Robin et al. 2003)]. Abundance results showed that thick disk stars are generally old (10-013 Gyr) and metal-poor, and their α–element abundances are higher than those of their thin disk counterparts at fixed metallicity. These results have led to a significant rethinking of earlier models of rapid or dissipative collapse, supporting instead a scenario of repeated, hierarchical mergers.

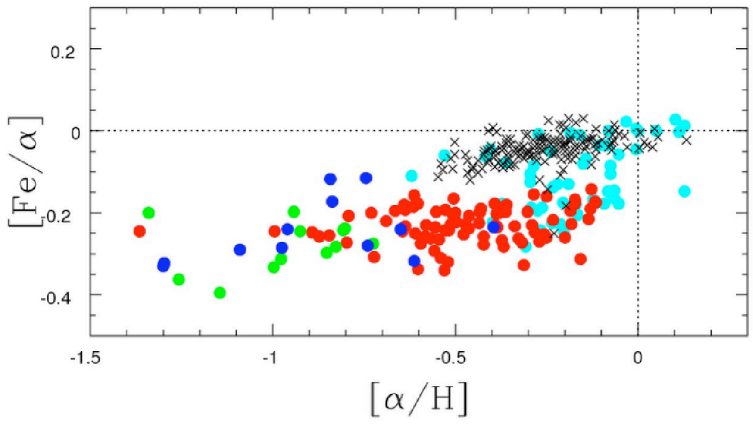

Figure 22: The fossil record of chemical evolution in the Galactic disk, from Reddy (2010). Thick disk and thin disk stars are shown as red circles and black crosses, respectively.

However, there remain important gaps in our understanding of thick disk component and its overall connection to the Galactic disk. For example, we do not know for sure the complete metallicity range of thick disk stars, which is quite important in understanding the kind of star formation and enrichment history it underwent. There are reports that the thick disk is not just a "frozen" entity within the disk, but had itself an active star formation history (Bensby et al. 2007; Reddy 2010). There are efforts underway to define the extreme ranges in metallicity of the distinct components: i.e., metal-weak, thick disk stars vs. metal-rich, thick disk stars. But, at present, such studies are limited by the lack of accurate astrometry, a problem that will soon be solved by the Gaia mission. The complexity of the

problem is illustrated in Figure 22 which summarizes the current picture of the Galactic disk chemical evolution. Thin disk stars are represented by black crosses and thick disk stars by filled red circles. The blue and green symbols represent stars of halo and the metal-weak thick disk as defined in the study of Reddy & Lambert (2008). The most intriguing aspect of the observed relation are the stars represented by light blue circles. Some of these stars have kinematics that are similar to thick disk but with thin disk abundances; a few of them have intermediate thick and thin disk chemistries. This finding suggests that the disk is a complex structure with its multiple subcomponents having chemical properties that reflect disk formation at different epochs.

Despite decades of study, the primary mechanism for formation of the thick disk remains elusive. Partly, this may be due to the incomplete observational data (i.e., astrometry and high-resolution spectroscopy). However, results from the Hipparcos mission and high-resolution spectroscopic surveys have inspired a number of hybrid scenarios for Galaxy formation and evolution (e.g., accretion plus secular heating of the existing thin disk, and *in situ* formation due to gas-rich mergers and radial migration. Needless to say, such models require more complexity to explain the observations. The observed flat radial metallicity gradient of the thick disk is not expected in the case of an accretion scenario of stars from disrupted satellites (e.g., Abadi et al. 2003). Likewise, pre-heating of an existing thin disk through a minor merger (e.g., Quinn, Hernquist & Fullagar 1993) cannot explain the flat metallicity gradient either, and the theory needs the pre-existing thin disk to have a flat metallicity gradient as well (Bekki & Tsujimoto 2011). The observed higher Vϕ values at metal rich end of the thick disk (Lee et al. 2011) are not expected in the case of minor merger scenario (see Bekki & Tsujimoto 2011) while radial migration of stars by spiral arms (e.g; Schönrich & Binney 2009) has also been proposed as an explanation of the observables, but the details are still being worked out. In a series of papers, Brook et al. (2007 and references therein) proposed the formation of the thick disk through heating of the thin disk by gas-rich mergers. If correct, this could explain the higher [α/Fe] and the flat metallicity gradient. Rapid star formation ensures higher [α/Fe] even at higher metallicities with significantly older age compared with thin disk stars having similar metallicities. Models also predict very low velocities for the merged stars and some are expected to show counter-rotation. Simulations do not predict the observed drop in [α/Fe] which is the telltale signature of SN Ia contributing to thick disk chemical enrichment. Mn abundance trends also point to SN Ia contributions.

Most of the current high-resolution spectroscopic studies are limited to stars in the immediate solar neighbourhood (within 100–200 pc). Locally, only 5–6$\%$ of the stars are associated with the thick disk, and fewer still belong to the halo ($\sim$ 1$\%$). The remaining stars belong to the thin disk. Whereas the astrometry from Hipparcos was limited to these relatively nearby stars, the Gaia mission will provide accurate astrometry for about one billion stars distributed over the entirety of the Galaxy. While this mission promises to revolutionize our understanding of the Galactic disk and its subcomponents, Gaia requires detailed abundances and precise radial velocities for its faintest targets in order realize this potential. For instance, beyond $z = 1$ kpc, the thin disk population is reduced dramatically compared to the thick disk population. Reaching these faint limits for *in situ* studies of the thick disk population will require a comprehensive, high-resolution spectroscopic survey, covering thousands of square degrees, using a dedicated 10m-class telescope. The ngCFHT Galactic Archaeology Survey would be the definitive resource for exploring the formation and evolution of the Galactic disk and its subcomponents.

Key Science. C. Formation of the Galactic Bulge

Whereas dissipation was likely not important for the Milky Way's stellar halo, the disk is certainly a highly dissipated structure. The bulge, on the other hand, may be somewhere in between. It is a small box-shaped structure, and its stars are now known to mostly old ($\sim$ 12 Gyr). Because of highly influential CDM simulations, the bulge was long believed to have formed through the mergers of our Galaxy with other smaller systems. During the last decade, though, new observations and N-body simulations have made it clear that the boxy/peanut-shaped bulges that are commonly seen in later-type spiral galaxies like the Milky Way are actually barred systems viewed edge on (e.g., Athanassoula 2005). Thus, it now seems much more likely that the Galactic bulge formed as a result of bar-forming and bar-buckling instabilities in the early disk. The subsequent growth and evolution of the bar/bulge depends on angular momentum transfer between the bar and the nearby dark matter halo. In this way, the formation and evolution of the bulge are closely related to both the inner disk, and the inner regions of the Milky Way's dark halo.

Although the dynamics of this bulge-formation process is well understood theoretically, its observational underpinning is only now starting to be developed. The theory makes detailed predictions about the interplay between chemical element abundances and kinematics, and these need to be tested in detail by chemical and kinematical observations for large numbers of stars throughout the bulge and the surrounding disk. High-resolution observations are needed

to measure a range of elements produced by nuclear processes that have distinct timescales and locations (i.e., SN II, SN Ia, AGB stars). In this way, it will be possible to understand the star formation history that occurred before, and during, the formation of the bulge.

The data available already from medium-resolution surveys show that the bulge has the characteristic cylindrical rotation pattern predicted by the disk instability picture (e.g., Howard et al. 2009). It has so far been difficult to determine whether there is also a minor merger-generated, "classical" bulge component. This is an important unknown, because it would affect our understanding of the early evolution of the inner Galaxy. Stellar kinematics alone cannot answer this question because a small, classical bulge is rapidly spun up by the torque of the bar/bulge, and its kinematics become indistinguishable from those of the main bar/bulge itself (Saha et al. 2012). Again, we must depend on detailed chemical studies for many elements in order to identify the presence of a separate, classical bulge component.

Results to date from medium-resolution, spectroscopic studies of the bulge have been tantalizing. Simulations show that the first stars to have formed in our Galaxy are likely to be found today in the bulge region (e.g., Diemand et al. 2005). They are expected to be in the bulge region but are not part of the bulge itself. They formed in small overdensities in the early universe before the Galaxy itself had formed, and were subsequently accreted by the Galaxy. Recent medium-resolution surveys of the bulge, like the ARGOS survey (Freeman 2012), have identified a population of metal-poor stars in the bulge region with metallicities as low as [Fe/H] $= -3$. These are candidates for the first stars. Detailed high resolution studies of these stars are needed to determine whether they are chemically different from the stars of the inner halo which are also expected to be found in this region.

High-resolution spectroscopy of bulge giants enables study of elements from a wide range of element groups (i.e., light elements, alpha elements, Fe-peak and n-capture elements; see also Figure 19). The targets would all be giant stars, and indeed there is no real astrophysical benefit in studying giants fainter than the dominant red clump ($M_V \sim 0.5$). Such studies would provide much more insight into the formation and chemical evolution of the bulge than is available from the limited current data for large medium-resolution surveys which give only Fe, Al and α-element abundances. For example, the ARGOS survey with the AAT at resolution $\mathcal{R} = 11\,000$ has already observed $\sim 28\,000$ red clump giants in the bulge and inner disk: see Figure 23).

While a small volume of high-resolution optical spectra can be acquired with existing telescopes, it is not possible to observe the large numbers of stars ($\sim 50\,000 - 100\,000$) that are needed to get the full picture of element distributions throughout the bulge and inner disk. A wide-field, high-resolution facility capable of reaching the clump stars throughout the bulge ($g \sim 18$) is essential to attack this problem. Note that ongoing high-resolution infrared surveys like APOGEE will provide more accurate data for iron and the α-group elements in the brightest giants, but cannot access the crucially diagnostic heavy n–capture elements.

A high-resolution bulge survey, which would be possible with the 10m ngCFHT, would provide especially good complementary information to Gaia data for bulge stars since spectra would enable better distance estimates than will likely be possible with Gaia for red clump giants in high-density bulge fields.[12] This is because the high-resolution data would allow much more accurate *spectroscopic* estimates of the stellar $\log g$ and $T_{\rm eff}$, and, hence, more accurate isochrone distances. These spectroscopic distance estimates are essential for unraveling the structure of the bulge; the distance errors from medium-resolution spectroscopy are about 0.9 kpc for clump giants and about 3 kpc for the brighter giants. These errors are significant relative to the scale of the bar/bulge (~ 3 kpc). Higher spectral resolution would reduce the distance uncertainties to a much more useful level of 0.7 kpc, all along the giant branch.

What bulge science would be enabled with ngCFHT that is not possible now? The high resolution survey competition has been discussed previously; all except VLT (FLAMES), VLT(UVES) and the proposed VLT(MOONS) instrument are on smaller telescopes. The former two instruments cannot compete in terms of multiplexing ability with ngCFHT, whereas the latter is similar, but with a much smaller field ($\sim$ 1/10th that of ngCFHT). The niche for ngCFHT, therefore, is a large-scale, high-resolution survey of bulge stars in the northern bulge — a region that is readily accessible from Mauna Kea, at a declination of $\delta \simeq 19\overset{\circ}{.}8$ (see Figure 23). The fibre density of ngCFHT is also well matched to the requirements of this survey; the density of red clump giants in the bulge fields shown in Figure 23 is high, and there will be plenty of stars within the 1.5 deg^2 field to assign all 800 fibres. Accurate element abundances (i.e., with uncertainties of ~ 0.1 dex) require S/N ≥ 100, which is achievable for stars with $g \leq 18$ in $\sim$ a 1-hour exposure. Thus, it would be straightforward to integrate this bulge survey into the main Galactic Archaeological Survey described above.

The observational goal of this bulge survey would to measure abundances for a wide range of elements for stars in the bulge and the surrounding inner disk. The scientific aim is to understand the chemical evolution of the inner

[12] As the APOGEE survey has shown, the much of the Galactic bulge is readily observable from the north: i.e., seen from Mauna Kea, the Galactic centre lies at an airmass $X \geq 1.5$ for up to 7 hours per night during the summer (see Figure 23)

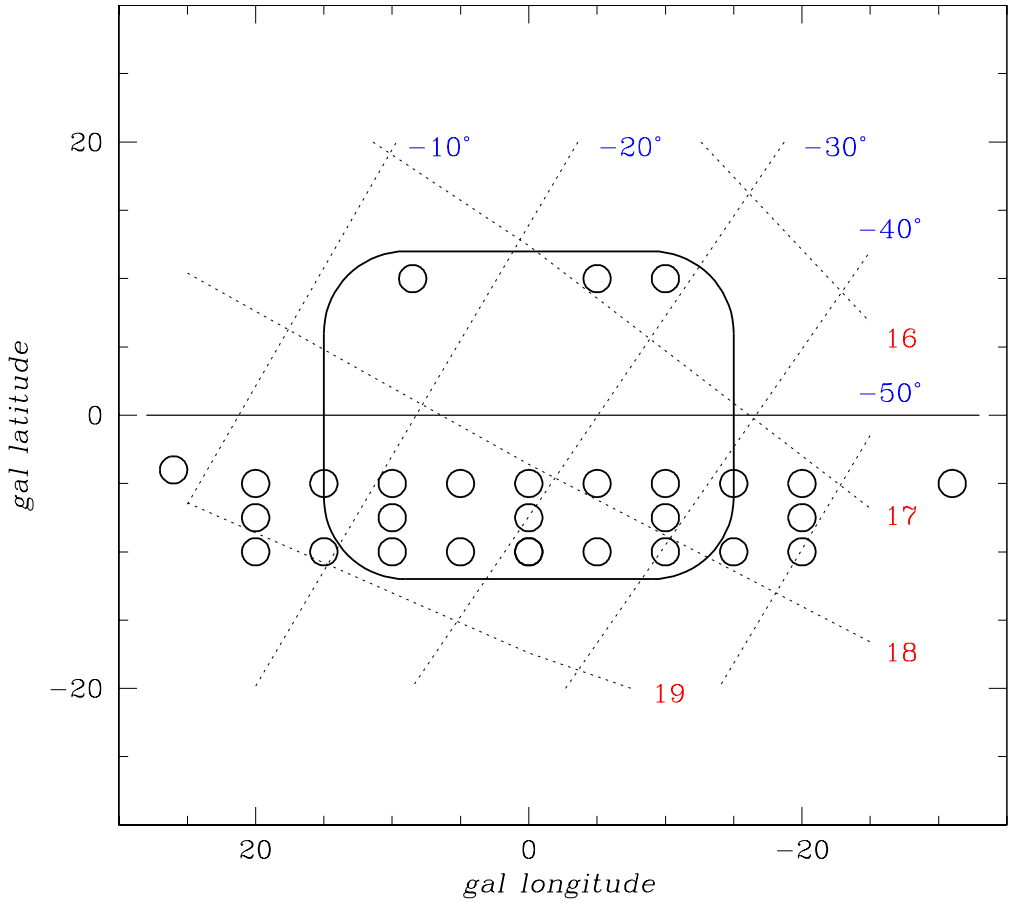

Figure 23: The circles show fields for the ARGOS survey, which were chosen to have reddening E(B-V) $\lesssim$ 0.5 mag. The central box shows the approximate boundary of the bulge. Lines of constant right ascension (red numbers) and declination (blue numbers) are also shown. Much of the northern bulge is readily accessible from Mauna Kea.

Galaxy within the context of the bulge formation event and its subsequent evolution. It was clear from the medium-resolution ARGOS survey that 28 000 stars is not enough to characterize properly MDF variations over the bulge. To investigate the detailed complexities of the MDF in the inner Galaxy, a sample of *at least* $50,000 - 100,000$ stars is needed, covering the accessible regions of both the bulge and the inner disk. The wide field of ngCFHT and its large number of fibres make it possible to consider a survey on this scale. It would be a landmark step forward in assessing the chemical state of the inner Galaxy.

Finally, the high-resolution spectra would allow accurate radial velocities measurements that could be useful for detecting very cold kinematic substructures in the inner galaxies (if such substructures are present). These would be either likely relics of gas infall and star formation in the inner Galaxy, or debris of small, dense galaxies accreted by the Milky Way. A high-resolution survey on this scale may also allow the chemical tagging of dispersed substructures that are no longer visible kinematically.

Future Considerations I. Higher Spectral Resolution Although the discussion above outlines a unique and important role that ngCFHT could play in testing bulge formation scenarios, we note here that there are significant science gains to be achieved by implementing an even higher resolution mode of $\mathcal{R} \simeq 45\,000$. Such an extension in capabilities needs to be studied in the context of all science cases and instrument functionality, but the added costs may be acceptable if the scientific gains and legacy benefits are improved significantly. The limiting magnitude of the resulting survey need be no more than about 0.5 mag brighter: a 1 hour exposure at $g = 18$ would give SN = 95 at $\mathcal{R} = 45\,000$.

Resolutions of $\mathcal{R} \sim 20\,000$ have been demonstrated to be relatively easily achievable while enabling a great swath of science (as shown throughout this document). Furthermore, the stellar research being done at ESO with the FLAMES/GIRAFFE system to observe stars in the Milky Way, LMC and dwarf spheroidal galaxies is a good

illustration of this strategy for chemical studies in the bulge. Of course, $R \sim 20,000$ has its limitations for some scientific questions, primarily due to line blending in metal-rich stars, which are a major component of the Galactic bulge (and the disk). This blending makes it difficult to perform accurate measurements of the weak lines of most of the n–capture elements. Most of the recent, high-quality comprehensive chemical studies have been done with higher-resolution systems (e.g., VLT/UVES, Keck/HIRES, Magellan/MIKE), all of which offer resolutions of $\mathcal{R} \sim 45\,000$. The advantage of the higher resolution is that more elements can be measured, and the precision of the element abundances is significantly better. These higher-resolution spectra can also provide a superior radial velocity accuracy for preliminary Doppler planet search studies (see §2.2). Other applications, such as detailed studies of damped Ly-α and Ly-forest absorption systems in quasar spectra, and studies of the ISM, could also be improved with the implementation of such an observing mode (see §2.1 and §2.7).

Future Considerations. II. A Near-IR Capability

For Galactic studies, there is also a case for a near-IR, high-resolution, multi-object capability in the H-band, as pioneered by the APOGEE project. The H-band has a double advantage of reduced line blending in the spectra of cool, metal-rich stars and lower interstellar extinction.[13] The H-band is thus well suited to studies of abundances and kinematics in low latitude fields in the Galactic disk and bulge. From existing optical bulge surveys, like the ARGOS survey, it is clear that the abundances and kinematics in bulge regions change with position. Data in the low-b, highly reddened fields are important for understanding the details of how the Galactic bulge formed. The capability of H-band spectroscopy would therefore be very attractive for aspects of bulge science which are otherwise out of reach.

The disadvantage of the H-band is that there are few lines of n–capture elements in this band. Although some of the near-IR bulge science will be done by APOGEE using the brightest cool stars, and some can be done by the relatively narrow-field MOONS instrument (if approved), the low-latitude, inner disk and bulge provide some real opportunities for a large-scale, near-IR spectroscopy of giants. One vital science issue is to understand how the MDF changes with position in the bulge and the inner disk at low Galactic latitudes. There is no other instrument on the horizon that could perform the required observations. Note that fainter giants are required because the brightest stars provide a chemically biased sample and are not suitable for this study. As part of the future development of ngCFHT, an extension to longer wavelengths should be investigated vigorously from both the scientific and technical perspectives.

[13] While lower extinction is certainly important for the bulge and some parts of the Galactic disk, it is also true that only a small ($\sim 5\%$) fraction of the sky suffers from an extinction of $A_V \sim 1$ mag or more.

2.4 The Local Group

2.4.1 Abstract

The collection of galaxies in the immediate vicinity of the Milky Way — the Andromeda Galaxy, Triangulum, and the $\sim$ 70 dwarf galaxies that constitute the "Local Group" — are the nearest examples of galaxies spanning a wide range of morphological types. Generally speaking, they are the only galaxies in the Universe — aside from the Milky Way itself — for which individual stars can be observed from the ground. As such, these nearby systems offer unique insights into galaxy formation and evolution. Because they subtend large angles on the sky and consist of a multitude of stars that are, individually, quite faint, both the wide field and 10m aperture of ngCFHT are essential for their study. Here, we describe a number of key ngCFHT science projects for Local Group galaxies along with their top level science requirements. These include the chemodynamical deconstruction of $L^\star$ and sub-$L^\star$ galaxies, the characterization of the outer dark matter profiles and tidal interaction histories of dwarf galaxies, and derivation of the chemical enrichment histories of Galactic satellites.

2.4.2 Introduction

Over the next decade, we can expect that some of the most significant discoveries in cosmology and astrophysics will come from detailed studies of Local Group galaxies. Today, wide-area photometry from surveys like SDSS or the Pan-Andromeda Archaeological Survey (PAndAS; McConnachie et al. 2009) can map the halos of our own Galaxy (Belokurov et al. 2006) and that of M31, while "pointed" observations from programmes using Subaru/SuprimeCam or CFHT/MegaCam can disentangle the stellar populations of individual dwarf galaxies. When combined with low-resolution spectroscopy (radial velocities), medium-resolution spectroscopy (metallicities, alpha-abundances and basic stellar parameters), and/or high-resolution spectroscopy (individual chemical abundances), it is possible to extract a wealth of information relating to galaxy internal structure, star formation history, and chemical evolution (as well as the complex interplay between these three). Nowhere else in the universe can we hope to obtain such a detailed view of galaxy evolution.

In the coming years, there are plans for a number of ambitious, large-scale photometric surveys in which "near-field cosmology" figures as a key theme; for Local Group science, the principal obstacle to fully realizing the potential of these surveys is the lack of comprehensive spectroscopic follow up. Because Local Group galaxies generally subtend large angles on the sky and consist of individually faint stellar targets that are beyond the reach of spectrographs on 4m-class telescopes, both a wide field of view and an 8m- to 10m primary aperture is needed. Existing 8m-class spectrographs such as VLT/FLAMES, Keck/DEIMOS or Gemini/GMOS have made good progress in some aspects of these science cases (see the recent review by Tolstoy et al. 2009), but are limited in both their degree of multiplexing and the mismatch between their fields of view (usually measured in arcminutes) and the extent of the nearest galaxies (which often extend over scales of degrees).

Spectroscopic studies of resolved stellar populations are expected to be a major science driver for ngCFHT. Stellar astrophysics and stellar populations in the Milky Way have been discussed in §2.2 and $2.3, so here we focus on the remaining galaxies in the Local Group, as these constitute the majority of galaxies in the universe for which spectroscopy of individual stars is possible with a 10m-class facility. Celestial coordinates for the 75 galaxies that are currently known to make up the Local Group are shown in an Aitoff projection in Figure 24. The first panel shows the known satellites of the Milky Way in red, while the second panel shows all remaining Local Group galaxies, with the M31-system in blue and "isolated" galaxies in green.

2.4.3 ngCFHT in Context: Competition and Synergies

Over the past decade, significant research time and observing resources have been devoted to characterizing the structure and chemodynamics of the closest galaxies. This has been partly spurred on by a string of new discoveries, in the SDSS, of previously unknown Galactic satellites: both globular clusters and faint dwarf galaxies (e.g., Willman et al. 2005ab; Belokourov et al. 2006). Spectroscopy of their constituent stars has, in some cases, revealed large velocity dispersions that imply these objects could be the most dark-matter-dominated systems in existence (Martin et al. 2007; Simon & Geha 2007).

Very wide field photometric surveys such as the SDSS provide the necessary data for the discovery of new Milky Way satellites; deeper and more accurate photometric studies of their stellar populations requires the wide field capabilities of 4m- and 8m-class telescopes. In particular, CFHT/MegaCam, Subaru/SuprimeCam and other instruments have

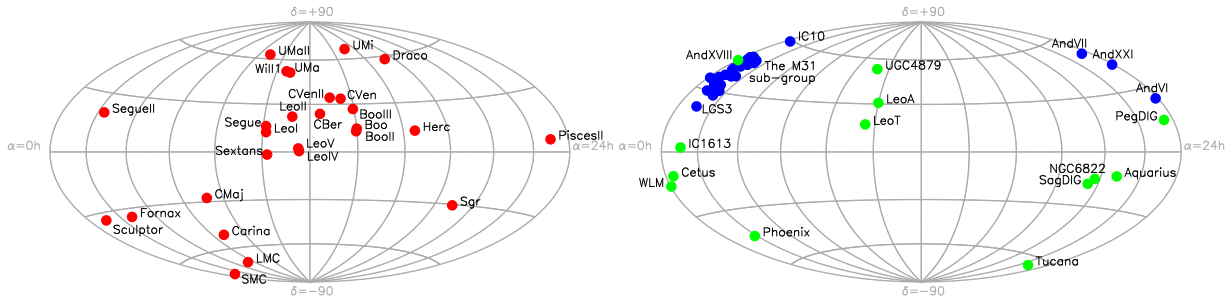

Figure 24: Aitoff projections of the Celestial coordinates of all galaxies in the Local Group. The left panel shows the Galactic satellites (red), while the right panel shows M31 sub-group galaxies (blue) and isolated Local Group galaxies (green).

played key roles in obtaining deep, photometric follow-up observations. In the future, PanSTARRS/PS1, SkyMapper, Euclid, LSST and the Subaru/HSC Strategic Survey will likely provide the data in which new Milky Way and Local Group dwarfs (at least for LSST and HSC) will be discovered. Imaging that is deep enough to supply stellar targets for spectroscopy with 8m-10m-class telescopes is already in hand for every known dwarf galaxy, or can be easily obtained with current or future wide-field cameras. For M31, the PandAS survey with CFHT/MegaCam provides the necessary data out to 150 kpc for M31 and M33. Probing this galaxy to still larger radius would be possible with either CFHT/MegaCam or, more easily, with the forthcoming Subaru/HSC instrument. We note that although foreground contamination from dwarf stars will likely be significant in sparse fields in M31 and in some dwarf galaxies, the multiplexing gain of ngCFHT would ensure high completeness for genuine members in any field.

Spectrographs that are currently used for studies of this sort include Keck/DEIMOS, VLT/FLAMES(GIRAFFE), VLT/FLAMES(UVES) and Magellan/MMFS. Their primary limitation is often either field of view and/or level of multiplexing; for the closer galaxies that subtend larger areas on the sky, and for which there are more bright targets, the limited fields of view and multiplexing are not ideal for richly populated galaxies (and this is particularly true at high resolution, where one would like to take advantage of their proximity to get high order abundance information). For more distant galaxies, increased throughput would be greatly beneficial. For the M31 and M33 galaxies, the field size of any of existing $\sim$ 8m-class spectrograph is inadequate for a comprehensive spectroscopic survey.

For spectrographs that are on the immediate horizon, the primary competition will come from Subaru/PFS[14] As a facility instrument, it is not yet clear how much time PFS will have to devote to studies of stellar populations, but it is clear from the recent summary of the PFS design by Ellis et al. (2012) that they are contemplating a survey of 65 deg^2 surrounding M31, building on the photometric survey of PAndAS and possibly HSC. PFS will work at a resolution of around $R \sim 2\,000$ at optical wavelengths, and will obtain complete spectral coverage over the 0.38–1.3 μm range. For data with reasonable S/N, analyses such as those performed by SDSS/SEGUE suggest this will be good enough to derive a global [Fe/H] measurement accurate to a few tenths of a dex, an estimate of [α/Fe], as well as T$_{eff}$ and log g estimates, in addition to velocity estimates to accuracies of order $\sim$ 10 km s^{-1}.

Given the possibility that PFS may be used for resolved stellar population studies in M31 — and potentially in any of the northernly ($\delta \gtrsim -30^\circ$) dwarf galaxies as well — it is natural to ask what role ngCFHT might play. We propose the following requirements to ensure maximal ngCFHT impact in the field of Local Group research:

- ngCFHT should operate at a resolution of $\mathcal{R} \sim 6\,000$ with very broad wavelength coverage (similar to $\mathcal{R} \sim 2\,000$ mode), for all 3200 objects. Ultimately, a resolution of $R \sim 2000$ is sub-optimal for studies of the more distant Local Group galaxies, as numerous studies using Keck/DEIMOS and other instruments have amply shown. For dwarf galaxies and stellar halos, a nominal velocity resolution of 10 km s^{-1} is the same or larger than the expected velocity dispersions of the dwarf galaxies and stellar streams; thus, an optimal kinematic study should aim for resolutions of a few km s^{-1}. In terms of chemistry and metallicity, the higher resolution allows for much more accurate determination of the same quantities than $\mathcal{R} \sim 2\,000$, and in the future may offer possibilities for extracting some additional abundance information, based on techniques similar to those pioneered by E. Kirby and collaborators (e.g., Kirby et al. 2008a). The higher resolution will also make measurement of the equivalent widths of individual features easier, especially if wavelength range is limited. This is of particu-

[14] All 4m class facilities are seriously limited in their ability to study all but the very brightest (i.e., youngest) stars beyond the Milky Way.

lar importance for gravity-sensitive indicators to enable good dwarf/giant separation — a key ability for sparse fields.

- A significant fraction of ngCFHT time should be available for "key programmes" such as those discussed below. This capability is important since PFS will likely not be able to perform multiple, long-term, dedicated observing programmes due to time pressures on Subaru.

2.4.4 Legacy Science

We now highlight two high-impact studies that ngCFHT could undertake to study chemodynamical aspects of galaxy evolution using the resolved stellar content of Local Group galaxies. Note that both of these programmes address a multitude of interrelated science goals that are, when considered collectively, transformational in scope compared with present-day studies.

2.4.4.1 A Chemodynamical Deconstruction of $L_\star$ and sub-$L_\star$ Galaxies

Table 9: Technical Requirements and Survey Implementation: A Spectroscopic Survey of the M31-M33 Subgroup

Survey Area (Ω)	The M31-M33 subgroup: $\Omega \approx 350$ deg^2.
Field Location	$\alpha_{2000} \simeq 15^\circ$, $\delta_{2000} \simeq 42^\circ$
Number of ngCFHT Fields ($N_{\rm field}$)	$N_{\rm field} = \Omega/{\rm FOV}_{\rm ngCFHT} \approx 240$ for complete areal coverage of M31 and M33.
Number of Configurations per Field ($n_{\rm config}$)	$\langle n_{\rm config} \rangle = 1 - 10$, a strong function of radius and magnitude limit (central regions)
Total Number of Exposures ($N_{\rm exp}$)	$N_{\rm exp} = N_{\rm field} \times \langle n_{\rm config} \rangle \approx 240$ (minimum)
Primary Imaging Resources for Target Selection	CFHT/MegaCam PAndAS Survey; possibly Subaru/HSC for outer regions; possibly HST/PHAT for some of M31 disk
Observing Conditions	Mostly dark time. Cloud cover $< 20\%$.
Instrumental Configuration(s)	[All observations taken as part of PI-style programme] (1) $\mathcal{R} = 6000$ $T_{\rm exp} \sim 1$ hr; all fields except for main disks (2) $\mathcal{R} = 20000$ $N_{\rm point} = 1$, $T_{\rm exp} = 6$ hr (young stars in main disks)
Wavelength Coverage and Velocity Precision (ϵ_v)	(1) 0.40–0.95μm (ideal; window of a few hundred nm around CaT absolute minimum) and $\epsilon_v \approx 5$ km s^{-1} at $\mathcal{R} = 6000$ (2) Wavelength range same settings as for Milky Way surveys at high resolution; velocity precision $\epsilon_v \approx 5$ km s^{-1} at $\mathcal{R} = 20000$
Limiting (point source) Magnitude	$g_{\rm AB} > 23.0$, corresponding to at least the top half magnitude of TRGB ($\mathcal{R} = 6000$ only).
Total Time Needed for Program ($T_{\rm tot}$)	$T_{\rm tot} >$ [1×(238×1 hr) + (2×6 hr)] + 20% overhead ≈ 300 hrs.

During the coming decade, the astrophysics community will witness a revolution in the amount and quality of high-resolution multi-wavelength data on large galaxies and their constituent components — the result of massive international infrastructure investments in space- and ground-based observing facilities. Of particular importance to the Local Group research theme will be the launching of the Gaia satellite (currently scheduled for 2013). Gaia, ESA's sixth cornerstone mission, will provide unprecedented astrometric measurements with the accuracies needed to produce a stereoscopic and kinematic census of about one billion stars in our Galaxy and throughout the Local Group. Radial velocity measurements and chemical information will also be provided by onboard instruments. This dramatic advance in our ability to map the six-dimensional phase-space structure of a galaxy will likely usher in a "Golden Age" of Milky Way and Local Group research. However, although Gaia (with complementary information from many other multi-wavelength surveys) will provide a very detailed view of the structure and dynamics of our Galaxy, this information will have to be put into context by comparing the results with observations of other galaxies. This will allow us to ascertain the relative importance of cosmic variance, environment, merger history, mass, etc, in the evolution of galaxies. Without this essential complementary information, any conclusions that we may draw about the process of galaxy formation from observations of the Milky Way would be premature.

It is in this context that we must consider next-generation studies of the large Local Group galaxies, M31 and M33. These galaxies represent the obvious stepping stones between our highly detailed description of the Milky Way, and the low-resolution studies of more distant galaxies, in the realm of a few Mpc and beyond, where we can obtain significant samples of galaxies (as a function of galaxy type, environment, mass, etc). By $\sim$ 2020, M31 and M33 will have been studied in detail by many existing and imminent instruments/observatories. Nevertheless, a gaping chasm in our understanding of these structures will remain: i.e., their kinematics and chemistry from resolved stellar populations.

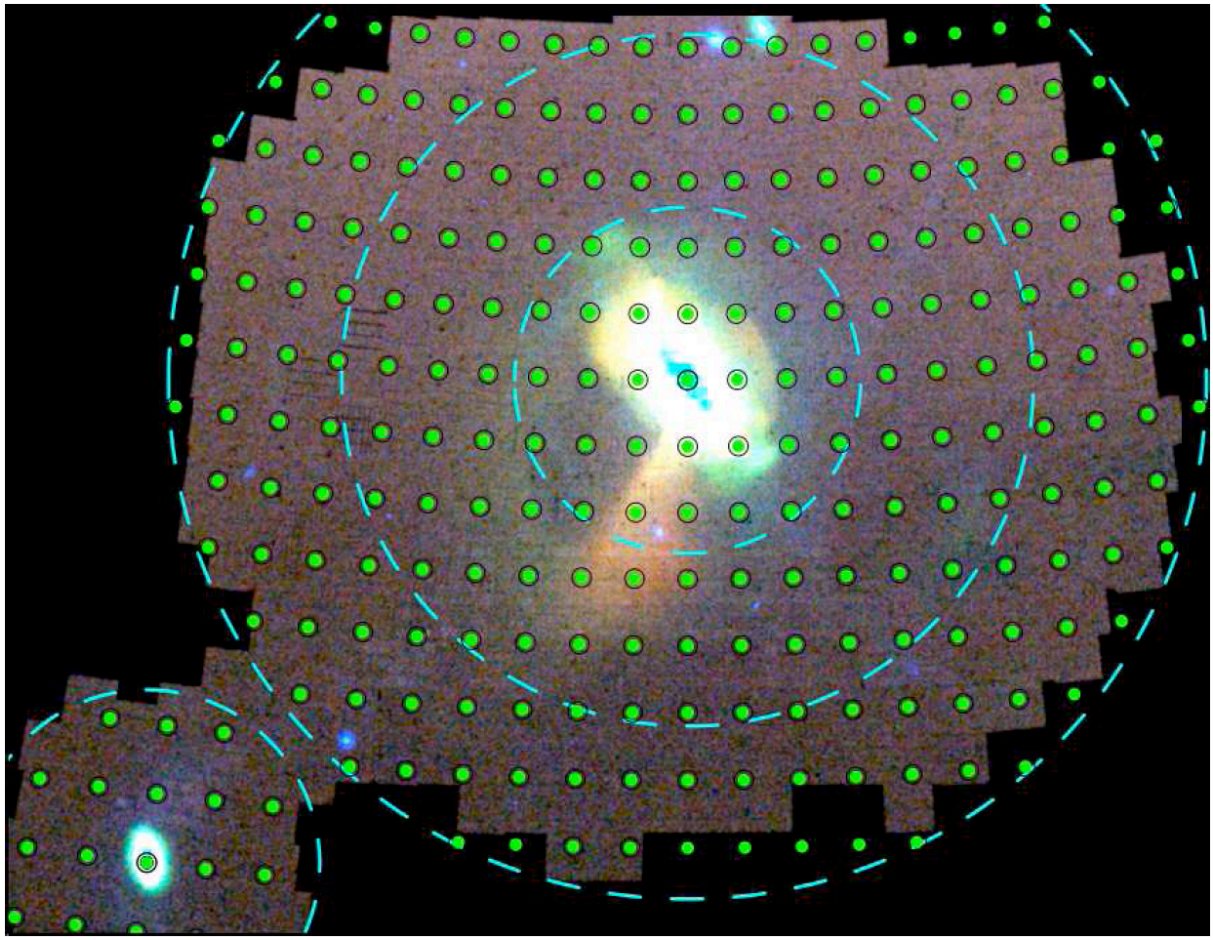

Figure 25: Spatial distribution of candidate RGB stars in the environs of M31 and M33, as identified from colour-magnitude cuts from the CFHT/MegaCam PAndAS Large Program. Dashed circles highlight maximum projected radii of 50, 100 and 150 kpc from M31, and 50kpc from M33. Filled dots indicate *the central coordinates* (not the FOV) of ngCFHT pointings that would give complete areal coverage of the M31/M33 system.

ngCFHT would be a unique opportunity in this time-frame to make a pivotal contribution to the subject by undertaking a large spectroscopic survey of these two Local Group galaxies. The goal would be to obtain a statistically significant sample of stars belonging to their constituent structural components. The scientific aim of this "Galactic archaeology" theme is to understand the galactic formation process, which is clearly an open-ended endeavour. Our power to address the key issues (e.g., thick disk formation, halo formation, streams, chemical enrichment history), depend on the spectral resolution that the survey affords. In the Milky Way, current state-of-the-art spectroscopic surveys (e.g., RAVE) aim to sample of order one million stars. This is feasible with a reasonable allocation (i.e., a few months) on ngCFHT. In contrast to the very local (few kpc) view provided by RAVE and others, this proposed M31/M33 study would provide a uniquely powerful, global panorama of these galaxies.

Figure 25 shows the spatial distribution of candidate red giant branch (RGB) stars in the environs of M31 and M33, as identified by colour-magnitude selection from 400 deg^2 of contiguous gi imaging with CFHT/MegaCam as part of PAndAS. Colour-coding corresponds to the colour of the RGB stars, such that redder RGB stars (likely higher metallicity) appear red, and bluer RGB stars (likely metal-poor) appear blue. Dashed circles correspond to maximum projected radii of 50, 100 and 150 kpc from M31, and 50 kpc from M33. PAndAS resolves point sources at the distance of M31 (D = 783 kpc; McConnachie et al. 2005) to $g \simeq 25.5$ and $i \simeq 24.5$ at S/N ~ 10.[15] The typical colour of TRGB stars in M31 is $(g-i) \sim 1.3$ so $g_{TRGB} \sim 22.5$. PAndAS therefore reaches down (nearly) to the horizontal branch

[15] In the CFHT filter system, the absolute magnitude of stars at the tip of the red giant branch (TRGB) is $M_i = -3.44$, so $i_{TRGB} \sim 21$.

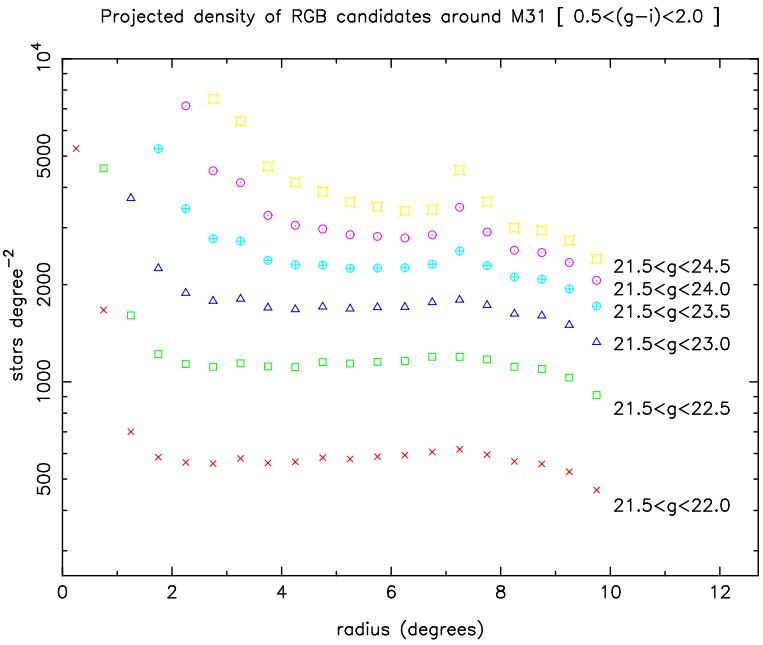

Figure 26: Radial distribution of stars surrounding M31 with colours in the range $0.5 < (g-i) < 2.0$. Densities have been averaged over circular annuli, and results are shown for a range of limiting g-band magnitudes. Note that red giant branch stars in M31 have $g \gtrsim 22.5$. The bump at $R \approx 7.5^\circ$ is due to the NGC147/185 subsystem.

level, providing photometry of sufficient depth that potential spectroscopic targets for a 10m facility could be selected.

In Figure 25, the effective surface brightness of the faintest visible features is of order 32–33 mag arcsec^{-2}. This corresponds literally to a few RGB stars per square degree. Note that the disk of the Milky Way is located to the North so there is increasing contamination in the colour-magnitude of the RGB locus by foreground dwarfs; the reddest RGB stars are particularly affected by this source of contamination. Young, blue stellar populations — and even intermediate-age populations such as asymptotic giant branch (AGB) stars — are not present in the outer regions of M31 in any significant numbers. Thus, any spectroscopic study of the outer regions of the M31 halo will necessarily concentrate on the older, evolved, RGB population. For this reason, we consider separately surveys of the *outer halo* (characterized by a low surface density of evolved, giant star candidates) and the *inner galaxy* (with a high surface density of targets from a mixture of stellar populations).

At present, the best instrument with which to study M31 and M33 spectroscopically is Keck/DEIMOS. This multi-object spectrograph has a $5\farcm0 \times 16\farcm7 \sim 80$ arcmin^2 field of view, and can observe ≈ 200 targets simultaneously in dense fields. At its highest resolution ($\mathcal{R} = 6\,000$), it is capable of obtaining spectra at the Ca II triplet (850 nm) with S/N = 10 for stars within the brightest 1 mag of TRGB in a 1-hour exposure. Spectra of this quality are sufficient to measure accurate kinematics (i.e., better than $5\,\mathrm{km\,s^{-1}}$) and also provide a rough estimate of the metallicity from the Ca II equivalent widths. The wide wavelength coverage of ngCFHT at a similar resolution will allow derivation of addition stellar parameters, as discussed earlier. Table 9 summarises the overall parameters of a survey of this subgroup, which we now discuss in more detail.

A. An Outer Halo Survey of M31/M33

Principal science aim: To obtain a complete, magnitude-limited, spectroscopic census of every star in the outer regions of an $L_\star$ galaxy halo, to provide complete kinematics and metallicities for every star, and, ultimately, to deconstruct a nearby galactic halo into its accreted "building blocks".

Area and number density: Figure 26 shows the number density of all potential evolved stars in the outer reaches of M31, averaged over circular annuli. These are very broadly defined as having colour in the range $0.5 < (g-i) < 2.0$, and magnitudes within the quoted limits. Within ~ 0.5 mag of the TRGB, there are typically < 2000 stars deg^{-2} for

Table 10: Signal-to-Noise Ratios and Velocity Accuracies for M31/M33 Surveys†

g	$\mathcal{R}$ = 1 500 (S/N, σ_v)	$\mathcal{R}$ = 3 500 (S/N, σ_v)	$\mathcal{R}$ = 5 000 (S/N, σ_v)	$\mathcal{R}$ = 7 500 (S/N, σ_v)
22.5	(19, 10)	(12, 7)	(10, 6)	(8.5, 5)
23.0	(12, 17)	(8, 11)	(7, 9)	(5, 8)
23.5	(8, 25)	(5, 17)	(4, 15)	(3.5, 11)
24.0	(5.5, 36)	(3, 29)	(2.8, 21)	(2.1, 19)
24.5	(3, 67)	(2, 43)	(1.8, 33)	(1.3, 31)

† – *S/N per resolution element at 850 nm and nominal velocity accuracy, σ_v, obtained in 1 hour observing using "rule of thumb" approximations, whereby nominal accuracy = FWHM/SN and FWHM = c/$\mathcal{R}$. These numbers were obtained using the ngCFHT Exposure Time Calculator.*

$R > 4^\circ$ ($\simeq 60$ kpc). This is well matched to the ngCFHT fibre density of 3200 fibres per 1.5 deg^2, or 2150 deg^{-2}. Note that, at these radii, 90–99.9% of targets are likely interloping foreground stars (hence the flattening of the radial profile at large radii). Thus, a complete survey of these regions *necessitates* extreme multiplexing in order to identify the few genuine RGB stars over the strong foreground contamination. Even within 2 mag of the TRGB, the number density of target stars is $\sim$ 3000–4000 deg^{-2}.

Defining the outer halo of M31 as $R \geq 4^\circ$ implies a survey area of ~ 260 deg^2 out to the limits of the PAndAS area (150 kpc projected radius, or about half the cosmological virial radius of M31). Including the area around M33 increases this area by ~ 40 deg^2. Figure 25 shows an example survey strategy, where each circle represents the centre of possible ngCFHT pointings, based on a hexagonal field of view of 1.5 deg^2 (not shown). Approximately 200 pointings are required for complete areal coverage of the other halo of M31. Depending on the efficiency of the fibre positioning setup, the survey could be essentially complete for all stars within 0.5 mag of the TRGB using a single pointing per position (and would correspond to observations of more than a half million stars), or complete for all stars within ~ 1 mag of the TRGB with two pointings per position (more than a million stars). It is worth emphasizing the faintness of the target stars; clearly, any gain in throughput would be significant for a programme of this sort.

Spectral resolution: As a simple illustration of the need for moderate resolution, we considered 1-hour exposures at resolutions of $\mathcal{R} = 1\,500, 3\,500, 5\,000$ and $7\,500$. Results are listed in Table 10 for a variety of limiting magnitudes. Two points should be kept in mind when considering these values:

1. The first aim of this survey is to map velocity structures in the halo. These will generally arise from dwarf galaxies in various stages of disruption. Typical velocity dispersions of dwarf galaxies (and, hence, lower limits on the velocity dispersions of the streams) are $\sigma_v \sim 8$ km s^{-1}. Thus, typical velocity accuracies should be 8 km s^{-1}, or better, in order to resolve low-mass structures kinematically.

2. The second aim of this survey is to obtain spectroscopic metallicities for a large fraction (and possibly all) of RGB targets. This is most easily done at intermediate resolution using the CaT feature at 850 nm. For these measurements, higher resolution is generally favorable at S/N $\approx$ 10. For high-S/N spectra and good wavelength coverage, spectral synthesis techniques should also be explored to extract maximal stellar parameter information.

We conclude that a resolution of $3\,500 \lesssim \mathcal{R} \lesssim 7\,500$ is necessary to obtain the requisite velocity accuracy. This is not surprising since most studies that use the CaT as a metallicity indicator (e.g., DART; Tolstoy et al. 2004) use resolutions in the range 5 000–7 500. Typically, S/N $\sim$ 10 is required for [Fe/H] estimates with accuracies of ~ 0.25 dex. At current specifications, exposures of 1 hour at $\mathcal{R} \sim 6\,000$ targeting the CaT region should obtain both the necessary velocity precision for stars within the upper 1–1.5 mag of the RGB, and metallicities accurate to ~ 0.2 dex for all stars at or near the TRGB. Resolutions closer to $\mathcal{R} \sim 2\,000$, while providing useful data, will not be optimal for a full chemodynamical analysis of these stars. Full wavelength coverage is desired to allow maximal data to be extracted from the stellar parameters.

B. Inner Regions I: "Faint" Stellar Populations

The inner regions of M31 and M33 offer a high surface density of stellar targets for ngCFHT. Unlike their outer regions, there is a broad variety of stellar populations that span all ages. In what follows, it is convenient to separate

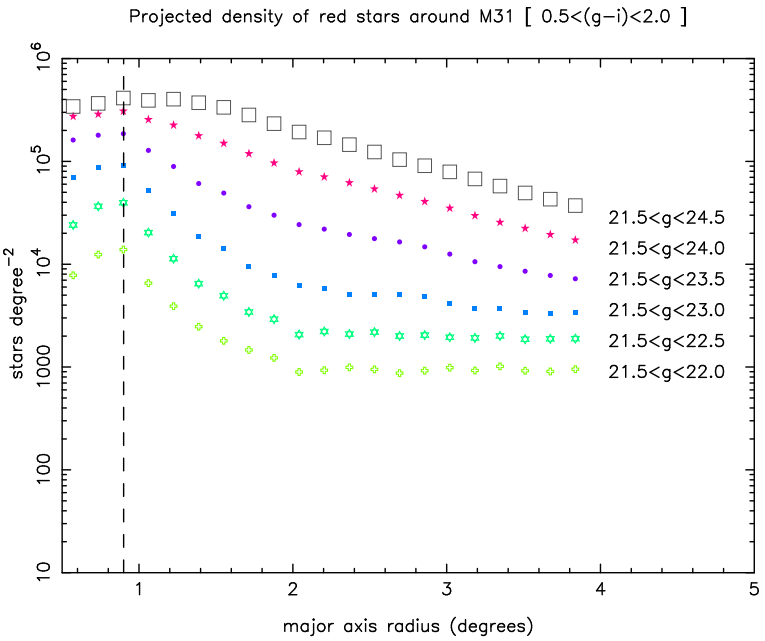

Figure 27: Radial distribution of red giant branch candidates in the central parts of M31 averaged over elliptical annuli ($e = 0.775$, matching the shape of the M31 disk) and plotted as a function of major axis distance. As in Figure 26, results are shown for different limiting magnitudes. It is clear that crowding affects the photometry in the inner degree or so.

these populations loosely into two groups: i.e., "bright" stars (generally from young or intermediate-age, many of which are luminous enough to warrant high-resolution spectroscopic observations), and "faint" stars (generally fainter than the TRGB, and which are either old or intermediate-age giants, similar to the outer halo survey).

Principal science aims: To study the disk/thick-disk/halo transition region, to characterize the relationship between these components, and to determine the role of mergers in thick-disk evolution.

Area and number density: Figure 27 shows the number density of RGB candidates in the inner regions of M31, in the same way as Figure 26, except averaged over elliptical annuli corresponding to the projected shape of the disk of M31. A far smaller area would need to be surveyed than for the outer halo — a (circular) radius of 40 kpc corresponds to an area of $\sim$ 22 deg^2, or about 15 individual ngCFHT fields. For M33, the main optical disk fits entirely within a single ngCFHT pointing. However, the density of targets rises rapidly with decreasing distance from either of these two galaxies, and multiple (a few to tens) of setups would be required, per position, in order to obtain the desired, magnitude-limited survey for stars at or near the TRGB. The benefit of the large number of sources, however, is the corresponding increase in average S/N per target obtained compared with the outer regions, since only the brightest targets need to be selected. This would ensure that precise radial velocities and accurate CaT-based metallicities are obtained for *all* stars in the sample. Additionally, contamination by foreground dwarfs will be very low. In only one week of dark time (anticipating 6 setups per night with 1 hour exposures) more than 125 000 radial velocities, accurate to a few km s^{-1}, could be obtained for genuine RGB stars in the central regions of M31, each with metallicity estimates accurate to better than a few tenths of a dex.

Additional considerations: Most requirements in this case are the same as for the outer halo survey. The only additional concern is the effect of crowding; from Figure 27, this clearly becomes a problem at major-axis distances of $<$ 1degree (i.e., within the main optical disk of M31). This can be mitigated, in part, by targeting only the brightest stars, and/or by using smaller fibres. High-resolution imaging of some of the disk of M31 will soon be available from the Panchromatic Hubble Andromeda Treasury (PHAT; Dalcanton et al. 2012) survey, enabling better target selection in these regions. Nevertheless, crowding is likely to remain the fundamental limitation in pushing this study into the inner 10 kpc or so of M31.

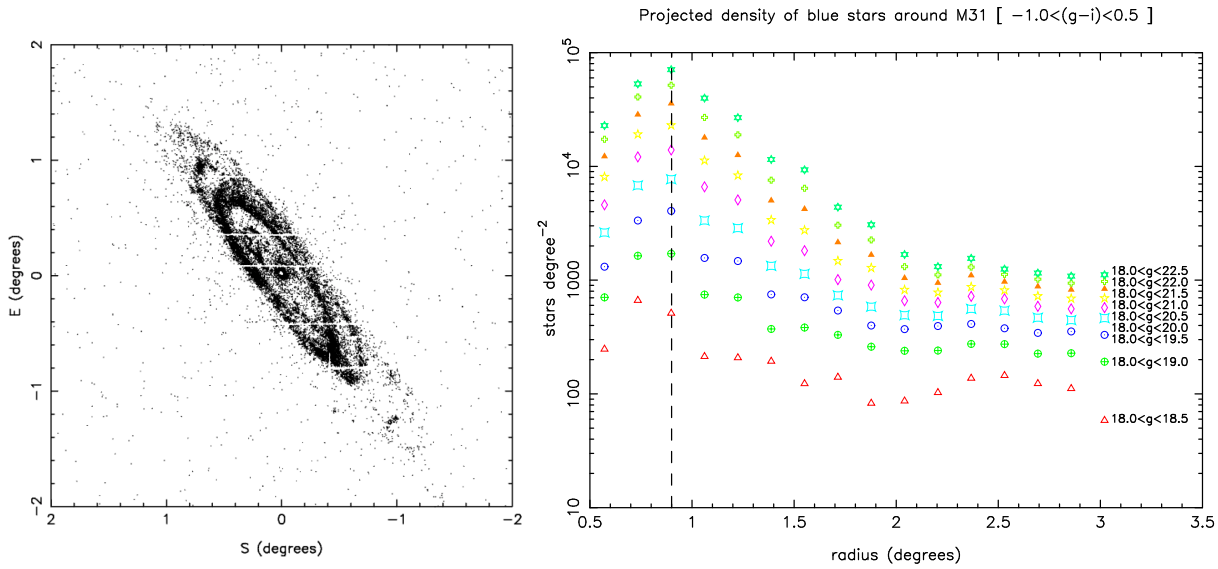

Figure 28: (Left Panel). Spatial distribution of young blue stars selected from the central PAndAS fields. (Right Panel). Radial distribution of young blue stars around M31 with $-1.0 < (g-i) < 0.5$ averaged over elliptical annuli ($e = 0.775$, matching the shape of the M31 disk) and plotted as a function of major axis distance. As in the previous figure, it is clear that crowding affects the photometry in the inner degree or so.

C. Inner Regions II: Bright (Young) Stellar Populations

Principal science aim: To observe a large fraction of the brightest young stars across the entirety of a galaxy disk at high ($\mathcal{R} = 20\,000$) resolution in order to determine individual chemical abundances (O, Fe, α elements, etc), examine the chemical composition of a star-forming disk, and characterize disk kinematics. A related goal is to compare young stellar populations as a function of environment both within, and between, galaxies (cf., LMC, MW, etc)

Area and number density: The left panel of Figure 28 shows the spatial distribution of all bright blue stars selected from PAndAS data using a colour-magnitude cut that isolates only bright, blue stars. These stars clearly follow the disk and spiral arm structure of M31, tracing young star-forming regions. Indeed, cross correlating this map with the GALEX image of the M31 disk shows conclusively that the two populations follow each other, and that this CMD selection resolves many of the stars responsible for the UV emission.

The right panel of this figure shows the number density profile of the candidate blue stars. The young stars are entirely concentrated in the disk, and so literally, just one or two pointings with ngCFHT are needed to provide complete areal coverage. The number density of the brightest stars ($g \lesssim$19–20) is well matched to the expected fibre density for ngCFHT, in either the high- (N=800, $\mathcal{R}$=20 000) or low-resolution modes (N=3200, $\mathcal{R}$=2,000 or 6 500). A majority of the brightest stars in M31 could therefore be observed in a handful of setups at high resolution. The ngCFHT exposure time calculator indicates that, in approximately 6 hours, a S/N of > 100 per $\mathring{A}$ can be obtained for stars with $g = 20$.

2.4.4.2 Dark matter and Baryons at the Limits of Galaxy Formation

The CDM model is strongly supported by a wealth of data on large spatial scales (e.g., by CMB data, measurements of the matter power spectrum on scales above $\sim$ 10 Mpc, and cluster gravitational lensing). Dwarf galaxies are the most dark-matter dominated systems known, and for this reason, it is widely assumed that their stars can be used as a straightforward tracer of their overall potentials. Because these potentials should be close to the predictions of dark-matter-only numerical simulations, the dynamics of stars in dwarf galaxies can test the behaviour of dark matter on sub-kpc scales in collapsed objects.

Intensive spectroscopic surveys are required to advance our understanding of dwarf galaxy dynamics in a meaningful way. For example, the Fornax dSph has attracted much interest as the brightest of the classical dSphs, which

Table 11: Technical Requirements and Survey Implementation: A Representative Survey for a Local Group Dwarf Galaxy

Survey Area (Ω)	A Local Group dwarf galaxy, $\Omega \approx\sim$few deg^2.
Field Location	Any RA, Dec
Number of ngCFHT Fields ($N_{\rm field}$)	$N_{\rm field} = \Omega/{\rm FOV}_{\rm ngCFHT} \approx 1 - 7$ (typically 1 for distant dwarfs, but nearest MW dwarfs will require some tiling).
Number of Configurations per Field ($n_{\rm config}$)	$\langle n_{\rm config} \rangle = 1 - 10+$, a function of distance (50-1000kpc), limiting magnitude, and dwarf luminosity
Total Number of Exposures ($N_{\rm exp}$)	$N_{\rm exp} = N_{\rm field} \times \langle n_{\rm config} \rangle \approx 1$ -10+
Primary Imaging Resources for Target Selection	Wide field 4 or 8m class ground based photometry (e.g., CFHT/MegaCam)
Observing Conditions	Mostly dark time. Cloud cover $< 20\%$.
Instrumental Configuration(s)	[All observations taken as part of PI-style programme] (1) $\mathcal{R} = 6000$ $T_{\rm exp} \sim 1 - 8$ hr (depending if focus is on RVs or chemistry) (2) $\mathcal{R} = 20000$ $N_{\rm point} = 1, T_{\rm exp} \sim 3$ hr (function of distance, luminosity of dwarf (number of bright targets))
Wavelength Coverage and Velocity Precision (ϵ_v)	(1) 0.40–0.95μm (ideal; window of a few hundred nm around CaT absolute minimum) and $\epsilon_v \approx 5$ km s^{-1} at $\mathcal{R} = 6000$ (2) Wavelength range same settings as for Milky Way surveys at high resolution; velocity precision $\epsilon_v \approx 5$ km s^{-1} at $\mathcal{R} = 20000$
Limiting (point source) Magnitude	Faint end limit of $g_{\rm AB} \sim 23.0$, suitable for most distant dwarfs
Total Time Needed for Program ($T_{\rm tot}$)	$T_{\rm tot}$ $1 - 24$ hrs

CDM would expect to reside in one of the most massive halos mentioned above; intensive efforts to acquire spectra for ~ 2600 stars in Fornax have yielded the most robust mass measurement of any dwarf galaxy so far, with velocity data extending to the peak of the rotation curve (Walker et al. 2009). ngCFHT would bring about an entirely new era for such studies, enabling accurate kinematic measurements like this to be performed *much* more efficiently, with a larger number of stars, and well beyond the peak of the rotation curve, for *all* Local Group dwarf galaxies with $\delta \gtrsim -30^\circ$. Crucially, ngCFHT would be well-positioned to understand how the dynamics of dwarf galaxies respond to evolutionary effects, in particular tidal stripping, due to its ability to explore sparse outer fields while ensuring high completeness in the presence of strong contamination.

Connecting the dynamics of dwarf galaxies to their metallicities and chemical abundances is a key area of current research and will likely remain so, well into the era of ngCFHT. Indeed, there are at least three important open questions regarding the chemistries, metallicities and star formation histories of dwarf galaxies that would take advantage of a highly multiplexed, wide-field instrument on a 10m telescope:

1. The full metallicity distribution (which requires CaT with a minimum S/N of ~ 10), including spatial gradients in metallicity and/or stellar populations. This would provide important information on whether star formation propagated inwards or outwards. These data would also indicate if there were significant metallicity variations with time, and would make it possible to break the age-metallicity-reddening degeneracy definitively in colour-magnitude diagram studies.

2. The dispersion in abundance ratios at fixed metallicity: e.g., the patterns of [α/Fe] vs. [Fe/H] and the relative proportions of other element groups in relation to the iron-peak elements (i.e., light elements, odd-Z elements, light and heavy s-process, r-process). These abundances hold important clues to the history of star formation in these galaxies as well as their initial mass function.

3. A census of rare stellar species (extremely metal-poor stars, carbon stars, etc), including their overall numbers and spatial distributions.

As with the M31-M33 research projects, the first of these goals requires a resolution of around $\mathcal{R} \sim 6\,000$. At present, the second and third goals can be achieved easily only for Galactic satellites; the largest existing samples of stars with $\mathcal{R} = 20\,000$ spectroscopy are of the order of 70–150 for a few Galactic satellites and generally cover only their central regions. ngCFHT would not only allow an increase of a factor of $\sim$10 or more in sample size, but would also reach to the tidal radii (and beyond) in the target galaxies. Sextans is a good example of a key target for ngCFHT, as it is largely beyond the reach of the current instruments. The left panel of Figure 29 shows the CMD for roughly 7 000 stars in the central regions of Sextans. The right panel shows stars that have been targeted by VLT/FLAMES. Here green indicates lower resolution CaT measurements and red shows the stellar subset selected for high-resolution ($\mathcal{R} \simeq 20\,000$) spectroscopy. A possible mapping strategy for ngCFHT is indicated by the circles, which makes clear the vast improvement in efficiency that ngCFHT would provide.

The high-resolution spectra can deliver the most accurate abundances for the largest number of elements. ngCFHT's high resolution mode ($\mathcal{R} \sim 20\,000$) is thus most appropriate for the brightest stars. However, if the wavelength range is large enough (i.e., $400 - 900$ nm, which is comparable with, but shorter than, the X-Shooter UVB and VIS ranges), a resolution of $\mathcal{R} \sim 6\,000$ is an excellent option for fainter stars, offering a $\sim$0.2 dex accuracy.

As an illustration of the sheer power of ngCFHT for chemodynamical studies of nearby dwarf galaxies we consider NGC 6822, one of the nearest dwarf irregular galaxies — at an "intermediate" distance of 500 kpc for Local Group galaxies. It is one of the more intriguing targets for detailed study because of ongoing disturbances in its HI velocity field and very active star formation. There is some evidence for young stellar populations associated with infalling HI clouds, and for deviations from circular disk rotation. However, the large angular scale of the system (~ 1 degree across) and the likelihood that the substructures are represented by only a small fraction of the stars means that the system remains poorly understood, even with a small (but steadily growing) sample of stellar spectra from VLT/FLAMES and Keck/DEIMOS.

The number of potential targets in NGC6822 available for spectroscopy with ngCFHT dwarfs the capabilities of existing multi-object spectrographs on 8-10m-class telescopes. For instance, the number of potential "red star" targets (i.e., stars with ages > 500 Myr, most of which are likely older than 1 Gyr) is:

1. ~ 2500 stars *above* the TRGB, including ~ 103 carbon stars ($18 < I < 19.5$).
2. ~ 7500 stars within 0.5 mag of the TRGB ($19.5 < I < 20$).
3. ~ 30000 stars between 0.5 and 1.5 mag of the TRGB ($20 < I < 21$).

Likewise, there are large numbers of potential "blue star" targets:

1. ~ 1000 stars with ages < 50 Myr ($15.5 < g < 18.5$).
2. ~ 1000 stars with ages 50–200 Myr ($18.5 < g < 20.5$).
3. ~ 2000 stars with ages 200–400 Myr ($20.5 < g < 21.5$).

With these stellar densities and spatial distributions, it would be possible, for example, *to measure radial velocities accurate to better than 5 km s^{-1} for every AGB and red supergiant star, and nearly all RGB stars within 0.5 mag of the TRGB, in just one night on ngCFHT, at medium resolution and with S/N ∼10–20.* A single pointing, with three different configurations of the 3200 fibres, each observed for roughly a 1 hour, would provide a complete census of these bright red stars. With samples of $> 10^4$ stars, sub-populations representative of just 1% of the total number of stars would become detectable with high significance. To obtain spectra further down the RGB would take more time, but not unimaginably so. For instance, at $I = 21$, S/N ~ 10 per hour would be achieved in the red/near-IR region, meaning that homogeneous, high-quality kinematic and metallicity results for $\sim 30\,000$ stars could be achieved in only 10 nights: i.e., 6-8 hours per setup, with 10 configurations needed to reach every target. If the shallower survey were repeated multiple times over a period of several years, the sensitivity and multiplexing would allow unprecedented studies of variability and evolutionary changes for stars in the late phases of evolution. Similarly, intermediate-resolution radial velocities could be obtained for *every main-sequence star in the galaxy younger than* ~ 400 *Myr in just* ~ 3 *nights at S/N* $\sim 10 - 15$ *for* $g < 21.5$. At medium resolution, the baseline specifications for ngCFHT are fibre-density limited and not field-of-view limited for dwarf irregular galaxies.

High-resolution work would be significantly more limited in sample size. However, a dramatic increase relative to current samples would be possible thanks to ngCFHT's large field of view and high level of multiplexing. For TRGB stars with $I = 19.5$, S/N ~ 100 per $\mathring{A}$ could be achieved for $\lambda > 600$ nm in $6 - 9$ hours, depending on observing conditions. However, the rich spectral region with $\lambda < 500$ nm would not be accessible at that magnitude level. The prospects are better for the young main-sequence stars, where $> 10^3$ stars younger than ~ 100Myr would be accessible to spectroscopy at $\mathcal{R} \sim 20,000$ and high S/N in $3 - 5$ hours of stacked exposures. A high-resolution survey of the upper main sequence from $400 - 700$ nm could provide key constraints on iron peak elements, [α/Fe] and some neutron capture elements for the most recent generations of stars in the galaxy. Table 11 summarises a strawman survey of a NGC6822-like galaxy; such a survey would be transformational compared with current capabilities.

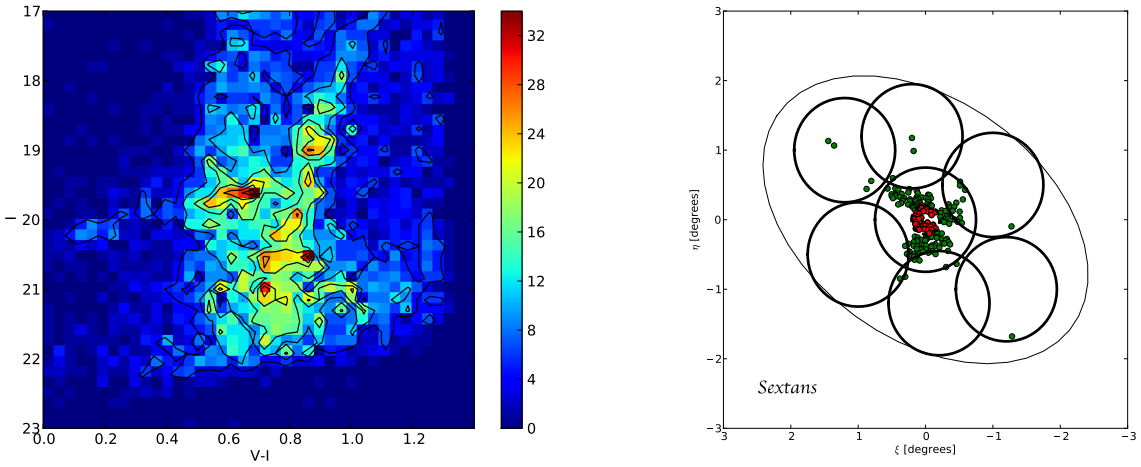

Figure 29: (Left Panel). The colour magnitude diagram of approximately 7 000 stars in the inner $\approx 0.9^\circ \times 0.9^\circ$ of the Sextans dSph galaxy, plotted as a Hess diagram where the colour-bar corresponds to the stellar number density. (Right Panel). Points indicate the coordinates of stars in Sextans for which VLT/Flames spectra have been obtained: green points correspond to lower resolution CaT measurements, while red points indicate high resolution, $R = 20\,000$ observations. The circles correspond to the field of view of ngCFHT, and show a possible mapping strategy for this galaxy. The ellipse shows the fitted tidal radius of the galaxy. Figure adapted from Battaglia et al. (2011).

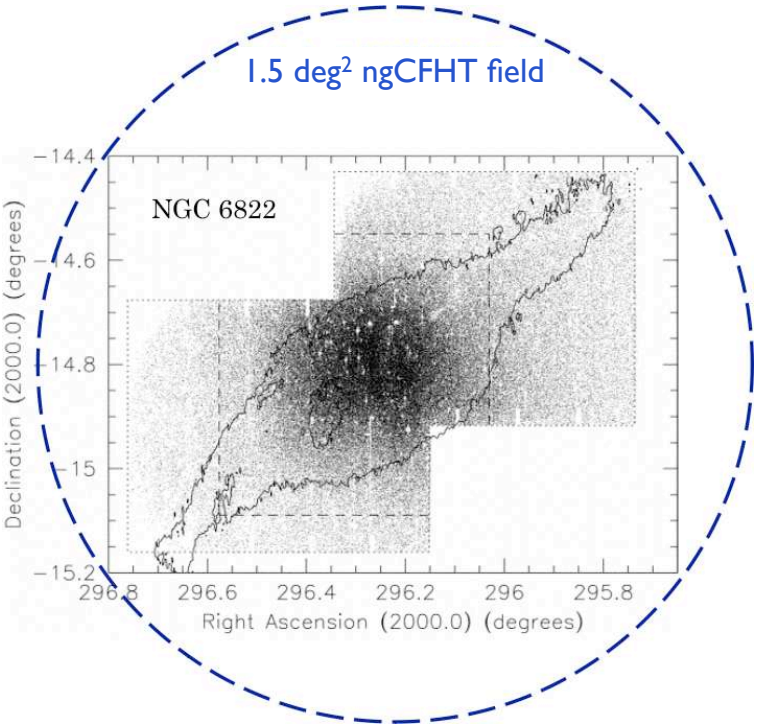

Figure 30: Spatial distribution of red giant branch stars (dots) in the barred irregular galaxy NGC6822 from Subaru/SuprimeCam observations. The contour shows the 5×10^{20} cm^{-2} boundary of the HI disk. The ngCFHT field of view is indicated for comparison. Figure adapted from Figure 16 of de Blok & Walter (2006).

2.5 Nearby Galaxies and Clusters

2.5.1 Abstract

Dark matter (DM) halos are the fundamental building blocks of the universe, but they are very difficult to observe directly. Instead, we observe their luminous counterparts — individual galaxies, galaxy groups and galaxy clusters — via the baryons that have turned into stars or are hot enough to shine in X-rays. These baryonic systems are the fossil records of hierarchical structure formation in the local universe. Because they can be studied in a level of detail that will never be possible with more distant systems, they provide astronomers with an opportunity to decode the history of mergers, interactions, star formation and chemical enrichment that have operated in different environments, and across a vast range in galaxy mass. Indeed, it is the low-mass end of the galaxy and halo mass spectrum that is most poorly understood at the present time. The nature of DM — whether it is cold, warm, or even mixed or decaying — can dramatically affect the abundance of low-mass halos. Moreover, star formation becomes increasingly inefficient in lower mass halos, though the reasons for this remain obscure. A complete understanding of the DM content, internal dynamics, ages, and chemical abundances of nearby galaxies and clusters will only be possible once a dedicated, highly-multiplexed, 10m-class spectroscopic facility — such as ngCFHT — becomes available. Key science questions to be addressed in this area include the abundance and density structure of DM halos, the faint end of the galaxy luminosity function, the physics of star formation in the lowest-mass stellar systems, and tests of competing models (i.e., cold/warm/decaying DM, tidal heating and modified gravity) for the kinematics of high- and low-mass galaxies alike.

2.5.2 Introduction

In field of galaxy formation, there are a number of outstanding problems that can roughly be grouped into two related themes:

1. *The abundance and structure of dark matter halos, particularly for the lowest mass scales that correspond to dwarf galaxies*. A longstanding mystery in galaxy formation is the so-called "missing satellites" problem. Cluster-mass halos have many thousands of satellite subhalos, and these are observed as galaxies. So too should galaxy-mass halos have thousands of dwarf satellites, but these are not observed in the expected abundance. This problem is not limited to the lowest mass galaxies, but extends to relatively massive dwarfs, similar to the Magellanic clouds (Boylan-Kolchin et al. 2011). A second problem (which may be related to the missing satellite problem) is the internal structure of dark-matter-dominated dwarf galaxies: numerical simulations suggest that their central density profiles should be cuspy (i.e., $\rho \propto r^{-1}$), but this is not observed.

2. *Star formation, the quenching of star formation, and the roles of environment and "feedback"*. A detailed understanding of star formation in dwarf galaxies is almost certainly needed to solve the missing satellite problem. For example, "feedback" (from supernova-driven winds) has been proposed as the primary mechanism for quenching star formation in dwarf galaxies, and might also solve the abundance and structure problems discussed above. However, it has also been shown that environment (through ram-pressure or tidal stripping) is also likely to play a critical role in quenching star formation. And what about the role of AGN, which are thought to be critical in quenching the star formation in giant galaxies? Do these mechanisms play a role in dwarf galaxies as well? A physical understanding of star formation in dwarf galaxies, including quenching and feedback, remains a crucial piece of the puzzle in galaxy formation.

In cosmology, the most important outstanding questions are the nature of Dark Energy and the validity of general relativity (see §2.9 for possible contributions in this area by ngCFHT). Many innovative approaches to these problems have been proposed. One of these is the evolution of the abundance of rich clusters as a function of redshift, which combines the cosmological volume element (which depends on the nature of Dark Energy) and the growth of structure (which also depends on the nature of Dark Energy and also on whether gravity is well described by general relativity or some variant). High-redshift observations of the cluster abundance are the target of large projects such as South Pole Telescope (SPT; Carlstrom et al. 2011) and eROSITA (Cappelluti et al. 2011). To understand and calibrate the evolution, however, it is essential to know how an observable (such as cluster richness, or gas mass) is correlated with total mass in the mean, and also the scatter in this mass-observable relation. ngCFHT would allow an exquisite, low-redshift calibration of the observable-richness relation and its scatter in the nearby universe.

This section makes frequent reference to three ngCFHT dark time surveys that are described in detail in §2.6 (see especially Tables 16, 17, and 18). These surveys (the Dark-Wide, Dark-Medium and Dark-Deep surveys, respectively) cover areas of $\Omega = 4\,300$, 100 and 1.5 deg^2 to approximate depths of $i \simeq 23.5$, 24.25 and 26, with varying levels of target completeness.

2.5.3 ngCFHT in Context: Competition and Synergies

For the study of nearby galaxies and clusters, the most important spectroscopic survey in the last few decades has been the SDSS. This survey, and a variety of related projects on 4m-class telescopes (e.g., the 2dF galaxy redshift survey, GAMA), have surveyed much of the local universe, providing an unprecedented characterization of galaxies with luminosities close to $L^\star$ ($\sim 10^{10} L_\odot$). With the advent of deeper, multi-colour, optical imaging surveys (e.g., CFHTLS, SDSS Stripe 82, Pan-STARRS, KIDS, VISTA, DES, Hyper-Suprime Cam, and ultimately, LSST), radio surveys (e.g., WALLABY, EMU, DINGO) as well as space surveys such as WISE, eROSITA and Euclid, there will be a wealth of deep, multi-wavelength data from which to draw samples for spectroscopic surveys. ngCFHT's 10m aperture, its multiplexing capabilities, and its range of spectral resolutions (i.e., low, medium and high) would make it the preeminent spectroscopic instrument of the next decade, the closest competition being PFS on Subaru.

2.5.4 Legacy Science

2.5.4.1 The Abundance of Dark Matter Halos and the Connection to Galaxy Formation

The overall abundance of DM halos as a function of mass, $dN/d\log M$ is among the most important outstanding issues in modern astrophysics. This quantity is sensitive to both the form of the inflationary perturbations and to the nature of the DM particle itself: i.e., whether it is collisional or collisionless, decaying, self-interacting, warm (light), or cold (massive). Establishing its functional form at low redshift, and with high precision, is critical for measuring its evolution, which in turn is sensitive to fundamental cosmological parameters.

In the ΛCDM paradigm, galaxy formation takes place within DM halos. Therefore, linking the luminous mass to DM halos is critical, both to understand the halo abundance and to understand galaxy formation. A general class of models, collectively known as the "halo model", has been devised to attack galaxy formation from a statistical view point (see also §2.6). Among these models, the conditional luminosity function (CLF) and stellar mass function (SMF), both as a function of halo mass, and the halo occupation distribution (HOD), are the most popular. Briefly, these approaches employ a few simple physical quantities to make predictions for the clustering properties, luminosity (or stellar mass) functions of galaxies, as well as galaxy-galaxy lensing results. Models that simultaneously reproduce these observables are then representative of the underlying association between galaxies and DM halos. Thus, the halo model provides a powerful, statistical description of the relationship between the halo mass and its baryonic content.

In the low-redshift ($z \leq 0.1$) universe, the majority of stellar mass is contained in Milky-Way-like galaxies ($\sim 10^{11}$ M$_\odot$). These, in turn, reside within halos having masses similar to the Local Group ($\sim 10^{12}$ M$_\odot$; Eke et al. 2005). At late times, the primary mode by which galaxies like the Milky Way are assembled is via a combination of cold gas accretion and minor mergers of low-mass companions (Guo et al. 2011). Both of these processes are probably regulated by the mass of the halo in which they reside. To understand these processes in detail, and the role of the parent halo, we need to reach the lowest possible limits on both galaxy and halo mass. Doing so requires a deep ($r \leq 24$) spectroscopic survey covering a significant area (i.e., more than 100 deg^2). Previous shallow, wide-area surveys such as the SDSS and the 2dF galaxy redshift survey (2dFGRS ; Colless et al. 2001) are only sensitive to massive galaxies and intermediate-mass halos (Eke et al. 2006; Yang et al. 2007). And while a handful of very low-mass systems have been found in both these surveys, neither the 2dFGRS or SDSS were able to identify halos below 10^{12}M$_\odot$, thereby barely sampling the dominant halo mass at their sensitivity limits.

A key focus for ngCFHT should therefore be the comprehensive sampling of both the halo mass function *and* the stellar mass function to the faintest possible limits. For a fully sampled, $r \leq 24$ mag survey covering 100 deg^2 (i.e., the Dark-Medium Survey; see §2.6 for details), it should be possible to detect ≈ 200 halos with $\log M/M_\odot = 10.75 \pm 0.5$ dex (Figure 31). This is 50 times greater than the density found in the GAMA survey (Robotham et al. 2011) — the deepest precursor for halo measurements — and more than an order of magnitude beyond the mass range probed by the SDSS and 2dFGRS datasets.

Equally important, the Dark-Medium survey would extend well into the regime of dwarf galaxies (i.e., to stellar masses of $\sim 10^7\ M_\odot$ at $z < 0.1$ and down to an ultimate, low-z mass limit of $10^{5.5}\ M_\odot$), enabling studies of halo occupancy, halo dependent mass functions, halo substructure, and star formation efficiency. Figure 32 shows the

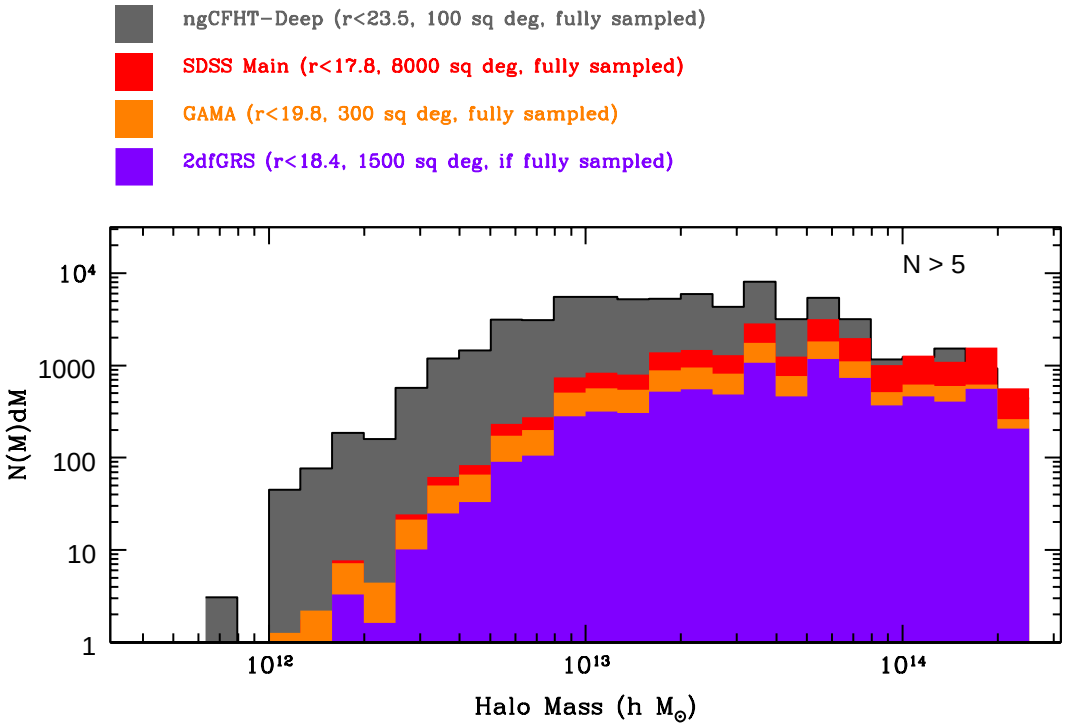

Figure 31: The abundance of halos with at least five kinematic tracers showing the expected improvement with ngCFHT over previous surveys that extend to halo masses below that of the Milky Way

current constraints on the $z < 0.1$ galaxy SMF from GAMA (Baldry et al. 2012), the SDSS (Baldry et al. 2008), the 2dFGRS (Cole et al. 2001), and the ngCFHT Dark-Medium survey. The stellar mass function is of particular interest because numerical simulations have long argued that halos such as the Local Group should contain thousands of galaxies, rather than the ≈ 100 that are known (Moore et al. 1999; Klypin et al. 1999). Indeed, observations find that the Local Group mass function is relatively flat (Driver & de Propris 2003). There are two principal mechanisms which have been proposed to reconcile this apparent discrepancy (Benson et al. 2003): (1) supernova feedback, whereby SN II explosions heat and expel a significant fraction of the baryons from lower mass halos; and (2) early photo-ionization, in which the primordial baryons in low-mass halos are heated by external sources (AGN and Pop III stars) and are thereafter unable to cool due to low gas metallicities. These two mechanisms give quite distinct, qualitative predictions for the faint-end slope of the galaxy SMF, as the former mechanism leaves a relic stellar population in every halo while the latter does not. Hence, by sampling to very low mass levels, the Dark-Medium survey should be able to distinguish between these mechanisms. In addition, it has also been proposed that the Local Group may not be representative (see discussion in Boylan-Kolchin et al. 2012), or that the local observational census is incomplete (Tollerud et al. 2008). Both of these suggestions can be best addressed by sampling a statistically significant sample of groups with Local Group halo masses.

These topics (i.e., missing satellites, group finding, merger rates, the study of the galaxy populations with respect to halo mass, and the halo mass function and SMF) are all key areas in which ngCFHT would be preeminent, allowing the sampling of the galaxy SMF right down to the Jean's limit of $10^{5.5}$M$_\odot$ from rich clusters to group, filament, and void environments. Critical factors for success will be *complete* sampling over regions no smaller than squarish 50 deg^2 "chunks", at a spectral resolution sufficient to obtain $\pm$ 20 km s^{-1} accuracy, in established regions with high-quality, multi-wavelength data. High completion is critical because many low-mass halos will typically contain only a few galaxies and all of these galaxies will need to be sampled to attain robust velocity dispersions (i.e., halo masses). Inevitably, this will require a multiple-pass survey to unpick the close pairs, triplets and compact groups (i.e., $\sim 5-10$ resamplings of the same region). 50 deg^2 chunks are essential in order to minimize the impact of boundary effects on the groups sampled within the survey area. A reasonable resolution (i.e., $\mathcal{R} \sim 2\,000$) is needed to measure the velocity dispersions of the lowest-mass groups (note that the Local Group velocity dispersion is 60 km s^{-1}). For full

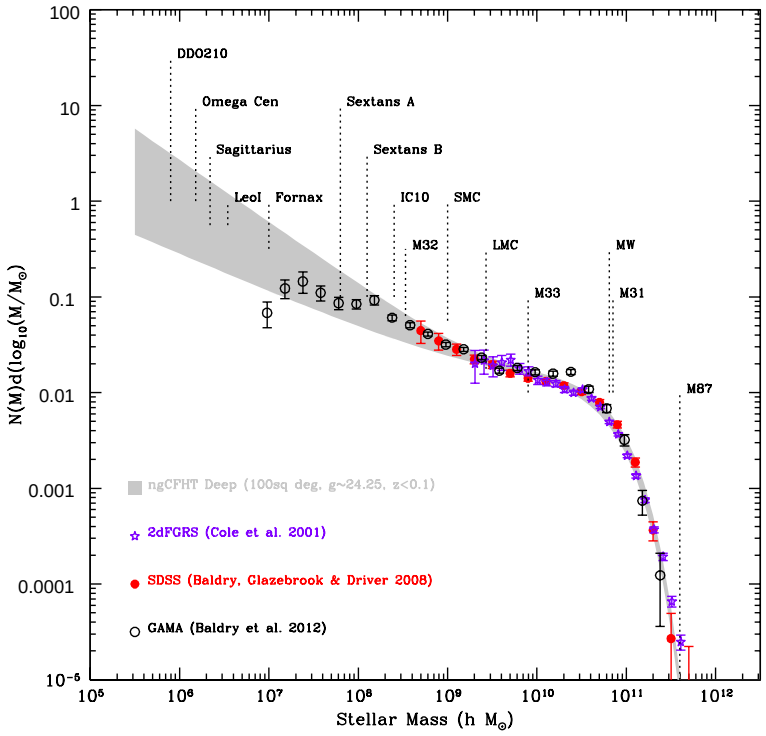

Figure 32: The galaxy stellar mass function (SMF) at $z < 0.1$ from the SDSS, 2dFGRS and GAMA compared to the ngCFHT Dark-Deep survey. For simplicity, the r-band selection assumes a constant mass-to-light ratio.

characterization of the galaxy population within each halo, excellent multi-wavelength data would be required such as that assembled by the GAMA team. As discussed in §1, many suitable regions are accessible from Mauna Kea.

Survey regions might include equatorial GAMA 9h, GAMA12h and GAMA 15h regions (Driver et al. 2011) which contain deep GALEX, VST, VISTA, WISE, HERSCHEL, GMRT, and ASKAP data over contiguous $5^\circ \times 12^\circ$ chunks. These provide comprehensive coverage of any AGN, stars, neutral gas, and dust components. Ideally, targets should be selected from deep, high-resolution, optical/near-IR imaging (to overcome high and low surface brightness selection biases), in the extinction-corrected $(r - K)$ wavelength range where fluxes at $z < 0.1$ are most closely correlated with stellar mass.

2.5.4.2 Rich Clusters: Benchmarks for Cosmology

The redshift evolution in the abundance of rich clusters is a critical test of Dark Energy and/or alternative gravity models because it combines a measurement of the cosmological volume element with the observed growth rate of structure. High-redshift observations of the cluster abundance are the focus of several high-profile projects. The ongoing SPT survey is expected to detect large cluster samples via the Sunyaev-Zeldovich (SZ) effect. Beginning in the summer of 2012, the Atacama Cosmology Telescope (ACT; Fowler et al. 2007) with the new polarization-capable receiver (ACTpol) will conduct a deep cluster search via the SZ effect within the HSC footprint. Planck, as an all-sky mission, will also deliver high-quality cluster samples detected through the SZ effect. Finally, the German-Russian satellite eROSITA will be launched in 2014; it will conduct the first all-sky X-ray survey since ROSAT in the 1990s.

The weakness of this cosmological test is that the cluster mass — the key parameter whose evolution is predicted by theory or N-body simulations — cannot be observed directly. Traditionally, cluster masses for large samples of clusters could only be inferred statistically, via various "observable"–mass scaling relations. Popular observables include X-ray temperature/luminosity, SZ flux, and cluster richness, $N_{\rm gal}$. To derive cosmological parameters based on cluster abundance, we need to calibrate these relations which involves knowledge of their scalings with mass and, critically, the *scatter* in the relations. While weak lensing can calibrate the *mean* mass-observable relations and its scaling, it is too noisy to measure the masses of individual clusters to the required precision.

By observing thousands of galaxies per rich cluster, ngCFHT would offer the great advantage of measuring cluster velocity dispersions to a few percent, translating into a $\lesssim 10\%$ accuracy in mass. This would provide a superb method for calibrating the various cluster mass proxies. The statistical accuracy could be further improved by "stacking" clusters of similar values of observables (e.g., richness, X-ray temperature). In short, ngCFHT data could provide the ultimate determination of cluster mass relations and their scatter.

In addition to its importance as a calibrator for cosmological surveys, large spectroscopic datasets are important for understanding the physics of cluster evolution and the link between cluster physics and galaxy formation. For example, by correlating the group and cluster sample derived by ngCFHT with that from eROSITA (or ACTpol/Planck), it would possible to examine the association of intracluster gas and dark matter halos, and thereby answer a fundamental question of cluster physics and cluster cosmology: at a given halo mass, what is the diversity in the gas mass fraction? Are there massive (optically-rich) yet X-ray/SZ faint (gas deficient) clusters? As the gas mass fraction has been employed as a powerful cosmological probe, measuring the level of diversity (among high mass clusters) underpins the robustness of such an approach.

With a deep cluster survey, it would be possible, for the first time, to measure the redshift of every nearby galaxy above some mass threshold, irrespective of morphology, colour, and host DM halo (see also §2.9). With the large cluster sample, the detailed cluster membership information will provide a prime opportunity to *completely* measure the HOD — the number of galaxies as a function of cluster mass, $N_{\rm gal}$, its scatter, and the spatial and velocity distributions of galaxies within clusters — for various kinds of galaxies (e.g., blue, red, active, passive, etc) at the high-mass end. Measuring $N_{\rm gal}$, its second moment, and the central galaxy luminosity in individual groups and clusters would allow us to investigate their scatter at fixed mass, which are crucial information for the HOD framework, and contains important signatures of the galaxy formation process.

2.5.4.3 The Star Formation Histories of Galaxies

A. Spatially-Resolved Stellar Populations and Star Formation Histories of Dwarf Galaxies

The star formation and chemical enrichment histories of galaxies, particularly *dwarf* galaxies, remain poorly understood. For instance, it is well known that dwarf galaxies are inefficient star formers, but the mechanisms that quench star formation in some, and allow it to proceed in others, are poorly understood. Like any galaxy, the fossil record of star formation for dwarfs is encoded in their present-day stellar populations. Recent results suggest that, while the ages of giant galaxies depend on the mass of the galaxy, and are relatively insensitive to environment, the reverse is true for low-mass galaxies: i.e., quenched fractions (red vs. blue) and mean stellar ages are both strong functions of clustercentric radius and/or local density (see Figure 33)

To disentangle these effects, a comprehensive redshift survey of low-mass dwarf galaxies over a wide range of environments is needed. The Dark-Wide survey would provide a large sample of dwarfs in the field and poor groups. The Virgo cluster survey discussed above will provide a measure from the cluster outskirts into the core of the cluster. This will also provide basic demographics of red and blue fractions as a function of environment. While colours are useful for distinguishing currently star-forming galaxies from passive ones, to break the age-metallicity degeneracy and so obtain more precise ages of the dominant red population, one needs absorption line indices from high S/N (> 25) spectra. For red galaxies, mean stellar ages and metallicities can be determined to 20% and 0.1 dex respectively, on a galaxy-by-galaxy basis in 1-hr exposures on ngCFHT for galaxies with $r < 17.5$. At the distance of the Virgo cluster, this magnitude limit corresponds to $M_r = -13.7$, about ~ 7.5 magnitudes below L_*, or the roughly the luminosity of the Fornax dwarf spheroidal in the halo of the Milky Way. Thus, a deep survey of Virgo (and other nearby clusters) would connect the star formation histories of dwarfs in clusters to those of the Local Group satellites. In Coma and similarly rich clusters, repeated configurations in the central regions would allow us to place fibres repeatedly on the same galaxy and so build up exposure times of ~ 6 hours, reaching magnitudes $r \sim 18.5$. In Coma, for example, there are nearly a thousand such dwarf galaxies ($M_r > -16.5$) within the virial radius.

Recent work (van Dokkum & Conroy 2010; Capellari et al. 2012; Smith et al. 2012a) has also suggested the intriguing possibility that the slope of the stellar initial mass function (IMF) varies as a function of galaxy mass and/or morphological type. The importance of exploring the IMF via the dwarf-sensitive Na I 8183 Å, 8195 Å and FeH 9916 Å (Wing-Ford) lines has been highlighted by van Dokkum & Conroy (2010). Very-high-S/N (> 200) spectra are needed to measure these absorption lines, however, requiring a 10m-class telescope. With the large aperture and multiplexing capabilities of ngCFHT, it would become possible for the first time to obtain IMF measurements for large samples of giant and dwarf galaxies in nearby clusters (and to probe possible variations in IMF within individual galaxies using multiple configurations with ngCFHT in "SparsePak" mode; see below and Figure 34). In Virgo, one

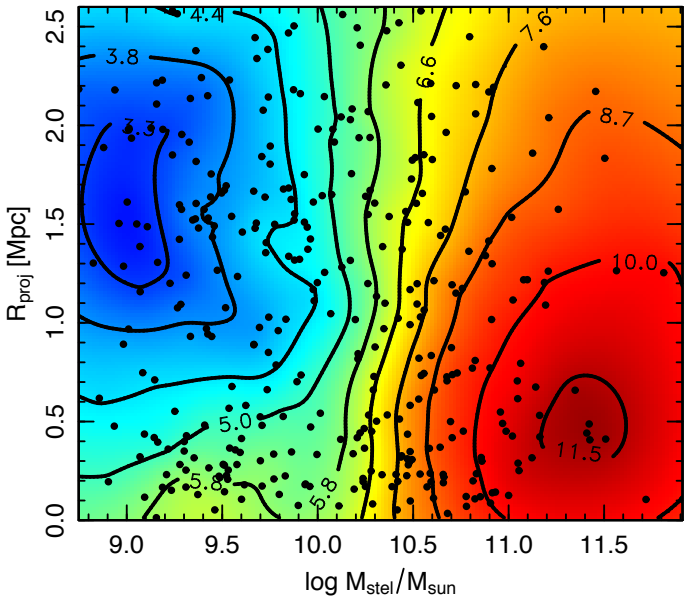

Figure 33: The dependence of the mean stellar age of red galaxies in the Coma cluster as a function of stellar mass and distance from the cluster centre. At high masses ($M \gtrsim 10^{10}\mathcal{M}_{\odot}$) the contours run vertically, indicating that the driving parameter modulating stellar age is stellar mass. However, at low masses, the contours become horizontal, suggesting that the distance from the cluster centre is strongly correlated with stellar age. This suggests that, for low-mass galaxies, it is cluster environment that quenches star formation. Figure from Smith et al. (2012b).

might obtain sufficient signal-to-noise spectra in one hour for dwarf galaxies $\sim$ 2–3 magnitudes below $L^{\star}$.

Finally, of particular interest is a systematic survey of intermediate-mass black holes in the centres of dwarf galaxies. Most currently-known extragalactic black holes have masses well in excess of 10^6 M$_{\odot}$, while few black holes with $M_{\rm BH} < 10^6$ M$_{\odot}$ have been detected unequivocally. Green & Ho (2004, 2007) pioneered the construction of a sample of < 230 low-mass black holes, with $M_{\rm BH} < 2 \times 10^6 M_{\odot}$, based on the SDSS. Most of these objects radiate at a high fraction of their respective Eddington rates. Black holes in this mass regime provide unique tests of the relationship between black holes and galaxies, since their late-type galaxy hosts do not necessarily contain classical bulges. Once again, a comprehensive survey of the Virgo cluster would be invaluable in this regard: HST imaging of the early-type galaxy population in Virgo has shown that most intermediate- and low-mass galaxies contain compact, structurally distinct stellar nuclei that may follow similar scaling relations as supermassive black holes (e.g., Côté et al. 2006; Ferrarese et al. 2006). Thus, a survey of Virgo with ngCFHT would allow the direct measurement of nuclei masses, ages and metallicities for a *complete* sample (i.e., many hundreds) of galaxies down to $g \simeq 17$, with clear implications for models of supermassive black hole growth.

In short, ngCFHT would make it possible to probe galaxy centres (and their central black holes) well down the galaxy luminosity function to unprecedently low flux levels. We would thus be able to determine conclusively the fraction of low-luminosity, low-mass black holes in the more typical galaxies that populate most of the known universe.

B. Spatially-Resolved Stellar Populations and Star Formation Histories of Giant Galaxies

The internal distribution of the stellar populations within individual galaxies yields important clues to their assembly, merger and the progression of star formation. For example, in spiral galaxies, chemical abundance gradients reveal in the disk the progression of star formation and the replenishment of the disk from gaseous corona. As an example, in starburst galaxies (including circumnuclear star-forming regions/rings), the mechanisms responsible for both triggering and propagation of their activity are not well understood. To better understand these processes, it is necessary to map the dynamics, reddening and age distributions of individual, star-forming regions in order to discriminate between stochastic and sequential star formation. Star-formation rates can be determined from dereddened Hα fluxes, while reddening values can obtained quite straightforwardly from Hα and CaII triplet equivalent widths. For the prevailing

nuclear starbursts, both Hα and Hβ are needed to correct for reddening in the ionized gas. Differences and similarities in the stellar populations between bulges, bars and disks can shed light on whether the former is correlated with the latter (as expected in secular evolution models). In "red and dead" galaxies, age and metallicity gradients reveal the relative importance of dry and wet mergers — a critical but poorly understood aspect of the histories of these objects.

In regions where the target density is very high (e.g., in rich clusters), there would be multiple fibre configurations of the same fields with ngCFHT. We would use this opportunity to perform spatially-resolved spectroscopy of bright giant galaxies, by applying repeated offsets in specific directions (e.g., along the disk major axis). There would be almost no "cost" for this revised observing strategy as the density of very bright target galaxies, and hence the number of fibres consumed, is relatively low. But the benefit would be high: it would be possible to obtain *spatially-resolved* abundances (cf. Figure 34), chemical enrichment histories, star formation rates and kinematics of the target galaxies, to derive their star formation timescales and history, and place these in the overall context of galaxy evolution scenarios. For very bright galaxies, one may be able to place as many as ~ 10 fibres across the galaxies. For somewhat less bright objects (say the brightest $\sim 20\%$ of nearby galaxies), it should be still possible to obtain simple but useful dynamical and abundance gradient information by offsetting fibres to ~ 2.2 disk scale-lengths from the galaxy centre (where the contribution of the disk to the rotation curve peaks).

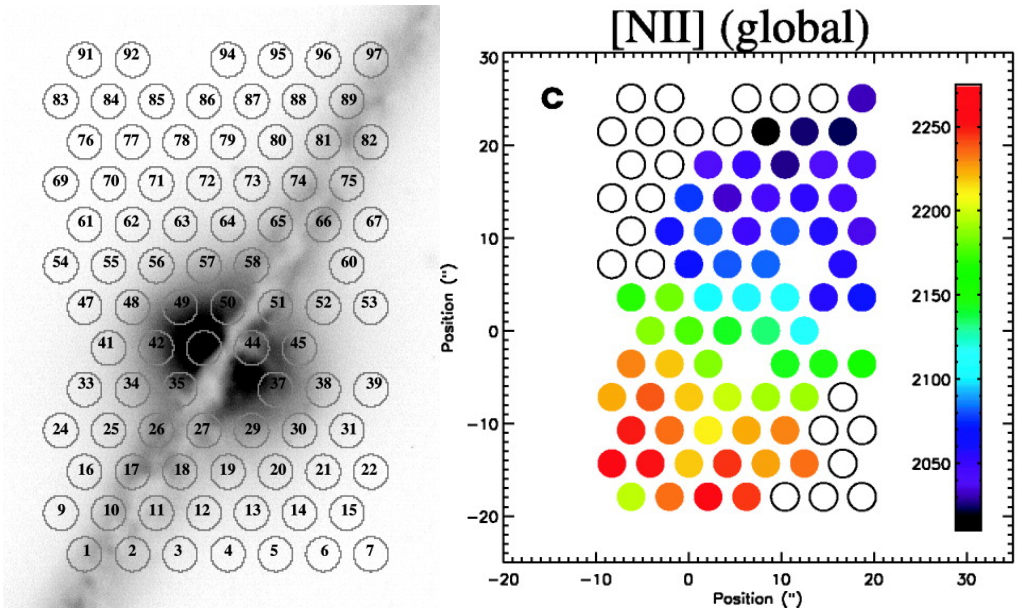

Figure 34: (Left Panel). An example of sparse IFU coverage for a central galaxy using fibres, based on WIYN observations of UGC 10043, a late-type galaxy at ∼30 Mpc, with the DensePak instrument (Matthews & de Grijs 2004). The DensePak fibres have $3''$ diameters and separations of $4\farcs15$. ngCFHT could mimic the multiple pointings across the face of the galaxy if it were observed in a field with repeated observations (and configurations). (Right Panel). The kinematics of the ionized gas in this system extracted from a single feature: the forbidden ionized nitrogen doublet [NII] at $\lambda\lambda 6548.0, 6583.4$Å. One could measure simultaneously the kinematics of the stellar components from, e.g., the Ca II triplet, while abundances and star formation rates could be determined from many other lines in the optical. In both panels, the field is roughly $1'$ on a side.

A 1-hour exposure would reach a surface brightness level of $\mu_g = 23.0$ mag arcsec^{-2} (for a generic elliptical galaxy) with a S/N per Å of ~ 5 in the range from 600 to 800 nm. Taking the Coma cluster as an example of a rich cluster, reaching an IFU-like configuration for $N = 10$ therefore requires 10, 1-hour observations. Although this is a modest fibre investment, it would be of tremendous importance in narrowing down the origin of stellar population and metallicity differences within a large number of massive cluster galaxies, simultaneously and homogeneously.

2.5.5 Legacy Surveys and Key Projects

To achieve the science goals listed above, there are several key requirements: (1) a *large area* in order to attain a fair sampling of the field, spanning all environments from deep voids, to rich clusters, in the nearby universe; (2)

depth, in order to reach dwarf galaxies of the lowest possible masses; and (3) *multiple fibre configurations* on the same fields in order to: (a) obtain complete samples of dynamical tracers with which to measure halo masses; and (b) obtain spatially-resolved spectra of larger galaxies. The ngCFHT Dark-Medium survey satisfies conditions (2) and (3), although over a relatively small area on the sky (100 deg^2). The ngCFHT Dark-Wide survey covers a large area (4 300 deg^2), but has low completeness (10%), even in regions of average density. We therefore describe two supplementary surveys, or key projects, that have been designed to meet these science goals. These are: (1) a wide, nearly complete survey of galaxies in the low-z universe; (2) a targeted survey of nearby, rich clusters; and (3) an ultra-deep, high-completeness survey of Virgo, the nearest cluster.

2.5.5.1 Key Project I. A 1000 deg^2 Complete Survey of the Nearby Universe (LOWZ)

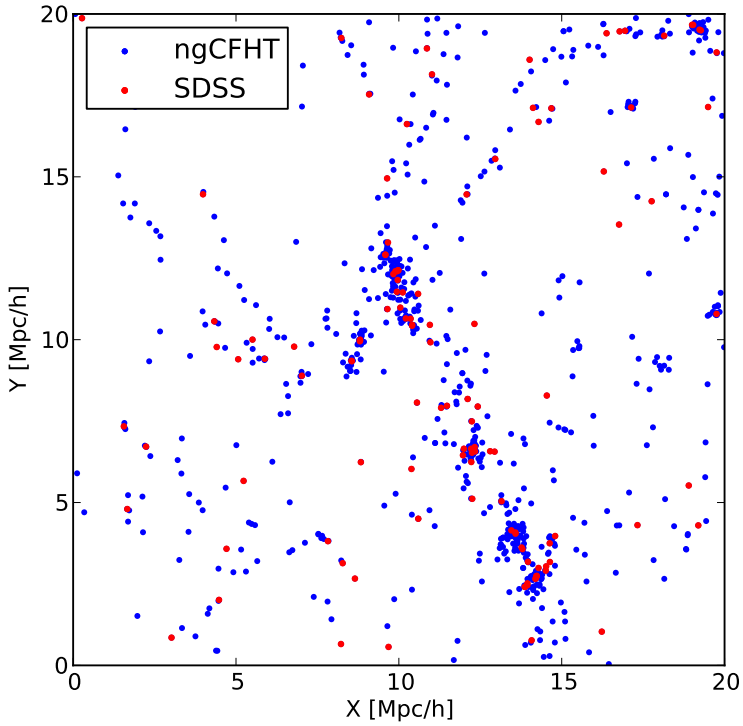

Figure 35: A simulated, 10 Mpc/h-thick slice at a depth of $z = 0.05$ from the Millenium-II semi-analytic models (Guo et al. 2011). Galaxies that meet the SDSS selection criteria are shown in red, while those that could be detected with ngCFHT are shown in blue. Note the many small groups of faint dwarfs that would be within reach of ngCFHT, and how these low-mass galaxies fill the voids.

Optimized for galaxy evolution and cosmological studies, the ngCFHT Dark-Wide survey would have a completeness of $\approx 10\%$ (§2.6). For a unbiased measurement of the dynamics and masses of the lowest-mass DM halos, their baryonic content, and the dependence of these parameters on local environment, we would require a $\sim$ 1000 deg^2 survey with high completeness at $i' < 22$ for galaxies with $z < 0.15$ (see Figure 35). For this particular project, near-complete sampling is crucial in order to obtain reliable masses for the low-mass groups. We anticipate pre-selecting targets using photometric redshifts from multiwavelength data, limited to $z < 0.21$ so that the $z < 0.15$ volume is $\sim 95\%$ complete. The surface density of targets would then be $\sim 1\,400$ deg^{-2}, which is well matched to the ngCFHT fibre-positioning system. Of course, galaxies are clustered, and so repeat configurations within the same pointings would be necessary for a complete sample. Given the short reconfiguration time expected for ngCFHT (40 sec or less), the optimal strategy would be multiple, short (15 min) exposures, with a total depth of 8×15 minutes (2 hrs total) exposure per field. In a small percentage of fields containing a very high density of targets (i.e., rich groups or clusters), this would need to be increased by a factor ~ 3.

The completed survey would cover an area four times larger than the GAMA survey and reach ≈ 2 mag deeper,

Table 12: Technical Requirements and Survey Implementation: The LOWZ Survey

Survey Area (Ω)	$\Omega \approx 1000$ deg^2.
Field Location	TBD
Number of ngCFHT Fields ($N_{\rm field}$)	$N_{\rm field} \approx 600$, excluding coverage already available from the Dark-Wide survey; assumes 5% overlap.
Number of Configurations per Field ($n_{\rm config}$)	$\langle n_{\rm config} \rangle \sim 4$, with some variation between 2–6 depending on surface density of targets.
Total Number of Exposures ($N_{\rm exp}$)	$N_{\rm exp} = 8 \times 600 \approx 4800$.
Primary Imaging Resources for Target Selection	GALEX, VST, LSST, Euclid, VISTA, WISE, HERSCHEL, GMRT, ASKAP, etc
Observing Conditions	Lunar illumination $< 50\%$.
Instrumental Configuration(s)	(1) $\mathcal{R} = 2\,000$ (i.e., Dark-Wide survey), $N_{\rm point} \simeq 700$, $T_{\rm exp} = 1$ hr (2) $\mathcal{R} = 2\,000$ (i.e., Dark-Medium Survey), $N_{\rm point} \simeq 70$, $T_{\rm exp} = 4$ hr (2) $\mathcal{R} = 2\,000$ (i.e., LOWZ Survey), $N_{\rm point} \simeq 600$, $T_{\rm exp} = 0.25$ hr
Wavelength Coverage and Velocity Precision (ϵ_v)	(1) 0.37–1.3μm and $\epsilon_v \approx$ 15–30 km s^{-1} at $\mathcal{R} = 2\,000$
Limiting (point source) Magnitude	$i' \simeq 22$.
Total Time Needed for Program ($T_{\rm tot}$)	$T_{\rm tot}$ = [8×600×0.9×0.25 hr] + 20% overhead $\approx$ 1 300 hrs. [Excluding time allocated to the Dark-Wide and Dark-Medium surveys.]

yielding $\sim 500\,000$ redshifts within $z < 0.15$. We anticipate that 10% of the targets will be covered by the Dark-Wide survey, and that 100 deg^2 of this area would be covered fully by the Dark-Medium survey. Therefore, to cover 800 deg^2 with 2-hour exposures would require $\sim 1\,300$ hours, including overheads.

2.5.5.2 Key Project II. A Deep Survey of Rich Clusters

Rich clusters are a linchpin of several cosmological studies that probe dark energy and the growth of structure. They are also ideal targets for exploiting ngCFHTs extreme multiplexing capabilities. The LOWZ survey described above would be likely to pick up only a few clusters with masses comparable to the Coma cluster. An obvious ancillary project would therefore be a study of about 20 rich clusters down to a depth of $r \sim 22$ ($M_r \sim -13$ at the distance of Coma) and extending beyond each cluster's virial radius. Note that the eROSITA mission (scheduled for launch in 2014) is expected to detect about 10^5 clusters down to a mass of $\sim 2 \times 10^{14} M_\odot$. It is thus reasonable to expect that there will be a very large sample of nearby ($z < 0.1$) clusters with high-quality, multi-wavelength and weak lensing data from which to select a sample of 20 suitable clusters. We anticipate 12 hours of exposure per cluster, with one or two configurations on the cluster outskirts and multiple overlapping configurations in the central regions, yielding 40 000 fibre-hours of exposures per cluster. The repeat configurations are needed, first, to sample dense regions of the cluster but, importantly, to give the added flexibility of stacking exposures (by repeated fibre placement on the same target) of targets of interest, or to simulate a sparse IFU-like mode (using offset pointings on the same galaxy; see Figure 34). For instance, for each cluster, one could observe 20 000 faint galaxies targets as well as 1 000 large galaxies with 10 IFU pointings per galaxy and 1 000 dwarfs with deep 10-hr exposures for individual ages and metallicities. Of course, for fainter red galaxies, the spectra could be stacked to obtain mean ages and metallicities for the stacked population. Such a programme would require ~ 290 hours, including overheads.

Table 13: Technical Requirements and Survey Implementation: The Rich Cluster Survey

Survey Area (Ω)	20 cluster fields at $z < 0.1$; total coverage of $\Omega \sim 30$ deg^2.
Field Location	TBD
Number of ngCFHT Fields ($N_{\rm field}$)	$N_{\rm field} \approx 20$, excluding dithers.
Number of Configurations per Field ($n_{\rm config}$)	$\langle n_{\rm config} \rangle \sim 3$, with some variation between 2–6 depending on the distribution of targets.
Total Number of Exposures ($N_{\rm exp}$)	$N_{\rm exp} \approx 12$ per cluster.
Primary Imaging Resources for Target Selection	eROSITA, Pan-STARRS (3π), LSST, Euclid (Wide), ASKAP, etc
Observing Conditions	Lunar illumination $< 50\%$.
Instrumental Configuration(s)	$\mathcal{R} = 2\,000$, $N_{\rm point} = 30$, $T_{\rm exp} = 12$ hr
Wavelength Coverage and Velocity Precision (ϵ_v)	0.37–1.3μm and $\epsilon_v \approx$ 15–30 km s^{-1} at $\mathcal{R} = 2\,000$
Limiting (point source) Magnitude	$r \simeq 22$
Total Time Needed for Program ($T_{\rm tot}$)	$T_{\rm tot}$ = [12×20×1 hr] + 20% overhead $\approx$ 290 hrs.

2.5.5.3 Key Project III. The Virgo Cluster Spectroscopic Survey

While statistical studies are essential, it is also important to study some benchmark objects in detail. An obvious key project with ngCFHT is therefore a comprehensive spectroscopic survey of the Virgo cluster (see Table 14). With a gravitating mass of $M \simeq 4 \times 10^{14} M_\odot$, the Virgo cluster contains about 700 galaxies (DM subhalos) with stellar

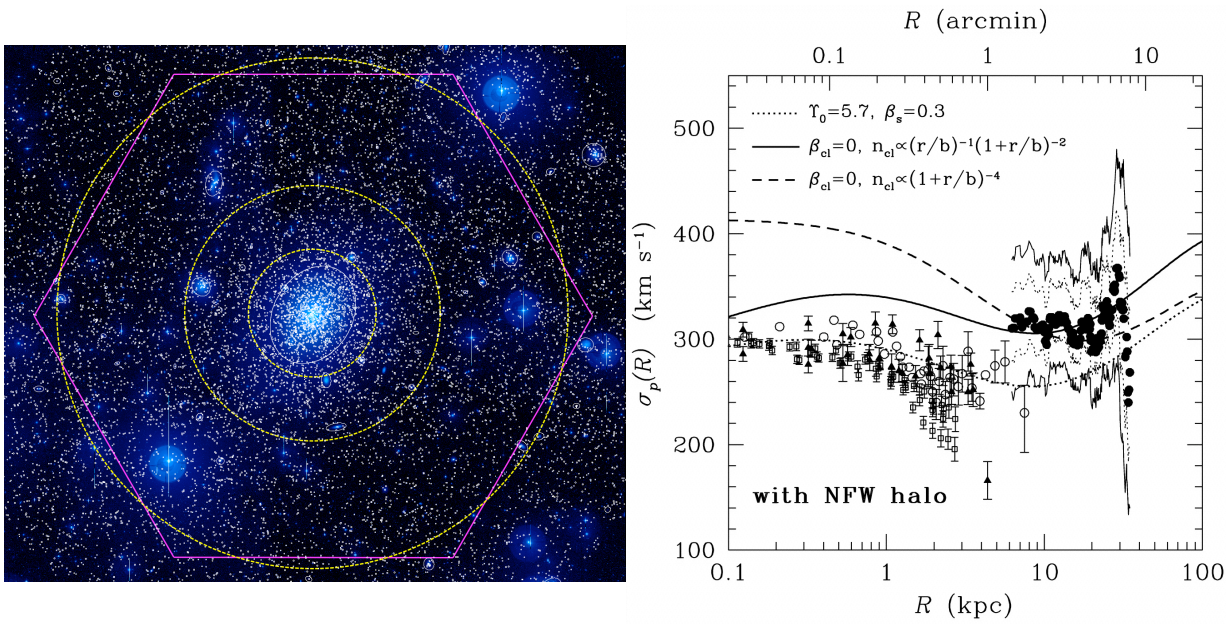

Figure 36: (Left Panel). The central region of the Virgo B subcluster based on deep, wide-field CFHT imaging from the Next Generation Virgo Cluster Survey (Ferrarese et al. 2012). The 1.5 deg^2 field of ngCFHT is shown by the hexagon. White symbols show confirmed or probable baryonic substructures (e.g., giant galaxies, dwarf galaxies, UCDs, and star clusters) within the Virgo cluster, selected to have $g_{\rm AB} \leq 23.5$. The yellow circles have radii of 50, 100 and 200 kpc. (Right Panel). Stellar velocity dispersion profile for the central galaxy (M49) in the preceding panel, as well as for 263 globular star clusters based on multi-object spectroscopy from the Keck 10m telescope (Côté et al. 2003). The curves show models for different baryonic tracer populations embedded in the cluster dark matter potential, for a variety of velocity anisotropy parameters, β. A 210-hr ngCFHT survey of the Virgo cluster could be supplemented with data from the Dark-Wide survey to derive radial velocities for more than $\sim$ 600,000 sources located inside the cluster's virial radius. Spectroscopically confirmed members of Virgo would then be used as dynamical test particles to measure the distribution of dark matter in the cluster and the orbital properties of the embedded baryonic tracers.

masses larger than $M_* \simeq 10^9 M_\odot$. The internal velocity dispersions of these galaxies vary from $\sigma_v \approx$ 15–20 km s^{-1} at $\mathcal{M}_* = 10^9 \mathcal{M}_\odot$ to $\sigma_v \approx 300$ km s^{-1} for the most massive galaxies. Spectra collected as part of the Dark-Wide survey that encompasses the Virgo cluster region would therefore be well suited to this programme, although these data alone would be insufficient for a comprehensive survey, for two reasons. First, large variations in target surface density over the cluster would require multiple pointings and/or fibre configurations to achieve a high level of completeness for tracers located near the centres of high-mass galaxies (see the left panel of Figure 36). Second, while a spectral resolution of $\mathcal{R} = 2\,000$ (which corresponds to a velocity precision of $\epsilon_v \sim$ 15–30 km s^{-1}) would be adequate for studying the internal dynamics of the roughly 200 galaxies that are more massive than $\mathcal{M}_* \simeq 6 \times 10^9 \mathcal{M}_\odot$ (which have $\sigma_v \sim 75$ km s^{-1}), additional observations at a spectral resolution of $\mathcal{R} \sim 6\,500$ ($\epsilon_v \sim$ 5–10 km s^{-1}) would be needed to resolve the internal velocity structure of the lower mass galaxies ($15 \gtrsim \sigma_v \gtrsim 75$ km s^{-1}).

Recently, SDSS data have been used to identify $\sim$ 10 000 GC candidates within $\sim$ 2 Mpc of the cluster centre (Lee et al. 2010), while a much deeper $ugriz$ survey of the Virgo cluster with CFHT (the Next Generation Virgo Cluster Survey; NGVS) will soon produce a catalogue of many tens of thousands of star clusters, faint galaxies and ultra-compact dwarf (UCD) candidates over the full $\approx$ 100 deg^2 extent of the cluster (Ferrarese et al. 2012; Figure 36). Many of these objects — to which we refer collectively as *baryonic substructures* — are sufficiently bright that they are within reach of ngCFHT while and their density on the sky is also well matched to the ngCFHT fibre density. PNe are also attractive targets for ngCFHT, and these have already been detected in the halos of galaxies and in intracluster space in Virgo (e.g., $\Sigma \sim 350$ deg^{-2}; Feldmeier et al. 2004). Moreover, it will soon be possible to generate much more extensive PNe catalogues, covering the full extent of the cluster, by combining $ugriz$ imaging from NGVS (and, eventually, high-resolution IR imaging to a depth of $J_{\rm AB} \sim 24.5$ from Euclid) with narrow-band [OIII] λ5007 imaging collected with wide-field 4-8m telescopes.

Table 14: Technical Requirements and Survey Implementation: The Virgo Cluster Spectroscopic Survey

Survey Area (Ω)	The Virgo cluster ($r \leq r_{200}$): $\Omega \approx 100$ deg^2.
Field Location	$\alpha_{2000} \simeq 188^\circ$, $\delta_{2000} \simeq 12^\circ$
Number of ngCFHT Fields ($N_{\rm field}$)	$N_{\rm field} = \Omega / {\rm FOV}_{\rm ngCFHT} \approx 70$ for complete areal coverage.
Number of Configurations per Field ($n_{\rm config}$)	$\langle n_{\rm config} \rangle = 3$, with some variation between 2–5 depending on surface density of targets.
Total Number of Exposures ($N_{\rm exp}$)	$N_{\rm exp} = N_{\rm field} \times \langle n_{\rm config} \rangle \approx 210$ (including 70 from the Dark-Wide Survey).
Primary Imaging Resources for Target Selection	CFHT (NGVS), Pan-STARRS (3π), Subaru/HSC, Euclid (Wide)
Observing Conditions	Lunar illumination $< 50\%$. Cloud cover $< 20\%$.
Instrumental Configuration(s)	(1) $\mathcal{R} = 2\,000$ (i.e., Dark-Wide survey), $N_{\rm point} = 70$, $T_{\rm exp} = 1$ hr
	(2) $\mathcal{R} = 2\,000$ (i.e., Virgo Spectroscopic Survey), $N_{\rm point} = 70$, $T_{\rm exp} = 1$ hr
	(3) $\mathcal{R} = 6\,500$ (i.e., Virgo Spectroscopic Survey), $N_{\rm point} = 70$, $T_{\rm exp} = 1.5$ hr
Wavelength Coverage and Velocity Precision (ϵ_v)	(1) 0.37–1μm and $\epsilon_v \approx$ 15–30 km s^{-1} at $\mathcal{R} = 2\,000$
	(2) 0.37–0.58μm and $\epsilon_v \approx$ 5–10 km s^{-1} at $\mathcal{R} = 6\,500$
Limiting (point source) Magnitude	$g_{\rm AB} \simeq 23.6$, corresponding to a mass of $\sim 3 \times 10^5 M_\odot$ for old stellar populations.
Total Time Needed for Program ($T_{\rm tot}$)	$T_{\rm tot}$ = [(70×1 hr) + (70×1.5 hr)] + 20% overhead $\approx$ 210 hrs.
	[Excluding (70×1 hr) + 20% overhead $\approx$ 84 hrs available from the Dark-Wide Survey.]

The key parameters for a spectroscopic survey of the Virgo cluster are summarized in Table 14. The survey would require three visits and configurations for each of the 70 ngCFHT fields that are needed to cover the cluster in its entirety; note that this total of 210 configurations includes 70 that would be obtained in the Dark-Wide survey. In other words, in roughly 210 hrs of dark time — over and above the 84 hrs that would be devoted to surveying this same region in the Dark-Wide survey — it would be possible to collect spectra for a sample of more than *a half million* sources in the direction of Virgo (including "contaminating" foreground stars and background galaxies). Using the database of spectroscopically confirmed baryonic substructures in Virgo, it would be possible to carry out an unprecedented characterization of the mass function and density structure of DM halos and subhalos across the whole of the cluster. Such a survey would also provide the first complete and unbiased census of compact stellar systems (i.e., ultra-compact dwarfs, extreme cE-type galaxies, etc) for *any* environment. Without spectroscopy to identify such objects and place them unambiguously within the cluster (i.e., they appear "star-like" in normal conditions of ground-based seeing), their detection must rely on either statistical arguments, or pencil-beam surveys with HST (Hasegan et al. 2005) and narrow-field spectrographs on 8m-class telescopes (see Brodie et al. 2011 and references therein).

To appreciate the power of ngCFHT for a spectroscopic survey of this sort, consider the time required to conduct an equivalent survey with existing telescopes and multi-object spectrographs. As we have seen, it is possible to survey the full 100 deg^2 cluster area and down to a depth of $g_{\rm AB} \sim 23.5$ in about 294 hrs of dark time (yielding spectra for $\sim 500\,000$ sources). It would therefore be possible to complete this survey in, at most, two observing seasons with ngCFHT. Assuming that Virgo is observable during dark time for an average of ~ 200 hrs per year, then a comparable programme with VLT-FLAMES, VLT-VIMOS, Keck-DEIMOS or MMT-Hectospec would require 39, 14, 27 and 10 years to complete.

2.6 Galaxy Evolution

2.6.1 Abstract

Galaxies grow over time through a combination of *in situ* star formation, gas accretion, and mergers. The CDM model provides robust predictions for the growth of structure, but gas and stellar dynamics, heating and cooling processes, dust, and chemical evolution all make the formation of galaxies a much more complex process. The SDSS revolutionized the field of galaxy evolution by providing spectroscopy for ~ 1 million nearby galaxies distributed over an area of $\sim 10\,000$ deg^2. This has led to secure measurements of how galaxy properties — such as morphology, star formation rate, metallicity, gas content — depend on their stellar mass, dark halo mass and environment. However, these local trends are generally only indirectly related to the driving physical mechanisms of galaxy evolution, as they represent a snapshot of the present-day universe. While *ab initio* models provide some insight into the type of processes that might be important (e.g., AGN feedback, photoionization, mergers, ram pressure stripping), they are generally not sophisticated enough to put tight constraints on the relevant parameters, and there remain some serious discrepancies with observations that defy explanation. Spectroscopic surveys that are analogous in scope to the SDSS, but aimed at higher redshift, can directly measure the rate of galaxy evolution for different types of galaxies in different environments. While good progress has been made with surveys like DEEP2, zCOSMOS, GDDS, and VVDS, none of these have the combination of depth, completeness, width and sample size necessary to make measurements with the precision of SDSS. The three darktime surveys proposed for ngCFHT are poised to make a transformational contribution to our understanding of galaxy formation.

2.6.2 Introduction

The basic model of galaxy formation has been in place for more than twenty years (White & Frenk 1991). The growth of dark matter structure appears to be well described by the gravitational growth of fluctuations observed in the CMB. Radiative cooling of baryons leads to efficient star formation, and various mechanisms must then work to reheat, or expel, this gas in order to match the low efficiency of star formation observed today. Through ambitious, spectroscopic surveys of galaxies at $z \sim 0$ such as the SDSS (York et al. 2000) and 2dFGRS (Colless et al. 2001), and surveys at higher redshift, most notably GDDS (Juneau et al. 2004), DEEP2 (Willmer et al. 2006; Faber et al. 2005) and zCOSMOS (Lilly et al. 2007), a reasonable picture of stellar mass growth since $z \sim 1$ is in place. At higher redshifts, deep imaging surveys, with some spectroscopic follow-up, have established the growth of the most massive galaxies up to $z \sim 8$ (e.g., Bouwens et al. 2011).

However, there remain many unsolved problems. For example:

1 *How does stellar mass growth relate to halo mass growth?* Great advances have been made here through techniques like abundance matching (Yang et al. 2008) or Halo Occupation Distribution (HOD) modeling (Zheng et al. 2007), where the galaxy distribution is linked to the growth of dark matter halos. Applied to SDSS data at $z \approx 0$, this demonstrates that galaxy formation efficiency peaks in halos of $M \sim 10^{12} M_{\odot}$. At higher redshift, the constraints are poorer, as they either rely on photometric redshifts (e.g., Wake et al. 2011; Leauthaud et al. 2011; Coupon et al. 2011), or spectroscopic surveys over small areas (e.g., Abbas et al. 2010; Knobel et al. 2009). Nevertheless, this can be used to trace the evolution of star formation efficiency since about $z \sim 1$ over a wide range of masses, as shown in Figure 37. The cosmic star formation rate is observed to be rising with time between $z \sim 8$ and $z \sim 3$, where it remains high and roughly constant until $z \sim 1$ (Hopkins & Beacom 2006; Seymour et al. 2008; Kistler et al. 2009; Magnelli et al. 2011). Since ΛCDM models predict a declining infall rate at all epochs, this observation has proved difficult to explain theoretically (e.g., Weinmann et al. 2011; Krumholz & Dekel 2011). Better constraints on halo occupation at this redshift are needed, and these will require deep, spectroscopic surveys.

2. *How does satellite galaxy evolution differ from that of central galaxies?* A key component of HOD models, and many *ab initio* galaxy formation models (Bower et al. 2006), is that galaxies that are central in their dark matter halo evolve differently from those that are satellites. This is due to differences in the way gas flows into these galaxies. Although clear differences between central and satellite galaxy properties are indeed observed — both locally (e.g., Peng et al. 2010; Weinmann et al. 2010) and at higher redshifts (e.g., Poggianti et al. 2006; Cooper et al. 2006; McGee et al. 2011; Cooper et al. 2010; Balogh et al. 2011) — the interpretation, and possible explanation, of these trends remain poorly constrained (e.g., Balogh et al. 2009; Weinmann et al. 2010; Wetzel & White 2010; Weinmann et al. 2012).

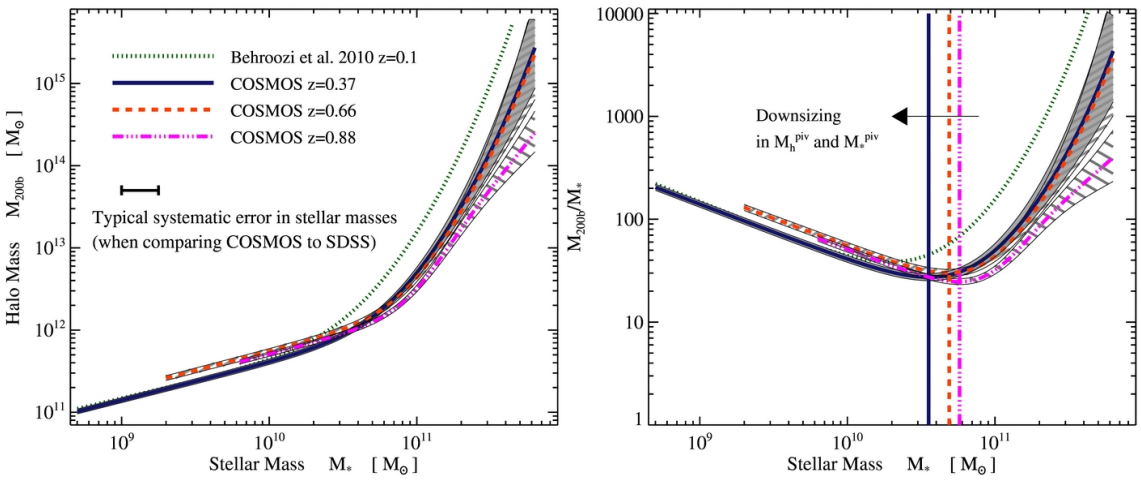

Figure 37: The redshift evolution of the correlation between stellar and halo mass, taken from Leauthaud et al. (2011). The left panel shows the correlation between stellar mass and halo mass, determined from the COSMOS survey over three redshift ranges. The results indicate an evolution in the stellar and halo mass at which M_{200b}/M_* reaches a minimum (see the panel on the right). At high masses, there is an interesting hint that the amplitude of the relation is decreasing at higher redshifts, but the volume of COSMOS is too small to claim a clear detection.

3. *What are the effects of environment on galaxy formation and evolution?* The large-scale environment likely influences both the mass accretion rate (e.g., Wechsler et al. 2002; Maulbetsch et al. 2006; Gao & White 2007) and the way that gas is accreted (Cattaneo et al. 2008; Dekel et al. 2009). The evolution of most galaxy properties (e.g. luminosity, colour, morphology) are sensitive to the gravitational and hydrodynamic interactions between galaxies, and the rate and type of such interactions is determined by the environment. These are generally complex, nonlinear effects and often subdominant to more local effects like feedback (q.v.). Spectroscopic observations of *millions* of galaxies are needed to disentangle the effects of environment from the other parameters driving galaxy evolution.

4. *How does feedback work?* It seems clear that supernova feedback and galaxy winds play a strong role in reducing star formation efficiency for most galaxies (e.g., Davé et al. 2011). In general, this can work either through heating gas or expelling it from the system. It is also clear that neither mechanism is sufficient to prevent overcooling in the most massive galaxies. The most promising explanation for the latter problem is that accretion onto supermassive black holes provides the energy, but we lack a convincing description of how this works. There are also relatively unexplored mechanisms, such as cosmic ray heating (Enßlin et al. 2011; Sironi & Socrates 2010) and heating from blazars (Pfrommer et al. 2011), that may prove to be important.

5. *How do galaxies get their gas?* The amount of cold gas in disks is insufficient to sustain star formation at their current rates for a Hubble time, and it is necessary that galaxies be "fueled" by gas on larger scales. This could come either through cooling of a hydrostatic hot halo, or through "cold flows" — i.e., cold, clumpy gas accreted for example along filaments. Both modes are likely important, at different epochs and for different mass galaxies (Birnboim & Dekel 2003; Kereš et al. 2005; Dekel et al. 2009).

2.6.3 ngCFHT in Context: Competition and Synergies

Astronomy is entering an era dominated by large surveys, and the majority of these (both current and planned) are restricted to imaging, with limited or negligible spectroscopy. Collectively, surveys like Pan-STARRS, DES, LSST and *Euclid* will image most of the sky in optical and IR filters. These exquisite data are necessary to make significant progress in our understanding of galaxy evolution, and a great deal of progress has already been made through wide-field imaging studies alone. However, spectroscopy is absolutely essential to address the science cases outlined here, for the following reasons.

1. Precise redshifts (i.e., distances) are only possible with moderate-resolution spectroscopy. With good photometric filter coverage it is possible to achieve a precision of $\sigma/(1+z) \sim 0.03$ (Mobasher et al. 2007); this is the expected precision of the Euclid/LSST combination (e.g., Sorba & Sawicki 2011). Catastrophic errors can be almost completely eliminated in such a survey, if objects with large uncertainties on their photo-z are discarded. As shown in Table 15, this is sufficient to identify the epoch at which a galaxy is observed, to within 300 Myr or better for galaxies at $z > 0.3$. It is also sufficient to measure the total galaxy luminosity (and, hence, closely related quantities like SFR or stellar mass), to within thirty per cent, at all $z > 0.3$. However, the uncertainty on luminosity distance is always > 100Mpc and increases with redshift, to over 1 Gpc at $z = 3$. With additional, narrow-band filters, one can do better; using 30 filters the COSMOS survey yielded $\sigma/(1+z) \sim 0.008$ (Ilbert et al. 2009). But even this (much more expensive!) strategy corresponds to a > 30 Mpc uncertainty on luminosity distance (i.e., more than 100 Mpc at $z = 1$). This makes it very difficult to identify large-scale structure from imaging surveys alone, due to large line-of-sight projections. Massive clusters and some large-scale filamentary structure can be identified through other techniques (e.g. X-ray or SZ observations), but spectroscopy is required to associate individual galaxies with those structures, to measure dynamical masses of these structures through the velocity distribution of their members, and to identify close pairs of interacting or merging galaxies.

Table 15: Precision in Distance, Time and Luminosity for a Redshift Uncertainty of $\sigma/(1+z) \sim 0.03$.

Redshift	Δz	ΔD_L (Mpc)	ΔD_A (Mpc)	Δt (Mpc)	$\Delta L/L$
0.1	0.033	162.7	111.38	399.4	0.705
0.5	0.045	306.3	60.29	320.0	0.216
1	0.06	489.4	23.12	237.9	0.148
2	0.09	854.6	8.57	141.1	0.110
3	0.12	1223.1	18.82	94.0	0.096

2. Some measurement of star formation history can be inferred from the stellar populations by fitting the spectral energy distribution from multi-band imaging alone. Although the uncertainties for an individual galaxy can be large, many of the statistical and systematic errors inherent in photometric studies can be overcome through averaging. With samples of $> 100\,000$ galaxies the statistical and any randomly distributed systematic uncertainties become negligible. However, this technique is prone to biases (Lee et al. 2010); there is a tendency to underestimate the mass and age of galaxies, by up to a factor of ten, due to the fact that light from young stars dominates the emission (Kannappan & Gawiser 2007; Maraston et al. 2010). Such systematic errors lead to a factor ~ 3 uncertainties on the stellar mass fractions (Conroy et al. 2010; Behroozi et al. 2010). Other physical quantities such as the star formation history, dust content and metallicity are more poorly constrained (Sawicki & Yee 1998; Walcher et al. 2008; Lee et al. 2010). Spectroscopy, combined with photometric information, substantially improves estimates of age, dust extinction, current star formation rate and star formation history, through both improved spectral resolution and a more precise redshift (Kriek et al. 2008).

3. For some galaxies, spectroscopy allows independent measures of dust extinction and metallicity. The former especially requires a measurement of the $H\alpha$ emission line. Good red throughput is therefore important, and sensitivity at 1.3μm would enable detection of the $H\alpha$ line to almost $z = 1$. Finally, tracers of current (Hα, [OII] emission) and recent ($H\delta$ absorption) star formation provide independent and complementary information to that measured from the UV or IR continuum. In particular, the presence of strong Hδ absorption lines in a galaxy without evidence for significant, ongoing star formation can be a good indication of recent "quenching", where evolution is driven by a drop in star formation rate. Such galaxies can thus be used to trace the evolution of this quenching process (Le Borgne et al. 2006; Yan et al. 2009; Poggianti et al. 2009). Notably, this quenching can *only* be identified reliably with spectroscopy. Unlike star formation rates, which can be estimated from photometry in several ways, recent quenching can best be measured with good S/N measurements of stellar absorption lines.

4. The need for averaging in purely photometric surveys makes it difficult or impossible to study the variation in galaxy properties. Stellar populations clearly depend on more than just cosmic time: i.e., even galaxies of fixed stellar mass and observed at the same epoch show a large diversity of stellar populations. Some of this diversity

is likely related to environment (e.g., satellite vs central galaxies) and to distributions of dust and metallicity — quantities that are difficult to constrain independently using photometry alone.

For these reasons, follow-up spectroscopy is an essential component for all these imaging surveys. While small-field telescopes like ALMA, TMT, E-ELT and JWST will make exciting contributions to the follow up of small numbers of galaxies, wide-field spectroscopy is necessary to address fundamental questions about the galaxy population as a whole, which requires statistically robust samples.

ngCFHT will face competition on this front from other wide-field spectrographs on both 10m-class (i.e., PFS on Subaru) and smaller (e.g., BigBOSS) telescopes. However, because Subaru is a user facility, it will not be able to devote a large fraction of time to PFS surveys; present plans for a "strategic program" of 300 nights over a five-year period (Ellis et al. 2012). Meanwhile, BigBOSS could perform a highly complete survey of ~ 100 deg^2, to a fairly bright limit of $I_{AB} = 20.5$, in just ~ 500 h of exposure time; however, the current plan for short exposures of only 15 min would not reach even that depth. Their strategy is to overlap tiles, and to select just luminous red galaxies (LRGs) and emission line galaxies (ELGs) (and other classes of objects, like quasars), to achieve 80 per cent completeness overall. Part of the BigBOSS survey strategy is to observe a few selected "calibration" fields multiple times. By the end of the survey, this will yield $\sim$ 30–40 deg^2 with high completeness, reaching $i = 22$–22.5 through repeat observations. Thus, it will have a depth comparable to the zCOSMOS survey, over an area ~ 20 times larger. While this will provide a much better range of environments compared with zCOSMOS, the depth will still be insufficient to reach galaxies that are most sensitive to environment (see § 2.6.4.2). There is, nevertheless, potential for an excellent synergy between the BigBOSS and ngCFHT surveys; by targetting BigBOSS fields ngCFHT can take advantage of the existing spectroscopy on brighter galaxies, and also pre-select appropriate fields for the Dark-Medium and Dark-Deep surveys.

2.6.4 Legacy Science

Three proposed dark surveys on ngCFHT would enable a wide number of investigations of distant galaxies. The average, expected source density of galaxies in a ngCFHT field is shown in Figure 38, based on the COSMOS photometric redshift catalogues of Capak et al. (2007). Assuming that the Dark-Wide survey reserves ~ 15 per cent of fibres for sky, and ~ 10 per cent of the remaining science fibres for quasars and other targets of interest, each configuration would be able to target ~ 2600 galaxies. At $I_{AB} = 23.5$, the approximate depth expected for the Dark-Wide survey[16], the target density is about 30 000 deg^{-2}. Thus, sampling will necessarily be sparse (< 10 per cent), but would nevertheless result in a sample of $\sim 7.4 \times 10^6$ galaxies. *This allows a study of galaxies over seven different epochs between* $0.5 < z < 1.5$*, each with the same statistical power as SDSS.*

Table 16: Technical Requirements and Survey Implementation: The Dark-Wide Survey

Survey Area (Ω)	$\Omega \approx 4\,300$ deg^2.
Field Location	Contiguous coverage over an equatorial field; field location and geometry TBD.
Number of ngCFHT Fields ($N_{\rm field}$)	$N_{\rm field} = \Omega/{\rm FOV}_{\rm ngCFHT} \approx 3010$ with 5% overlap.
Number of Configurations per Field ($n_{\rm config}$)	$\langle n_{\rm config} \rangle = 1$, with $n_{\rm config} > 1$ for nested Dark-Medium and Dark-Dark surveys.
Total Number of Exposures ($N_{\rm exp}$)	$N_{\rm exp} = N_{\rm field} \times \langle n_{\rm config} \rangle \approx 3010$.
Primary Imaging Resources for Target Selection	Euclid (Wide), Pan-STARRS (3π), LSST, eRosita, EMU, etc.
Observing Conditions	Lunar illumination $< 50\%$. Cloud cover $< 20\%$.
Instrumental Configuration(s)	$\mathcal{R} = 2\,000$, $T_{\rm exp} = 1$ hr
Wavelength Coverage and Spectral Resolution	0.37–1.3μm at $\mathcal{R} = 2\,000$
Limiting (point source) Magnitude	$i_{\rm AB} \simeq 23.5$.
Total Time Needed for Program ($T_{\rm tot}$)	$T_{\rm tot}$ = [3010×1 hr] + 20% overhead ≈ 3600 hrs.

Multiplexing permits the study of dense environments and close pairs of galaxies — important science drivers that are discussed below. By targeting fields with good existing photometric and bright spectroscopic data, it is possible to efficiently preselect galaxies in the desired redshift range and improve completeness further. The heavy multiplexing proposed for the Dark-Medium survey achieves a density of $\sim 22\,000$ science targets per deg^2 over the full 100 deg^2 field. This is well-matched to the space density of $0.5 < z < 1$ galaxies at the depth of the Dark-Medium survey (Figure 38), allowing this population to be measured with high (> 70 per cent) completeness if they are pre-selected from existing data. In total, spectra for ~ 2 million galaxies will be obtained from this survey, bringing the total (when

[16]For distant galaxy studies, g-band selection is not optimal; selection in I or redder bands is necessary to reach the lowest-mass, passively-evolving galaxies.

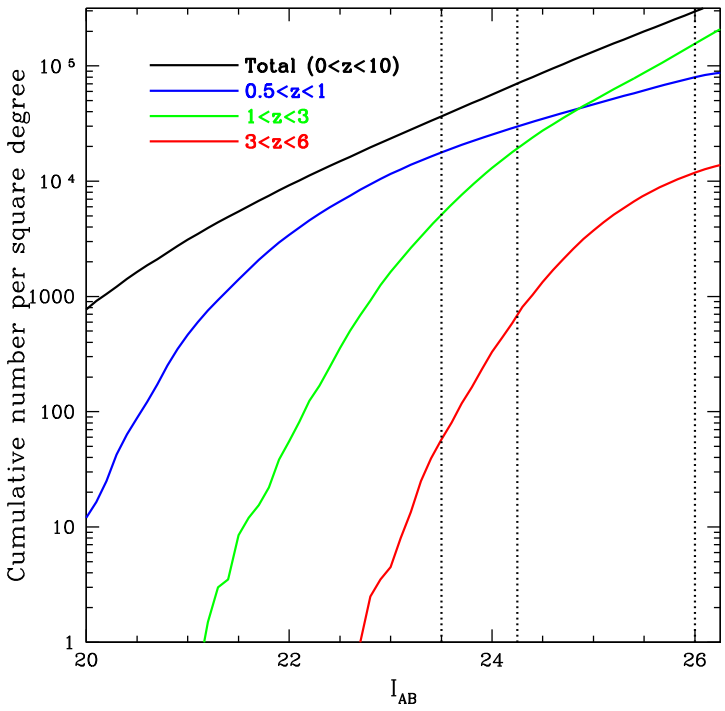

Figure 38: The cumulative number of galaxies per square degree as a function of I magnitude, in different redshift ranges, as determined from photometric redshifts (Capak et al. 2007). The proposed limits on the ngCFHT Dark-Wide, Dark-Medium and Dark-Deep surveys are shown as vertical lines.

combined with Dark-Wide) to almost 10 million, — an order of magnitude larger than SDSS. The high-redshift galaxy population, at $3 < z < 6$, will be explored primarily through the Dark-Deep survey. With six fibre configurations, and allowing for $\sim 1/6$ of the science fibres to be placed on quasars for the reverberation mapping project (sec §2.7), a sample of $\sim 14\,000$ galaxies over 1.5 deg^2 would be obtained; this is very well matched to the space density of such high-redshift galaxies (see § 2.6.4.4).

These three galaxy sample would enable a wide range of scientific investigations of distant galaxies. A few of the highest profile cases are described in detail below. Needless to say, ngCFHT would almost certainly lead to exciting and unexpected discoveries, raising new questions that cannot be anticipated.

2.6.4.1 Clustering and Halo Models

Galaxies are believed to be hosted by massive dark matter halos that make up more than 85% of their total mass. An essential aspect of galaxy evolution is the underlying complex baryonic processes that take place within these dark-matter halos. Processes such as gas infall and outflow, star formation, metal enrichment, negative feedback to star formation, black hole growth, and galaxy merging, should all work differently for different dark matter halo masses at different cosmic times. However, directly measuring dark halo masses either requires observations that are very challenging, especially at high redshift (e.g., Conselice et al. 2003; Swinbank et al. 2006; Mandelbaum et al. 2006), or rely on unusual and rare circumstances such as strong gravitational lensing events (e.g.,Treu 2010).

Thankfully, halo clustering is a strong function of halo mass, with more massive halos being more strongly clustered. Galaxies of different stellar masses and different star formation histories will correlate with dark matter halos of different masses and this relationship will evolve with time (e.g., Foucaud et al. 2010; Wake et al. 2011; Lin et al. 2012). Studies of galaxy clustering in large, local surveys have shown how clustering at $z \sim 0$ does depend significantly on several specific properties. These include luminosity (e.g., Norberg et al. 2002a; Zehavi et al. 2005), colour or spectral type (e.g., Norberg et al. 2002b; Zehavi et al. 2002), morphology (e.g. Guzzo et al. 1997), stellar mass (e.g.

Table 17: Technical Requirements and Survey Implementation: The Dark-Medium Survey

Survey Area (Ω)	$\Omega \approx 100$ deg^2.
Field Location	Contiguous coverage within the boundaries of the Dark-Wide survey.
Number of ngCFHT Fields ($N_{\rm field}$)	$N_{\rm field} = \Omega/{\rm FOV}_{\rm ngCFHT} \approx 70$ with 5% overlap.
Number of Configurations per Field ($n_{\rm config}$)	$\langle n_{\rm config} \rangle = 10$.
Total Number of Exposures ($N_{\rm exp}$)	$N_{\rm exp} = N_{\rm field} \times \langle n_{\rm config} \rangle \approx 700$.
Primary Imaging Resources for Target Selection	Euclid (Wide), Pan-STARRS (3π), LSST, eRosita, EMU, etc.
Observing Conditions	Lunar illumination $< 50\%$. Cloud cover $< 20\%$.
Instrumental Configuration(s)	$\mathcal{R} = 2\,000$, $T_{\rm exp} = 4$ hr
Wavelength Coverage and Spectral Resolution	0.37–1.3μm at $\mathcal{R} = 2\,000$
Limiting (point source) Magnitude	$i_{\rm AB} \simeq 24.25$.
Total Time Needed for Program ($T_{\rm tot}$)	$T_{\rm tot}$ = [700×4 hr] + 20% overhead $\approx$ 3360 hrs.

Table 18: Technical Requirements and Survey Implementation: The Dark-Deep Survey

Survey Area (Ω)	$\Omega = 1.5$ deg^2.
Field Location	Single, ultra-deep pointing within the Dark-Wide survey.
Number of ngCFHT Fields ($N_{\rm field}$)	$N_{\rm field} = \Omega/{\rm FOV}_{\rm ngCFHT} = 1$.
Number of Configurations per Field ($n_{\rm config}$)	$\langle n_{\rm config} \rangle = 6$.
Total Number of Exposures ($N_{\rm exp}$)	$N_{\rm exp} = N_{\rm field} \times \langle n_{\rm config} \rangle \approx 6$.
Primary Imaging Resources for Target Selection	Euclid (Wide), Pan-STARRS (3π), LSST, eRosita, EMU, etc.
Observing Conditions	Lunar illumination $< 90\%$. Cloud cover $< 20\%$.
Instrumental Configuration(s)	$\mathcal{R} = 2\,000$, $T_{\rm exp} = 100$ hr
Wavelength Coverage and Spectral Resolution	0.37–1.3μm at $\mathcal{R} = 2\,000$
Limiting (point source) Magnitude	$i_{\rm AB} \simeq 26.0$.
Total Time Needed for Program ($T_{\rm tot}$)	$T_{\rm tot}$ = [6×100 hr] + 20% overhead $\approx$ 720 hrs.

Li et al. 2006) and environment (e.g., Abbas & Sheth 2006). In recent years, deep spectroscopic surveys have made it possible to extend these investigations to $z \lesssim 2$, yielding results on how these dependencies evolve with time (e.g., Le Fèvre et al. 2005; Coil et al. 2006; Meneux et al. 2008, 2009). More luminous and massive galaxies tend to be more clustered, and this segregation seems stronger at $z \sim 0$ than at $z \sim 1$.

These results support a scenario in which the stellar mass of a galaxy is essentially proportional to the mass of the most recent dark matter halo in which it was the central object (Conroy et al. 2006; Wang et al. 2006). Investigating such results at higher redshift is essential, as the relationship between the galaxies and their halos is expected to be more straightforward. However, samples at $z > 2$ are limited and based mainly on multi-colour photometric selections or photometric redshifts and suffer from limitations in sample size, area covered and incompleteness. In order to compare the correlation function $\xi(r_p, \pi)$ and its projection $w_p(r_p)$ at high redshifts ($z > 2$) with similar measurements at $z < 2$, a deep, accurate, complete and unbiased sample of spectroscopic redshifts over a large area is required.

It is natural to use a halo-based prescription where galaxies form by the cooling of gas within bound and virialized clumps of dark matter. Galaxies occupy dark matter halos following a HOD model. In turn, the HOD fully describes the bias in the distribution of galaxies with respect to the underlying dark matter distribution, in terms of the probability distribution that a halo of virial mass M_h contains N galaxies of a given type (Berlind & Weinberg 2002). HOD models can be used to directly investigate the changing relationship of dark matter and luminous matter, and to separate contributions from satellite and central galaxies, and relate them to the masses of the dark matter halos. Until now, the majority of analyses conducted using HOD modeling to interpret galaxy clustering have been based either on large, low-redshift surveys such as the SDSS (e.g., Zehavi et al. 2011a), or at higher redshifts, smaller ($\sim$ 1deg^2) deep fields such as COMBO-17, VVDS and COSMOS (e.g., Phelps et al. 2006; Abbas et al. 2010; Leauthaud et al. 2011). Photometric redshifts enable clustering measurements in the framework of the halo model over a larger redshift baseline and larger area (e.g., Coupon et al. 2011), but such studies suffer from a lack of accuracy at all scales required to constrain the models. In particular, the dark matter halos in the lower-mass regime suffer from the lack of precision on the line-of-sight dimension due to the reliance on photometric redshifts. Such imprecision tends to bias the results for faint galaxies toward being satellite galaxies in large halos, rather than central galaxies in low-mass halos.

The clustering approach to extract information on the dark matter halo masses has proven an efficient way to identify the physical processes driving galaxy evolution at the dark-matter scale. For instance, it is now established that the fraction of luminous-to-dark matter is a strong function of dark-matter halo mass (e.g., Foucaud et al. 2010; Wake

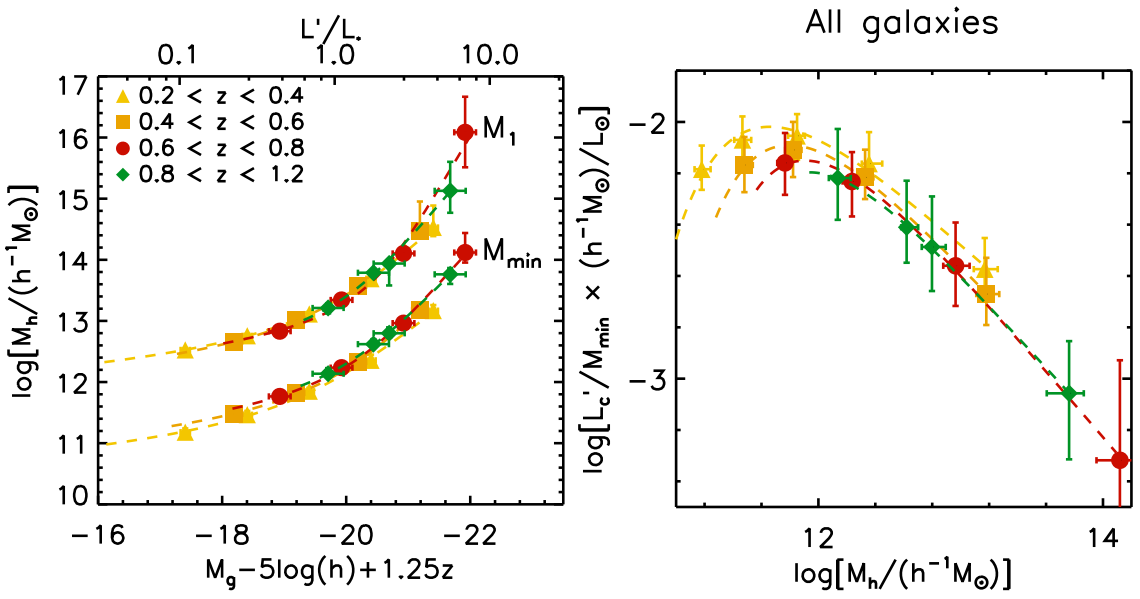

Figure 39: (Left Panel). Halo mass estimates, $M_{\rm min}$ and M_1, for all galaxy samples from the CFHTLS-wide survey, as function of luminosity threshold, corrected for passive redshift evolution to approximate stellar mass selected samples. The dashed lines correspond to the relation between central galaxy luminosity, $L'_{\rm c}$, and the halo mass stated in Zehavi et al. (2011b). (Right Panel). Light-to-halo mass ratios, $L'_{\rm c}/M_{\rm min}$, with identical parameters as those fitted with the same relation but as function of halo mass. Figure from Coupon et al. (2011).

et al. 2011; Leauthaud et al. 2012, Figure 37). This fraction decreases toward lower masses, because the dynamical time is long and supernovae feedback is strong, preventing efficient star formation. The fraction also decreases toward higher masses, where star formation is prevented by the cooling time and strong AGN feedback. Thus, the efficiency of star formation peaks at an intermediate mass range ($\sim 10^{12}{\rm M}_\odot$ at $z \sim 0$), and the location of this peak evolves to higher masses at higher redshift. Figure 39, extracted from Coupon et al. (2011), demonstrates that HOD modeling can probe the light-to-halo-mass ratio. This figure also shows that the technique is limited in the lower mass regime, especially at high redshifts, due to the lack of reliable redshifts at the faint end.

Interestingly, when looking at the clustering properties of galaxies selected according to their star-formation rates, even more complex phenomena can be explored. Figure 41, extracted from Lin et al. (2012), illustrates the evolution of the correlation length with different specific star formation rates (sSFR). Two distinct regimes are apparent, with galaxies having sSFR$\lesssim 2 \times 10^{-9}$ yr $^{-1}$ showing increasing correlation power with decreasing specific star-formation rates, and galaxies above this threshold show the opposite behaviour. The positive correlation observed at high sSFR reflects the "main sequence" evolution of galaxies, with galaxies in deeper dark matter halos showing more efficient star formation. On the other hand, the anticorrelation observed at low sSFRs can be understood as an environmental effect similar to that seen at lower redshifts: i.e., these are likely to be galaxies that are falling into the denser environments where their star-formation activity is more effectively suppressed. Large samples of galaxies with accurate spectroscopic redshifts are required to make further progress in understanding these trends. For instance, in the context of HOD models, the previous correlation between sSFR and correlation length could be understood as a physical processes in action for satellite and central galaxies. It is also essential to probe higher redshifts to be able to understand when, and how, such relationships were established.

To exploit the full potential of the HOD technique for the low-mass regime and at large redshifts, a deep, large and complete spectroscopic survey is essential. The ngCFHT Dark-Medium survey would be well-suited to address this science. The depth of $I_{AB} = 24.25$, corresponds to a stellar mass of $M \sim 2{\times}10^9 M_\odot$ at $z = 0.3$, and $M \sim 5{\times}10^9 M_\odot$ at $z = 1$, crucially probing below the mass level that dominates the star formation rate density of the universe (Gilbank et al. 2010, 2011).

A wide-area survey is necessary to reduce "cosmic variance" to a negligible level (Somerville et al. 2004) and to include a fair sample of rare, high- and low-density regions in the survey. Table 19 shows the expected number

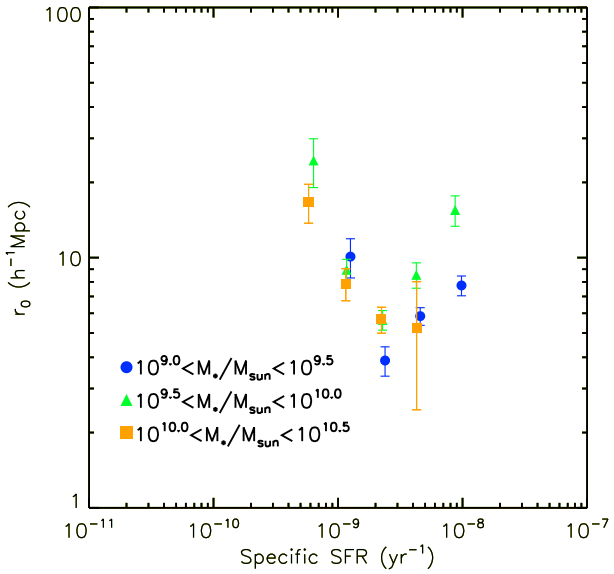

Figure 40: The relationship between the correlation length, r_0, and specific star formation rate of *sBzK* galaxies for three different stellar mass bins: $9.0 < \log(M_*/\mathrm{M}_\odot) < 9.5$ (blue circles), $9.5 < \log(M_*/\mathrm{M}_\odot) < 10.0$ (green triangles) and $10.0 < \log(M_*/\mathrm{M}_\odot) < 10.5$ (orange squares). Figure adapted from Lin et al. (2012).

Table 19: Number of Clusters in a 100 deg^2 Region.

$M/M_\odot$	$> 1 \times 10^{14}$	$> 5 \times 10^{14}$	$> 1 \times 10^{15}$
$z < 0.25$	400	4	0.2
$0.35 < z < 0.9$	2300	4	0.076

density of clusters per 100 deg^{-2} above three different mass limits and in two redshift intervals, based on numbers from Vikhlinin et al. (2009), Klypin et al. (2010), Crocce et al. (2010) and de Boni et al. (2011). Even a blind, 100 deg^2 survey would be adequate for sampling moderate clusters up to $M \sim 5 \times 10^{14} M_\odot$. But there is no clear value in choosing the area blindly, or even contiguously, and instead we envision carefully sampling a wide range of environments and redshifts as identified from existing imaging and spectroscopic surveys. The fields could even be selected based on results from the ngCFHT Dark-Wide survey itself. For example, if a subset of fibres from the wide field ngCFHT field were assigned to LRGs (roughly 1100 deg^{-2}; Schlegel et al. 2011), then regions of high and low density could be identified. A selection of these fields could then be followed up with multiple fibre configurations to greater depth. One possibility would be to preselect halos that span a range in mass — from the most massive clusters, through small groups, to individual galaxies. Though high completeness would be necessary, the number of fibre configurations required would depend on the amount of preselection possible and the availability of existing spectroscopy. Such a survey would permit an accurate measurement of halo properties (mass density profiles, mass-to-light ratios, sphericities, etc) as a function of mass and redshift.

The Deep-Dark survey would provide complementary data, with redshifts for early-type galaxies of mass $M = 1 \times 10^9 M_\odot$ up to $z \sim 1$. With $> 100\,000$ targets deg^{-2} at $z > 1$, high completeness would not be practical; but $\sim$10 configurations, with sensible target selection, would return a unique sample of $> 30\,000$ galaxies.

2.6.4.2 Environment

The "environment" of a galaxy could refer to its status as a central or satellite galaxy, its location within a dark matter halo, or the surrounding mass density on large or small scales. Each of these definitions are expected theoretically to have some influence on galaxy evolution, for different reasons. The satellite–central distinction arises because, although central galaxies are largely fueled by cold flows or rapid cooling of hot atmospheres, satellites are not ex-

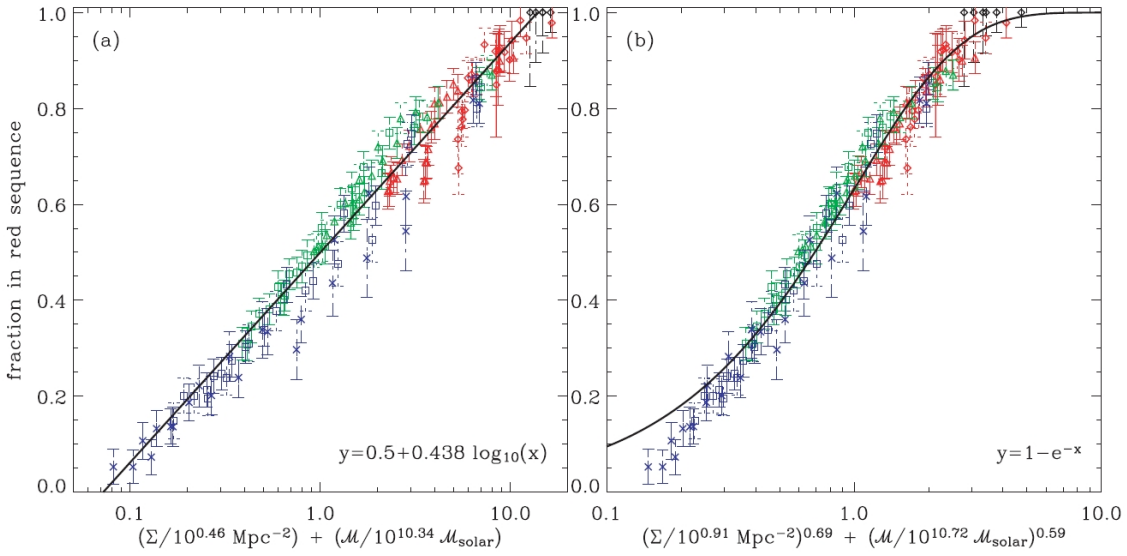

Figure 41: The fraction of red (passive) galaxies is shown as a function of two different combinations of stellar mass, M, and local density, Σ. The symbols represent different stellar mass ranges, from $10^9 < M/M_{\rm solar} < 10^{10}$ in blue to $M/M_{\rm solar} > 10^{10.8}$ in red. The red fraction depends on both environment and stellar mass, in a surprisingly simple way. From analysis of the SDSS by Baldry et al. (2006).

pected to have access to as much of this material, leading to a rapid depletion of fuel for star formation (Larson et al. 1980; Cattaneo et al. 2006). To understand the evolution of central and satellite galaxies requires studying the effects of environment from the scales of massive clusters (e.g., Park & Hwang 2009) to small-mass, galactic-scale halos (Ann et al. 2008). A correlation with large-scale environment might be expected because of the halo assembly bias seen in dark matter simulations (e.g., Maulbetsch et al. 2006; Gao & White 2007), although this effect has not been observed in the galaxy population at low redshift (Tinker et al. 2011). A correlation with location within a halo is expected, and observed, as a result of a correlation between accretion time and present-day location (e.g., Ellingson et al. 2001; Balogh et al. 2000). Finally, independent correlations with local density could be related to tidal interactions and mergers between close pairs of galaxies (e.g., Lin et al. 2007; Ellison et al. 2008; Park & Choi 2009; Patton et al. 2011).

After many years of speculation based on small samples with poorly understood selection criteria, the field was transformed by the large, homogeneous survey data provided by the SDSS. The sample size and wavelength coverage allowed researchers to explore correlations with both environment and the stellar mass of the galaxy. This immediately demonstrated that galaxy properties (such as morphology, age, metallicity, etc) depend strongly on their stellar mass. Many of the trends with environment reported previously turned out to be at least partly due to the fact that the stellar mass function depends on environment (Balogh et al. 2001; Baldry et al. 2006). After accounting for this, however, a strong environmental dependence remains: the fraction of "red sequence" galaxies (at fixed stellar mass) is larger in dense environments than in the general field (e.g., Baldry et al. 2006). In fact, the fraction of red galaxies is well described by a relatively simple function of just stellar mass and local density, as shown in Figure 41.

Since all galaxies must have been blue, star-forming systems at some point, the red fraction must be linked somehow to the decline, or quenching, of star formation in blue cloud galaxies. To understand the nature of this transformation, one must either identify galaxies in the process of moving between the two populations (e.g. in the "green valley"), and/or trace the redshift evolution of these correlations. Locally, the relatively low gas fractions and star formation rates, combined with low infall rates into groups and clusters, mean that the fraction of galaxies in the process of transformation today is probably quite small. This could be why observations have shown the properties of star-forming galaxies at $z < 0.2$ to be at most weakly dependent on environment (Balogh et al. 2004; Wolf et al. 2009; Vulcani et al. 2010; McGee et al. 2011; Wijesinghe et al. 2012). Thus, although these trends are now measured quite precisely, we still have very little insight into the physical mechanisms that might be driving any such transformation. A simple assumption is that satellite galaxies are deprived of the gaseous halos and cold flows that normally perpetu-

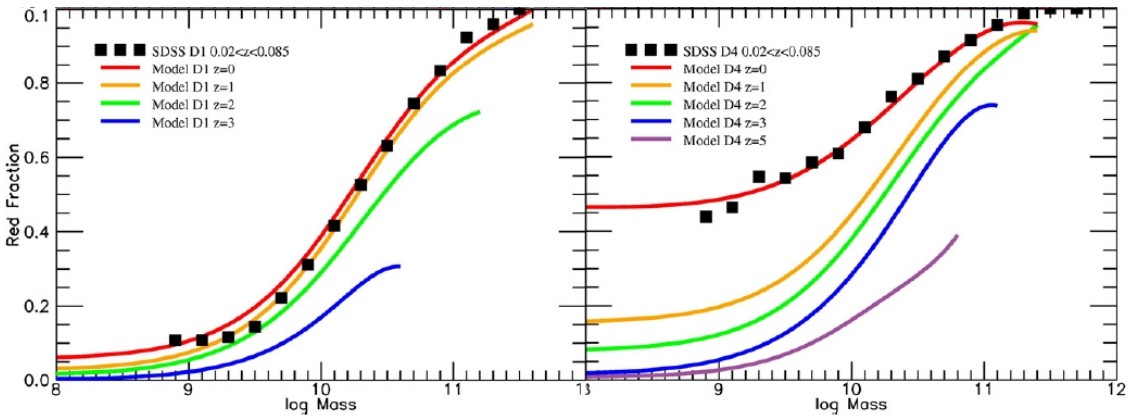

Figure 42: The fraction of red (passive) galaxies is shown as a function of stellar mass for the low- and high-density quartiles of the density field (left and right panels, respectively). The model parameters are fixed to reproduce the SDSS data (black squares) at $z \sim 0$ (red curve), while the other curves show predictions for higher redshifts. From analysis of the SDSS by Peng et al. (2010).

ate star formation, an assumption that is at least partly supported by numerical simulations (e.g., Kawata & Mulchaey 2008; McCarthy et al. 2008; Cen 2011; Bahe et al. 2012). However, a simple implementation of this effect in *ab initio* galaxy formation models leads to a predicted environmental signature that is much too strong when compared with observations (e.g. Weinmann et al. 2006; 2012).

Peng et al. (2010, 2011) have recently taken the observation of Baldry et al. (2006) a few steps further and presented an especially attractive, simple model in which galaxy evolution is driven by two "quenching rates" that are independent of one another — one related to stellar mass and the other to local density. From this they are able to predict how the stellar mass functions of star–forming and passive galaxies will evolve to $z \sim 3$. This predicted evolution is shown in Figure 42.

It is important to measure these correlations with comparable, or better, precision at higher redshifts in order to establish the timescales of transformation and solve this problem. Essentially, including a third axis for cosmic time in Figure 41 allows a direct measurement of the rate at which galaxies evolve in different environments (McGee et al. 2009). Even more directly, the higher star formation rates and infall rates into clusters at $z > 0.5$ should lead to a substantial, and measureable, population of galaxies caught in the midst of their transformation. In the model of Peng et al. (2010), for example, normalization of the "transition galaxy" mass function, relative to that of the star–forming population, is equal to the transition timescale divided by the inverse of the average specific star formation rate at M^*.

Of course, such measurements have been attempted in the past, beginning with Butcher & Oemler (1978), and continue with large redshift surveys today (e.g., Poggianti et al. 2006; Cooper et al. 2006; Park & Hwang 2009; Cooper et al. 2010; McGee et al. 2011; Balogh et al. 2011; Raichoor & Andreon 2012). The best constraints to date have come from the zCOSMOS and DEEP2 surveys due to their depth and relatively high sampling completeness. However, even combined these surveys consist of 70 000 redshifts covering only ~ 2 deg^2 and spanning ~ 9 Gyr in cosmic time. The sample size alone (per Gyr) is ~ 50 times smaller than the SDSS, and the small areas severely limit the range of environments probed.

It is clear that ngCFHT has the potential to provide to a breakthrough in this field, likely exceeding in importance the paradigm shift that resulted from the SDSS analysis. The Dark-Medium survey will cover ~ 100 deg^2 with ~ 12 fibre configurations at each position, and will yield over 10 million galaxy redshifts over $0 \lesssim z \lesssim 1.5$. *It will thus have the statistical power of the SDSS per Gyr of cosmic time, with similar completeness and limiting stellar mass.* Although 100 deg^2 is relatively small compared to the SDSS, a judicious choice of fields will ensure that a wide range of environments is sampled. For example rare, dense environments like galaxy clusters can be identified from existing data and included in the survey. Complementing this, the Dark-Wide survey will cover $\sim 4\,300$ square degrees, only a factor ~ 2 smaller than SDSS. While the completeness and depth will not be as high as for the Dark-Medium survey, it will be sufficient to identify over- and under-dense regions which could be intentionally targeted by the deeper survey.

The high level of completeness planned for the Dark-Medium survey is essential for studies of environment: i.e., structures on scales from kpc to ∼tens of Mpc need to be identified robustly. Given the importance of correctly

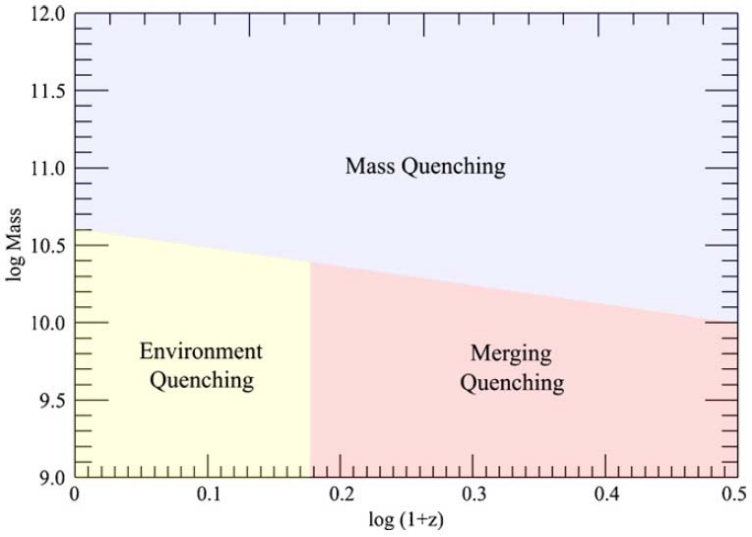

Figure 43: The redshift and stellar mass ranges over which various galaxy evolution mechanisms are believed to dominate. In this model, galaxy evolution is assumed to be dominated by independent quenching parameters that are related to the stellar mass of the galaxy (i.e., "mass" quenching) and to the merging of dark matter halos (i.e., "environment" and "merger" quenching). To measure quantitatively the timescale related to environment quenching will require reaching to stellar masses below $M \simeq 10^{9.5} M_{\odot}$ at $z = 1$. From analysis of the SDSS by Peng et al. (2010).

identifying neighbour galaxies when studying environmental effects (see Park et al. 2008), it is desirable that the sampling rate exceed 80 per cent. Indeed, the study of strong, small-scale environments is highly compromised if the completeness is ~ 50 per cent or less (Park & Hwang 2009).

It is apparent from Figure 42 that the influence of environment is most important at stellar masses $M < 10^{10.5} M_{\odot}$, since the mass-quenching term dominates at higher masses. This is shown schematically in Figure 43, also from Peng et al. (2010), which shows how "environment quenching" and "merger quenching", both of which are related to the merging of dark matter halos, are expected to dominate in even lower mass galaxies at higher redshift. Thus, it is important to observe galaxies of all types (passive and star-forming), with masses at least as low as $\sim 10^{9.5} M_{\odot}$. This corresponds to $I_{\rm AB} \sim 24.25$ at $z = 1$ (e.g., Ilbert et al. 2010) and is substantially deeper than any large spectroscopic survey has achieved today.

2.6.4.3 Mergers

In the hierarchical structure formation paradigm, galaxy merging is expected to play a crucial role in the build-up of galaxy mass at early times. In addition to contributing directly to mass assembly, galaxy mergers can also trigger starbursts, transform the galaxy morphology, induce AGN activity, and, ultimately, quench the star formation (e.g., Springel et al. 2005; Hopkins et al. 2006, 2010). In order to understand both the mass assembly history of galaxies, and their subsequent evolution, it is therefore essential that we quantify galaxy merger rates and characterize the overall effects of mergers.

There are two popular methods of identifying merger systems. The first one is to look for morphologically disturbed galaxies through non-parametric methods such as Gini-M_{20} and asymmetry, which have been widely applied to high-resolution imaging data (Conselice et al. 2003; Lotz et al. 2004). However, morphological tracers are sensitive to tidal disturbances and can appear in different stages of mergers, which makes translating them into galaxy merger rates difficult without a good understanding of the timescale for such signatures. It is also not easy to exclude the contributions of minor mergers or stochastic star formation in galaxies from major mergers by morphologies alone. A second approach relies on the search for kinematic close galaxy pairs identified based on their line-of-sight velocity difference and the projected separation (Patton et al. 2002; Carlberg et al. 2000). This method has served as a robust means of identifying merger candidates, and thus estimating merger rates, out to $z \sim 1$ (e.g., Lin et al. 2008; de Ravel et al. 2009). It is also the only way to properly classify merger types based on galaxy properties (colours, stellar mass

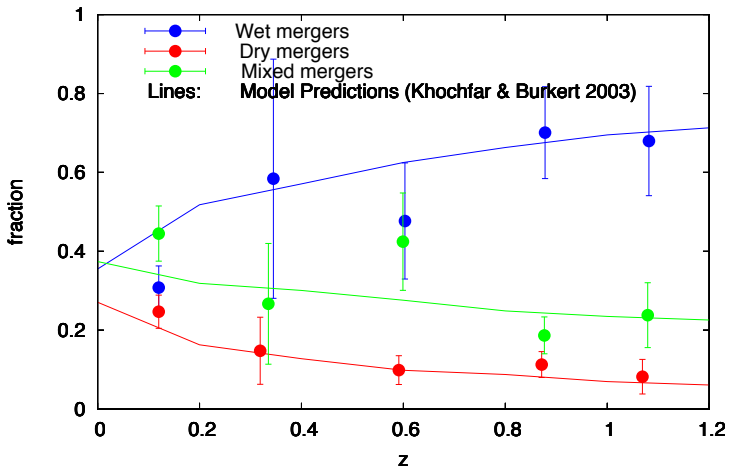

Figure 44: Fraction of major mergers for wet (open triangles), dry (open circles), and mixed mergers (solid circles) as a function of redshift (Lin et al. 2008). The three curves show the semi-analytical predictions for Sp-Sp, E-E, and E-Sp mergers from Khochfar & Burkert (2003).

ratio, luminosity ratio, etc) because they are in a stage predating the coalescence of their nuclei.

Recent work using close pairs has attempted to pin down the relative contributions among different types of mergers as a function of cosmic time (Lin et al. 2008; de Ravel et al. 2009; Bundy et al. 2009; Lin et al. 2010). It has became clear that the gas-rich (wet) mergers dominate the merger events at higher redshifts ($z \sim 1$) while the relative abundance of gas-poor (dry) and mixed mergers gradually increases toward lower redshifts (see Figure 44; Lin et al. 2008). This implies that galaxies assembled through wet mergers at earlier times likely experienced a starburst phase, followed by the quenching of star formation that moved them gradually toward the red sequence. On the other hand, dissipationless (dry) mergers may have played a key process at recent epochs, in building up the mass of present-day early-type galaxies.

Extending the merger rate measurements beyond $z \sim 1$ is of great interest since it is now well established, using a wide variety of star formation diagnostics, that the peak of the cosmic star formation rate occurs between $z \sim 1$ and $z \sim 3$. It was commonly believed that galaxy mergers were responsible for the elevated cosmic star formation rate at $z \sim 2$, given that extreme star-bursting systems at that epoch (such as submillimeter galaxies) were found to be associated with merging systems (Tacconi et al. 2006). However, following the launch of the Herschel telescope, several studies have demonstrated that LIRGs (luminous infrared galaxies) and ULIRGs (ultraluminous infrared galaxies) account for the majority of the star formation density at $1 \lesssim z \lesssim 2$ and they are not necessarily mergers but instead normal disk-like galaxies (Melbourne et al. 2005; Kartaltepe et al. 2010). Whether the gas-rich mergers continue to increase with look-back time, and are responsible for the elevated cosmic star formation rate beyond $z \sim 1$, remains a mystery. On the other hand, the so-called "cold accretion model' (Dekel et al. 2009) has recently been proposed as an alternative to the gas-rich mergers for the greater star formation at higher redshifts by accreting cold gas from the surrounding large-scale structures. While it is observationally challenging to detect cold flows and quantify their importance, one way to decipher the contributions from the aforementioned two mechanisms is to measure directly the merger rates at high redshift.

Reliable merger rate measurements using the close pair technique require a large spectroscopic sample covering a wide area with a high sampling rate. ngCFHT would enable such a survey to be conducted in an efficient way, thanks to its proposed large field, heavily multiplexed spectrograph, and 10m aperture. Intermediate spectral resolution ($\mathcal{R} > 2\,000$) is required to pick up kinematic close pairs so as to exclude the interlopers. The proposed ngCFHT surveys would dramatically improve upon existing studies in three key areas related to galaxy mergers:

1. The Dark-Medium survey, which covers an area of ~ 100 deg^2 down to $i \sim 24.25$, would yield a sample size that surpasses the current spectroscopic samples at $z \sim 1$ by more than an order of magnitude, allowing the measurement of the merger rates, not only as a function of redshift and galaxy types, but also of environment. The latter is of particular interest as it is linked directly to the questions of how, and when, massive galaxies grow

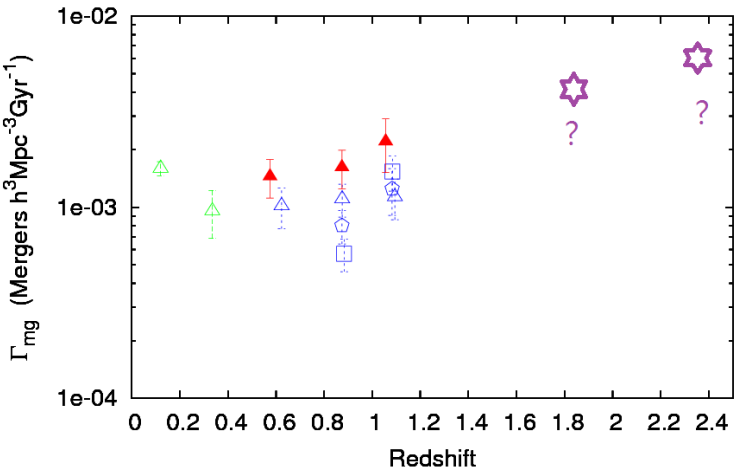

Figure 45: The volume-limited, co-moving galaxy merger rate as a function of redshift. The data points at $z < 1.2$ show observational results taken from Lin et al. (2008). The star symbols mark the redshift range that samples the peak of the cosmic star formation rate density; this range would be thoroughly explored by ngCFHT.

in different environments (Lin et al. 2010). The large coverage of the survey is essential to ensure a statistically meaningful sample of the most extreme large-scale structures, such as very massive clusters of galaxies, so that one can probe directly the environments (field vs. group vs. cluster) where galaxy mergers preferentially occur, and in which part of the clusters (i.e., outskirts vs. core) mergers are likely to take place.

2. The IR arm of the ngCFHT would enable the detection of [OII] emission lines out to $z \sim 2.4$. This makes it possible to extend the measurements of the gas-rich merger rates to $1 < z < 2.4$, the critical epoch of star formation in the galaxies (Figure 45). Furthermore, [OII] is a good tracer of recent star formation and could potentially be used to study interaction induced star formation. When combined with the comoving density measurement of galaxy merger rates, one could gain key insights into the contribution of gas-rich mergers to the global cosmic star formation rate density. The close pair sample can also be cross-correlated with the far-IR and submillimeter-selected, extreme star-forming galaxies to explore the linkage between mergers and dusty, starbursting galaxies.

3. Recent studies of the UV luminosity function of high-redshift galaxies have found that the characteristic luminosity increases from $z \sim 6$ to $z \sim 4$, suggesting a hierarchical build-up of galaxies during this epoch (Bouwens et al. 2007). While it is currently very difficult to resolve the structures of very high-redshift galaxies to study their association with the merging activities, the Dark-Deep survey will be able to detect Ly$_\alpha$ emission out to $z \sim 7$ or so, which would provide a great chance to study the merger rates at the earliest phases of galaxy formation, through the close pair technique.

2.6.4.4 Galaxies at the Epoch of Formation

The universe at $z > 2$ looks profoundly different from that at the present time. Massive galaxies are actively forming stars, the Hubble sequence is not yet in place, and massive clusters of galaxies are almost entirely absent. It is during this early time that today's massive galaxies were being assembled. Galaxies at these high redshifts can now be readily identified from deep imaging surveys (e.g., Adelberger et al. 2004; Sawicki & Thompson 2006; Dahlen et al. 2007), and/or as strongly lensed galaxies that have been greatly magnified (e.g., Jones et al. 2010; Richard et al. 2011). Current samples are impressive (over a thousand spectroscopically confirmed galaxies) but still tiny compared to large nearby surveys like the SDSS, and generally restricted to the most massive galaxies at this epoch (Shapley et al. 2011). This will change as deep, wide-field imaging surveys such as LSST come online.

From their angular clustering it is possible to estimate the average masses of such high-redshift objects (e.g., Brodwin et al. 2008; Williams et al. 2011; Wake et al. 2011), and thus to intercompare the various samples selected (for example) by UV continuum, infrared dust emission, or nebular emission. From broadband photometry alone

it is possible to estimate stellar masses and star formation rates, and these studies have established a reasonably tight correlation between these two quantities, with specific star formation rates at $z = 2$ about a factor ~ 4 times larger than at $z \sim 1$ (e.g., Daddi et al. 2007; Sawicki 2012). But for a true understanding of the physical properties of such galaxies, spectroscopy is essential. Deep spectroscopic observations on either individual galaxies, or on stacked averages, have been used to measure outflow velocities (e.g., Shapley et al. 2003), star formation histories, metallicities, and Lyman continuum escape fractions (e.g., Iwata et al. 2009; Nestor et al. 2011). It is known, for example, that large-scale outflows are common at $z > 2$ (e.g., Steidel et al. 2010), but there are few constraints on the actual mass outflow rates, or on the high gas accretion rates predicted by theory.

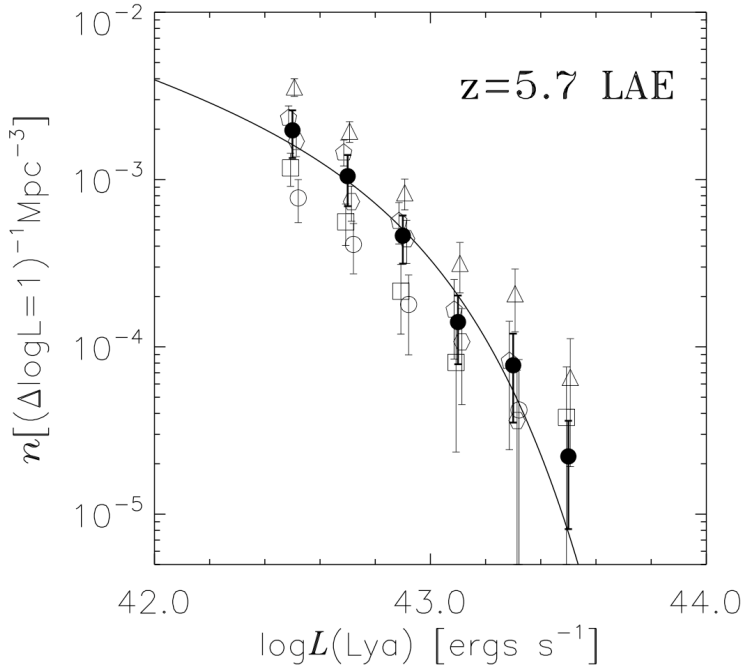

Figure 46: The luminosity function of Ly-α emitters (LAEs) at $z = 5.7$; the different symbols correspond to different surveys. A 100-hour survey with ngCFHT could reach $L = 2 \times 10^{42}$ ergs/s at $z \approx 7$, where more than 1000 LAEs are expected per 1.5 deg^2 field. Figure from Ouchi et al. (2008).

Moreover, there is, at present, very little information on the correlation of galaxy properties with large-scale environment at $z > 2$. Although large-scale structures can be identified to some degree from deep imaging data (e.g., Ouchi et al. 2005; Venemans et al. 2007), spectroscopic sampling of galaxies in these structures is at a very early stage.

ngCFHT would greatly advance this field by obtaining long exposures on large samples of photometrically-selected galaxies. For example, the number density of Lyman-break galaxies at $2 < z < 3$, and brighter than $R \simeq 25.5$, is about ~ 4500 deg^{-2} (e.g., Steidel et al. 2003). This is well matched to the number density of fibres on ngCFHT, and thus a pair of fibre configurations would be sufficient to obtain a complete sample over a ~ 20 Mpc area. Although ngCFHT would not compete with ELTs for targeted observations of individual galaxies at higher redshifts, it would still be able to probe massive galaxies over large scales, up to $z \sim 6$.

The Dark-Deep survey would also provide great insight in the high-redshift, emission-line population over large scales, reaching emission line fluxes as low as $\sim 3 \times 10^{-18}$ergs s^{-1} cm^{-2}. This corresponds to a Ly-α luminosity at $z = 7$ of $\sim 2 \times 10^{42}$ ergs s^{-1}. The cumulative volume density of LAE galaxies brighter than this limit is about $\sim 10^{-4}$Mpc^{-3} (see the differential luminosity function in Fig 46, from Ouchi et al. 2008). Thus, there should be well over 1000 LAEs per ngCFHT field. With spectroscopic redshifts for well over a thousand LAEs, it would be possible to measure their stellar mass function, and to improve constraints on their halo masses from measurements of their clustering. Crucially, the precise spectroscopic redshifts will enable efficient follow-up with narrow-field telescopes like ALMA, JWST and the proposed E-ELT or TMT.

The multiplexed, ultra-deep exposures from the Dark-Deep survey represent a unique contribution of ngCFHT,

as being the only method for probing individual $M_{\rm star} < 10^{10} M_{\odot}$ galaxies to $z \approx 5$. This science requires high throughput and excellent sky subtraction, which are achievable with stable, high-quality fibres (e.g., Sharp & Parkinson 2010), and a number of algorithms now exist for accurate sky subtraction with fibres (e.g., Battaglia et al. 2008; Bolton & Schlegel 2010). An alternative approach, albeit one with potentially significant design implications, is the "nod-and-shuffle" technique (Cuillandre et al. 1994; Glazebrook & Bland-Hawthorn 2001), whereby the telescope is nodded on and off the target, while the charge is shuffled on the detector to make room for both on- and off-target data. The preferred strategy for sky subtraction will need to be examined carefully at a later stage. In any case, greater depths can be achieved for galaxies with strong emission lines, and since the wavelength coverage of ngCFHT extends to 1.3 μm it would formally allow the spectroscopic confirmation of Ly-α emission to redshifts as high as $z \sim 9$.

2.7 The Intergalactic Medium

2.7.1 Abstract

The intergalactic medium (IGM) is the rarefied material that spans the vast distances between galaxies in the universe. The IGM therefore straddles the interface between studies of galaxy formation and the evolution of large-scale structure, and its observable properties are closely intertwined with both processes. One of the key observational probes of the IGM is the Lyα forest of H I absorption lines in the spectra of distant quasars. Its study provides a valuable cosmological tool for exploring dark matter and dark energy, and allows insight into the interactions between galaxies and the IGM.

Establishing the connections between the properties of foreground galaxies and measured parameters of the IGM is an additional outstanding issue in the field of galaxy formation. At the large HI column density end, the so-called Damped Lyman-α Absorbers (DLAs) are an observational tool for probing galaxy-scale objects. DLAs remain our best diagnostic of the ISM within high-redshift galaxies and have yielded results that are relevant to fields ranging from cosmology and galaxy evolution to star formation and stellar nucleosynthesis.

2.7.2 Introduction

Observations of the Lyα forest — the manifestation of the IGM and cosmic gas web — have driven numerous investigations of galaxy evolution and cosmology. For example, comparisons of line statistics are a critical test of cosmological simulations: i.e., the IGM's thermal history and opacity is direct test of reionization of both helium and hydrogen, while the detection of metal species allows us to probe chemical enrichment and the extent of the circumgalactic medium (CGM).

There are two types of datasets that have been used most often to study the Lyα forest during the last decade: (1) the SDSS, which consists of thousands of low- to moderate-resolution ($\mathcal{R} \sim 2\,000$), low S/N (~ 5) spectra (e.g., McDonald et al. 2006); and (2) VLT/UVES and/or Keck/HIRES data consisting of far fewer, high-resolution ($\mathcal{R} \sim 40\,000$) high-S/N (> 50) spectra (e.g,. Kim et al. 2004). The complementarity between quality and quantity is well demonstrated by studies of the matter power spectrum that can be inferred from the distribution of Lyα flux. While SDSS data have been used to place constraints on the Lyα flux power spectrum that have small (0.6%) statistical error bars, the higher quality UVES data are better suited to studying astrophysical effects on small scales. Although analyses of both datasets yield broadly similar cosmological constraints, there remains some tension between these Lyα forest measurements and other data. These issues could be addressed by surveys that yield large numbers of moderately high resolution spectra, combining the strengths of the SDSS and UVES surveys.

For exploring the connection between galaxies and the IGM, it is particularly important to establish the link between the absorption line properties — such as N(HI), velocity spread and Voigt profile parameters — and the properties of the associated galaxy. Similarly, the connection between metal absorption (like C IV, Si IV, N V and O VI) in the low-density IGM and foreground galaxies and determining the length scale over which a typical star-forming galaxy influences the IGM metallicity and ionization state of the gas are important issues. The impact of such work is epitomized by recent observations of O VI associated with relatively low-redshift galaxies, where it has been calculated that there is as much mass in metals in the CGM as in the galactic disk (Tumlinson et al. 2011).

At higher redshifts, state-of-the-art work connecting galaxies and absorbers has come from the Keck Baryonic Structure Survey (e.g., Steidel et al. 2010) and similar work done at the VLT. To date, the distribution of galaxies around a combined sample of two dozen high-z quasars has been mapped with these two telescopes (see the summary in Rudie et al. 2012; Crighton et al. 2003); These quasar spectra have high-resolution ($\mathcal{R} \geq$ 45,000) and the galaxy spectra have resolution $\mathcal{R} \sim$ 300 to 1,000. Perhaps surprisingly, it has been found that the flux transmission in the Lyα forest correlates with Lyman break galaxies up to a scale of 5 Mpc (Adelberger et al. 2003; Crighton et al. 2003). These programmes have also revealed the connection between metal absorption lines and the CGM, again to the surprising scale of many hundreds of kpc (Rudie et al. 2012). Such studies are clearly in their infancy, but are indicators of the powerful combination of wholesale pairings of high-quality QSO spectra with galaxy surveys.

At the highest hydrogen column densities, the DLAs are expected to trace galaxies. The largest haul of DLAs to date comes from the SDSS; 937 absorbers with $2.15 < z < 5.2$ (Noterdaeme et al. 2009), permitting an estimate of the cosmic density of neutral gas which is thought to trace the evolution of neutral gas reservoirs for star formation. However, to move beyond the pure statistics of DLA numbers and HI gas content, high resolution follow-up with echelle, or echellette, spectrographs on 8-10m-class VLT/Keck telescopes is still required. This is because the metal lines used to determine the metallicities and element ratios are weak, narrow and cannot be easily detected with

resolutions of a few thousand. Therefore, although some 1,000 DLAs are known, detailed properties such as chemical abundances, kinematics and element ratios are known for just ∼10% of these. ngCFHT would provide a sample of moderate-resolution spectra that would allow astronomers to increase dramatically the number of metallicity estimates for large samples of DLAs.

2.7.3 ngCFHT in Context: Competition and Synergies

In the near future, large scale spectroscopic surveys such as the SDSS-III Baryon Oscillation Spectroscopic Survey (BOSS) and the proposed BigBOSS already aim to measure the baryon acoustic oscillation (BAO) scale using the Lyα forest (amongst other tracers) at $z \simeq 2 - 3.5$ (Slosar et al. 2011). The BOSS survey in particular will collect spectra of 150,000 quasars over 10,000 deg^2, while BigBOSS proposes to survey $14\,000\,\mathrm{deg}^2$ and target about five times as many quasars at higher resolution ($\mathcal{R} \sim 3\,000 - 4\,800$) with the 4m Mayall telescope (Schlegel et al. 2009). While BOSS and BigBOSS would represent a significant competitor to ngCFHT for any very large Lyα forest survey at low resolution, moderate to high resolution spectra are not required to accurately measure the ~ 150 comoving Mpc BAO scale (the trade-off between quasar number density and S/N is instead more important, e.g., McQuinn & White 2011). A smaller sample of high-resolution spectra would, however, enable correlations in the small-scale IGM structure to be probed by Lyα absorption (as induced by, e.g., ionisation or temperature fluctuations during He II reionisation). This would be an exciting area in which ngCFHT could capitalize.

At present, the VLT and Keck telescopes are used most frequently to connect quasar absorbers with galaxies. At Keck, Steidel and collaborators are conducting the Baryonic Structure Survey, which targets 15 quasars with HIRES while collecting $\sim$ 800 galaxy spectra with LRIS. At VLT, the Durham group is using VIMOS to collect spectra for galaxies surrounding six quasars that have high-resolution spectra from HIRES or UVES. The main requirement for increasing the number of absorbers (for association with the foreground galaxies) is the large number of quasars with high-resolution (R≥40 000) and high-S/N spectra. In particular, it is important to have wide wavelength coverage so that large numbers of metal species can be associated with a given absorber. In the VLT/UVES and Keck/HIRES archives, high-resolution spectra for $\sim$ 400 quasars are available. Therefore, a campaign with ngCFHT to amass spectra for large numbers of galaxies in these fields would yield a 10 to 20 fold increase in the number of sight lines studied. Since BOSS will observe a large number of quasars brighter than 20 mag, it would therefore be possible to identify fields with an excess of quasars within a ngCFHT field. At present, there is no planned or proposed facility that equals the capabilities of ngCFHT in this area.

For DLAs, the unique contribution of the ngCFHT would be two-fold. First, it would be the first facility to provide survey level statistics at high spectral resolution. For instance, a bright-time survey of 10,000 deg^2 at a resolution of $\mathcal{R} = 20\,000$ would yield S/N∼20 spectra (in 1 hr) at the survey limit ($g \sim 20.4$). This resolution is comparable to X-shooter on the VLT (currently most highly oversubscribed instrument at ESO) or ESI on Keck. Both instruments have a proven track record for quasar absorption line studies, demonstrating that abundance studies can be done at $\mathcal{R} \simeq 20\,000$. However, in order to convert the measured metal line strengths into useful chemical abundances, the HI content of the absorber must also be measured. The Lyα line is considerably bluer (at 1216 Å) than most of the metal lines, and with equivalent widths (EWs) typically in excess of 10 Å can be measured in much lower resolution spectra. The second benefit of the ngCFHT is therefore the addition of the Dark-Wide survey which, with $\mathcal{R} = 2\,000$ and coverage from 0.37–1.3μm could measure HI in DLAs over a redshift range of $2 \lesssim z \lesssim 9$. The combination of coverage in both the blue (at lower resolution) and at red wavelengths at $\mathcal{R} = 20\,000$ would yield an extraordinary gain in the statistics of high-redshift DLAs.

2.7.4 Legacy Science

2.7.4.1 The IGM Probed by the Lyα Forest

As explained in §2.7.2, the Lyα forest is a powerful probe of structure formation, but there are some important inconsistencies between current, complementary datasets. For example, the amplitude of the power spectrum, σ_8, inferred from the Lyα forest flux power spectrum is somewhat larger than the value obtained from the CMB. This may be an indication that there are as yet unidentified physical effects that influence the individual measurements, such as the uncertain thermal state of the IGM (Viel et al. 2009).

A large, independent sample of moderate-resolution quasar spectra at $2.1 < z < 4.5$ (corresponding to about $0.38 < \lambda_{\rm obs} < 0.67\mu$m for Ly$\alpha$ in the observed frame) would probe the flux power spectrum down to the Jeans scale and allow significant progress relative to existing studies. A PI-led quasar spectroscopic survey targeting at least

several hundred quasars with $\mathcal{R} \simeq 5\,000$ and $\mathrm{S/N} \sim 20$ (see Figure 47 for examples of simulated Lyα forest spectra) would allow an exploratipn of possible systematic effects while providing much improved statistical power relative to studies at higher resolution. McQuinn & White (2011) estimate a quasar number density of $4 \times 10^{-5}\,\mathrm{Mpc}^{-2}$ ($1.5 \times 10^{-3}\,\mathrm{Mpc}^{-2}$) for B-band magnitude limit of $m_{\mathrm{AB}} = 20$ (23) at $z = 3$, based on the luminosity function of Hopkins et al. (2007). This is equivalent to a quasar number density of $0.5\,\mathrm{deg}^{-2}$ ($19.5\,\mathrm{deg}^{-2}$). A large sample of medium-resolution spectra ($\mathcal{R} = 5\,000 - 7\,000$) would therefore offer valuable insights when compared to low-resolution SDSS data and the much sparser, higher-resolution spectra.

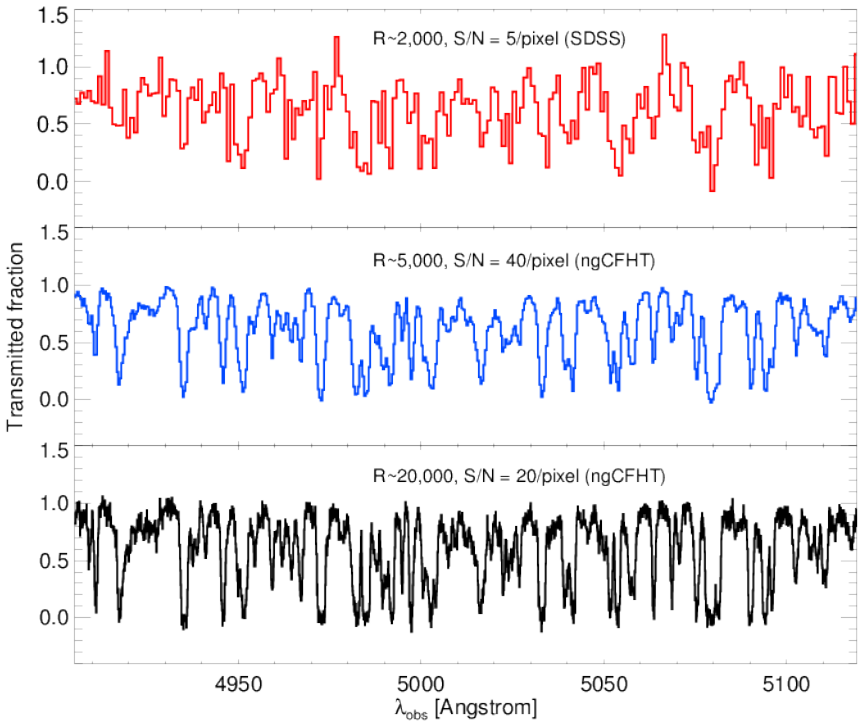

Figure 47: A comparison of simulated SDSS and ngCFHT Lyα forest spectra drawn from a high-resolution hydrodynamical IGM simulation at $z = 3.2$. The spectra have been convolved with a Gaussian instrumental profile and then rebinned; random Gaussian noise has been added to each pixel in order to approximate observational data. Note that no quasar continuum has been added to these spectra. (Top Panel). A simulated SDSS spectrum with $\mathcal{R} \sim 2\,000$ (FWHM$= 140\,\mathrm{km\,s}^{-1}$) and S/N$= 5$ per 1.06 Å pixel. (Middle Panel). Simulation of an $\mathcal{R} \sim 5\,000$ (FWHM$= 60\,\mathrm{km\,s}^{-1}$) ngCFHT spectrum with S/N$= 40$ per 0.44 Å pixel. (Lower Panel). Simulation of an $\mathcal{R} \sim 20\,000$ (FWHM$= 15\,\mathrm{km\,s}^{-1}$) ngCFHT spectrum with S/N$= 20$ per 0.11 Å pixel.

An additional application of Lyα forest observations would be the measurement of its opacity, which is sensitive to the ionization and thermal state of the IGM, and provides an indirect probe of the sources responsible for maintaining the IGM in its highly ionized, post-hydrogen-reionization state. Precise measurements of the redshift evolution of the mean transmission through the Lyα forest, $\langle F \rangle = \langle e^{-\tau} \rangle \equiv e^{-\tau_{\mathrm{eff}}}$, where τ_{eff} is the effective optical depth, provide a means to measure the intensity of the UV background (Bolton et al. 2005, Faucher-Giguere et al. 2008). This is an important probe of the ionizing emissivity of sources in the early Universe, and is therefore a key constraint on models of the H I reionization era. In addition, the epoch of singly ionized helium reionization is thought to complete by $z \approx 3$, roughly coinciding with the peak in quasar numbers (Furlanetto & Oh 2008). An increase in the IGM temperature due to the associated He II photo-heating is observed at $z < 4$ (Becker et al. 2011), and will also impact on the observed Lyα forest opacity.

Measurements of the τ_{eff} redshift evolution would therefore be valuable for improving existing constraints, exploring systematic uncertainties, and investigating the thermal history of the IGM. The latter has an effect on τ_{eff} through the temperature dependence of the H II recombination rate, such that the number density of neutral hydrogen $n_{\mathrm{HI}} \propto T^{-0.7}$. At $z \sim 3.2$ a "dip" in the otherwise monotonic redshift evolution of τ_{eff} has previously been measured from spectra obtained with the SDSS survey (Bernardi et al. 2003) and more recently in ESI/HIRES Keck

spectra (Faucher-Giguere et al. 2008). It has been suggested that this feature may be due to heating of the IGM during He II reionization, although it is very difficult to explain this feature theoretically (Bolton et al. 2009). A large, independently-selected sample of moderate- to high-resolution spectra would enable further examination of this key issue. A homogenous set of several hundred $\mathcal{R} \sim 6\,500$, S/N$= 20$ quasar spectra would improve the statistical uncertainties on existing high-resolution studies by a factor of ~ 5 (see Figure 48).

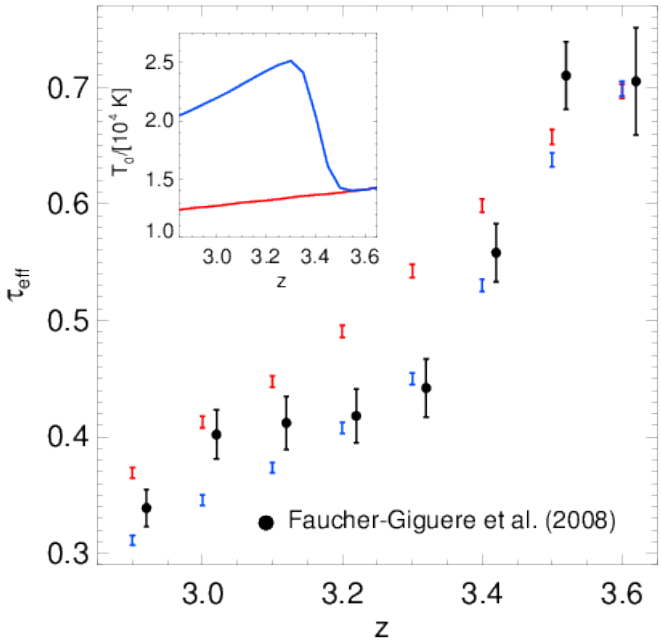

Figure 48: The Lyα forest effective optical depth plotted against redshift. The filled circles with error bars (1σ statistical only, offset for clarity) display the measurements of Faucher-Giguere et al. (2008) from a sample of 86 ESI/HIRES Keck spectra at $2 \leq z \leq 4.2$. However, other analyses find no evidence for this feature (e.g., Paris et al. 2011). For comparison, simulated ngCFHT data (at $\mathcal{R} \sim 5\,000$, S/N$= 20$) drawn from two different high-resolution hydrodynamical simulations are shown as the red and blue 1σ error bars. The spectra are drawn from models with different IGM thermal histories (see inset) which result in different temperatures at mean density, T_0, and hence different $\tau_{\rm eff}$. Each bin contains a total Lyα forest path length of $4\,000$ proper Mpc (corresponding to ~ 200 independent quasar spectra for a single $\Delta z = 0.1$ bin at $z = 3.4$), and the statistical uncertainties show the standard error on the mean obtained by averaging over three proper Mpc chunks. A large, independently-selected sample of medium- to high-resolution ngCFHT spectra would be well suited for examining the presence of this feature, as well as providing precise measurements of the effective optical depth.

A second, related area is measuring the temperature of the IGM, which is sensitive to the photo-heating of the IGM during reionization. Directly measuring the IGM thermal state requires the relatively narrow thermal widths of Lyα absorption lines to be resolved:

$$b_{\rm HI} = 12.9\,{\rm km\,s^{-1}} \left(\frac{\rm T}{10^4\,{\rm K}} \right)^{1/2} \tag{2}$$

Ideally, this requires high-resolution ($\mathcal{R} \sim 40\,000$) spectroscopy. However, lower resolution data (e.g., the $\mathcal{R} \sim 20\,000$ mode on ngCFHT) would still resolve the larger scale on which the IGM is pressure (Jeans) smoothed. The lower number density of sufficiently bright quasars for moderate S/N would clearly preclude a BOSS-like survey at this resolution, but a large number of quasars obtained in a PI-led programme could still be used very effectively to probe the pressure smoothing scale in the IGM along — and, for sufficiently close quasar pairs, *transverse to* — the line of sight.

This "Jeans smoothing" scale is set predominantly by photoheating during reionization. In principle, when combined with measurements of the instantaneous temperature, constraints on the IGM Jeans scale from quasars can thus

yield insights into the timing and duration of the reionisation history. The uncertain thermal history is furthermore an important systematic when attempting to measure the instantaneous temperature of the IGM (Becker et al. 2011). The thermal structure of the IGM is also expected to be patchy on large scales due to the inhomogeneous nature of He II reionisation (McQuinn et al. 2009). Studying the line-of-sight variation in the data would thus provide a novel way to test both H I and He II reionization scenarios.

2.7.4.2 Galaxy/IGM Connection

The IGM is known to be the major reservoir of baryons at high-redshifts. Using this reservoir, galaxies draw fuel for star formation. Thanks to the large samples of $z \sim$3 galaxies that are now available, it is possible to study observationally the connection with this reservoir of ionized gas. Several interactions have been identified, ranging from accretion of the gas for star formation within the galaxies, to galactic winds polluting the IGM with metals up to low over-densities (i.e., Ryan-Weber et al. 2009).The next challenges for studies of the structure of galaxies is to understand the physical processes involved in the formation of galaxies and their interactions with the surrounding medium. Unfortunately, details of the cycling of gas into, through, and out of galaxies remain poorly understood. What is currently missing is an understanding of the gas belonging to the CGM, which is believed to be both the repository of the *inflowing* gas and the receptacle of the feedback of energy and metals generated *within* the galaxy.

Adelberger et al. (2005) used Lyman-Break techniques to select $z \sim 3$ galaxies in the fields of quasars. In this way, they were able to study the cross-correlations of Lyα and C IV absorbers seen in quasar spectra with the galaxy population in the field, finding that C IV is detected in most of the galaxies halos up to a hundred of kpc. They further found that the cross-correlation function of galaxies and C IV systems appears to be the same as the autocorrelation length of the galaxies, consistent with the idea that C IV systems and galaxies reside in similar parts of the universe. Similarly, they established that Lyα is associated with galaxies up to distances within 5–6 h^{-1} Mpc. More surprisingly, their observations hinted at a decrease of this cross-correlation at small distances within 1 h^{-1} Mpc, possibly due to enhanced star formation in these galaxies heating their surrounding IGM.

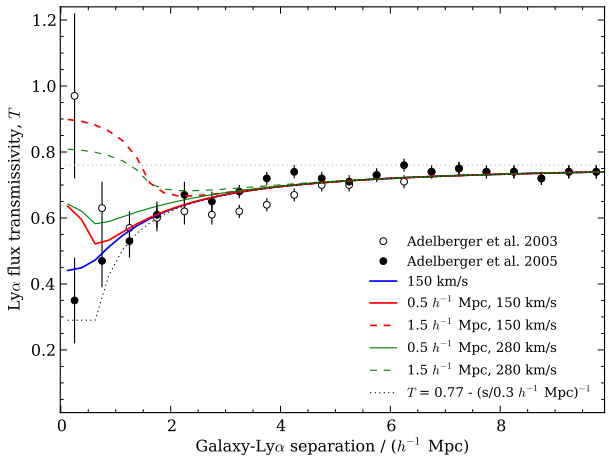

Figure 49: Mean Ly-α forest transmissivity in quasar spectra plotted as a function of distance from the nearest Lyman break galaxy from Aldelberger et al. (2003, 2005) and Crighton et al. (2011). The dotted line shows the unconvolved power-law model, and the blue line shows this model convolved with the expected uncertainty for LBGs in the NIRSPEC sample of Aldelberger et al. (2005). The green and red lines show models with a transmission spike of width 1.5 or 0.5 Mpc, convolved with two different velocity dispersions.

Crighton et al. (2011) measured the cross-correlation between H I gas causing the Lyα forest and 1020 Lyman break galaxies at $z \sim 3$. In agreement with the Adelberger et al. (2003) power-law relation, they measured the cross-correlation between C IV absorbers and Lyman break galaxies for scales 5-15 h^{-1} Mpc. They found an increase in H I absorption compared to the mean absorption level within $\sim$5 h^{-1} Mpc of a galaxy, in agreement with the results of Adelberger et al. (2005; see Figure 49). They argued that the Lyα-Lyman break galaxy cross-correlation can be

described by a power law on scales larger than 3 h^{-1} Mpc. After taking galaxy velocity dispersions into account, the results at <2 h^{-1} Mpc are also in good agreement with the results of Adelberger et al. (2005). There is little indication of a region with a transmission spike above the mean IGM value which might indicate the presence of star formation feedback.

More recently, Rudie et al. (2012) studied a sample of 886 star-forming galaxies, located close to background quasar sightlines, in the range $2.0 \lesssim z \lesssim 2.8$. Using high resolution data from Keck, their programme aimed to study the gas properties in these systems, such as column density and temperature. From their $N_{H\,I}$ measurements, they found that absorbers with log $N_{H\,I} > 14.5$ cm^{-2} are tightly correlated with the locations of galaxies, while the absorbers with lower column densities are correlated with galaxy positions only on $\gtrsim$ Mpc scales.

Given the differing results in studies of the transmissivity of the Ly-α forest, a new and larger sample of quasar absorbers and galaxy spectra from ngCFHT would represent an important new addition to the field. Moderate-resolution ($\mathcal{R} \sim 1\,000$–$3\,000$) spectra for galaxies at $2 \leq z \leq 3$ and lying close to the sightlines of bright quasars are needed to firmly establish the link between foreground galaxies and gas detected in absorption in the quasar spectra. For best results, good coverage is needed for all galaxies within the projected physical separation of 1 Mpc. For high spatial completeness, one may wish to visit each field several times in order to cover the galaxies around the quasars.

The galaxies observed in existing spectroscopic samples have a limiting magnitude of $R \approx 25.5$, and only $\sim 30\%$ of the galaxies show Ly-α emission. Since redshifts based on Ly-α emission can be offset with respect to the redshift based on absorption by up to several hundred km s^{-1}, it is preferable to have measurements based on absorption lines. A minimum S/N of ~ 5 per pixel would then be needed at $R \sim 25.5$. A reasonable goal for such a survey would be to target at least 100 bright quasar fields, with perhaps three visits to ensure coverage of all galaxies within $\sim 1'$. This corresponds to roughly 600 hrs of dark time. Based on the known number densities, dn/dz, we would expect about 40 000-45 000 Ly-α absorbers with log N(HI)>12.00, about 600 OVI systems (with log N(OVI)>13.2) and nearly 1000 C IV systems (with log N(CIV)>12.3). These represent 7- to 10-fold gains over any existing sample.

2.7.4.3 Galaxy-Scale Absorbers: Damped Lyα Systems (DLAs)

Metallicity studies of DLAs — see, e.g., Figure 50, which shows the evolution of metals from $z \sim 1$ to $z \sim 4$ — have many different applications in astrophysics. The ratio of alpha-to-iron peak elements is known to depend on star formation history, and very metal-poor DLAs offer an alternative to extreme metal-poor stars as diagnostics of early nucleosynthesis. Similarly, the primordial abundance of deuterium constrains Big Bang nucleosynthesis models, while studies of specific elements provide independent constraints on nucleosynthetic origins. Finally, fine structure lines provide independent information on star formation rates, and allow tests for possible time variations in physical constants. For these reasons, the efficient study of ever larger DLA samples is likely to be a priority in the coming decade, and, as we now explain, ngCFHT could play a leading role in such efforts.

Although the last two decades has seen a steady increase in the use of DLAs as probes of chemical abundances at high redshift, the very large number of DLAs that would be available from ngCFHT surveys would allow rare examples of extreme-metallicity DLAs to be identified. At low-metallicities, extremely metal-poor DLAs would provide an excellent complement to the abundance studies based on metal-poor Galactic halo stars (§2.3). The most metal poor DLAs also offer excellent independent tests of low-metallicity yields (e.g., Akerman et al. 2005). The recent discovery of a carbon-enhanced metal-poor DLA (Cooke et al. 2011) is currently the only one of its kind, but potentially represents the missing link between Population III enrichment and standard chemical evolution models. At the other end of the scale, extremely metal-enriched DLAs represent the rare cases of galaxies that have self-enriched to close to solar metallicity already by $z \sim 2$ (Kaplan et al. 2010).

For high-resolution observations at the bluest wavelengths, there would be further exciting opportunities. Most notably, at $\mathcal{R}$ = 20 000, it is possible to search for molecular gas, which has been detected in only a handful of DLAs to date (Noterdaeme et al. 2008). In survey mode, ngCFHT could detect hundreds of molecule-bearing (mostly H_2) galaxies. There would be multiple scientific dividends from such detections. Obviously, this would be the first truly statistical census of H_2 at high redshift. Measurement of the various J level populations also provides one of the few ways that the internal temperatures and densities can be measured (Noterdaeme et al. 2010) and the detection of CO gives a measurement of the CMB temperature (Srianand et al. 2008, Noterdaeme et al. 2011). Perhaps of greatest physical importance, follow-up observations of the molecule-bearing DLAs could be used to search for time variation in the fundamental constants (e.g., Murphy et al. 2008). To date, such research has relied on just a few individual absorbers.

Although a partnership between the ngCFHT bright-time and dark-time surveys is truly great for high-redshift

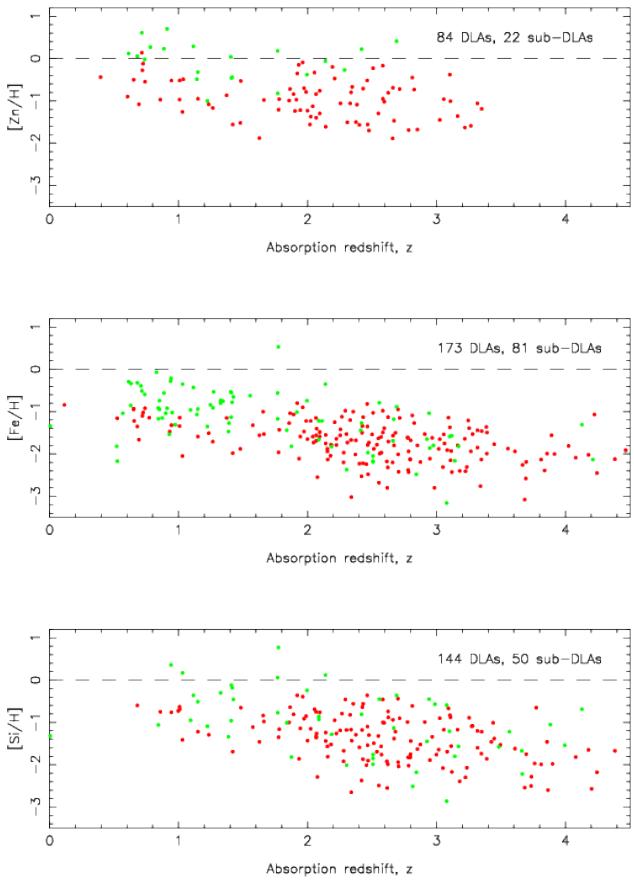

Figure 50: DLA abundances as a function of redshift according to the current literature. ngCFHT would dramatically improve the number of systems in which such measurements are possible.

abundances, the best science results would require a careful matching of the wavelengths so that the metals and HI are covered for the same redshift range. For example, an excellent line for this work is the SiII 1808 Å line: it is relatively strong, but usually not saturated, and Si is relatively unrefractory (compared with iron, for example). For absorbers in the range $1.8 \lesssim z \lesssim 3.5$ the blue low-resolution coverage (for Lyman α) would need to be approximately 0.34–0.55μm. The high resolution coverage would need to be $\approx$ 0.50–0.80μm, which, for selected programmes, could be obtained in the red arm using two instrumental setups. This is, in fact, further motivation for good blue sensitivity (in addition to studies of H_2). In general, work on the IGM and ISM benefits greatly from blue sensitive instruments, and such science cases have driven the design of, for example, UVES, and blue upgrades to instruments such as LRIS and HIRES on Keck. This is one of the primary scientific drivers for the high sensitivity of ngCFHT at blue wavelengths.

In order to calculate the approximate absorption line numbers that will be covered in a survey covering $\sim$ 10 000 deg^2, we adopt a typical quasar colour of (g–i) = 0.2. The bright survey limit is therefore approximately i =19.5. Combined with the quasar luminosity function, this yields the redshift path per square degree as shown in Figure 2.7.4.3. The redshift path is hence Δ z $\sim$ 1 per square degree for a survey with i <19.5. At redshifts of 2–3, the number density (i.e, the number per unit redshift path) of DLAs is n(z)$\sim$0.2. So, for an area of 10 000 deg^2, we can expect 10 000 $\times$ 1 $\times$ 0.2 = 2 000 DLAs.

With the newly available large number of spectra and images from SDSS in the last few years, it has been possible to undertake a "statistical" approach to some aspects of quasar absorbers studies, including stacking of spectra with low S/N. Examples of this include looking at the lensing effect (Menard & Peroux 2003), dust content (Murphy & Liske 2004; York et al. 2006; Frank & Peroux 2010; Khare et al. 2012) in composite spectra, stacking images with absorbers (Zibetti et al. 2005) or statistically correlating galaxies-absorbers (Bouche et al. 2004; Gauthier et al. 2009; Lundgren et al. 2009). With much enlarged samples of this kind, one would be able to divide surveys into data subsets

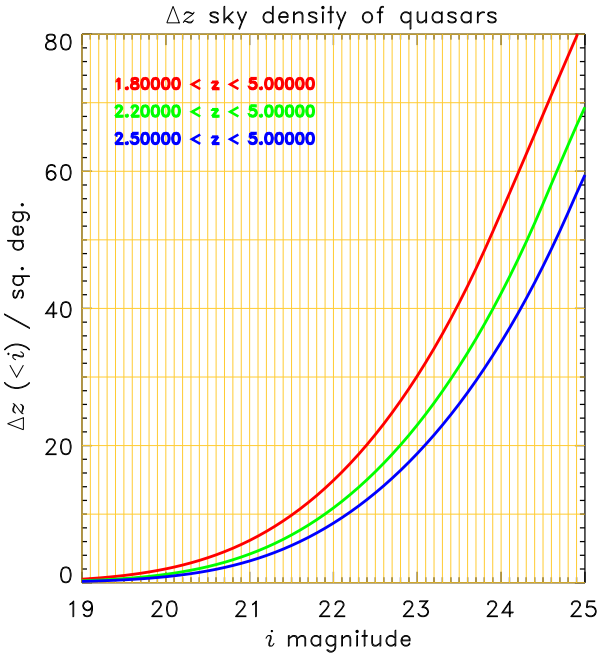

Figure 51: Surface density on the plane of the sky for quasars, in various redshift bins, brighter than a given i-band magnitude, as indicated on the horizontal axis. Note that the survey density of quasars at all z is much higher: i.e., $\approx$ 150–200 deg^{-2} for $i \lesssim 23$.

that could be used to study some specific aspects in more details (e.g., influence of metallicity on DLA dust content).

Studies such as these have laid the foundation for our understanding of the properties of gas in distant galaxies. However, our current understanding of the ISM at high redshift has clearly reached the point where it is limited by statistics, and this is where the combination of the bright and dark surveys with ngCFHT could make an enormous impact on this field. Finally, we point out that some of the projects discussed here could be carried out in conjunction with those outlined in the two following chapters.

2.8 QSOs and AGNs

2.8.1 Abstract

Active Galactic Nuclei (AGNs) and quasars (by which we mean the most luminous broad-line AGNs) are now thought to lurk at the hearts of all sufficiently massive galaxies. However, we remain ignorant about much of the basic picture of AGNs. How does the distribution of black hole masses and accretion rates in AGNs change with time? Do black holes grow to their observed masses steadily or intermittently? How does the light of an accretion disk relate to its fundamental physical properties and those of the black hole it surrounds? How do AGN outflows impact the current and future star formation in AGN host galaxies? Our ignorance in these and other areas of AGN and quasar science is likely to persist until the availability of a facility — such as ngCFHT — that is capable of delivering high-quality spectra for vast numbers of faint targets distributed over very wide fields.

2.8.2 Introduction

When we observe active galactic nuclei — highly luminous sources of radiation at the centres of distant galaxies — we know that the emission comes from metal-enriched gas surrounding a black hole. We can deduce the mass of the black hole at the heart of an AGN from the width of broad emission lines in its spectra. For certain quasars, we can estimate, using high-resolution spectroscopic observations, the distance from the black hole of the outflowing gas observed in the spectrum, as well as the outflow's kinetic energy and momentum fluxes. We can determine statistically the typical masses of quasar host galaxies and their halos from the clustering properties of quasars. In short, we can use quasars as beacons with which to study the distribution of gas and elements around — and between — distant galaxies over almost the entire history of the universe.

Nonetheless, we still have much to learn about quasars and AGNs. How *well* can we use a quasar's spectrum and multi-wavelength SED to determine its black hole mass, accretion rate, and other parameters such as gas-phase metallicity? How do the distributions of these properties change with quasar luminosity and with cosmic time? How did quasars cluster relative to galaxies and other quasars during the quasar epoch at $z > 2$? How did the black holes at the hearts of AGNs grow to the masses observed for them today and during the quasar epoch, and how did AGN light at all wavelengths track that growth? How much can we learn about quasar accretion disks and outflows from studies of variability in both quasar fluxes and absorption line profiles? Can we use reverberation mapping (RM) time delays to measure quasar luminosities with systematic uncertainties small enough to construct a quasar Hubble diagram of distance vs. redshift for comparison with models of dark energy? In the coming decade, astronomers will be attempting to increase our understanding of these and other issues surrounding AGN as best as possible with current datasets. To go beyond those datasets will require a new spectroscopic facility such as ngCFHT.

Above all, ngCFHT is needed for quasar and AGN science because quasars and AGN are rare objects. To assemble large quasar and AGN samples requires surveys with large areal coverage. To extend quasar and AGN science beyond their current frontiers will require reaching to significantly lower luminosities without a significant reduction in spectral S/N. The large aperture of ngCFHT would allow it to study AGNs to significantly lower luminosities at fixed S/N than any current or planned AGN survey on 2.5m- or 4m-class telescopes. Wide-field, high-quality spectroscopy was responsible for the extraordinary scientific impact of the SDSS, and will do the same for the ngCFHT.

2.8.3 ngCFHT in Context: Competition and Synergies

For AGN and quasar science, the most influential surveys to date have been SDSS-I and II, and SDSS-III/BOSS. The SDSS includes $\sim$ 10,000 deg^2 of $ugriz$ imaging data plus high-quality spectra for targeted and serendipitous quasars and AGNs. Deeper imaging surveys of this size or larger will soon be available (see, e.g., §1). However, most spectroscopic surveys that wish to go fainter than existing surveys are restricted to smaller areas, limiting their science (e.g., SDSS-IV/eBOSS). The ngCFHT would execute the largest-area spectroscopic surveys, at every magnitude, within reach of a 10m-class telescope.

Quasar targets for ngCFHT could be drawn from the SDSS down to its photometric limits (Richards et al. 2009). Quasar selection can be optimized and extended by combining SDSS data with additional optical data (from, e.g., CFHTLS, other Megacam projects, or many other surveys with other telescopes), near-infrared data (from various WIRCAM projects, UKIDSS, etc), far-infrared data (WISE, Planck, Herschel, SCUBA-2, etc), radio data (NVSS, FIRST, JVLA, LOFAR, SKA pathfinders, etc), ultraviolet data (GALEX or UVIT), X-ray data (Chandra, XMM, Astro-H, eROSITA, etc), and astrometric data from Gaia. Combining spectroscopic data on quasars from ngCFHT

with multi-wavelength data from these and other instruments, telescopes and surveys would enable far more science — and far more *interesting* science — than can be done with any individual dataset. In particular, ngCFHT would have immense AGN science synergy with Pan-STARRS and LSST, despite the latter being located in a different hemisphere. The combination of deep, multicolour, photometric monitoring from Pan-STARRS or LSST with spectroscopic observations with ngCFHT would yield greater scientific impact than either photometry or spectroscopy alone, even when confined to the equatorial regions accessible to both telescopes.

Because ngCFHT will have 3,200 fibres on a 10m telescope, its prime competition is the PFS instrument on Subaru (2,400 fibres on an 8m telescope; Ellis et al. 2012). While this will be an impressive instrument, the largest survey currently planned for it would cover an area of 1,400 deg^2, one-third the area of the ngCFHT Dark-Wide survey. The only other wide-field spectroscopic survey that comes close to competing with ngCFHT for AGN studies is the proposed 5000-fibre BigBOSS (Schlegel et al. 2011) on the KPNO 4m telescope, which would obtain $\mathcal{R} \gtrsim 3,000$ spectra over the $0.34 - 1.06\mu$m range of 500,000 quasars at $2.2 \lesssim z \lesssim 3.5$ covering 14,000 deg^2. There is no doubt that this would be an impressive survey, but BigBOSS would never be able to reach targets as faint as ngCFHT.

In short, ngCFHT would be, for AGN and QSO science, the world's premier wide-field spectroscopic survey telescope — a legacy that is ensured by its large collecting area, high throughput and multiplexing, wide spectral coverage, and overall efficiency for survey operations.

2.8.4 Legacy Science

The AGN science legacy datasets from the ngCFHT would consist of:

1. Low-resolution spectroscopy of 375,000 $z \lesssim 2.2$ quasars, 200,000 quasars in the range $2.2 \lesssim z \lesssim 4$ (400,000 if BigBOSS has not already observed $2.2 \lesssim z \lesssim 4$ quasars at $g \leq 23$), and 26,000 $z \geq 4$ quasars obtained as part of the Dark-Wide and Dark-Medium Surveys (a total of 150–200 quasars deg^{-2}) for studies of baryon acoustic oscillations (Sawangwit et al. 2012) and quasar physics, clustering, and luminosity functions (§2.8.4.1).

2. High-resolution spectroscopy of up to 50,000 quasars (50 deg^{-2}) obtained as part of the bright-time survey for studies of intrinsic absorbers and AGN feedback (§2.8.4.2) as well as for studies of intervening absorbers.

3. 100 epochs of low-resolution spectroscopy for more than 500 quasars in a single 1.5 deg^2 field obtained as part of the Dark-Deep Survey for variability studies of accretion disks, outflows, and emission-line regions (§2.8.4.3).

We discuss below the primary science drivers for these datasets, but it cannot be overemphasized that a vast range of other scientific projects would be enabled by such large datasets, and *only* by them.

2.8.4.1 AGN Luminosity Functions, Clustering, and Binaries

Surveys with ngCFHT would provide enormous samples of Type 1 (broad-line, optically unobscured) and Type 2 (narrow-line, optically obscured) AGNs, as well as control samples of galaxies that show no evidence for currently hosting optically detectable AGN. The relationships between galaxies and AGNs can be quantified in large measure using the AGN luminosity function (LF), the clustering of AGNs relative to galaxies and to other AGNs, and the evolution with redshift of both quantities out to $z \simeq 6.5$. Photometric redshifts enable coarsely-binned LF and clustering studies using multicolour photometry alone (i.e., Richards et al. 2009), but are useful primarily for extending such studies to fainter AGN candidates which lack spectroscopy (rather than as a substitute for spectroscopy).

The LF and its redshift evolution can constrain AGN black hole masses, accretion rates, duty cycles, and lifetimes (e.g., Hopkins, Richards & Hernquist 2007). Such constraints are only possible, however, with samples that extend past the break in the double-power-law AGN LF at luminosity L^*. For example, in the merger+feedback model of Hopkins et al. (2006), the faint-end slope constrains how long visible AGNs typically accrete at sub-Eddington rates, while the bright-end slope constrains the space density of massive galaxy mergers that lead to briefly visible episodes of Eddington-limited accretion onto black holes. Understanding how the AGN LF changes with cosmic time will help us refine such models for the formation of AGNs and the influence of their radiative and kinetic luminosities on the evolution of massive galaxies. Even better constraints would be possible by combining observations of the AGN LF and AGN clustering.

Clustering. Clustering measurements, when combined with quasar LF measurements, constrain quasar lifetimes, t_q (Martini & Weinberg 2001; Haiman & Hui 2001; Shen 2009; Shankar, Weinberg, & Shen 2010). Quasar lifetimes,

and their dependences on other quasar parameters, can be predicted by models of galaxy formation incorporating AGN feedback (e.g., Booth & Schaye 2009) and thus can be used to test such models.

Measurements of quasar-quasar and quasar-galaxy clustering also constrain the masses of the dark matter halos that quasars inhabit. The strength of clustering measured by the two-point correlation function, $\xi(r) \simeq (r/r_0)^{-\gamma}$, can be approximated by the value of r_0, the projected radius around one galaxy within which the chance of detecting other galaxies is higher than random: i.e., stronger clustering yields larger r_0.[17] The concordance cosmological model predicts the autocorrelation of dark matter, but galaxies and AGN are believed to be biased tracers of dark matter with scale-dependent bias, $b(r)$, defined by $\xi(r) = [b(r)]^2 \xi_{DM}(r)$. The higher the average halo mass hosting a subsample of AGN, the higher the average bias, and the stronger the clustering within that subsample and between it and other AGN and galaxy samples. The quasar-galaxy $\xi(r)$ can be measured by targeting $z < 2.2$ quasars (Sawangwit et al. 2012), while measuring the quasar-quasar $\xi(r)$ at $z > 2.2$ can discriminate between different models of black hole mass growth that are degenerate at $z < 2.2$ (see Figure 52).

The clustering evolution of optically-selected quasars has been measured at redshifts $z \leq 2.2$ (e.g., Croom et al. 2005; Ross et al. 2009) and $z > 2.9$ (Shen et al. 2007), but even the full SDSS is limited by small-number statistics in the latter case. The need for a statistically significant number of pairs at very small separations to measure the '1-halo' term and constrain the triggering of AGNs in mergers and interactions drives the demand for ever larger samples (e.g., Myers et al. 2008; Ross et al. 2009).

Binary AGNs. With a $6''$ minimum on-sky separation between fibres, ngCFHT will have the advantage of being able to probe quasar clustering at sub-arcminute scales. Binary AGN (e.g., Liu et al. 2011) can be identified via dual narrow-line or broad-line redshifts or in very close pairs through multiple spectroscopic visits (which will also be needed for small-scale galaxy clustering studies). A statistical study of dual AGNs and their host galaxies would have important implications for theories of galaxy and black hole formation and growth (Bogdanović et al. 2008; Volonteri, Miller, & Dotti 2009), and for predictions of the potential detection rate of gravitational wave signatures from merging black holes (Loeb 2010).

Observational Considerations. While the ngCFHT Dark-Wide and Dark-Medium surveys (see §1) will inevitably turn up vast numbers of faint AGNs in their galaxy targets, targets must also include objects identified as AGN candidates via quantitative selection criteria utilizing all available information (e.g., multiwavelength photometry, variability, astrometry). We refer to these candidates as quasars to distinguish them from lower-luminosity AGNs targeted as galaxies as a result of emission from the host galaxy.

In the Dark-Wide survey, the total surface density of quasar targets to $g = 23.5$ ($i = 23$) at all redshifts (150–200 deg^{-2}) reduces the number of galaxies targeted per pointing by $\leq 6\%$ at most. The 4300 deg^2 Dark-Wide survey would obtain spectra for 375,000 $z \lesssim 2.2$ quasars, 400,000 $2.2 \lesssim z \lesssim 4$ quasars (or only 200,000 if BigBOSS has already targeted the bright half of the sample), and 25,500 quasars at $4 \lesssim z \lesssim 5$. The luminosity range probed by ngCFHT would straddle the break in the LF, but to determine an accurate faint-end slope at high redshift requires targeting quasars to $i = 24$ in the Dark-Medium 100 deg^2 survey. This survey would contain an additional $\sim$500 quasars at $4 \lesssim z \lesssim 5$.

2.8.4.2 AGN Outflows as Feedback

The properties of black holes and their host galaxy spheroids correlate with each other, suggesting that the formation and evolution of a galaxy spheroid is strongly affected by feedback generated through accretion onto its central black hole (e.g., Ferrarese et al. 2006). AGN feedback consists of the heating caused by the AGN's radiation field and the kinetic energy and momentum fluxes of outflows of matter from, e.g., the accretion disk (e.g., Murray, Quataert, & Thompson 2005; Ostriker et al. 2010). Heating and physical feedback can inhibit star formation in the surrounding galaxy, while physical feedback can in principle trigger it as well. Depending on the details of these feedback inputs, AGNs can dramatically affect the evolution of star formation in their host galaxies (Hopkins & Elvis 2010, and references therein), the cooling of gas in surrounding galaxy clusters (e.g., McNamara 2010), and the nearby intergalactic medium (e.g., Martel 2011). An improved understanding of AGN outflows is therefore needed for a better understanding of the formation of galaxies and structure in the universe.

We can divide AGN outflows into narrow, relativistic *jets* (which can be studied at radio, X-ray and γ-ray wavelengths) and *winds* (which can be seen as absorbers in AGN spectra; see Figure 53). These winds range from broad absorption line (BAL) systems — which can be tens of thousands of km s^{-1} wide (e.g., Hall et al. 2002) and which

[17] In detail, there is a scale dependence of $\xi(r)$ due to a transition from '1-halo' clustering within a dark matter halo to clustering between different dark matter halos.

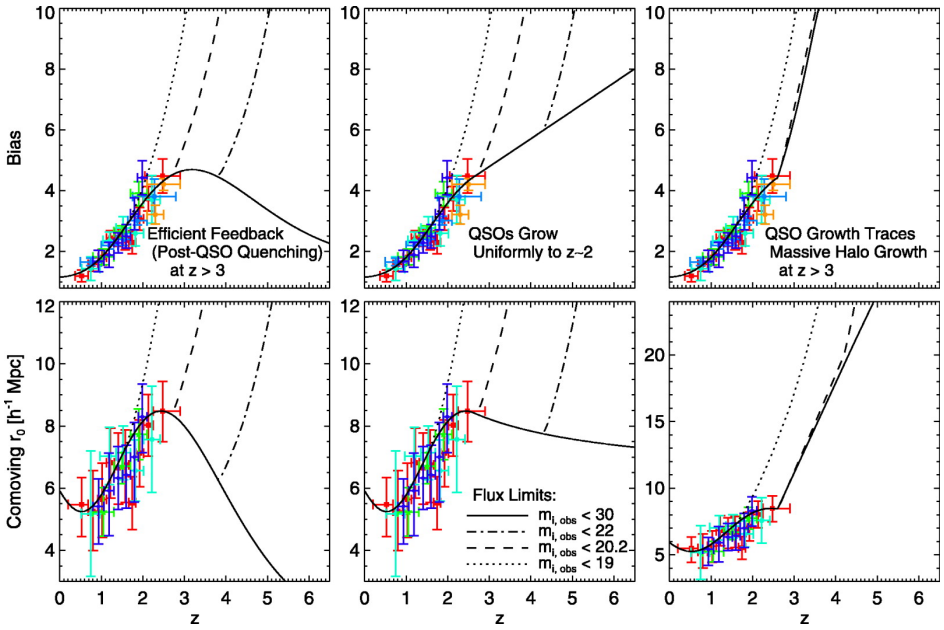

Figure 52: Predictions for quasars' clustering correlation length (bottom row) and inferred bias (top row) at redshifts $z \gtrsim 3$, from Hopkins et al. (2007). Results from existing surveys are shown by points of various colours. The effects the observed-frame i-band flux limits given in the lower centre panel are shown as different lines ($i = 20.2$ corresponds to the SDSS completeness limit). Quasars seen at brighter fluxes preferentially have more massive black holes, which preferentially inhabit more massive dark matter halos, and thus exhibit greater clustering. The left panels assume that black hole growth shuts down after a quasar episode, so that at $z \gtrsim 2.5$ quasars trace the increase with cosmic time of the mass of halos collapsing for the first time. The centre panels assume that all $z > 2.5$ black holes grow to characteristic peak luminosities at $z \sim 2.5$, and then shut down. The right panels assume quasar growth tracks host halo growth, even after a quasar episode, until $z \sim 2.5$. Observations at $z \gtrsim 3$ with ngCFHT would break the degeneracies between these models at $z \lesssim 2.5$ and enable tests of more detailed models.

also absorb a quasar's X-ray emission (e.g., Gallagher et al. 2006) — through to narrow systems of width $<$100 km s^{-1} (e.g., Hamann 2001).

Feedback From UV Absorbers. Of particular interest for ngCFHT are outflows with unblended UV troughs from ground and excited states of the same ion; e.g., S IV (Dunn et al. 2012), C II, Si II, Fe II, etc., which enable characterization of the mass, kinetic energy flux, and momentum flux of the $T \sim 10^4$ K gas in the outflows (e.g., Dunn et al. 2010). The relative strength of the excited state absorption tracks the relative population of the collisionally populated excited state. Measurement of the ground and excited state absorption therefore constrains the electron density in the absorbing gas, and the observed abundances of ions of different ionization energies constrains the ionization parameter U of the gas. With a model for the total number of hydrogen-ionizing photons per second emitted by the quasar (Q_H), the distance d of the absorbing gas is found from the defining relation $U = Q_H/4\pi d^2 n_e$. The outflow's mass flux is $\dot{M} = \Omega d N_H v$, where Ω is the solid angle of the absorbing gas around the black hole and N_H its total hydrogen column density (obtained assuming solar metallicity unless a metallicity measurement can be obtained using ions from multiple elements). The outflow's momentum flux is $\dot{p} = \Omega d N_H v^2$, and its kinetic energy flux is $\dot{E}_k = \frac{1}{2}\Omega d N_H v^3$. To date, such outflows have been shown to reach $\dot{E}_k = 0.01 L_{bol}$ (Dunn et al. 2010) even without including any contribution from a hot gas component which may contribute 5–50$\times$ higher N_H (Netzer et al. 2003; Faucher-Giguère et al. 2012).

High-Resolution Observations. High-resolution ($\mathcal{R} = 20,000$) observations are needed to resolve the sometimes complex velocity structure of intrinsic absorbers and to accurately determine the ionic column densities in them. The required spectra of bright quasars could be incorporated into the ngCFHT "bright-time" surveys covering $\sim$ 10,000 deg^2 or more (see, e.g., §1, 2.1, 2.2, 2.3). For instance, an allocation of 10% of the survey fibres for the proposed high-resolution, Galactic Archaeology Survey (i.e., 80 fibres per pointing, on average) would be sufficient to obtain SN $\geq 20/$Å spectroscopy for **all quasars at** $0.5 \lesssim z \lesssim 4.1$ **brighter than** $i = 20$ over the entire 10,000 deg^2 survey footprint at high Galactic latitude (up to 50,000 quasars in total). This sample would enable a characterization of the

energy, mass and momentum fluxes of hundreds of quasar outflows with unblended ground and excited-state troughs. It would also enable unprecedented studies of intervening and intrinsic narrow Mg II absorbers (at $z > 0.5$) and C IV absorbers (at $z > 1.65$), and a thorough catalogueuing of DLAa at $2.3 \lesssim z \lesssim 4.1$.

Low-Resolution Observations. By observing ∼150 quasars deg^{-2} in the Dark-Wide and Dark-Medium surveys, ngCFHT would also extend the detection and study of intrinsic absorbers to larger numbers, fainter quasars, and longer variability baselines than is possible with SDSS/BOSS:

1. Larger samples enable finer binning in studies of the interdependences of outflow and quasar properties.

2. Fainter samples are key to understanding the connection between outflows with obscuration and intrinsic quasar luminosity. The presence of dust in, or near, outflows can lead to an underestimate of the fraction of quasars with outflows (Allen et al. 2011); spectroscopy of fainter samples better constrains that fraction.

3. ngCFHT spectroscopy combined with previous SDSS spectroscopy would quantify the variability in intrinsic absorption in thousands of quasars over rest-frame years, even when only two epochs are available (e.g., Gibson et al. 2010). ngCFHT would also provide an opportunity to monitor ∼ 400 broad-line AGNs for absorption-line variability (including trough appearance and disappearance) over rest-frame timescales of days to years, as part of the Dark-Deep survey (§2.8.4.3).

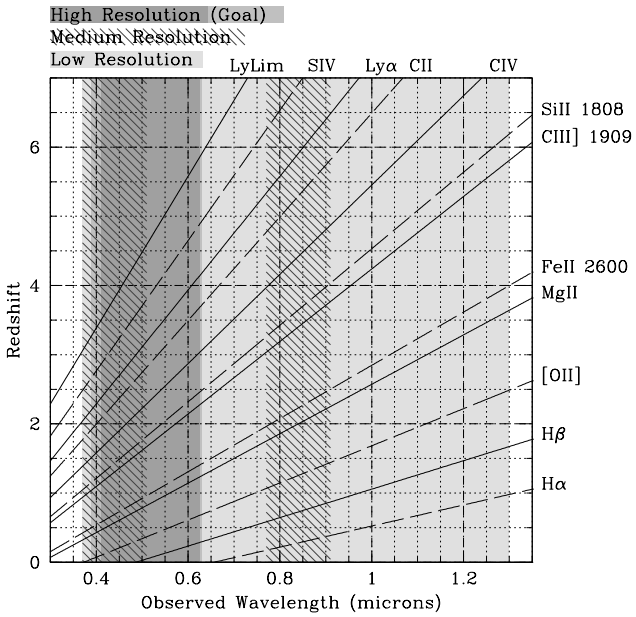

Figure 53: Observed wavelengths of important quasar emission and absorption lines as a function of redshift (diagonal tracks) overplotted on the planned ngCFHT spectral coverage. The wavelength region to be covered by low resolution spectroscopy ($\mathcal{R} \sim 2,000$), including coverage at wavelengths >1 μm from a near-IR arm, is shaded light grey. The two regions of medium resolution ($\mathcal{R} \sim 6,000$) coverage are hatched. The design requirement for high resolution ($\mathcal{R} \sim$ 20,000) coverage is the dark grey shaded region, while the goal is coverage of the slightly wider medium grey shaded region.

2.8.4.3 Reverberation Mapping: Black Hole Masses and Dark Energy Constraints

Even the nearest AGNs are too far away for the continuum- and line-emitting regions surrounding their black holes to be imaged at optical wavelengths using current facilities. We can nonetheless "image" AGNs using time resolution as a substitute for angular resolution by using repeated spectroscopic observations to measure the time delay, τ_d, between a change in the continuum flux and the resulting change in flux of a broad emission line (Blandford & McKee 1982). Once the size of that broad-line region (BLR) $s_{BLR} = c\tau_d$ is measured, the mass of the black hole is given

by $M_{BH} = f(\Delta v)^2 s_{BLR}/G$ where G is the gravitational constant, Δv is a measure of the width of the emission line studied, and f is a factor of order unity which accounts for the geometry and kinematics of the BLR (see, e.g., Peterson 2011, and references therein). With spectral coverage from 0.37–1.3μm, ngCFHT would enable RM in two or more strong lines at all redshifts $\lesssim 3.5$ (Hβ+Mg II or Mg II+C IV). Such observations would also enable statistical studies of continuum variability in *all* quasars, and absorption-line variability in quasars with intrinsic absorption (§2.8.4.2). A large sample of reverberation-mapped quasars would also allow a characterization of the spread of BH and BLR properties (i.e., viewing angle, fueling rate, BH spin) corresponding to the spread expected in velocity-resolved time delay maps (Denney et al. 2010).

Understanding the black hole mass function and its evolution over cosmic time helps us understand the impact of AGN feedback on the evolution of galaxies. While single-epoch quasar spectroscopy can yield black hole masses calibrated via RM, the calibration for distant, luminous quasars has to date been inferred entirely from observations from nearby, lower-luminosity quasars. *In situ* measurement of black hole masses at high redshift is the only way to ensure that the calibration is not dependent on either luminosity (due, for example, to changing BLR structure with luminosity; Richards et al. 2011) or cosmic time (due, for example, to changes in the average fueling rate at a given black hole mass).

A good introduction to the state of the art in black hole mass measurements and RM is given in Peterson (2011); see also Zu, Kochanek, & Peterson (2011). While the general technique behind black hole mass measurements is known to work, this remains an area of active research aimed at determining the ultimate observational and theoretical limitations of the technique (e.g., Croom 2011; Assef et al. 2012; Ho et al. 2012). For instance, work is needed to understand just how well the usually unobserved far-UV ionizing luminosity tracks the observed near-UV continuum (Arav et al. 2012). The current status of black hole mass measurements is conceptually similar to the current status of SNe Ia as standard candles despite our incomplete understanding of their progenitors and explosion mechanisms.

Dark Energy Constraints. Reverberation mapping has the potential to measure not just black hole masses but quasar luminosities, using the dependence of BLR size on quasar luminosity. With measured quasar luminosities and observed quasar fluxes, a quasar Hubble diagram of distance versus redshift can be constructed and used to constrain possible time variation in the dark energy equation of state, which would change the distance-redshift relation (Watson et al. 2011). Based on SNe Ia, the distance-redshift relation is constrained only out to $z \sim 1.7$. Luminosity distances are given by $\sqrt{L/4\pi F}$ where F is the observed flux and intrinsic quasar luminosities, L, are inferred from their BLR sizes measured from RM according to the empirically well-established relationship $s_{BLR} \propto L^{1/2}$ (Kaspi et al. 2007; Bentz et al. 2009). The intrinsic scatter in a RM measurement of the luminosity of a quasar is estimated to be 0.08 dex, or 0.20 mag (Watson et al. 2011). Of course, considerable work remains to be done over the coming decade to ensure that this limit can be reached in a large fraction of randomly selected quasars.

Technical Considerations. Requirements for accurate RM have been discussed by Horne et al. (2004). The peak emission-line time delay, τ_d, measured in a given RM campaign is the light-crossing time of the BLR in that line at that time (the BLR increases in size with increasing quasar luminosity; Cackett & Horne 2006). High-fidelity velocity-delay maps (i.e., line responsivity as a function of line-of-sight velocity and time delay) can be obtained if the RM campaign has duration $T_{dur} > 3\tau_d$. The velocity resolution is only limited by the spectral resolution, while the delay resolution is $\Delta\tau_d \simeq 2\Delta t$ where Δt is the sampling time interval. Sampling with $\Delta t \leq \frac{1}{6}\tau_{\rm pred}$, where $\tau_{\rm pred}$ is the predicted τ_d, enables detection of that lag at $\geq 3\sigma$. The detection of low-amplitude, short-timescale continuum and emission-line variations requires high-S/N spectra (~ 30 per resolution element at the line centre). Contemporaneous photometric monitoring can help guard against spectrophotometric errors in absolute fluxes.

RM campaigns with the potential to constrain dark energy are feasible with ngCFHT. RM can be done with Hβ and Mg II at $z \lesssim 1.7$ ($z \lesssim 3.5$ with a NIR spectrograph arm), and C IV at $z \gtrsim 1.7$. The requirement of observing simultaneously a large number of RM targets pushes the survey to the faintest practical magnitudes, and the requirement of $\gtrsim 18$ spectra per target means the required total exposure time can be obtained only in the context of an extremely deep "pencil-beam: survey. Thus, the necessary spectroscopic epochs would be obtained primarily during the ngCFHT Dark-Deep galaxy spectroscopic survey. RM requirements do not strongly constrain the preferred location of an ngCFHT Dark-Deep field, although they do favour a location with $+5^\circ < \delta < +50^\circ$ (to maximize the accessible time at airmass $X < 1.5$) or at least $0^\circ < \delta < +65^\circ$ (to maximize the accessible time at airmass $X < 2$).

The main RM requirements on the Dark-Deep (DD) survey are on the nightly depths and the visit timing. Each night's coadded spectra of RM targets must reach $\mathrm{S/N} \sim 30$ per resolution element in the line centre. The simplest timing for the visits would be every $\frac{1}{6}\tau_d$ or less for a span of $3\tau_d$. But, as shown in Table 20, such timing is not achievable at magnitudes where large numbers of quasars lie within a single ngCFHT field of view, due to time dilation and the scaling of $\tau_d \propto L^{1/2}$. Fortunately, modern RM analysis methods can cope with irregularly spaced

visits and seasonal gaps (Zu, Kochanek, & Peterson 2011), especially if frequent photometric monitoring occurs in between spectroscopic epochs (Fine et al. 2012).

Table 20: Observational Cadence and Duration Required for Quasar Reverberation Mapping (RM)†

g (mag)	$z = 1$ τ_d (obs)	Observe Hβ/ Mg II Every	For T_{dur}=	$z = 2.2$ τ_d (obs)	Observe C IV Every	For T_{dur}=	$z = 4$ τ_d (obs)	Observe C IV Every	For T_{dur}=
18.5	175 (350)	50 d	3 yr	71 (227)	1 mo	2 yr	150 (750)	3 mo	6 yr
21.0	56 (112)	16 d	1 yr	22 (70)	9 d	7 mo	47 (235)	1 mo	2 yr
22.95	23 (46)	7 d	4.5 mo	9 (29)	4 d	2.8 mo	19 (95)	13 d	10 mo
23.5	18 (36)	5 d	3.5 mo	7 (22)	3 d	2.2 mo	15 (75)	10 d	7.5 mo

† *Each line of the table above lists values for a different observed g-band magnitude. At that magnitude, for each of three different redshifts z, a set of three columns gives the expected τ_d in rest (observed) days and the cadence and duration T_{dur} (in days, months and years) required to reliably measure that τ_d using Mg* II *or Hβ at $z = 1$ and C* IV *at $z > 1.7$. (A NIR spectrograph arm would enable Mg* II *RM at $z = 2.2$ with timescales similar to those for C* IV *RM at $z = 4$.) For example, a $g = 18.5$ quasar at $z = 1$ should be observed every 50 days for 3 years to measure its $\tau_d = 175$ rest-frame days. Values of τ_d for C* IV *follow the results of Kaspi* et al. *(2007); the τ_d for Mg* II *are 2.5 times longer.*

For observations at airmass $X < 2$ (and preferably $X < 1.5$), the maximum practical exposure time is roughly 6 hours per night. With that total exposure time and the RM S/N requirement, the limiting magnitude for RM targets will be $g = 22.95$ ($i = 22.7$). To these limits there are approximately 545 $z < 4$ quasars per ngCFHT field (1.5 deg^2). This is about 1/6th the total number of science fibres. (All RM targets could be confirmed as quasars in advance, via shorter pilot exposures if needed, so as not to waste survey mode fibres on identification.)

Of course, not every scheduled survey night will yield the goal of 6 hours of spectroscopy on the Deep-Dark field. Visits cut short due to unacceptable observing conditions could be given priority status to be finished within two subsequent nights. That would ensure the co-added spectra remain useful for RM measurements on all but the faintest $z \lesssim 2.2$ quasars (see Table 20). Alternatively, or in addition, sufficient numbers of 6-hour visits could be ensured as follows. The DD galaxy survey requires 6 configurations overlapping on a single ngCFHT field. We suggest including all RM targets on 5 of the 6 original configurations (#1–5, for convenience) and on a new configuration #7. The configuration without RM targets (#6) will include any galaxies of interest within $6''$ of RM targets. Configurations #1–5 will have the goal of 6 hours' total exposure time in each nightly visit, while #6 will have no such goal. Each configuration #1–6 will be retired after achieving 100 hours' total exposure time. Weather and other issues will cut short some visits for configurations #1–5, though visits of <6 hours will still be useful for RM of brighter quasars. Configuration #7 will be used to ensure that fainter quasars will have sufficient numbers of RM-quality observations. When the time since the last 6-hour visit in any configuration grows too long, configuration #7 will move to the top of the scheduling queue, thus prioritizing a 6-hour visit without compromising the Deep-Dark galaxy survey's desire for a total of 100 hours/configuration in visits of any length. Configuration #7 can be changed over time to include different galaxy targets as long as all quasar RM targets remain on it. More refined scheduling of observations could also be done to observe more slowly varying high-luminosity objects less often than more rapidly varying low-luminosity objects.

Table 21: Technical Requirements and Survey Implementation: Quasar Reverberation Mapping (RM)

Survey Area (Ω)	The Dark-Deep ngCFHT pointing: $\Omega \approx 1.5$ deg^2.
Number of Configurations ($n_{\rm config}$)	$n_{\rm config} = 6$, with each RM target included in all configurations
Primary Imaging Resources for Target Selection	SDSS, Pan-STARRS (3π), LSST
Observing Conditions	Lunar illumination < 50%, Cloud cover < 20%
Number of Visits and Exposure Time per Visit	$N_{\rm visit} = 17$ per configuration (102 visits per RM target), $T_{\rm exp} = 6$ hr per visit
Wavelength Coverage	0.37–1.3μm at $\mathcal{R} \lesssim 2000$
Limiting (point source) Magnitude per Visit	$g_{\rm AB} \simeq 22.95$ or $i_{\rm AB} \simeq 22.7$
Total Time Needed for Program ($T_{\rm tot}$)	$T_{\rm tot}$ = 6 × (17×6 hr) + 20% overhead ≈ 735 hrs over 6 yrs [Includes 5 × (17×6 hr) + 20% overhead ≈ 612 hrs available from the Dark-Deep Survey]

The ngCFHT RM component of the Dark-Deep survey will result in a fraction, x, of quasars with successful measurements of the BLR time lag τ_d in at least one line, yielding $315x$ τ_d measurements at $0.2 < z < 1.7$ and $240x$

at $1.7 < z < 4$. At the highest luminosities, only about 1 in 6 quasars are variable enough for RM measurements in any given length of time T_{dur} (Kaspi et al. 2007; Botti et al. 2008). However, lower luminosity quasars are much more variable (e.g., Peterson et al. 2002). Assuming conservatively $x = 0.5$, we expect 155 $0.2 < z < 1.7$ and 120 $1.7 < z < 4$ RM measurements per field. For dark energy studies, that sample would match the statistical power of the "Gold" SNe Ia sample of Riess et al. (2007) at $0.2 < z < 1.7$ (i.e., six bins of $n\Delta z = 6$ each) and extend the same power to $1.7 < z < 4$, where SNe Ia are not seen. Another way of expressing this power is in terms of Δw, the deviation in the equation of state parameter $w(z) = \frac{P(z)}{\rho(z)}$ from the cosmological constant value of $w(z) = -1$. *With 50% RM detection efficiency, the ngCFHT RM sample would yield a* $\geq 4\sigma$ *detection of any* $|\Delta w| \geq 0.07$ *in any of five bins in the unexplored redshift range* $1.7 < z < 4$. That result will be a significant new contribution to constraining models of dark energy, which is arguably the most outstanding unsolved issue in all of astrophysics.

2.9 Cosmology and Dark Energy

2.9.1 Abstract

Over the past century, cosmology has evolved from a theoretically motivated science to one driven mainly by observations. Indeed, the exponentially growing volume of data is now the key factor in driving the development of new theories in cosmology. This is especially in the study of Dark Matter and Dark Energy. Here we explore a possible cosmological spectroscopic survey — using the ngCFHT facility to map galaxies and quasars tracing the large-scale structures beyond $z > 0.5$ — that has the following goals:

1. Determine with high accuracy (i.e., better than 1%) Baryonic Acoustic Oscillation (BAO) distances over the range $1< z <3$ using redshifts for galaxies and quasars collected in a massive, wide-field (up to $\sim$10,000 deg^2) cosmological spectroscopic survey.

2. Measure in this same wide-field survey: (1) the Redshift Space Distortions, thereby providing strong constraints on the growth factor and opening the further possibility of constraining the law of gravitation on large scales; and (2) the shape of the power spectrum in order to probe both neutrino masses and the non-gaussianity of the primordial density fluctuations.

3. Conduct a dedicated pointed survey of the $\sim$500 massive galaxy clusters identified in optical, SZ and X-ray surveys (mostly in the redshift range $0.3 < z < 1$) and probe the growth of these massive clusters over the last half of the Hubble time.

4. Carry out a deep survey of the many transient objects, such as supernovae and/or their hosts, that will be identified in forthcoming synoptic imaging surveys (e.g., LSST) or other transient search experiments (such as the Zwicky Transient Factory).

We also investigate the possibility of mapping, to first order, the velocity field of stars in distant galaxies which, when combined with weak-lensing shape measurements, would increase significantly cosmological constraints from weak lensing. Such project would, however, require modification of the current ngCFHT instrumental design: e.g., by replacing single fibres by bundles of fibres.

2.9.2 Introduction

With the discovery of the acceleration of the Universe expansion (Riess et al. 1998; Perlmutter et al. 1999) possibly driven by a new form of energy with negative pressure, astronomers and physicists have concluded that 96% of the energy density of the universe is in an undetected — or "dark" — form. Over the last decade, there has been a growing realization that understanding these new components of the universe (*i.e.*, the dark matter and dark energy) may require fundamentally new physics. Numerous ideas have been advanced to explain the acceleration and predict its redshift evolution (e.g., see the review of Frieman et al. 2008).

Determining the cosmological world model has thus become one of the hottest questions of contemporary cosmology. Current and expected technologies (in terms of telescopes and instrumentation) offer the possibility to probe most of the volume of the universe (both in imaging and spectroscopy) to a steadily increasing depth. The resulting three-dimensional mapping of galaxies would provide the information needed to accurately determine the galaxy power spectrum and its evolution, thereby constraining the various cosmological parameters. Specifically, the isotropic power-spectrum of any large-scale structure tracer — such as galaxies, quasars or the Ly-α forest absorbers — probes universe geometry, the accelerated universal expansion, the matter and energy content of the universe, the law of gravitation on large scales, neutrino masses, and the level of primordial non-Gaussianity. The anisotropic galaxy power-spectrum is caused by an effect called Redshift Space Distortions (RSDs), which also provide a good testbed for our theory of gravity.

In general, deep, wide-field spectroscopic surveys are needed to the determine the isotropic and anisotropic power-spectrum of any large-scale structure tracer. Moreover, such surveys can provide an important set of redshifts needed to calibrate the enormous number of photometric redshifts that will soon be delivered by planned weak lensing and photometric surveys (e.g., Pan-STARRS, DES, HSC, LSST). Recent or imminent spectroscopic surveys include:

1. The Wiggle-z dark energy survey measured the Baryonic Acoustic Oscillations (BAO) with a 3% accuracy from $z \sim 0.3$ to $z \sim 0.7$ using 200,000 ELGs over 800 deg^2 (Blake et al. 2011).

2. SDSS-III/BOSS was started in 2009 with the goal of surveying 10,000 deg^2 and measuring redshifts for 1.4 million LRGs within $0.3 < z < 0.6$ as well as for 160,000 quasars at $z > 2.2$. BOSS has already provided a first measurement of BAO using one-third of their LRG sample (Anderson et al. 2012). It will also use the absorbers in the Ly-α forest of distant quasars to provide a first measurement of BAO at $z \sim 2.5$ (with $\sim 3\%$ accuracy). The final BOSS BAO measurement accuracy should reach about 1% at $0.4 < z < 0.6$ by mid-2014.

3. Between 2011 and 2014, the VIPERS project will use VIMOS on the VLT to conduct a survey of 100,000 galaxies in the $0.5 < z < 0.9$ window over an area of 24 deg^2, focusing on RSD measurements.

4. Starting in 2013, the HETDEX survey will provide BAO measurements targeting 800,000 Lyman-break galaxies at $1.9 < z < 3.5$. HETDEX will cover an area of 420 deg^2.

5. Between 2014 and 2020, eBOSS will conduct a 3,000 deg^2 BAO survey focusing on: (1) the $0.6 \lesssim z \lesssim 1$ window using 150,00 LRGs and 525,000 ELGs; and (2) in the $1 \lesssim z \lesssim 2.5$ window using 320,000 quasars.

These surveys have tended to focus on medium- to wide-field BAO and RSD measurements, and no major survey has systematically targeted massive clusters at $z > 0.3$ on large scales. The observational strategies needed to target massive clusters must be adapted those employed in galaxy surveys, which benefit from the much higher density of targets. For transient observations, most of the current follow-up programmes are performed on object-by-object basis in view of their low number densities and the limited flexibility of multi-object spectrographs. A massive transient follow-up survey, which could be linked with deep spectroscopy survey projects, will only be practical when highly multiplexed, rapidly reconfigurable spectrographs become available, along with larger input catalogues.

Many of the major astronomical projects that are currently underway or in the planning stages — including WiggleZ, SDSS/BOSS, DES, HSC, *Planck*, LSST and *Euclid* — are cosmology driven. Nevertheless, there are many aspects of cosmology that will not be addressed by the above approved projects. In particular, there is no dedicated spectroscopic facility that will supersede the SDSS/BOSS spectrograph in multiplexing capability before 2018. It is therefore critical to think of the next steps in this important area. From a cosmology perspective, the key features for a multi-object spectrograph are the following:

- A wide field of view, in order to probe the largest cosmological scales ($\Omega \sim$ a few square degrees).
- A high level of multiplexing, in order to target a large numbers of sources ($\Sigma_{\rm MOS} \sim 1$ arcmin^{-2}).
- A short reconfiguration time ($t \leq$ a few minutes)
- A large collecting area telescope ($D > 4$m) and high system throughout, in order to minimize exposure times, allow the detection of faint sources, and maximize sample size.

2.9.3 ngCFHT in Context: Competition and Synergies

A wealth of available (or imminent) imaging and astrometric data is suitable for planning and implementing new spectroscopic surveys. For instance, in the northern hemisphere, surveys and/or faciltities of interest include:

1. CFHT-Megacam, which has already imaged more than 6,000 deg^2 of the northern sky. It could also survey a much larger area in the coming years, if the communities and agencies were committed such a project. The Synergistic Sky Survey, or S^3, was proposed (but not approved) in 2012 as part of the most recent call for large programmes. S^3 was aiming to image 8,000 deg^2 of the northern sky in at least two filters to a depth of 24 AB magnitude, for a total of $\sim$1100 hours.

2. Palomar Transient Factory, which is surveying the sky in the g band to search for transient objects. There is a plan to replace the current camera by a new powerful one which would cover 35 deg^2 in a single exposure. If this goes well, the new camera could be on the sky as soon as 2014 leading to the *Zwicky* Transient Factory project. The primary limitation of these data will be the poor image quality ($\sim 2''$ at best).

3. Pan-STARRS is a dedicated 1.8m facility that is now surveying the entire northern sky. Its main goal is the detection of potentially hazardous objects in the solar system. But the wide-field, repetitive nature of the Pan-STARRS observations makes the survey ideal for a host of other astronomical purposes, ranging from solar

system astronomy to cosmology. The current limitation of PS-1 (the first telescope and survey of the Pan-STARRS project) is the depth of its imaging, which is basically limited to $\sim$ 22 AB magnitude (i.e., similar to the depth of the SDSS). However, Pan-STARRS is aiming to build a PS-2 telescope that is very close in design to PS1, except for a few mechanical improvements based on PS-1 experiences. During normal operations, PS1 and PS2 will then be pointed at the same patch of sky, and the resulting images will be stacked, resulting in significant improvements in S/N and faster elimination of detector artifacts.

4. Hyper Suprime Cam (HSC) on the 8.2m Subaru telescope is a new, powerful red-sensitive CCD camera that can cover 1.8 deg^2 in one exposure. Because of the exquisite image quality at the Subaru site, and the large aperture of the telescope, this facility will probably be the state-of-the-art ground-based imager for the near future. The commissioning of the camera began in August 2012; survey observations could therefore start as early as 2013. The widest imaging survey planned for the next three years will cover 1,500 deg^2 to 26 AB magnitude. While this survey alone would not be wide enough for a dedicated wide-field cosmological survey with ngCFHT, there are proposals to image a much larger region of the extragalactic sky in subsequent years.

5. The WISE (Wide-field Infrared Survey Explorer) satellite has recently conducted an all-sky survey at wavelengths of 3.4, 4.6, 12 and 22 μm (Wright et al. 2010). In the course of its 10-month mission, 99.99% of the sky has been imaged at least eight times, while regions near the ecliptic poles have been observed more than 100 times. The key WISE channels are the 3.4 and 4.6 μm band, which can improve red galaxy selection, yielding 95% completeness down to a flux limit of 70μJy (19.3 mag AB) in areas with 10-fold coverage (almost all of the sky), and reaching the confusion noise limit of 63 μJy (19.4 mag AB) in the deepest regions (E. Wright, priv. comm.). The final WISE public data release occurred in March 2012. A further data release comprising all the data effectively taken may happen in the future, with the full WISE dataset.

6. LSST, with an effective aperture of 6.5m, is equipped with a wide-field camera that will image $\gtrsim$ 20,000 deg^2 of the southern and equatorial sky. The overlap with ngCFHT would be appreciable: nearly 10,000 deg^2. LSST will rapidly scan the sky, finding and charting objects that change in brightness or move in position — from exploding supernovae to potentially hazardous near-Earth asteroids. The resulting deep images $\sim$27 AB magnitude (after a 10-year survey), will provide multiple probes of dark matter and dark energy. First light is expected around 2019.

7. The *Euclid* space mission will ultimately survey 15,000 deg^2 of the extragalactic sky with high photometric accuracy to a depth of $\sim$25.5 AB magnitude in the visible and $\sim$24.5 in Y, J, and H near-infrared bands. It could thus provide legacy imaging suitable for extragalactic and cosmology surveys with ngCFHT. *Euclid* should be launched in 2020, but as with any space mission, there are risks of delays and/or more serious problems (i.e., launch failure).

8. The Gaia space mission will soon provide the best astrometric database for tying any photometric imaging to a spectroscopic survey with ngCFHT. Gaia will be launched in 2013.

The two spectroscopic facilities that have played the most important roles in wide-field cosmological surveys are the 4m AAT (e.g., 2dF Galaxy Redshift Survey, 6dF and the Wiggle-z survey) and the 2.5m SDSS telescope (e.g., SDSS-I and II, and now the SDSS-III/BOSS). For future cosmological surveys, both facilities are limited by their primary aperture, level of multiplexing (i.e., 400 fibres for AAOmega, $\sim$ 1000 for the BOSS spectrograph), and, to a lesser extent, site quality. Neither facility presently extends to wavelengths redder than 1 μm. A number of wide-field spectroscopic surveys (see Table 22) are therefore being considered for other facilities, although in many cases, the project is not yet funded or approved. Also, a clear cosmological programme has yet to be laid out in some cases.

1. BigBOSS is a proposed 5,000-fibre spectrograph that would cover the 0.36–1μm window at a resolution of $\mathcal{R} \approx$ 3,000 or higher. It would be installed on the 4m Mayall Kitt Peak telescope in 2018, and 500 nights of guaranteed time would be allocated to a major cosmological (BAO) survey. Although DOE and NOAO are showing interest, the project is not yet funded.

2. PFS/SUMIRE is a 2,400-fibre spectrograph that will cover the 0.36–1.3μm window at a resolution of $\mathcal{R} \approx$ 2,000 or higher. PFS is to be installed on the 8.2m Subaru telescope in 2017. However, only 300 nights will be reserved as guaranteed time, and one third of this will be set aside for a major cosmological survey.

Table 22: Current and Future Cosmological Spectroscopic Surveys

	Wiggle-z	BOSS	e-BOSS	BigBOSS	PFS	*Euclid*
Telescope (m)	AAT (3.9)	Sloan (2.5)	Sloan (2.5)	Mayall (4)	Subaru (8.2)	*Euclid* (1.2)
Image quality (arcsec)	$\sim$1.5-2	$\sim$1.5	$\sim$1.5	$\sim$1.2	$\sim$0.7	$\sim$0.6
Wavelength (μm)	0.37–0.95	0.36–1.0	0.36–1.0	0.36–1.0	0.4–1.3	1.2–2.0
Field-of-View (deg^2)	2	6.7	6.7	6.7	1.8	0.5
Multiplexing	400	1,000	1,000	5,000	2,400	—
Spectral Resolution	1,300	1,600-2,600	1,600-2,600	2,000-5,000	2,000-4,000	500
Imaging	SDSS/GALEX	SDSS	SDSS+DES	ZTF/PS?	HSC	*Euclid*
Mag Limit	$r < 22.5$	$i < 20$	$g < 22.5$	$r < 23.5$	$r < 23.5$	$H < 22$
Survey Area (deg^2)	800	10,000	3,000	14,000	1,500	15,000
Target density (deg^{-2})	275	140	500	2,300	1,500	$\sim$3,000
Survey Duration (year)	4.5	5	6	4	5	5
Night/year	60	150	150	120	60	—
Spectra (in million)	0.2	1.5	1.5	20	4	30
Redshift(Gal)	0.3–0.7	0.2–0.6	0.6–1.0	0.6–1.6	0.6–2	1–2
Redshift(QSO)	–	2.2–4	1–4	1–4	1–6	3–4(?)

3. DESpec is a 2,000-fibre spectrograph idea that aims to cover the 0.5–1μm window at resolution of $\mathcal{R} \approx 2{,}000$ or higher. It will be installed on the 4m Blanco CTIO not before 2018 (i.e., at the conclusion of the Dark Energy Survey). The main focus of this project is to follow up on the DES. However, there is at present no clear path to having this project approved by NOAO, or funded.

4. 4MOST is a proposed 1,500-fibre (possibly 3,000) spectrograph that would cover 0.42–1μm window at resolution larger than $\mathcal{R}$ = 3000 (de Jong et al. . 2012). This ESO instrument would be installed on either the VISTA or NTT telescope. The main focus of this project is to follow up on the Gaia and eROSITA space missions. A decision on the project is not expected until mid 2013.

5. MOONS (Multi-Object Optical and Near-infrared Spectrograph) is a proposed $\sim$1000 fibre spectrograph for the 8.2m VLT (Cirasuolo et al. 2012). Covering the 0.8–1.8μm window at a range of spectral resolutions (from $\mathcal{R}$ = 4,000 to 20,000), MOONS would have a somewhat limited field of view of ~ 0.14 deg^2. A decision on the project is not expected until mid 2013.

6. The space mission *Euclid* will have a slitless spectroscopic mode in its near IR channel that should cover the $\sim$1.2-2μm window. It will thus be quite powerful in identifying the Hα emission line of star-forming galaxies at $0.9 \lesssim z \lesssim 2$. However, the spectral resolution will be very limited — $\mathcal{R} \sim 500$ — and crowding issues may make the redshift identification complex, needing high-level, powerful algorithms. *Euclid* should be launched in 2020, but as with any space mission, there are risks of delays or more serious problems.

The power of ngCFHT for cosmological surveys lies in its large telescope aperture (10m), the dedicated nature of its operations, and the excellent image quality of the site. Its closest competitors are BigBOSS and PFS (see Table 22). Compared to BigBOSS, ngCFHT is unique in having coverage in the near IR region, along with a decided advantage in collecting area and, hence, sensitivity. Nevertheless, there could be interest in increasing the number of fibres on ngCFHT to $\sim$ 5,000, in order to match the level of multiplexing of BigBOSS. Compared to PFS, ngCFHT is unique in that the combination of aperture, throughput, fibre numbers and available survey time all contribute to a significantly higher efficiency. In addition, ngCFHT would have a high-resolution spectroscopic capability that PFS lacks. High spectral resolution enables some important cosmological observations (see, e.g., §2.3, 2.4, 2.7), including near-field cosmology and studies of the IGM.

For ngCFHT, it is important to dedicate enough resources to the data reduction and analysis software to ensure that operations run with the highest possible efficiency. As an example, the plan for BigBOSS (which is building on the SDSS legacy) is to process the spectra and measure redshifts for all targeted galaxies in a period of less than 24 hours. This is an important point to consider, as it could dictate the overall impact of the ngCFHT project in the era of large, synoptic imaging surveys.

2.9.4 Legacy Science

2.9.4.1 Measuring the Expansion Acceleration of the Universe with BAO

The expansion rate as a function of redshift is a sensitive probe of the content of the Universe: in particular, of the unknown "Dark Energy" component. Like supernovae-Ia standard candles, the spatial distribution of galaxies is a standard ruler for the Universe. By observing the apparent size of a standard ruler (and, therefore, the angular diameter distance) at different redshifts, we can measure the scale factor as a function of time.

The power spectrum of the galaxy distribution has two features useful as standard rulers. At $k \sim 0.01 h\mathrm{Mpc}^{-1}$, the power spectrum turns over from a k^1 slope (for a scale invariant spectrum of initial fluctuations), to a k^{-3} spectrum, caused by modes that entered the horizon during the radiation dominated era and were therefore suppressed. The precise position of this turnover is thus determined by the size of the horizon at matter-radiation equality. It corresponds to a physical scale determined by the matter $(\Omega_M h^2)$ densities and radiation densities $(\Omega_\gamma h^2)$. The second important feature is the oscillations in the power spectrum caused by acoustic waves in the baryon-photon plasma before hydrogen recombination at $z \sim 1000$, called the Baryon Acoustic Oscillations (hereafter BAO; Holtzman 1989; Wu & Sugiyama 1995; Eisenstein & Hu 1998). The scale of this feature is determined by the sound horizon at the recombination epoch, when the photons escaped from the baryonic plasma.

The imprint of Baryon Acoustic Oscillations is on a large scale (~ 105 Mpc$/h$) and was created when the Universe was still very close to homogeneous, with only very small perturbations; therefore, one can calculate the signature of BAO in a relatively straightforward way using linear theory. The fact that the signature of BAO occurs on such a large scale, and that it has a specific shape in the power-spectrum, makes BAO one of the least biased probes for exploring the properties of Dark Energy (Seo & Eisenstein 2003; Linder 2003).

The first BAO measurements were achieved by SDSS using the Luminous Red Galaxies sample as well as the 2dF experiment (Eisenstein et al. 2005, Cole et al. 2005). More recently, the BAO peak has been measured by the Wiggle-z and the SDSS-III/BOSS experiment (Blake et al. 2011; Anderson et al. 2012) in the z = 0.4–0.7 redshift window. In the coming months, SDSS-III/BOSS may provide the first BAO detection imprinted in the Lyα forest of $z > 2.2$ quasars. Thus, as of today, we have an unexplored region in the Universe between $0.7 < z < 2$ where we have no large-scale structure and BAO information (see Figure 54). Although this unexplored window is first to be explored with eBOSS, part of the post-Sloan III project, the expected accuracy of the BAO measurement will be limited, and future projects such as BigBOSS, PFS, *Euclid* or ngCFHT will be required to improve the measurement accuracy to better than the 1% level.

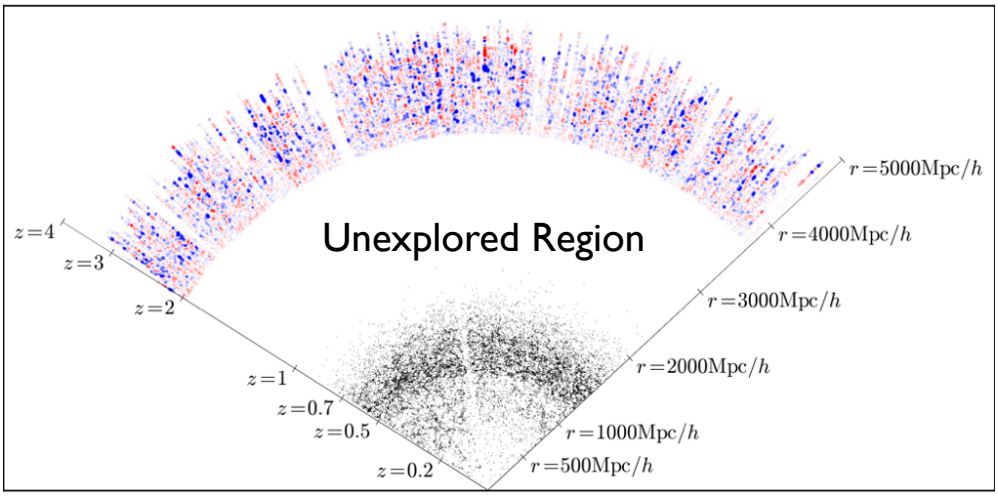

Figure 54: The status of wide-field redshift mapping by the BOSS survey. The "unexplored region" can be charted easily using emission line galaxies and quasars, which can then provide a complete evolution of the BAO peak from $z \sim 0$ to ~ 3. *Graphic adapted from Anze Slosar.*

In short, the measurement of the BAO feature is of prime interest for cosmology as it provides complementary and nearly systematic-free geometrical information compared to other cosmological probes such as the cosmic microwave background (CMB) and weak lensing (WL). Furthermore, the accuracy of the BAO measurement does not depend

strongly on our understanding of galaxy bias (Padmanabhan & White 2009; Mehta et al. 2011). In fact, Padmanabhan & White (2009) have demonstrated that the BAO shifts by sub-percent levels at bias $= 1$ to 2.

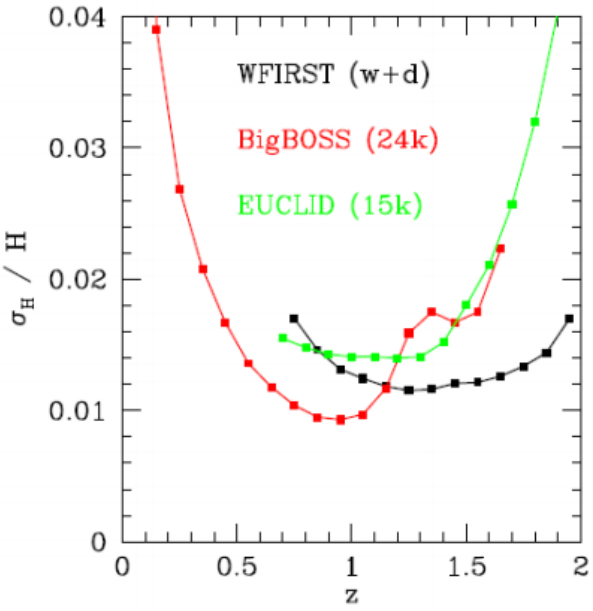

Figure 55: The fractional error in the Hubble expansion rate, H(z), as a function of redshift driven by the precise measurement of the BAO scale in the spectroscopic galaxy redshift survey. The constraints for the proposed WFIRST 1 year deep + 1 year wide survey, are shown alongside those for the prospective *Euclid* and BigBOSS surveys. *Figure from the Final SDT Report of the WFIRST mission [http://wfirst.gsfc.nasa.gov/science/WFIRST_IDRM_Report_Final_signed_Rev2.pdf]).*

BAO with Luminous Red Galaxies (LRGs). The BAO feature was first observed in early 2005 — both in the SDSS LRG sample (Eisenstein et al 2005) and in 2dFGRS data (Cole et al 2005) . Soon afterwards, it was detected using photometric Luminous Red Galaxies (LRGs) in 3500 deg^2 of SDSS data (Sanchez et al. 2009; Chuang et al. 2010; Kazin et al. 2010; Percival et al. 2010; Reid et al. 2010). More recently, the BAO peak was also measured by the SDSS-III/BOSS experiment (Anderson et al. 2012) at $z = 0.57$ using their "CMASS" galaxy sample (a somewhat broader sample than the LRG sample but at higher redshift) to a mean observed density of $\sim$150 per deg^2. The BOSS survey will be completed by summer 2014. Meanwhile, the eBOSS project plans to extend to $z \sim 0.8$ the detection of the BAO using red galaxies, and BigBOSS to $z \sim 1$. Both eBOSS and BigBOSS will likely use the WISE 3.4 μm data to help identify the red galaxies using the 1.6 μm bump which is redshifted in the first WISE band.

Note that large-scale structure measurements with LRG are not possible beyond a redshift of $\sim z$, given the sharp decrease in their space density.

BAO with Emission Line Galaxies (ELGs). An alternative strategy is to use the less biased ,and more (observationally) abundant, ELGs as large scale structure tracers. This is the basis of the WiggleZ survey (Drinkwater et al. 2010) and is the technique proposed to be used in *all* future BAO experiments (BigBOSS, SUMIRE/PFS, *Euclid* and the proposed ngCFHT in order to measure BAO at redshifts greater than one.

The now complete WiggleZ project used a combination of GALEX UV photometry and SDSS optical photometry data to select targets, finding a ELG density of $\Sigma_{\rm ELG} = 238$ galaxies deg^{-2} over $0.2 < z < 0.8$ (but covering only 800 deg^2). WiggleZ has completed their first analysis, detecting the BAO signal up to $z = 0.73$ (Blake et al. 2011) and demonstrating the validity of the BAO measurement with ELGs.

In the visible, an important factor in the redshift measurement of ELGs above $z \sim 1$ is the fact that only the [OII] emission line is available below $\sim$1μm. Nevertheless, there are two ways in which the identification of this line can be firmly established: i.e., (1) by extending the spectral coverage into the near IR region; or (2) by observing at a spectral resolution that is sufficient to resolve the [OII] doublet. Figure 57, show a preliminary trade-off analysis between the identification of the line, the S/N detection of the line and the spectral resolution. This analysis suggests that a minimum resolution of $\mathcal{R} \approx$ 3,000 would allow the identification of the doublet at reasonable S/N. While this

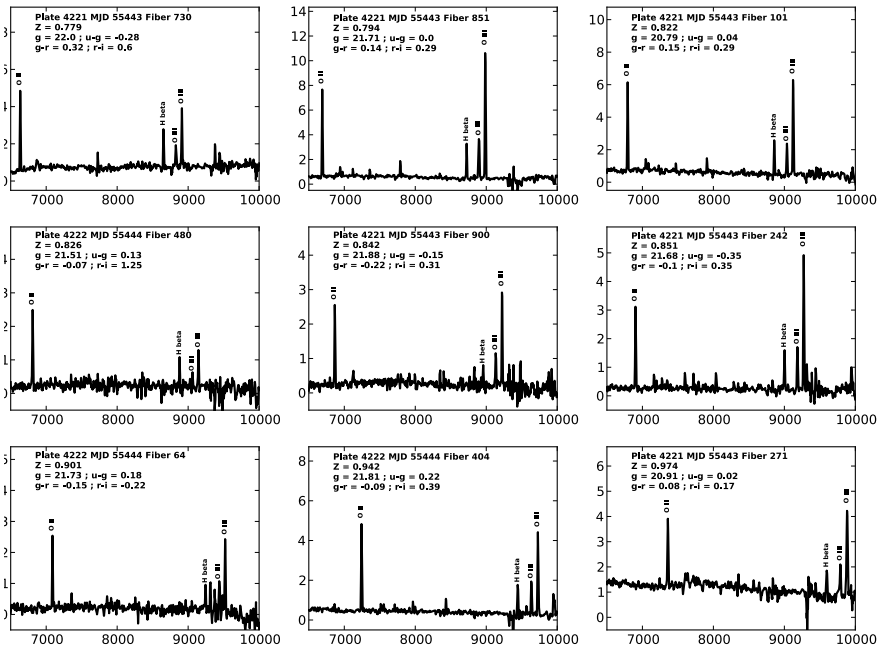

Figure 56: Representative spectra for emission line galaxies from the "ELG" BOSS ancillary project. These targets were selected from $(u-g)$ and $(g-r)$ colour cuts to a depth of $g = 22.5$ (corresponding roughly to $i \approx 21.3$). Fluxes are in units of 10^{-17} erg s^{-1} cm^{-2} Å^{-1}.

is somewhat larger than is currently available with ngCFHT in low-resolution mode, the wide spectral coverage (i.e., 0.37–1.3 μm at $\mathcal{R} \approx 2{,}000$) would allow unambiguous identification of the [OII] line.

BAO in the QSO Ly-α Forest. Several authors proposed using the Ly-α forest to measure the angular diameter distance and Hubble parameter at $2 < z < 4$ with the standard ruler provided by the BAO (McDonald 2003; White 2003; McDonald & Eisenstein 2007). To be competitive, the three-dimensional density field on the scale of the BAO feature should be sampled at high density. Such a measurement is the aim of the BOSS spectroscopic survey, where $z > 2.2$ quasars are targeted to an observed density of ~ 15 QSOs deg^{-2}. Because quasars at $2.2 < z < 3.5$ are located in the same regions as stars in most colour-colour diagrams, techniques using both photometry and variability have been developed that identify efficiently QSOs candidates at $z > 2.2$ (Palanque-Delabrouille et al. 2011; Ross et al. 2011) . While the BOSS analyses are underway, Le Goff et al. (2011) have simulated the BOSS QSO survey to estimate its statistical accuracy on the BAO scale determination. In particular, they simulated realistic mock samples of QSO Lyman-α, computed their power spectrum and estimated the BAO scales. Using 100 different simulations, they confirmed the Fisher matrix estimate and predicted that the BAO scale can be measured with an error of order 2.3%. They also showed that the uncertainty in the quasar absorption may increase the error on the BAO scale by 10 to 20% and results in a sub-percent bias on cosmological parameters.

Using a sample of approximately 14,000 quasars at $z >$2.1 that were observed in the first year of the BOSS survey, Slosar et al. (2011) measured the three-dimensional correlation function of absorption in the Ly-α forest. In particular, the angle-averaged correlation function of transmitted flux was securely detected for the first time out to comoving separations of 60 Mpc/h. They also detected a quadrupole distortion of the redshift-space correlation function by peculiar velocities. Fitting this feature assuming linear theory redshift-space distortion and linear bias of the transmitted flux, they find a linear bias parameter 0.16$< b <$0.24 and redshift-distortion parameter 0.44$< \beta <$1.20, at central redshift $z = 2.25$ with a well constrained combination b(1+β)=0.336$\pm$0.012. The value of β is somewhat low compared to theoretical predictions; it is likely depressed by the presence of high column density systems and metal line absorption. The data do not show an overwhelming contamination by the photoionization rate fluctuations or the effects of the temperature fluctuations in the intergalactic medium induced by the HeII reionization. Moreover, their analysis demonstrates that it is possible to measure the correlation function in the presence of instrument systematics such as imperfect sky subtraction and cross-talk between adjacent fibres. The early results by Slosar et al (2011) have

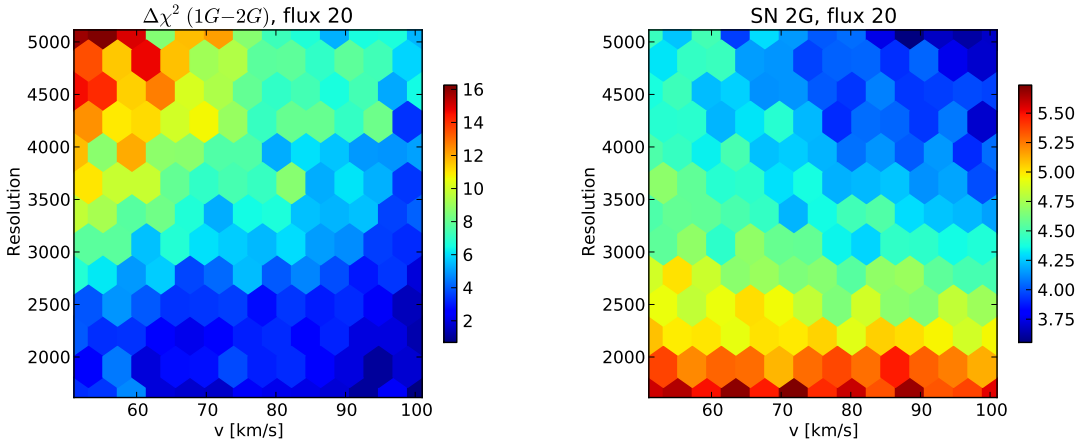

Figure 57: (Left) Variation of the $\Delta\chi^2$ between a 1-Gaussian fit and a 2-Gaussian fit as a function of spectral resolution and the velocity width of the [OII] line. (Right) Variation of the S/N ratio of the 2-Gaussian fit as a function of spectral resolution and the velocity width of the [OII] line. As shown in the analysis of the DEEP2 spectroscopic sample, 80% of the galaxies have $v < 70$ km s^{-1}, and so could be detected with a spectrograph having $\mathcal{R} \gtrsim 5\,000$. Note that the [OII] line flux chosen here is 20×10^{-17} erg s^{-1} cm^{-2} Å^{-1} with an exposure time adjusted to obtain a reasonable detection level.

set the stage for cosmological parameter determinations from three-dimensional structure in the Ly-α forest, including the first constraints on dark energy from BAO at $z > 2.2$ (expected in the near future).

BAO from QSO Clustering. The space density of quasars increases dramatically beyond $z \approx 0.5$, allowing us to use them as tracers of large-scale structures in the Universe. Down to $g \sim 22.5$, their number density is of the order of ~ 140 per deg^{-2}, opening the possibility of a clustering analysis on large scales. Sawangwit et al. (2011) have explored this idea by first searching for BAO and large-scale structure using $\sim 60,000$ QSOs from different surveys (SDSS, 2QZ and 2SLAQ) and then using the results (and simulations) to assess the science case for new QSO surveys. They did find evidence for a BAO peak at the same scale ($\sim$105 Mpc$/h$) as the one detected by Eisenstein et al. (2005), but only at low statistical significance. The use of mock catalogues to estimate the nominal survey size needed for a 3-4σ detection of the BAO peak shows that a redshift survey of $\sim$250,000 $z < 2.2$ QSOs is required over $\sim 3,000$ deg^2. Such a survey could, on its own, produce the first detection of, e.g., discontinuous dark energy evolution in the as yet uncharted $1 < z < 2.2$ redshift range.

The eBOSS survey is using QSOs to measure BAO at $z \sim 1.5$. When deeper imaging than SDSS becomes available (i.e., Pan-STARRS, LSST, etc), improved constraints from BAO measurements based on ngCFHT spectra for quasars could reach the percent level in accuracy. This would provide a measurement that is complementary to that obtained from ELGs, using a supposedly higher bias tracer.

Table 23: Technical Requirements and Survey Implementation: The BAO/Cosmology Survey

Survey Area (Ω)	$\Omega \approx 10\,000$ deg^2.
Field Location	The lowest foreground absorption regions at the North and South Galactic caps.
Number of ngCFHT Fields ($N_{\rm field}$)	$N_{\rm field} = \Omega/{\rm FOV}_{\rm ngCFHT} \approx 7\,000$.
Number of Configurations per Field ($n_{\rm config}$)	$\langle n_{\rm config} \rangle = 2$
Total Number of Exposures ($N_{\rm exp}$)	$N_{\rm exp} \simeq 14\,000$
Primary Imaging Resources for Target Selection	eROSITA, Pan-STARRS (3π), LSST, Euclid (Wide), ASKAP, etc
Observing Conditions	Lunar illumination $< 50\%$.
Instrumental Configuration(s)	$\mathcal{R} = 2\,000$, $T_{\rm exp} = 0.25$ hr
Wavelength Coverage and Velocity Precision (ϵ_v)	0.37–1.3μm at $\mathcal{R} = 2\,000$
Limiting (point source) Magnitude	$r = 23.7$
Total Time Needed for Program ($T_{\rm tot}$)	4 200 hrs

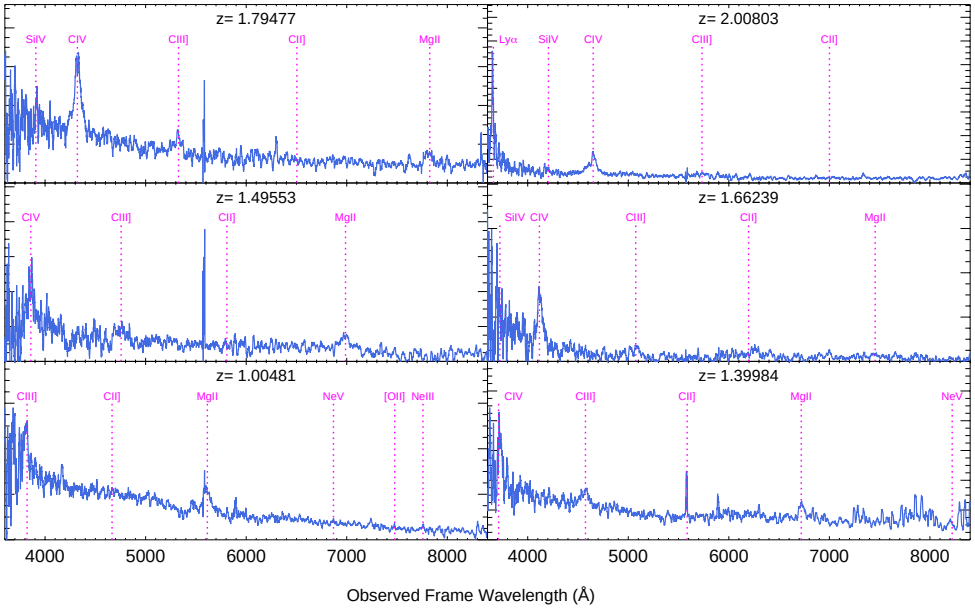

Figure 58: BOSS QSO spectra in the magnitude range $21.95 < g < 22.05$. BOSS exposure times are clearly sufficient for high quality QSO spectra even at $g = 22$. Although BOSS targets QSOs at $z > 2$, QSO identification and redshift assignation is unambiguous at all redshifts. Below $z = 1$, the unmistakable [OIII] and Hβ lines become visible (see Figure 56).

2.9.4.2 Constraining the Law of Gravitation with Redshift Space Distortions

The peculiar velocities of galaxies are induced by the gravitational pull of the mass content of the nearby universe. On large scales, these peculiar motions become coherent bulk flows toward over-dense regions and away from under-dense regions. The velocity bulk flows depend on the amplitude of the matter fluctuations and therefore are a measure of the growth rate of structure (Peebles 1980; Kaiser 1987). These coherent flows imprint a distinct anisotropic feature in the distribution of galaxies in redshift space, generally referred to as "Redshift Space Distortions" (RSDs). For example, the two-point correlation function gets compressed in the line-of-sight direction.

RSDs are now receiving significant attention as a potential cosmological probe. As a tracer of the growth rate of structure, RSDs are in principle capable of distinguishing dark energy from modified gravity models (e.g., Guzzo 2008,Percival & White 2009). Observationally, several projects carried out during the last decade have used RSDs to constrain cosmological parameters: i.e., the 2dFGRS (Peacock et al. 2001), the SDSS (e.g., Tegmark et al. 2006; Cabre & Gaztanaga 2009), 2SLAQ (Ross et al. 2007) and the VVDS (Guzzo et al. 2008). Currently, the VIPERS project is using ESO facilities to carry out a survey designed to measure RSDs. The WiggleZ survey has also just released their first results on RSDs (Blake et al. 2011). All major future cosmological spectroscopic surveys now highlight RSDs as one of their probes.

RSD detection by the standard method — measurement of the quadrupole anisotropy in the redshift-space two-point functions — is limited by the sample variance of the power spectrum in the surveyed volume V. This method yields a measure of fG, where G is the linear growth factor, and $f = d\ln G/d\ln a$. The sample-variance limit for standard RSD analyses is $\sigma_{\ln fG} \geq 35/\sqrt{k_{\rm max}^3 V}$ if accurate peculiar-velocity theory is available for $k < k_{\rm max}$. The WiggleZ survey attains $\sigma_{\ln fG} \approx 0.05$ assuming $k_{\rm max} = 0.3h\,{\rm Mpc}^{-1}$. A spectroscopic survey with ngCFHT would provide tighter cosmological constraints than achieved using RSDs by measuring a high density of sources over a much wider field of view than current RSD-motivated surveys, such as VIPERS.

2.9.4.3 Neutrino Masses

The large volume of ngCFHT survey data, together with the high density of the sample and the high bias of the quasars, would lead to an accurate measurement of the power spectrum on large scales. This would, in turn, provide accurate constraints on several cosmological parameters. For example, neutrinos free stream through the universe, but if they have mass, they suppress the growth of cold dark matter on scales below the free streaming scale, whereas no

suppression is expected on large scales. This leads to a broad feature in the matter power spectrum on scales of tens to hundred Mpc. The amplitude of the feature depends on neutrino mass, and one needs a very large survey volume to detect this effect. The quasar redshift survey would be the largest volume redshift survey available and so would be ideally suited to search for this effect.

2.9.4.4 Non-Gaussianity

Non-Gaussianity in the initial conditions of density perturbations has emerged as one of the most important discriminators among inflationary models for the early universe. A new method that has recently been proposed is based on theoretical models that indicate galaxy bias becomes scale dependent on very large scales due to non-Gaussianity (Dalal et al. 2008). This makes it possible to use galaxy and quasar clustering to learn about non-Gaussianity of the initial conditions in the universe. The method relies on tracers being highly biased since the effect scales as bias and vanishes for unbiased tracers. High-redshift quasars are particularly suitable for this purpose, as they are highly biased. Indeed, in the first application of this method to SDSS photometric data (Slosar et al. 2008), quasars give the strongest constraint. The result, $-29 < f_{nl} < 69$ (95% confidence levels), is comparable to the latest CMB constraints from WMAP, while having completely different systematic errors. This method is therefore competitive with the CMB bispectrum and should be pursued further.

The analysis in Slosar et al. (2008) was based on 235,000 photometric QSOs covering an area of 6,000 deg^2. The selection criteria are $g < 21$ and excess UV flux $(u-g) < 1.0$, in addition to other quasar selection cuts. Quasars were split into $z < 1.5$ and $z > 1.5$ samples, where the low-redshift sample has an effective redshift of 1.3 and contains 110,000 objects, while the high-redshift sample has an effective redshift of 1.7 and contains 125,000 objects. The effective bias of the low- and high-redshift bins is 2.4 and 2.75, respectively. The one sigma error on f_{nl} obtained solely from the quasar sample is 30.

Future redshift information from, e.g., ngCFHT, would allow one to go from a 2-D to a 3-D analysis, greatly increasing the number of available modes. The errors could be further reduced by bispectrum analysis, which contains information complementary to the power spectrum. The end result, as discussed below, is likely to be a constraint on non-Gaussianity comparable and independent to the expected Planck constraint of 5–10 on f_{nl}.

2.9.4.5 Strong Lensing

In SDSS-I, the Sloan Lens ACS Survey (SLACS; Bolton et al. 2006, 2008a) discovered over 100 strong gravitational lens systems through the spectroscopic signature of two redshifts along the same line of sight. Follow-up imaging of spectroscopic lens candidates with the *Hubble Space Telescope* and high-resolution ground-based facilities has enabled a unique experimental approach to the study of the structure and dynamics of massive galaxies at relatively low redshift (e.g., Koopmans et al. 2006; Bolton et al. 2008b). Within the BOSS project, the BOSS Emission-Line Lens Survey (BELLS: Brownstein et al. in prep; Bolton et al. in prep.) is successfully extending this technique to significant cosmological look-back time at redshift $z \sim$ 0.4-0.6, thereby probing directly the structural and dynamical *evolution* of LRGs.

A future spectroscopic survey with ngCFHT would allow this technique to be extended to redshifts of $z \sim 1$ and beyond (for ELG lenses), yielding a direct measurement of massive galaxy structure over an unprecedented cosmic time baseline. ELG lenses would also provide accurate measurements of the total aperture masses of galaxies beyond $z = 1$, for which masses are currently available only through relatively uncertain stellar-population synthesis techniques. This would provide a powerful new discriminant between competing models for the assembly and evolution of galaxy mass.

As an additional benefit, the main redshift-finding algorithms for future spectroscopic surveys, including those from ngCFHT, should be designed to find both emission-line redshifts (for ELGs) and absorption-line redshifts (for LRGs). This will make it possible to integrate the spectroscopic strong-lensing detection algorithms directly into the main survey redshifting pipeline, by looking for cases of different, and highly significant, pairs of redshifts (ELG+ELG or LRG+ELG) in the same spectrum.

2.9.4.6 A Cosmological Galaxy Clusters Survey

Clusters of galaxies are important cosmological probes (see also §2.5 and §2.6). The number and mass of clusters are highly sensitive to cosmological parameters including the mass density, the normalization of the mass power spectrum, and the dynamics of dark energy. Understanding the properties of clusters is vital for testing theories of

structure formation and mapping the distribution of cosmic matter on scales of ∼1–10 Mpc. In general, spectroscopic surveys can improve cluster cosmology in three complementary ways:

1. Calibration of photometric redshifts from spectroscopy.
2. Efficient cluster finding by virtue of improved photometric redshifts, which increase the purity of cluster measurements based on weak lensing.
3. Improved cluster mass proxies. Cosmology with clusters require the measurement of cluster mass, or its proxies. Three common proxies are:
   - *Cluster Richness.* In this case, spectra are essential for establishing membership for individual cluster galaxies.
   - *Weak lensing measurements.* The mass from lensing tomographic analysis can also be improved with better-calibrated photometric redshifts.
   - *Cluster Velocity Dispersion.* While this provides an excellent mass proxy with smaller scatter, it requires dedicated and massive spectroscopic campaigns on well-defined cluster samples (e.g., selected using homogenous X-ray or SZ surveys).

As the most massive clusters are intrinsically rare, one could imagine using ngCFHT to carry out spectroscopic follow up of the $\sim$ 500 most massive clusters in the $0.2 < z < 1$ window to: (1) measure their dynamical masses; and (2) trace out the large-scale structure in their vicinity. Such a programme would naturally require spectroscopy to higher galaxy densities than the BAO survey, thus entailing repeated observations of the same fields.

Table 24: Technical Requirements and Survey Implementation: The Cosmology Cluster Survey

Survey Area (Ω)	500 fields or $\simeq$ 750 deg^2.
Field Location	TBD; the 500 most massive clusters in the universe at low Galactic latitude.
Number of ngCFHT Fields ($N_{\rm field}$)	$N_{\rm field} = 500$.
Number of Configurations per Field ($n_{\rm config}$)	$\langle n_{\rm config} \rangle$ =2–4, (depending on cluster redshift) complementing the Dark-Wide or BAO survey information.
Total Number of Exposures ($N_{\rm exp}$)	$N_{\rm exp} \approx$ 1500.
Primary Imaging Resources for Target Selection	eROSITA, Pan-STARRS (3), LSST, Euclid (Wide), Planck
Observing Conditions	Lunar illumination $<$ 50%.
Instrumental Configuration(s)	$\mathcal{R} = 2\,000$, $T_{\rm exp}$ = 0.5–1.0 hr
Wavelength Coverage and Velocity Precision (ϵ_v)	0.37–1.3μm at $\mathcal{R} = 2\,000$
Limiting (point source) Magnitude	$i \simeq 23.5$
Total Time Needed for Program ($T_{\rm tot}$)	$T_{\rm tot}$ = [500×3×0.75 hr] + 20% overhead $\approx$ 1350 hrs.

2.9.4.7 A Massive Spectroscopic Survey of Supernovae and Other Transients

Type Ia supernovae (SNIa) are well established cosmological probes whose luminosity distances provide key constraints on the Dark Energy equation of state, w. Indeed, the current constraints of $\approx 6.5\%$ on w (including systematical effects) have yet to be matched by other probes. Even if future improvements on the Dark Energy Figure of Merit (FoM) from SNIa will not be as large as expected from other probes (e.g., Weak Lensing, BAO, etc), they are geometrical probes that are independent of large-scale structure growth, so more data at higher redshifts will be useful for comparing basic cosmological assumptions (particularly if the Universe is not simply described by ΛCDM). Of course, there is more to cosmology than merely improvements to the Dark Energy FoM, and having larger and more distant SNIa samples will, for instance, allow increasingly precise tests of isotropy.

Improvements on w to the $\sim 1\%$ level, using SNIa of redshifts $z \lesssim 0.8$, must involve better control of systematic effects: e.g., improved calibrations and better knowledge of the physics driving SN explosions. The analysis of nearby SN spectra suggests that standardization with spectra alone may be possible. This promises to reduce the intrinsic SNIa dispersions using accurate spectral sub-classifications.

While the number of high-redshift SNIa ($z > 0.8$) is still quite small, samples will improve dramatically with the next generation of imaging surveys (e.g., Euclid, LSST). We consider two examples where ngCFHT could play a key role in providing the all-important spectroscopic followup of SNe imaging surveys. First, LSST is aiming to perform high-cadence observations of $\sim$ 40–50 "deep drilling fields" (each covering $\sim$ 10 deg^2) in order to obtain

well-sampled lightcurves for $\sim$ 50 000 SNIa per year. Followup spectroscopy for these objects will be essential for obtaining their physical properties. Given their faintness, a wide-field, large-aperture telescope with a highly-multiplexed spectrograph will be essential. Most of these deep drilling fields will likely be at equatorial latitudes to facilitate this essential spectroscopic follow up. On average, each deep drilling field will contain roughly a thousand SNIa per year, so that a single pointing with ngCFHT would contain 150 SNIa over the course of a year. Thus, ngCFHT would be poised to become the de facto LSST SNe-followup telescope. Second, Euclid is considering a dedicated 6-month SNIa survey that could yield near-IR light curves for 1700 SNIa in the range $0.75 \lesssim z \lesssim 1.5$. Spectroscopy for those SNIa and their host galaxies will *not* be available from Euclid. Thus, there is an exciting opportunity for ngCFHT to serve as a major provider of spectra for transients and their host galaxies, which are crucial for typing the individual transient candidates, for redshift measurements, for sub-classifications based on key spectral features, and for investigating correlations between the properties of SNIa and those of their hosts.

Additional, exciting transient science (i.e., beyond SNIa cosmology) will certainly benefit from enormous numbers of spectra taken with a wide-field, 10m telescope: e.g., core-collapse supernovae, ultra-bright supernovae or pair-instability supernovae, supernovae associated with gamma ray bursts, and AGN flares. Future surveys will deliver thousands of candidates, and efficient spectroscopic follow up will be essential if we are to better understand the physics driving these events.

2.9.4.8 Internal Velocity Fields of Distant Galaxies

First-order velocity maps for a large sample of moderately extended galaxies would be of strong cosmological interest if combined with a weak lensing survey. Because the velocity field of a galaxy is not distorted by weak lensing, it provides a unique way of extracting the gravitational shear signal using a much smaller number of galaxies than would otherwise be required. Indeed, as shown by Morales (2006) for the (idealized) case of a perfect velocity measurement with only two lensed galaxies, one can retrieve the intrinsic gravitational shear! Of course, such an approach will, in practice, be compromised by the errors associated with the velocity measurements. Nevertheless, it is not unreasonable to hope for an improvement in the shear accuracy measurement of a factor of $\sim$10 (see Figure 59).

How could one measure such low-order velocity fields using ngCFHT? One option would be to observe the galaxies in a given field multiple times, re-configuring the fibres each time so that a low order "map" of each galaxy is built up progressively. Given the current ngCFHT — which emphasizes a wide field, large number of fibres and short ($\sim$ 40 sec) configuration time — this approach represents an efficient and cost-effective method for accumulating low-order, pseudo-IFU spectra for a large number of galaxies.

An alternative approach that could be considered on longer timescales, would be to implement a spectrograph mode in which, rather than assigning a single fibre to each object, compact bundles of 7 (or even 19) fibres are deployed across the telescope field, allowing the direct measurement of crude velocity maps for moderately extended galaxies (i.e., 1–2$''$ in size). Such an option would also provide excellent sky measurements, thereby ensuring the best OH sky-subtraction for compact and distant galaxies.

Although fibre bundles are still in early development (e.g., Croom et al. 2012) they hold great promise for scientific applications that require crude IFU spectroscopy for large numbers of targets. Of course, when the fibres are packed closely together, there is an important change at the spectrograph slit entrance, since the 7-fibre mode would need about five times more space at the entrance slit and detector than a single fibre.

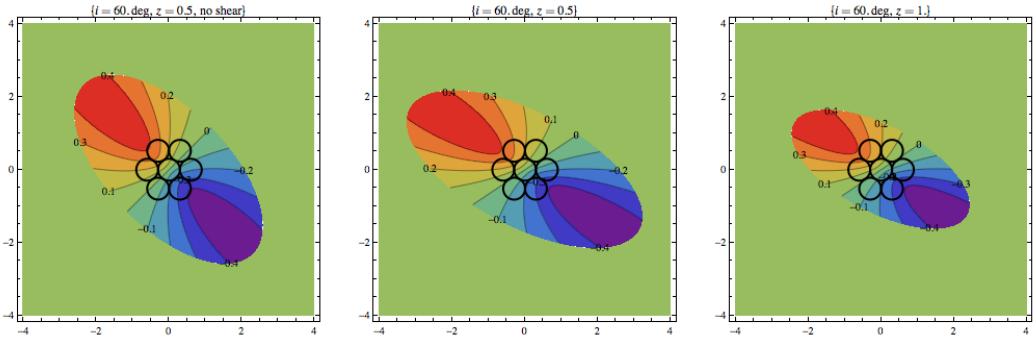

Figure 59: How gravitational shear can distort the intrinsic shape of a galaxy but *not* its velocity field The source galaxy is shown in the left panel, while the central and right panels show same galaxy with two different shear values. By measuring the velocity field orientation through, e.g., a seven fibre bundle IFU (as shown) and comparing it to the shape orientation, it is possible to measure directly the gravitational shear. This approach would allow an accurate measurement of the gravitational shear based on a minimum number of galaxies.

3 References

Abadi, M. G., Navarro, J. F., Steinmetz, M., & Eke, V. R. 2003, ApJ, 597, 21
Abbas, U., & Sheth, R. K. 2006, MNRAS, 372, 1749
Abbas, U., et al. 2010, MNRAS, 406, 1306
Adelberger, K. 2003, ApJ, 584, 45
Adelberger, K. L., et al. M. 2004, ApJ, 607, 226
Akerman, C. 2005, A&A, 440, 499
Albrecht, A., et al. 2006, arXiv:astro-ph/0609591
Allen, J. T., Hewett, P. C., Maddox, N., Richards, G. T., & Belokurov, V. 2011, MNRAS, 410, 860
Allende Prieto C., et al. 2008 AN, 329, 1018
Anderson, L. Aubourg, E. Bailey, S. Bizyaev, D. Blanton, M., et al. 2012, arXiv:1203.6594
Ann, H. B., Park, C., & Choi, Y.-Y. 2008, MNRAS, 389, 86
Arav, N., Edmonds, D., Borguet, B., Kriss, G.A., Kaastra, J.S., et al. 2012, A&A, 544, 33
Asplund M., et al. 2006, ApJ, 644, 229
Assef, R. J., et al. 2012, ApJL, submitted (arXiv:1203.2617)
Babusiaux C., Gilmore G., 2005, MNRAS, 358, 1309
Bahe, Y. M., McCarthy, I. G., Crain, R. A., & Theuns, T. 2012, ArXiv e-prints
Balcells, M., Benn, C. R., Carter, D., et al. 2010, Proc. SPIE, 7735
Baldry, I. K., Driver, S. P., Loveday, J., et al. 2012, MNRAS, 421, 621
Baldry, I. K., Glazebrook, K., & Driver, S. P. 2008, MNRAS, 388, 945
Baldry, I. K., et al. 2006, MNRAS, 373, 469
Balogh, M. L., Christlein, D., Zabludoff, A. I., & Zaritsky, D. 2001, ApJ, 557, 117
Balogh, M. L., Navarro, J. F., & Morris, S. L. 2000, ApJ, 540, 113
Balogh, M. L., et al. 2004, ApJL, 615, L101
Balogh, M. L., et al. 2009, MNRAS, 398, 754
Balogh, M. L., et al. 2011, MNRAS, 412, 2303
Barden, S., et al. 2009, WFMOS: A Feasibility Study for Gemini
Barden, S.C., Jones, D.J., Barnes, S. I., Heijmans, J., Heng, A., et al. 2010, Proc. SPIE, 7735
Battaglia, G., et al. 2008, MNRAS, 383, 183
Battaglia, G., et al. 2011, MNRAS, 411, 1013
Becker G.D, Bolton J.S., Haehnelt M.G., & Sargent W.L.W. 2011, 410
Behroozi, P. S., Conroy, C., & Wechsler, R. H. 2010, ApJ, 717, 379
Bekki, K., & Tsujimoto, T. 2011, ApJ, 738, 4
Belokurov, V., Zucker, D. B., Evans, N. W., Gilmore, G., Vidrih, S., et al. 2006, ApJ, 642, L137
Bensby, T., Feltzing, S., & Lundstrom, I. 2003, A&A, 410, 527
Bensby, T., Feltzing, S., Lundstrom, I., & Ilyin, I. 2005, A&A, 433, 185
Bensby, T., Zenn, A. R., Oey, M. S., & Feltzing, S. 2007, ApJ, 663, L13
Bensby T., et al. 2010 A&A, 521, 57
Bensby T., et al. 2011 A&A, 533, 134
Benson, A. J., Bower, R. G., Frenk, C. S., et al. 2003, ApJ, 599, 38
Bentz, M. C., et al. 2009, ApJ, 697, 160
Bergeron P., et al. 2005 ApJ 625, 838
Berlind, A. A., & Weinberg, D. H. 2002, ApJ, 575, 587
Bernardi M. et al. 2003, AJ, 125, 32
Bigiel F., et al. 2010, AJ, 140, 1194
Birnboim, Y., & Dekel, A. 2003, MNRAS, 345, 349
Blake, C., Brough, S., Colless, M., Contreras, C., Couch, W., et al. 2011, MNRAS, 415, 2876
Blake, C., Davis, T., Poole, G.B., Parkinson, D., Brough, S., et al. 2011, MNRAS, 415, 2892
Blandford, R.D., & McKee, C.F. 1982, ApJ, 255, 419
Blandford, R., et al. 2010, New Worlds, New Horizons in Astronomy and Astrophysics
Bogdanović, T., Smith, B. D., Sigurdsson, S., & Eracleous, M. 2008, ApJS, 174, 455
Bohlin, R.C. 2000, AJ, 120, 437
Bolton J.S., Haehnelt M.G., Viel M., & Springel V. 2005, MNRAS, 357, 1178
Bolton, A.S., Burles, S., Koopmans, L.E.V., Treu, T., & Moustakas, L.A. 2006, ApJ,. 638, 703
Bolton, A.S., Burles, S., Koopmans, L.E.V., Treu, T., Gavazzi, R. et al. 2008, ApJ, 682, 964
Bolton, A.S., Treu, T., Koopmans, LV.E., Gavazzi, R., Moustakas, L.A. 2008, ApJ, 684, 248
Bolton J.S., Oh S.P., & Furlanetto S.R. 2009, MNRAS, 396, 2405

Bolton, A.S., & Schlegel, D.J. 2010, PASP, 122, 248
Bonifacio, P., Caffau, E., Francois, P., et al. 2011, Astronomische Nachrichten, 332, 251
Bonifacio P., et al. , 2012 A&A 542 87
Booth, C. M. & Schaye, J. 2009, MNRAS, 398, 53
Botti, I., et al. 2008, arXiv:0805.4664
Bouche, N., et al. 2004, MNRAS, 354, 25
Bouwens, R. J., Illingworth, G. D., Franx, M., & Ford, H. 2007, ApJ, 670, 928
Bouwens, R. J., et al. 2011, ApJ, 737, 90
Bower, R. G., et al. 2006, MNRAS, 370, 645
Boylan-Kolchin, M., Bullock, J. S., & Kaplinghat, M. 2011, MNRAS, 415, L40
Boylan-Kolchin, M., Bullock, J. S., & Kaplinghat, M. 2012, MNRAS, 422, 1203
Brodie, J.P., Romanowsky, A.J., Strader, J., & Forbes, D.A. 2011, 2011, AJ, 142, 199
Brodwin, M., et al. 2008, ApJL, 687, L65
Bromm, V., & Loeb, A. 2003, Nature, 425, 812
Brooks A.M., et al. 2009, ApJ, 694, 396
Brott I., et al. 2011, A&A, 530, 116
Buchhave L.A., et al. 2012, Nature, 486, 375
Bundy, K., et al. 2009, ApJ, 697, 1369
Burgarella, D., et al. 2000, The Next Generation Canada-France-Hawaii Telescope
Butcher, H., & Oemler, A. 1978, ApJ, 219, 18
Côté, P., McLaughlin, D. E., Cohen, J. G., & Blakeslee, J. P. 2003, ApJ, 591, 850
Cabrè, A., & Gaztañaga, E. 2009, MNRAS 396, 1119
Cackett, E. M. & Horne, K. 2006, MNRAS, 365, 1180
Caffau, E., Bonifacio, P., François, P., et al. 2011, Nature, 477, 67
Capak, P., et al. 2007, ApJS, 172, 99
Cappellari, M., McDermid, R. M., Alatalo, K., et al. 2012, Nature, 484, 485
Cappelluti, N., Predehl, P., Böhringer, H., et al. 2011, Mem. della Societa Astronomica Italiana Supplementi, 17, 159
Carlberg, R., et al. 1999, A Wide-Field 8 Meter Telescope for Canadians
Carlberg, R. G., et al. 2000, ApJL, 532, L1
Carlstrom, J. E., Ade, P. A. R., Aird, K. A., et al. 2011, PASP, 123, 568
Carollo, D., Beers, T.C., Lee, Y.S., Chiba, M., Norris, J.E., et al. 2008, Nature, 451, 216
Cattaneo, A., Dekel, A., Devriendt, J., Guiderdoni, B., & Blaizot, J. 2006, MNRAS, submitted, astro-ph/0601295
Cattaneo, A., Dekel, A., Faber, S. M., & Guiderdoni, B. 2008, MNRAS, 389, 567
Cen, R. 2011, ApJ, 741, 99
Cescutti G., Matteucci F., 2011 A&A, 525, 126
Chen, C., Zhang, J., & Vogeley, M.S. 2009, Mapping the Global Impact of Sloan Digital Sky Survey
Cheng et al. 2012, ApJ, 746, 149
Cirasuolo, M., Afonso, J., Bender, R., Bonifacio, P., Evans, C., et al. 2012, arXiv:1208.5780
Clark, P.C., Glover, S.C.O., Smith, R. J.,et al. 2011, Science, 331, 1040
Coil, A. L., et al. 2006, ApJ, 644, 671
Cole, S., Norberg, P., Baugh, C. M., et al. 2001, MNRAS, 326, 255
Cole, S., Percival, W.J., Peacock, J.A., Norberg, P., Baugh, C.M., et al. 2005, MNRAS, 362, 505
Colless, M., et al. 2001, MNRAS, 328, 1039
Conroy, C., Wechsler, R. H., & Kravtsov, A. V. 2006, ApJ, 647, 201
Conroy, C., White, M., & Gunn, J. E. 2010, ApJ, 708, 58
Conselice, C. J., Bershady, M. A., Dickinson, M., & Papovich, C. 2003, AJ, 126, 1183
Cooke, R. 2011, MNRAS, 417, 1534
Cooper, M. C., et al. 2006, MNRAS, 370, 198
Cooper, M. C., et al. 2010, MNRAS, 409, 337
Côté, P., McLaughlin, D.E., Cohen, J.G., & Blakeslee, J.P. 2003, ApJ, 591, 850
Coupon, J., et al. 2011, ArXiv e-prints
Crighton, N. 2011, MNRAS, 414, 28
Crocce, M., Fosalba, P., Castander, F. J., & Gaztañaga, E. 2010, MNRAS, 403, 1353
Croom, S. M., et al. 2005, MNRAS, 356, 415
Croom, S. M., 2011, ApJ, 736, 161
Croom, S.M., Lawrence, J.S., Bland-Hawthorn, J., Bryant, J.J., Fogarty, L., et al. 2012, MNRAS 421, 872
Cui, X.-Q., Zhao, Y.-H., Chu, Y.-Q., Li, G.-P., Li, Q., et al. 2012, Research in Astronomy and Astrophysics, 12, 1197
Cuillandre, J.C., Fort, B., Picat, J.P., Soucail, J.P., Altieri, B., et al. 1994, A&A, 281, 603
Daddi, E., et al. 2007, ApJ, 670, 156

Dahlen, T., et al. 2007, ApJ, 654, 172
Dalal, N., White, M., Bond, J.R., & Shirokov, A. 2008, ApJ, 687, 12
Dalcanton, J.J., et al. . 2012, ApJS, 200, 18
Davé, R., Finlator, K., & Oppenheimer, B. D. 2011, MNRAS, 1158
de Blok, W.J.G., & Walter, F. 2006, AJ, 131, 343
de Boni, C., et al. 2011, MNRAS, 415, 2758
Dehnen, W., & Binney, J.J. 1998, MNRAS, 298, 387
de Jong R.S., et al. 2012, in SPIE Astronomical Instrumentation and Telescopes, astro-ph/1206.6885
Dekel A., et al. 2009, ApJ, 703, 785
Dekel, A., et al. 2009, Nature, 457, 451
Denney, K. D., et al. 2010, ApJ, 721, 715
de Ravel, L., et al. 2009, A&A, 498, 379
Dey, A., et al. 2003, KAOS: The Kilo-Aperture Optical Spectrograph
Drinkwater, M.J., Jurek, R.J., Blake, C., Woods, D., Pimbblet, K.A., et al. 2010, MNRAS 401, 1429
Driver, S. P., Hill, D. T., Kelvin, L. S., et al. 2011, MNRAS, 413, 971
Driver, S., & De Propris, R. 2003, A&AS, 285, 175
Dunn, J. P., et al. 2010, ApJ, 709, 611
Dwek E., et al. 1995, ApJ, 445, 716
Eisenstein, D.J., & Hu, W. 1998, ApJ, 496, 605
Eisenstein, D.J., Zehavi, I., Hogg, D.W., Scoccimarro, R., Blanton, M.R., et al. 2005, ApJ, 633, 560
Eisenstein D.J., et al. 2006 ApJS, 167, 40
Eisenstein et al. 2011 AJ 142, 72
Eggen, O.J., Lynden-Bell, D., & Sandage, A.R. 1962, ApJ, 136, 748
Eke, V. R., Baugh, C. M., Cole, S., Frenk, C. S., & Navarro, J. F. 2006, MNRAS, 370, 1147
Ekstrom S., et al. 2012, A&A, 537, 146
Ellingson, E., Lin, H., Yee, H. K. C., & Carlberg, R. G. 2001, ApJ, 547, 609
Ellis, R., et al. 2009, Wide-Field Fibre-Fed Optical Multi-Object Spectrometer WFMOS Study Summary
Ellis, R., Takada, M., Aihara, H., Arimoto, N., Bundy, K. et al. 2012, arxiv:1206.0737
Ellison, S. L., Patton, D. R., Simard, L., & McConnachie, A. W. 2008, AJ, 135, 1877
Enßlin, T., Pfrommer, C., Miniati, F., & Subramanian, K. 2011, A&A, 527, A99+
Eyre, A, & Binney, J., 2009, MNRAS 400, 548
Eyre, A. 2010, MNRAS 403, 1999
Faber, S. M., et al. 2005, ApJ, submitted, astro-ph/0506044
Faucher-Giguére C.-A., Prochaska J.X., Lidz A., Hernquist L., & Zaldarriaga M. 2008, ApJ, 681, 831
Faucher-Giguère, C.-A., Quataert, E. & Murray, N. 2012, MNRAS, 420, 1347
Federman, S.R. 1982, ApJ, 257, 125
Feldmeier, J. J., Ciardullo, R., Jacoby, G. H., & Durrell, P. R. 2004, ApJ, 615, 196
Ferrarese, L., Côté, P., Cuillandre, J.-C., et al. 2012, ApJS, 200, 4
Ferrarese, L., et al. 2006, ApJL, 644, L21
Fine, S., et al. 2012, MNRAS, in press (arXiv:1205.1401)
Firnstein M., Przybilla N., 2012 A&A, 543, 80
Fliri, J., & Vals-Gabaud, D. 2012, Ap&SS, 341, 57
Foucaud, S., et al. 2010, MNRAS, 406, 147
Fowler, J.W., Niemack, M.D., Dicker, S.R., Aboobaker, A.M., Ade, P.A.R., et al. 2007, ApOpt, 46, 3444
Frank, S. & Peroux, C. 2010, MNRAS, 420, 1731
Frebel A., Norris J.E., 2011, in Planets, Stars, and Stellar Systems, Chapter 5, (Springer), astro-ph/1102.1748
Freeman, K. C. 1987, ARA&A, 25, 603
Freeman, K., & Bland-Hawthorn, J. 2002, ARA&A, 40, 487
Freeman, K.C. 2012, Galactic Archaeology: Near-Field Cosmology and the Formation of the Milky Way, 458, 393
Friedman S,D., York, D.G., McCall, B.J., Dahlstrom, J. Sonnentrucker, P., et al. 2011, ApJ, 727, 33
Frieman, J.A., Turner, M.S., & Huterer, D. 2008, ARA&A 46, 385
Fukugita et al. 1998, ApJ, 503, 518
Fulbright et al. 2007, ApJ, 661, 1152
Furlanetto S.R., & Oh S.P. 2008, ApJ, 681, 1
Fuhrmann, K. 1998, A&A, 338, 161
Gallagher, S. C., et al. 2006, ApJ, 644, 709
Gao et al. 2010 MNRAS, 403, 1283
Gao, L., & White, S. D. M. 2007, MNRAS, 377, L5
Gauthier, J.-R., et al. 2009, ApJ, 702, 1

Geyl, R., et al. 2000, The New CFHT
Ghezzi L., et al. 2010 ApJ, 720, 1290
Gibson, R. R., et al. 2010, ApJ, 713, 220
Gilbank, D. G., et al. 2010, MNRAS, 405, 2419
Gilbank, D. G., et al. 2011, MNRAS, 414, 304
Gilmore, G., & Reid, N. 1983, MNRAS, 202, 1025
Gilmore G., et al. 2012, Messenger, 147, 25
Glazebrook, K., & Bland-Hawthorn, J. 2001, PASP, 113, 197
Godard, B., Falgarone, E., & Pineau Des Forêts, G. 2009, A&A, 495, 847
Gonzalez et al. 2011 A&A 530, 54
Greene, J. E., & Ho, L. C. 2004, ApJ, 610, 722
Greene, J. E., & Ho, L. C. 2007, ApJ, 667, 131
Green, J., Schechter, P., Baltray, C., Bean, R., Bennett, D., et al. 2012, arXiv:1208.4012
Grether, D., & Lineweaver, C.H. 2006, ApJ, 640, 1051
Greif, T.H., Springel, V., White, S.D.M., et al. 2011, ApJ, 737, 75
Groenewegen M.A.T., et al. 2007, A&A, 474, 975
Grundmann, W., et al. 1997, A CFH 12-16m Telescope Study
Guo, Q., White, S., Boylan-Kolchin, M., et al. 2011, MNRAS, 413, 101
Guzzo, L., Strauss,M. A., Fisher, K. B., Giovanelli, R., & Haynes, M. P. 1997, ApJ, 489, 37
Guzzo, L., Pierleoni, M., Meneux, B., Branchini, E., Le Fèvre, O., et al. , 2008, Nature, 451, 541
Haiman, Z. & Hui, L. 2001, ApJ, 547, 27
Hall, P. B., et al. 2002, ApJS, 141, 267
Hamann, F. 2001, astro-ph/9911505
Hanson B. et al. 2007 ApJ 671 380
Haşegan, M., Jordán, A., Côté, P., Djorgovski, S.G., McLaughlin, D.E, et al. 2005, ApJ, 627, 203
Helmi, A. 2008, A&ARv 15, 145
Ho, L., et al. 2012, ApJ, in press (arXiv:1109.4181)
Hobbs, L.M., York, D.G., Thornburn, J.A., Snow, T.P., Bishof, M., etal 2009, ApJ, 705, 32
Holberg J.B., et al. 2008, AJ, 135, 1225
Holtzman, J., 1989, ApJS 71, 1
Hopkins P.F., Richards G.T., & Hernquist L. 2007, ApJ, 654, 731
Hopkins, A. M., & Beacom, J. F. 2006, ApJ, 651, 142
Hopkins, P. F., Bundy, K., Hernquist, L., Wuyts, S., & Cox, T. J. 2010, MNRAS, 401, 1099
Hopkins, P. F., Somerville, R. S., Hernquist, L., Cox, T. J., Robertson, B., & Li, Y. 2006, ApJ, 652, 864
Hopkins, P. F. & Elvis, M. 2010, MNRAS, 401, 7
Hopkins, P. F., Richards, G. T., & Hernquist, L. 2007, ApJ, 654, 731
Hopkins, P. F., et al. 2006, ApJS, 163, 1
Hopkins, P. F., et al. 2007, ApJ, 662, 110
Horne, K., Peterson, B. M., Collier, S. J., & Netzer, H. 2004, PASP, 116, 465
Hunter I., et al. 2009, A&A, 496, 841
Ilbert, O., et al. 2009, ApJ, 690, 1236
Ilbert, O., et al. 2010, ApJ, 709, 644
Iwata, I., et al. 2009, ApJ, 692, 1287
Jones, T. A., Swinbank, A. M., Ellis, R. S., Richard, J., & Stark, D. P. 2010, MNRAS, 404, 1247
Juneau, S., et al. 2005, ApJL, 619, L135
Kaiser, N., 1987, MNRAS, 227, 1
Kalirai J.S., 2012, Nature, 486, 90
Kannappan, S. J., & Gawiser, E. 2007, ApJL, 657, L5
Kaplan, K. 2010, PASP, 122, 619
Kartaltepe, J. S., et al. 2010, ApJ, 721, 98
Kaspi, S., et al. 2007, ApJ, 659, 997
Kawata, D., & Mulchaey, J. S. 2008, ApJL, 672, L103
Kazin, E.A., Blanton, M.R., Scoccimarro, R., McBride, C.K., Berlind, A.A., et al. 2010, ApJ, 710, 1444
Kepler S.O., et al. 2007, MNRAS, 375, 1315
Kereš, D., Katz, N.,Weinberg, D. H., & Davé, R. 2005, MNRAS, 363, 2
Khare, P. 2012, MNRAS, 419, 1028
Khochfar, S., & Burkert, A. 2003, ApJL, 597, L117
Kilic M., et al. 2012, MNRAS, 423, 132
Kim T.S., Viel M., Haehnelt M.G., Carswell R.F., & Cristiani S. 2004, MNRAS, 347, 355

Kirby E. et al. 2008a, ApJ, 682, 1217
Kirby E. et al. 2008b, ApJ, 685, 43
Kistler, M. D., Yüksel, H., Beacom, J. F., Hopkins, A. M., & Wyithe, J. S. B. 2009, ApJL, 705, L104
Klypin, A., Kravtsov, A. V., Valenzuela, O., & Prada, F. 1999, ApJ, 522, 82
Klypin, A., Trujillo-Gomez, S., & Primack, J. 2010, ArXiv eprints
Knobel, C., et al. 2009, ApJ, 697, 1842
Komatsu, E., Smith, K.M., Dunkley, J., et al. 2011, ApJS, 192, 18
Koopmans, L.V.E., Treu, T., Bolton, A.S., Burles, S., & Moustakas, L.A. 2006, ApJ, 649, 599
Kordopatis, G., Recio-Blanco, A., de Laverny, P., et al. 2011, A&A in press, arXiv:1110.5221
Kriek, M., et al. 2008, ApJ, 677, 219
Krumholz, M. R., & Dekel, A. 2011, ArXiv e-prints
Kudritzki R.P., et al. 2012 ApJ, 747, 15
Kurucz, R.L. 2005, Memorie della Societa Astronomica Italiana Supplementi, 8, 189
Lallement, R., Welsh, B.Y., Vergely, J.L., Crifo, F., & Sfeir, D. 2003, A&A, 411, 447
Landecker T., Routledge, D., Reynolds, S.P., Smegal, R.J., Borkowski, K.J., et al. 1999, ApJ, 527, 866
Larson, R. B., Tinsley, B. M., & Caldwell, C. N. 1980, ApJ, 237, 692
Le Borgne, D., et al. 2006, ApJ, 642, 48
Le F‘evre, O., et al. 2005, A&A, 439, 877
Leauthaud, A., et al. 2011, ArXiv e-prints
Leauthaud, A., et al. 2012, ApJ, 746, 95
Lecureur A., et al. 2007, A&A, 465, 799
Lee, M. G., Park, H. S., & Hwang, H. S. 2010, Science, 328, 334
Lee, S.-K., Ferguson, H. C., Somerville, R. S., Wiklind, T., & Giavalisco, M. 2010, ApJ, 725, 1644
Lee, S.-K., et al. 2009, ApJS, 184, 100
Lee, Y.S., Beers, T.C., An, D., et al. 2011, ApJ, 738, 187
Le Goff, J.M., Magneville, C., Rollinde, E., Peirani, S., Petitjean, P., et al. 2011, A&A, 534, 135
Li, C., et al. 2006, MNRAS, 368, 37
Lilly, S. J., et al. 2007, ApJS, 172, 70
Lin, L., et al. 2007, ApJL, 660, L51
Lin, L., et al. 2008, ApJ, 681, 232
Lin, L., et al. 2010, ApJ, 718, 1158
Lin, L., et al. 2012, ApJ, 756, 71
Liu, X., Shen, Y., Strauss, M. A., & Hao, L. 2011, ApJ, 737, 101
Linder, E.V. 2003, Phys. Rev. D 68, 083504
Loeb, A. 2010, PRD, 81, 047503
Lotz, J. M., Primack, J., & Madau, P. 2004, AJ, 128, 163
Lundgren, B. 2009, ApJ, 698, 819
Madrid, J., & Macchetto, D. 2006, BAAS, vol 38, p. 1286
Madrid, J., & Macchetto, D. 2009, arXiv:0901.4552v1
Maeder A., Meynet G., 2010, New AR, 54, 32
Magnelli, B., et al. 2011, A&A, 528, A35
Majewski, S.R. 1992, ApJS, 78, 87
Majewski, S.R. 1993, ARA&A, 31, 575
Majewski, S.R., Munn, J.A., & Hawley, S.L. 1994, ApJ, 427, L37
Majewski S., 2012, AAS 21920506
Mandelbaum, R., Seljak, U., Kauffmann, G., Hirata, C. M., & Brinkmann, J. 2006, MNRAS, 368, 715
Maraston, C., et al. 2010, MNRAS, 407, 830
Marshall, D.J., Robin, A.C., Reylé, C., Schultheis, M., & Picaud, S. 2006, A&A, 453, 635
Martel, H. 2011, arXiv:1110.1061
Martin, N.F., Ibata, R.A., Chapman, S.C., Irwin, M., & Lewis, G.F. 2007, MNRAS, 380, 281
Martini, P. & Weinberg, D. H. 2001, ApJ, 547, 12
Matthews, L. D., & de Grijs, R. 2004, AJ, 128, 137
Maulbetsch, C., et al. 2006, ApJ, in press, astroph/0606360
McCarthy, I. G., et al. 2008, MNRAS, 383, 593
McConnachie, A.W., et al. 2005, MNRAS, 356, 979
McConnachie, A.W., et al. 2009, Nature, 461, 66
McDonald, P., 2003, ApJ, 585, 34
McDonald P. et al. 2006, ApJS, 163, 80
McDonald, P., & Eisenstein, D.J. 2007, Phys. Rev. D 76, 063009

McGee, S. L., Balogh, M. L., Bower, R. G., Font, A. S., & McCarthy, I. G. 2009, MNRAS, 400, 937
McGee, S. L., et al. 2011, MNRAS, 413, 996
McNamara, B. 2010, in 38th COSPAR Scientific Assembly, Vol. 38, 2612
McQuinn M. et al. 2009, ApJ, 694, 842
McQuinn M., & White M. 2011, MNRAS, 415, 2257
McWilliam A., Zoccali M., 2010, ApJ, 724, 1491
McWilliam et al. 2008, AJ, 136, 367
Mehta, K.T., Seo, H.-J., Eckel, J., Eisenstein, D.J. Metchnik, M., et al. 2011, ApJ, 734, 94
Melbourne, J., Koo, D. C., & Le Floc'h, E. 2005, ApJL, 632, L65
Melendez J., et al. 2012, A&A, 543, 29
Melis, C., Farihi, J., Dufour, P., Zuckerman, B., Burgasser, A.J., et al. . 2011, ApJ, 732, 90
Menard, B. & Peroux, C. 2003, A&A, 410, 33
Meneux, B., et al. 2008, A&A, 478, 299
Meneux, B., et al. 2009, A&A, 505, 463
Miceli M., etal 2010, MmSAI, 75, 282
Minniti, D., Lucas, P.W., Emerson, J.P., Saito, R.K., Hempel, M., et al. 2010, New Astronomy, 15, 433
Mobasher, B., et al. 2007, ApJS, 172, 117
Moore, B., Ghigna, S., Governato, F., et al. 1999, ApJL, 524, L19
Morales, M.F. 2006, ApJ 650, L21
Munari U., Tomasella, L., Fiorucci, M., Bienaymé, O., Binney, J., et al. 2008, A&A, 488, 969
Murphy, M. 2008, MNRAS, 384, 1053
Murphy, M., & Liske, J., 2004, MNRAS, 386, 1192
Murray, N., Quataert, E., & Thompson, T. A. 2005, ApJ, 618, 569
Myers, A. D., et al. 2008, ApJ, 678, 635
Nakamura, F., & Umemura, M. 2001, ApJ, 548, 19
Nardetto N., et al. 2011, A&A, 534, 16
Neilson H.R., et al. 2012, A&A, 541, 134
Nestor, D. B., Shapley, A. E., Steidel, C. C., & Siana, B. 2011, ApJ, 736, 18
Netzer, H., et al. 2003, ApJ, 599, 933
Newberg, H.J., Willett, B.A., Yanny, B., Xu, Y. 2010, ApJ 711, 32
Ngeow C.C., et al. 2012, A&A, 543, 55
Nissen, P.E., & Schuster, W.J. 2011, A&A, 530, A15
Norberg, P., et al. 2002a, MNRAS, 332, 827
Norberg, P., et al. 2002b, MNRAS, 332, 827
Norris J.E., et al. , 2010 ApJ , 723, 1632
Noterdaeme, P. 2008, A&A, 481, 327
Noterdaeme, P. 2009, 505, 1087
Noterdaeme, P. 2010, A&A, 523, 80
Noterdaeme, P. 2011, A&A, 526, 7
Okamoto S., et al. , 2012 ApJ, 744, 96
Origlia L., et al. 2012, ApJ, 726, 20
Ostriker, J. P., Choi, E., Ciotti, L., Novak, G. S., & Proga, D. 2010, ApJ, 722, 642
Ouchi, M., et al. 2005, ApJL, 620, L1
Ouchi, M., et al. 2008, ApJS, 176, 301
Padmanabhan, N., et al. 2007, MNRAS 378, 852
Padmanabhan, N., & White, M., 2009, Phys. Rev. D 80, 063508
Palanque-Delabrouille, N., Yeche, C., Myers, A.D., Petitjean, P., Ross, N.P., et al. 2010, A&A, 530, A122+
Paris I., et al. 2011, A&A, 530, 50
Park, C., Gott, III, J. R., & Choi, Y.-Y. 2008, ApJ, 674, 784
Park, C., & Choi, Y.-Y. 2009, ApJ, 691, 1828
Park, C., & Hwang, H. S. 2009, ApJ, 699, 1595
Patton, D. R., Ellison, S. L., Simard, L., McConnachie, A. W., & Mendel, J. T. 2011, MNRAS, 412, 591
Patton, D. R., et al. 2002, ApJ, 565, 208
Peacock, J.A., Cole, S., Norberg, P., Baugh, C.M., Bland-Hawthorn, J., et al. 2001, Nature, 410, 169
Peebles, P.J.E., 1980, The Large-Scale Structure of the Universe (Princeton, N.J., Princeton University Press)
Peng, Y., Lilly, S. J., Renzini, A., & Carollo, M. 2011, ArXiv eprints
Peng, Y., et al. 2010, ApJ, 721, 193
Penny L., Gies D.R., 2009, ApJ, 700, 844
Pepe, F.A., Cristiani, S., Rebolo Lopez, R., Santos, N.C., Amorim, A., et al. 2010, SPIE, 7735, 14

Percival, W.J., & White, M., 2009, MNRAS, 393, 297
Percival, W.J., Reid, B.A., Eisenstein, D.J., Bahcall, N.A., Budavar, T., et al. 2010, MNRAS, 401, 2148
Perlmutter, S., Aldering, G., Goldhaber, G., Knop, R.A., Nugent, P., et al. 1999, ApJ, 517, 565
Perryman, M.A.C., Lindegren, L., Kovalevsky, J., et al. 1997, A&A, 323, L49
Perryman, M.A.C., & ESA 1997, ESA Special Publication, 1200
Peterson, B., et al. 2011, arXiv:1109.4181
Peterson, B. M., et al. 2002, ApJ, 581, 197
Pfrommer, C., Chang, P., & Broderick, A. E. 2011, ArXiv e-prints
Phleps, S., Peacock, J. A., Meisenheimer, K., & Wolf, C. 2006, A&A, 457, 145
Pietrukowicz, P., Udalski, A., Soszyński, I., Nataf, D.M., Wyrzykowski, Ł., et al. 2012, ApJ, 750, 169
Pineau des Forêts G., Flower, D.R., Hartquist, T.W., & Dalgarno, A. 1986, MNRAS, 220, 801
Placco V.M., et al. 2011, AJ, 142, 188
Poggianti, B. M., et al. 2009, ApJ, 693, 112
Poggianti, B., et al. 2006, ApJ, 642, 188
Pohlen M., Trujillo I., 2006, A&A, 454, 759
Pudritz, R., et al. 2000, The Origins of Structure in the Universe (LRP2000), http://www.casca.ca/lrp/
Quinn, P.J., Hernquist, L., & Fullagar, D.P. 1993, ApJ, 403, 74
Raichoor, A., & Andreon, S. 2012, ArXiv e-prints
Raimond S., Lallement, R., Vergely, J.-L., Babusiaux, C., & Eyer, L. 2012 A&A, in press, arXiv:1207.6092
Ramirez I., et al. 2010 A&A, 521, 33
Ransom, R.R., Kothes, R., Wolleben, M., & Landecker, T.L. 2010, ApJ, 724, 946
Reddy, B.E., Tomkin, J., Lambert, D.L., & Allende Prieto, C. 2003, MNRAS, 340, 304
Reddy, B.E., Lambert, D.L., & Allende Prieto, C. 2006, MNRAS, 367, 1329
Reddy, B.E., & Lambert, D.L. 2008, MNRAS, 391, 95
Reddy, B.E. 2010, IAU Symposium, 265, 289
Reid, B.A., Percival, W.J., Eisenstein, D.J., Verde, L., Spergel, D.N., et al. 2010, MNRAS, 404, 60
Richard, J., et al. 2011, MNRAS, 413, 643
Richards, G. T., et al. 2009, ApJS, 180, 67
Richards, G. T., et al. 2011, AJ, 141, 167
Riess, A.G., Filippenko, A.V., Challis, P., Clocchiatti, A., Diercks, a., et al. 1998, AJ, 116, 1009
Riess, A.G., et al. 2007, ApJ, 659, 98
Riess, A.G., Filippenko, A.V., Challis, P., Clocchiatti, A., Diercks, A., et al. 2009, AJ 116, 1009
Robin, A.C., Reyle, C., Derriere, S., & Picaud, S. 2003 A&A, 409, 523
Robotham, A. S. G., Norberg, P., Driver, S. P., et al. 2011, MNRAS, 416, 2640
Roskar R., et al. 2008, ApJ, 675, 65
Ross, N.P., da Ângela, J., Shanks, T., Wake, D.A., Cannon, R.D., et al. 2007, MNRAS 381, 573
Ross, N. P., et al. 2009, ApJ, 697, 1634
Ross, N.P., Myers, A.D., Sheldon, E.S., Yèche, C., Strauss, M.A., et al. 2012, ApJS, 199, 3
Rudie, G. 2012, ApJ, 750, 67
Ryan-Weber, et al. 2009, , MNRAS, 395, 1476
Ryde N., et al. 2010, A&A, 509, 20
Salvadori, S., Schneider, R., & Ferrara, A. 2007, MNRAS, 381, 647
Sánchez, A.G., Crocce, M., Cabré, A., Baugh, C.M., & Gaztañaga, E., 2009, MNRAS 400, 1643
Sawangwit, U., Shanks, T., Abdalla, F.B., Cannon, R.D., Croom, S.M., et al. 2011, MNRAS, 416, 3033
Sawangwit, U., et al. 2012, MNRAS, 420, 1916
Sawicki, M. 2012, MNRAS, 421, 2187
Sawicki, M., & Thompson, D. 2006, ApJ, 642, 653
Sawicki, M., & Yee, H. K. C. 1998, AJ, 115, 1329
Schlegel D.J. et al. 2009, arXiv:0904.0468
Schlegel, D., et al. 2011, ArXiv e-prints
Schlegel, D., et al. 2011, arXiv:1106.1706
Schneider, R., Omukai, K., Bianchi, S., & Valiante, R. 2011, MNRAS, in press, arXiv:1109.2900
Schoenrich R., Binney J., 2009, MNRAS, 396, 203
Schuler S.C., et al. , 2011 ApJ 732 55
Searle, L., & Zinn, R. 1978, ApJ, 225, 357
Seo, H.-J., & Eisenstein, D.J., ApJ, 598, 720
Seymour, N., et al. 2008, MNRAS, 386, 1695
Shafter, A.W., Darnley, M.J., Bode, M.F., & Ciardullo, R. 2012, ApJ, 752, 156
Shankar, F., Weinberg, D. H., & Shen, Y. 2010, MNRAS, 406, 1959

Shapley, A. E. 2011, ARA&A, 49, 525
Shapley, A. E., Steidel, C. C., Pettini, M., & Adelberger, K. L. 2003, ApJ, 588, 65
Sharp, R., & Parkinson, H. 2010, MNRAS, 408, 2495
Shen J., et al. 2010, ApJ, 720, 72
Shen, Y, et al. 2007, AJ, 133, 2222
Shen, Y. 2009, ApJ, 704, 89
Simon, J.D., & Geha, M. 2007, ApJ, 670, 313
Schönrich, R., & Binney, J. 2009, MNRAS, 399, 1145
Schörck, T., Christlieb, N., Cohen, J.G., et al. 2009, A&A, 507, 817
Sironi, L., & Socrates, A. 2010, ApJ, 710, 891
Slosar, A., Hirata, C., Seljak, U., Ho, S., & Padmanabhan, N. 2008, Journal of Cosmology and Astro-Particle Physics 8, 31
Slosar, A., Font-Ribera, A.P., Matthew M., Rich, J., Le Goff, J.M., et al. 2011, JCAP, 9, 1
Smiljanic, R., Pasquini, L., Bonifacio, P., et al. 2009, A&A, 499, 103
Smith V.V., et al. 2002, AJ, 124, 3241
Smith, R. J., Lucey, J. R., Price, J., Hudson, M. J., & Phillipps, S. 2012b, MNRAS, 419, 3167
Smith, R. J., Lucey, J. R., & Carter, D. 2012a, ArXiv e-prints
Somerville, R. S., et al. 2004, ApJL, 600, L171
Sorba, R., & Sawicki, M. 2011, PASP, 123, 777
Sousa S.G., et al. 2011, A&A, 533, 141
Spitoni E., Matteucci F., 2011, A&A, 531, 72
Springel, V., DiMatteo, T., & Hernquist, L. 2005, ApJL, 620, L79
Srianand, R. et al. 2008, A&A, 482, 39
Steele P.R., et al. 2011 MNRAS, 416, 2768
Steidel C., et al. 2010, ApJ, 717, 289
Steidel, C. C., et al. 2003, ApJ, 592, 728
Steidel, C. C., et al. 2010, ApJ, 717, 289
Steinmetz, M., Zwitter, T., Siebert, A., et al. 2006, AJ, 132, 1645
Suda T., Hirschi R., Fujimoto M.Y., 2011, ApJ, 741, 61
Sugai, H., Karoji, H., Takato, N., Tamura, N., Shimono, A., Ohyama, Y., et al. 2012, arXiv:1210.2719
Swinbank, A. M., et al. 2006, MNRAS, 368, 1631
Tacconi, L. J., et al. 2006, ApJ, 640, 228
Tegmark, M., Eisenstein, D.J., Strauss, M.A., Weinberg, D.H., Blanton, M.R., et al. , 2006, Phys. Rev. D 74, 123507
Tinker, J., Wetzel, A., & Conroy, C. 2011, ArXiv e-prints
Tollerud, E. J., Bullock, J. S., Strigari, L. E., & Willman, B. 2008, ApJ, 688, 277
Tolstoy, E., Irwin, M.J., Helmi, A., Battaglia, G., Jablonka, P., et al. 2004, ApJ, 617, L119
Tolstoy, E., Hill V., Tosi M., 2009, ARAA
Tremblay P.E., Bergeron P., Gianninas A., 2011, ApJ, 730. 1289
Treu, T. 2010, ARA&A, 48, 87
Tumlinson J., et al. 2011, Science, 334, 948
Turon, C., Primas, F., Binney, J., Chiappini, C., Drew, J, et al. 2008, Report by the ESA-ESO Working Group on Galactic Populations, Chemistry and Dynamics
Valle, G., Ferrini, F., Galli, D., & Shore, S.N. 2002, ApJ, 566, 252
van Dokkum, P. G., & Conroy, C. 2010, Nature, 468, 940
Venemans, B. P., et al. 2007, A&A, 461, 823
Venn K.A., et al. 2002, ApJ, 565, 571
Vergely J.L., Valette, B., Lallement, R., & Raimond, S. 2010, A&A, 518, A31
Viel M., Bolton J.S., & Haehnelt M.G. 2009, MNRAS, 399, L39
Vikhlinin, A., et al. 2009, ApJ, 692, 1060
Vives, S., Le Mignant, D., Madec, F., Jaquet, M., Prieto, E. et al. 2012, arXiv:1210.2728
Volonteri, M., Miller, J. M., & Dotti, M. 2009, ApJL, 703, L86
Vulcani, B., et al. 2010, ApJL, 710, L1
Wake, D. A., et al. 2011, ApJ, 728, 46
Walcher, C. J., et al. 2008, A&A, 491, 713
Walker M., Mateo M., Olszewski E.W., 2009, AJ, 137, 3100
Wang, L., Li, C., Kauffmann, G., & De Lucia, G. 2006, MNRAS, 371, 537
Wareing, C.J., Zijlstra, A.A., O'Brien, T.J., & Seibert, M. 2007, ApJ, 670, L125
Watson, D., Denney, K. D., Vestergaard, M., & Davis, T. M. 2011, ApJL, 740, L49
Wechsler, R. H., Bullock, J. S., Primack, J. R., Kravtsov, A. V., & Dekel, A. 2002, ApJ, 568, 52
Weinmann, S. M., Kauffmann, G., von der Linden, A., & De Lucia, G. 2010, MNRAS, 406, 2249

Weinmann, S. M., van den Bosch, F. C., Yang, X., & Mo, H. J. 2006, MNRAS, 366, 2
Weinmann, S.M., Neistein, E., & Dekel, A. 2011, MNRAS, 1463
Weinmann, S.M., et al. 2012, ArXiv e-prints
Welsh, B.Y., Lallement, R., Vergely, J.-L., & Raimond, S. 2010, A&A, 510, 54
Wetzel, A. R., & White, M. 2010, MNRAS, 403, 1072
White, M. 2003, in The Davis Meeting On Cosmic Inflation. 2003 March 22-25, Davis CA., p.18
White, S. D. M., & Frenk, C. S. 1991, ApJ, 379, 52
Wijesinghe, D. B., et al. 2012, ArXiv e-prints
Williams, C. C., et al. 2011, ApJ, 733, 92
Willman, B., Dalcanton, J.J., Martinez-Delgado, D., West, A.A., Blanton, M.R., et al. 2005, ApJ, 626, L85
Willman, B., Blanton, M.R., West, A.A., Dalcanton, J.J., Hogg, D.W., et al. 2005, AJ, 129, 2692
Willmer, C. N. A., et al. 2006, ApJ, 647, 853
Wolf, C., et al. 2009, MNRAS, 393, 1302
Wolleben M., 2007, ApJ, 664, 349
Wolleben M., Fletcher, A., Landecker, T.L., Carretti, E., Dickey, J.M., et al. 2010, ApJ, 724, 48
Wright, E.L., Eisenhardt, P.R.M., Mainzer, A.K., Ressler, M.E., Cutri, R.M., et al. 2010, AJ, 140, 1868
Hu, W., & Sugiyama, N. 1995, ApJ, 444, 489
Yan, R., et al. 2009, MNRAS, 398, 735
Yang, X., Mo, H. J., van den Bosch, F. C., et al. 2007, ApJ, 671, 153
Yang, X., Mo, H. J., & van den Bosch, F. C. 2008, ApJ, 676, 248
Yanny, B., Rockosi, C., Newberg, H.J., et al. 2009, AJ, 137, 4377
Yoachim, P., & Dalcanton, J.J. 2008, ApJ, 682, 1004
York, D. 2006, MNRAS, 367, 945
York, D. G., Adelman, J., Anderson, Jr., J. E., et al. 2000, AJ, 120, 1579
Younger J.D., et al. , 2007, ApJ, 670, 269
Zibetti, S. ApJ, 2005, ApJ, 63L, 105
Zhao, G., Zhao, Y.-H., Chu, Y.-Q., Jing, Y.-P., & Deng, L.-C. 2012, Research in Astronomy and Astrophysics, 12, 723
Zoccali M. 2012, in The Chemical Evolution of the Milky Way (ESO LP 187.B-0909)
Zoccali M. et al. 2008, A&A, 486, 177
Zu, Y., Kochanek, C. S., & Peterson, B. M. 2011, ApJ, 735, 80

4 Acronyms

2dF	2 Degree Field
2dFGRS	2 Degree Field Galaxy Redshift Survey
2QZ	2dF QSO Redshift Survey
2SLAQ	2dF-SDSS LRG and QSO Survey
2MASS	Two Micron All Sky Survey
4MOST	4-Metre Multi-Object Spectroscopic Telescope
AAO	Australian Astronomical Observatory
AAT	Australian Astronomical Telescope
ACS	Advanced Camera for Surveys
ACSVCS	ACS Virgo Cluster Survey
ACT	Atacama Cosmology Telescope
AGN	Active Galactic Nuclei
ADC	Atmospheric Dispersion Compensator
ALMA	Atacama Large Millimeter Array
AO	Adaptive Optics
APO	Apache Point Observatory
APOGEE	APO Galactic Evolution Experiment
ARGOS	Abundances and Radial velocity Galactic Origins Survey
ASKAP	Australian Square Kilometre Array Pathfinder
BAO	Baryon Acoustic Oscillations
BigBOSS	Big Baryon Oscillation Spectroscopic Survey
BLR	Broad Line Region
BOSS	Baryon Oscillation Spectroscopic Survey
CFHT	Canada France Hawaii Telescope
CFHTLS	Canada France Hawaii Telescope Legacy Survey
CDM	Cold Dark Matter
CMB	Cosmic Microwave Background
CMD	Colour Magnitude Diagram
CGM	Circumgalactic Medium
COMBO-17	Classifying Objects by Medium-Band Observations: A Spectrophotometric 17-filter Survey
COSMOS	Cosmic Evolution Survey
DART	Dwarf Abundances and Radial velocities Team
DEC	Dark Energy Camera
DEEP2	Deep Extragalactic Evolutionary Probe 2
DEIMOS	DEep Imaging Multi-Object Spectrograph
DES	Dark Energy Survey
DESPEC	Dark Energy Spectrograph
DIB	Diffuse Interstellar Band
DINGO	Deep Investigation of Neutral Gas Origins
DLA	Damped Lyman-α Absorber
DOE	Department of Energy
DRAO	Dominion Radio Astrophysical Observatory
ELG	Emission Line Galaxy
ELT	Extremely Large Telescope
E-ELT	European Extremely Large Telescope
eBOSS	extended Big Baryon Oscillation Spectroscopic Survey
eROSITA	extended ROentgen Survey with an Imaging Telescope Array
ESA	European Space Agency
ESO	European Southern Observatory
ETC	Exposure Time Calculator
ESI	Echelle Spectrograph and Imager

ESPRESSO	Echelle SPectrograph for Rocky Exoplanet and Stable Spectroscopic Observations
EW	Equivalent Width
FIRST	Faint Images of the Radio Sky at Twenty-cm
FLAMES	Fibre Large Array Multi Element Spectrograph
FWHM	Full Width at Half Maximum
GALEX	GALaxy evolution EXplorer
GAMA	Galaxy And Mass Assembly
GDDS	Gemini Deep Deep Survey
GMOS	Gemini Multi-Object Spectrograph
GMRT	Giant Metrewave Radio Telescope
GR	General Relativity
GRB	Gamma Ray Burst
HARPS	High Accuracy Radial Velocity Planet Searcher
HDS	High Dispersion Spectrograph
HERMES	High Efficiency and Resolution Multi-Element Spectrograph
HETDEX	Hobby-Eberly Telescope Dark Energy Experiment
HIRES	HIgh Resolution Echelle Spectrograph
HOD	Halo Occupation Distribution
HSC	Hyper Suprime Cam
HST	Hubble Space Telescope
JVLA	Karl G. Jansky Very Large Array
JWST	James Webb Space Telescope
IGM	Intergalactic Medium
IMACS	Inamori Magellan Areal Camera and Spectrograph
IMF	Initial Mass Function
ISM	Interstellar Medium
IR	Infrared
KIDS	Kilo-Degree Survey
KPNO	Kitt Peak National Observatory
ΛCDM	Lambda Cold Dark Matter
LAE	Lyman Alpha Emitter
LAMOST	Large Sky Area Multi-Object Fibre Spectroscopic Telescope
LOFAR	Low Frequency Array
LSST	Large Synoptic Survey Telescope
LRG	Luminous Red Galaxy
LRIS	Low Resolution Imaging Spectrograph
MDF	Metallicity Distribution Function
MIKE	Magellan Inamori Kyocera Echelle
MMFS	Michigan/MIKE Fibre System
MOONS	The Multi-Object Optical and Near-infrared Spectrograph
FMOS	Fibre Multi-Object Spectrograph
MOS	Multi Object Spectrograph
MOSFIRE	Multi-Object Spectrometer for Infra-Red Exploration
MSTO	Main Sequence Turn Off
NGVS	Next Generation Virgo Cluster Survey
NSF	National Science Foundation
NTT	New Technology Telescope
NVSS	NRAO VLA Sky Survey
ODI	One Degree Imager
OHP	Observatoire de Haute-Provence
PAndAS	Pan Andromeda Archaeology Survey
Pan-STARRS	Panoramic Survey Telescope and Rapid Response System
PN	Planetary Nebula

PFS	Prime Focus Spectrograph
PHAT	Panchromatic Hubble Andromeda Treasury
PSF	Point-Spread Function
QSO	Quasi Stellar Object
RAVE	Radial Velocity Experiment
RGB	Red Giant Branch
RM	Reverberation Mapping
ROSAT	RÖntgenSATellit
RSD	Redshift Space Distortions
RVS	Radial Velocity Spectrometer
SDSS	Sloan Digital Sky Survey
SEGUE	Sloan Extension for Galactic Understanding and Exploration
SOPHIE	Spectrographe pour l'Observation des Phénomnes des Intérieurs stellaires et des Exoplanètes
SKA	Square Kilometer Array
SLACS	Sloan Lens ACS Survey
SNR	Supernova Remnant
SuMIRe	Subaru Measurement of Image and Redshifts
SWG	Science Working Group
SZE	Sunyaev Zel'dovich Effect
TMT	Thirty Meter Telescope
TRGB	Tip of the Red Giant Branch
UKIDDS	UKIRT Infrared Deep Sky Survey
UKIRT	United Kingdom Infrared Telescope
UVES	Ultraviolet and Visual Echelle Spectrograph
UVIT	Ultraviolet Imaging Telescope
VHS	VISTA Hemisphere Survey
VIKING	VISTA Kilo-degree Infrared Galaxy survey
VIMOS	Visible and Infrared Multi-Object Spectrograph
VIPERS	VIMOS Public Extragalactic Redshift Survey
VISTA	Visible and Infrared Survey Telescope for Astronomy
VLT	Very Large Telescope
VST	VLT Survey Telescope
VVDS	VLT Very Deep Survey
VVVS	VLT Vista Variables
WALLABY	Widefield ASKAP L-band Legacy All-sky Blind surveY
WEAVE	WHT Enhanced Area Velocity Explorer
WFC	Wide Field Camera
WFIRST	Wide-Field Infrared Survey Telescope
WHT	William Herschel Telescope
WIRCam	Wide Field Infrared Camera
WISE	Wide-field Infrared Survey Explorer
WIYN	Wisconsin Illinois Yale NOAO
WL	Weak Lensing
XMM	X-ray Multi-Mirror Mission